Coxiella burnetii control of the host transcription factors TFEB and TFE3

Bhavna Padmanabhan

ORCiD: 0000-0002-2993-2755

Submitted in total fulfilment of the requirements for the degree of

Doctor of Philosophy

June 2020

Department of Microbiology and Immunology

Peter Doherty Institute for Infection and Immunity

The University of Melbourne

Australia

This thesis is dedicated to my beloved parents for all their sacrifices, endless love & support.

Abstract

Coxiella burnetii, the etiological agent of the zoonotic disease Q fever, is an obligate Gram negative intracellular bacterial pathogen that replicates inside the lysosome-derived CCV (*Coxiella*-containing vacuole) within mammalian hosts. The CCV maintains the degradative and acidic nature of the host lysosome despite *C. burnetii* directing the massive expansion of this compartment to accommodate the replicating pathogen. To establish this unique replicative niche, *C. burnetii* requires the Dot/Icm type IV secretion system (T4SS). This T4SS translocates approximately 150 effectors into the host cell to modulate various cellular processes. To date, the functional role of very few of these effectors have been defined.

Given the CCV's origins it is not surprising that *C. burnetii* infection increases host autophagy and lysosome biogenesis. To investigate this at the protein level, we employed an elegant SILAC based proteome analysis of human cells infected with *C. burnetii*. This validated that many proteins involved in these processes are increased in abundance during infection. This prompted us to examine the role of the human transcription factor EB (TFEB) and its close homologue TFE3 during *C. burnetii* infection. TFEB is a master transcription regulator directly controlling the expression of a network of genes responsible for autophagy and lysosome biogenesis. 3 day's post-infection with *C. burnetii*, TFEB/TFE3 is activated as demonstrated by TFEB/TFE3 trafficking from the cytoplasm into the nucleus. The nuclear translocation of TFEB/TFE3 appears to be controlled by *C. burnetii* as blocking bacterial translation with chloramphenicol leads to TFEB/TFE3 movement back into the cytoplasm. siRNA silencing of *tfeb* and *tfe3*

additionally demonstrated their contribution towards the intracellular success of *C. burnetii*. Interestingly, these host factors did not contribute to the replication of *C. burnetii* but in the absence of TFEB and TFE3 the CCV did not undergo its typical massive expansion.

This research was able to demonstrate that *C. burnetii* induced activation of TFEB/TFE3 was dependent on the Dot/Icm T4SS thus we hypothesized that an effector(s) of this system may manipulate TFEB/TFE3. An unbiased visual screen was conducted to identify effectors that influence this process and two putative *C. burnetii* effector proteins, namely CBU1701 and CBU2016, were identified. We demonstrated that ectopic expression of these proteins leads to nuclear localisation of TFEB. Subsequent characterisation of the impact of CBU1701 and CBU2016, demonstrated that they influence the host proteome in similar ways but with surprisingly little impact on TFEB-regulated proteins. These results indicated that nuclear localisation of TFEB in response to CBU1701 and CBU2016 may be uncoupled from activation of this host transcription factor.

In addition to characterising the impact of these effector proteins on host cellular function we set out to understand the role they play in intracellular replication and virulence of *C. burnetii.* Genetic manipulation of this pathogen is in its infancy and remains technically challenging however this study reports the successful production of multiple mutant strains. Initial characterisation experiments demonstrate that CBU1701 and CBU2016

likely make important contributions to the establishment of the *C. burnetii* intracellular niche.

Overall, the research carried out in this thesis has worked towards elucidating the contribution of TFEB and TFE3 to *C. burnetii* infection and developing an understanding of the molecular players in this process. Significant tool development and foundational findings reported here will pave the way to a deeper understanding of the interplay between intracellular bacterial pathogens and the host response to infection. Additionally, using *C. burnetii* effector proteins as a novel biological toolbox may uncover important insights that will impact our understanding of a range of human molecular pathways that impact human health.

Table of contents

List of Figures

List of Tables

Declaration

This is to certify that:

i. The thesis comprises only my original work towards the degree of Doctor of Philosophy except where indicated in the preface,

ii. Due acknowledgement has been made in the text to all other material used,

iii. The thesis is less than 100,000 words in length, exclusive of tables, maps, bibliographies, and appendices.

Bhavna Padmanabhan
Department of Microbiology and Immunology
The University of Melbourne, Australia
June 2020

Acknowledgements

Firstly, I would like to thank my wonderful supervisor Dr. Hayley J Newton who gave me an opportunity to pursue research in her fantastic lab. She showed great patience, understanding, and provided insightful guidance to help me through the difficulties. Her enthusiasm, passion, leadership skills and dedication for science is truly admirable and inspiring. It has been a great pleasure to work with you. Thank you also for organising memorable annual dinner with your family.

I would also like to express my gratitude to my co-supervisor Dr. Patrice Newton for her support, scientific inputs and also for organising fun events in the lab. Chen Ai Khoo is acknowledged for making my initial journey into the lab comfortable and who has equally amazed us all with her skillfulness.

It has been a real pleasure getting to know and working with some fantastic and cool colleagues in the Newton lab, both past and present. I am extremely thankful to each one of their friendship, and enormous support during the last four years. In the team, I would like to acknowledge, Eleanor, Miku, Laura, Yilin, Nicole, Robson, Yi Wei, Dave, and Cameron.

My Ph.D. committee members Prof. Jason M Mackenzie, Dr. Nichollas E Scott, Dr. Abderrahman Hachani, and Dr. Jaclyn S Pearson are acknowledged for their valuable time during the committee meetings, insightful discussions, and scientific advice and for being supportive. Dr. Nichollas E Scott is acknowledged for his help and valuable suggestions during the mass spectrometry studies.

I would also like to acknowledge the Department of Microbiology and Immunology, The Peter Doherty Institute for the excellent facilities provided to us and also for organising various seminars and events. Being part of SPASIM (2017 committee) was a wonderful way to meet new people, organising various events, specially the

Annual Biennial Doherty Symposium, 2017. I would also like to thank Rebecca Whitsed, Aradhana Deoki and all DMI admin staff for their help and support.

I greatly appreciate Department of Microbiology and Immunology, Faculty of Medicine, Dentistry and Health Science, The University of Melbourne for providing me the postgraduate research scholarships and continuous support over the years.

My deepest appreciation to all my non-academic and academic friends, who supported me in my bad times and laughed with me in my good. I cannot thank you all enough as you guys made the pillars of my Ph.D., who directly or indirectly helped me complete my research work. I would like to thank my cousin and her family for making me a part of their family and for being there for me. Faculty and friends at the Department of Microbiology and Cell Biology, Indian Institute of Science, Bangalore, India for all the training and for being supportive.

Finally, I would like to thank all my family members and friends for their love, support and for having faith and for putting up with me for this long being this far.

Publication arising from this thesis

1) <u>Padmanabhan B</u>, Fielden LF, Hachani A, Newton P, Thomas DR, Cho HJ, Khoo CA, Stojanovski D, Roy CR, Scott NE, and Newton HJ (2019).

Biogenesis of the spacious *Coxiella*-containing vacuole depends on host transcription factors TFEB and TFE3. *Infection and Immunity.*

Published December 9, 2019. https://www.ncbi.nlm.nih.gov/pubmed/31818957

PMID: 31818957

Preface

In accordance with the regulations of The University of Melbourne, I acknowledge that some of the work presented in this thesis was collaborative. Specifically:

1) **Chapter three:** Biogenesis of the spacious *Coxiella*-containing vacuole depends on host transcription factors TFEB and TFE3. *Infection and Immunity.*
Padmanabhan B, Fielden LF, Hachani A, Newton P, Thomas DR, Cho HJ, Khoo CA, Stojanovski D, Roy CR, Scott NE, and Newton HJ (2019). PMID: 31818957

Co-authors on the manuscript included in Chapter 3 made important contributions to the study as outlined on page 77.

2) Chapter four: Screen to identify *C. burnetii* effectors that induces nuclear translocation of TFEB was performed with the help of Chen Ai Khoo, who was also involved in the generation of plasmids that was used in this study.

3) Chapter five: Knock-out generation was performed with the help of Chen Ai Khoo.

The remainder of this thesis comprises only my original work.

Chapter One

Introduction

1.1 Historical perspective

Coxiella burnetii is a Gram negative, obligate intracellular bacterium and the causative agent of human Q fever [1, 2]. *C. burnetii* is a short (0.3-1.0 µm) rod shaped bacterium. It was first described in 1937 by the physician, Edward Holbrook Derrick, in abattoir workers in Brisbane, Queensland, Australia [3, 4]. The infection was initially named Query fever, as the source of the illness was unknown.

To recapitulate the disease and prove it was caused by an infectious agent, Derrick, in collaboration with Frank Macfarlane Burnett and Mavis Freeman, injected guinea pigs with the patient blood and reproduced the clinical signs of illness including an enlarged spleen. Samples from these guinea pigs were examined, and the researchers reported organisms that appeared to be “rickettsial-like” organisms but failed to agglutinate when mixed with sera from patients infected with *Rickettsia typhi* [4].

At around the same time, Gordon Davis and Harold Rae Cox isolated an unfamiliar agent from ticks found in the Rocky Mountains, Montana, USA [5]. This isolated organism named Nine Mile agent displayed both bacterial and viral properties, was filterable but was unable to grow axenically. In due course, the Q fever and Nine Mile agent was discovered to be the same organism [6]. Subsequent phylogenetic analysis, based primarily on 16S ribosomal RNA sequencing, showed that *C. burnetii* is more closely related to the order *Legionellales* and is distant from the genus *Rickettsia* [7]. The agent of Q fever was named in honour of the two prominent scientists Harold Cox and Sir MacFarlane Burnet in 1948 [8].

1.2 Transmission and Epidemiology

C. burnetii is a zoonotic organism and can be found within a large variety of animals including reptiles, birds, ticks and mammals [9]. The most common animal reservoir for human infection are ruminants such as sheep, goats, and cattle [10]. These animals appear to be mostly asymptomatic [2]. However, infection during pregnancy can cause spontaneous abortion. When this happens very large numbers of *C. burnetii* are released into the environment. *C. burnetii* is shed into the environment during delivery, with as many as 10^9 bacteria per gram of placenta released during birthing [2, 11]. Not only is this devastating for contaminated farms, but it poses a large risk to public health because these bacteria can be transmitted to humans through inhalation of contaminated aerosols [12]. Human infection has also been associated with consumption of unpasteurised dairy products although this route of transmission is far less common [13]. Direct transmission between humans is very rare and only a few incidents have been reported [14].

The pathogen might also be found in soil, dust, environmental products that are contaminated and carried by wind and dispersed over longer distances [15]. A single inhaled organism has the capacity to elicit clinical infections [16]. The organism is resistant to various physical and chemical stressors and can survive in the environment for several years [17, 18]. The pathogen's low infectious dose, environmental stability and aerosol-mediated transmission makes *C. burnetii* one of the most infectious intracellular pathogen known thus leading to the characterisation of *C. burnetii* as a Category B biothreat agent by the U.S. Centers for Disease Control and Prevention [19-22].

1.3 Epidemiological profile of Q fever

C. burnetii has a global distribution as observed by several recent Q fever outbreaks in the Netherlands, Australia and Chile [23, 24]. It is endemic worldwide with the exception of New Zealand, where negative results were obtained by serological surveys on ruminants from this region [25-30]. In fact, during 1990-1991 in New Zealand, sera from 2,181 aborting cattle and 12,566 sheepdogs tested seronegative for Q fever. There have been no reports of Q fever in Antarctica either [31]. The disease in most cases is endemic, however sporadic outbreaks have been reported leading to epidemics.

The biggest Q fever outbreak to date occurred in the Netherlands between 2007 and 2010 [32]. During this period, more than 4000 confirmed human cases were reported, and the outbreak was linked to dairy goat farms. Amongst the affected population, 14 humans, with severe underlying disease conditions, died from the infection [2, 33] . To control further spread of the disease, more than 50,000 pregnant goats in 400 infected dairy farms were culled [34]. The total cost for containing this Q fever epidemic was estimated to be around 300 million Euro [35]. Implementation of control measures such as use of appropriate personal protective equipment, culling of infected animals and immunisation of abattoir workers has further reduced the number of Q fever cases reported in the Netherlands [36]. Over the last 36 years, Australia has had several outbreaks, with the first one being 110 abattoir workers being affected in 1979 [37-45]. Between 2012-2014, a Q fever outbreak was linked to a goat dairy farm in Victoria, Australia where there were 18 confirmed cases (17 employees and 1 family member) [38]. A recent news report discussed how drought conditions can increase the risk of Q fever in certain parts of

Australia as it can spread through dust and dirt, livestock's, pets and even through kangaroo faeces [46]. Such outbreaks demonstrate that Q fever is a major economic, agricultural, and public health concern worldwide and there is a pressing requirement for proper biological tools and therapeutic interventions to counter this potential biological threat.

1.4 Query fever

Symptoms of infection can appear within two weeks of one's exposure to *C. burnetii* [2]. The clinical presentation of the disease is quite varied including influenza-like symptoms such as high fever, hepatitis, pneumonia, malaise, headache, and myalgia [47]. The bacteria flourish primarily in the lungs and can invade the bloodstream and disseminate into heart valves, liver and even bones resulting in chronic illness such as hepatitis or endocarditis with severe mortality [47]. In 1 – 5 % of cases, the generally self-limiting acute disease can develop into chronic Q fever [2, 48, 49]. Interestingly, a recent study demonstrated an association between chronic Q fever and the auto-immune disease anti-neutrophil cytoplasmic autoantibody (ANCA)-associated vasculitis (AAV) [50].

The US CDC recommends PCR and serological tests for *C. burnetii* diagnosis, as the clinical signs of Q fever are indistinguishable from other febrile illnesses including influenza [13]. One of the major drawbacks of serodiagnosis is that there is a lag in the production of the antibody and only works later in infection and not at the initial onset of the infection [51]. Hence, real-time PCR based diagnosis is recommended to detect DNA of *C. burnetii* from serum samples [51, 52]. The fatality rate of Q fever is 2% and the

immune system becomes severely compromised due to *C. burnetii* infection thereby increasing the chances of other infections as well [13]. Continued follow up of individuals diagnosed with Q fever during the outbreak in the Netherlands has demonstrated that one third of the infected individuals were still having long-term health problems two years post-diagnosis [53].

1.5 Treatment

The acute phase of Q fever lasts for 1 to 2 weeks and is treatable using antibiotics such as third generation cephalosporins and tetracycline [54, 55]. Treatment with doxycycline or tetracycline is known to reduce the symptomatic duration of the infection [56]. In case of acute Q fever, a two-week treatment using doxycycline is recommended. A combination treatment of doxycycline and hydroxychloroquine for 18-24 months has been shown to significantly reduce the treatment time in the case of chronic Q fever infections compared to a two week course of doxycycline used for the treatment of acute Q fever [13, 55, 57]. This combinatorial treatment has been shown to reduce the *in vivo* acidity, thus maintaining the potency of doxycycline [58]. Treatment using these antimicrobial agents can have significant side-effects, so even with treatment, this infection has a significant impact on the individual's quality of life [57]. Antimicrobial resistance is not commonly reported and is not yet a significant problem for this infection [58].

Q–VAX , the only commercially available Q fever vaccine, is a purified suspension of formalin-inactivated *C. burnetii* containing the phase I Heinzerling strain (Q-Vax®; CSL Limited, Melbourne, Australia) that is licensed for use only in Australia [59]. Phase I whole-

cell vaccines have been shown to be highly antigenic [60]. The vaccine is recommended to those who are at high risk of *C. burnetii* infection such as farm workers, abattoir workers and others exposed to animals or animal products. The vaccine is considered 98% effective with protection lasting for 5 years. A caveat associated with this vaccine is the pre-requisite of skin testing prior to immunization. The two-step screening process involves identifying Q fever antibodies and conducting an intradermal skin test using diluted vaccine [61]. The screening process is crucial as adverse side-effects were observed in individuals with pre-existing immunity [40, 62, 63].

1.6 Axenic growth

C. burnetii is acidophilic and in nature it requires the acidic confines of the lysosome-derived replicative vacuole for replication [64, 65]. Until recently, this pathogen was considered an obligate intracellular bacterium, propagated only in eukaryotic host-cells. The challenge to cultivate *C. burnetii* axenically (host cell-free) in the laboratory imposes several experimental constraints, and this hindered research into this pathogen [2]. A series of important studies, characterising gene expression [66] and metabolic requirements of *C. burnetii* [67] provided the basis for the landmark development of axenic culture conditions [68]. The 2009 report of a complex axenic nutrient rich media that mimics the intracellular replicative niche of *C. burnetii*, ACCM (Acidified Citrate Cysteine Medium), made it possible to propagate this pathogen *in vitro* enabling the study of its genetics and molecular pathogenesis [69]. ACCM allows for approximately a 3 log increase in *C. burnetii* after 6 days of growth at 37 °C with 5% CO_2 and 2.5% O_2 [69]. Further, advancement of ACCM semisolid agar has enabled the isolation of single

isolated colonies of *C. burnetii* [70]. ACCM-2, a second-generation acidified citrate cysteine medium, was developed in 2011 facilitating increased viability and replication of *C. burnetii* [71]. ACCM-D, a nutritionally defined medium with defined amino-acid concentrations was recently developed, providing greater flexibility and the capacity to examine nutritional requirements of *C. burnetii* [72]. Development of axenic cultures has facilitated the ability to genetically manipulate the pathogen which in turn has allowed the identification of factors required for *C. burnetii* virulence, physiology and has also helped in gaining insights into the *C. burnetii* regulatory network [69].

1.7 *Coxiella burnetii*: The genome

The first complete genome sequence of *C. burnetii* Nine Mile (NM) phase I RSA493 strain was published in 2003 [73]. Over the last couple of years, many more genomes have been sequenced [74]. A comparative analysis of five sequenced *C. burnetii* genomes estimated the size of the genome to be approximately 2.1 Mb ranging from 1.5 to 2.4 Mb and encoding for approximately 2100 open reading frames (ORFs) with approximately 35% (746) of these genes having no known functions. Overall, *C. burnetii* has a guanine-cytosine content of 42.6% and is most closely related to the order *Legionallales* [73]. Analysis of the *C. burnetii* genome sequence revealed that the bacterium encodes for factors that have putative functions in virulence. This included genes encoding for proteins likely to be involved in adhesion, invasion, bacterial intracellular trafficking, host-cell modulation, and detoxification [73]. Every isolate of *C. burnetii* contains autonomously replicating plasmid critical for infection [75, 76]. The QpH1 plasmid from Nine Mile reference strain RSA439 is approximately 37 kb in length and bioinformatics analysis

revealed presence of Dot/Icm substrates with eukaryotic-like motifs encoded by the plasmid [75, 76]. Subsequent transfection and translocation assays using the identified substrates revealed the complete conservation of the plasmid encoded genes by the pathogen [75, 76].

1.8 Genetic modification of *C. burnetii*

The inability to apply traditional genetic manipulation tools to *C. burnetii*, due to its obligate intracellular nature, was overcome with the development of axenic culture media. Genetic transformation of *C. burnetii* was first achieved in 1996 by using a *C. burnetii* - *E. coli* shuttle vector, pSKO(+)1000, a construct produced by cloning a 5.8 kb *C. burnetii* autonomous replication sequence into the *E. coli* cloning vector pBluescript that has a β-lactamase gene (*blaM*) conferring ampicillin resistance [77]. *C. burnetii* was further transformed in 2009 using the *mariner*-based *Himar1* transposon (Tn) system [78]. This research was the first report of a mutant in *C. burnetii* [78]. The mutant disrupted *ftsZ* and it demonstrated that mutants could be generated without the use of axenic culture media [78]. In 2012, a targeted gene deletion and inactivation approach was established that made targeted gene deletion possible in *C. burnetii* [79]. This two-step “loop-in/loop-out” gene deletion involves chromosomal integration of the upstream and downstream regions of the gene of interest along with a counterselection marker, as the first step. The second step involves a second recombination event resulting in the removal of the target gene [79]. Deletion of the gene occurs when the plasmid cointegrant is resolved during the second cross-over event which occurs in the presence of sucrose that leads to loss of the plasmid because it encodes *sacB* [79]. In addition to traditional genetic manipulation

technique which involves homologous recombination, two large scale transposon mutagenesis screens have been reported that identified *C. burnetii* factors essential for intracellular replication and CCV biogenesis [80, 81].

1.9 Morphological forms of *C. burnetii*

Much like several intracellular bacterial pathogens, *C. burnetii* has two morphologically distinct forms with a bi-phasic developmental life cycle [35-37]. The small cell variants (SCVs) are highly infectious, metabolically inert, endospore-like cells that are resistant to harsh environmental conditions [82]. SCVs, 0.2 to 0.5 µm in size, are characterized by condensed chromatin and can survive outside of the host for several years while still being infectious [83]. The capacity to form these resistant SCVs contribute to the epidemiology of the outbreaks. Once the soil of a farm is contaminated with SCVs, it is very hard to eradicate the pathogen from the environment. Upon internalisation and traffic to the lysosome, an SCV develops into a metabolically active and replicative large cell variant (LCV) form [84]. LCVs, greater than 0.5 µm in size, have a typical Gram-negative looking envelope and dispersed chromatin [85]. LCVs replicate to large numbers within the intracellular niche [86]. The replication of *C. burnetii* within the lysosomal environment takes place for approximately 6 days, post which the LCV form differentiates back to SCVs [84]. Interestingly it has been shown that the alternative sigma factor RpoS acts as a central regulator of developmental cycle in *C. burnetii* playing a crucial role in intracellular replication and reversion to SCV [87]. Transcriptome profiling of *C. burnetii* to identify genes contributing to the morphological transition, revealed a unique profile for

SCVs containing a peptidoglycan modification contributing towards its environmental stability [85].

1.10 Biogenesis and maturation of the *Coxiella*-containing vacuole

The *C. burnetii* SCV, following aerosol transmission, passively enters host phagocytic cells, predominantly alveolar macrophages, by actin-dependent phagocytosis [83].
C. burnetii can also enter non-phagocytic cells through a less defined mechanism that appears to be mediated by the outer membrane protein OmpA [88]. Regardless of the mechanism of entry, *C. burnetii* containing phagosomes undergo the same fate within mammalian cells. Endocytic maturation and delivery of ingested material to the lysosome is an intrinsic mechanism to destroy microbes however *C. burnetii* is able to withstand the bactericidal environment of the lysosome [84, 89].

Five minutes after internalization, the bacterium resides in a nascent phagosome which matures through the endosomal cascade (Figure 1.1). The *C. burnetii* containing phagosome acquires early endosomal markers, such as RAB5 and EEA1 (Early Endosome Antigen 1), followed by RAB7, a marker of late endosomes/lysosomes and the vacuolar ATPase (vATPase) [42]. vATPase pumps protons into the phagosomal lumen, driving the pH from 5.4 to 5 [90]. In comparison to phagosomes containing latex beads that acquires lysosomal markers within five minutes of uptake, lysosomal fusion is delayed by 2 hours resulting in an acidic compartment called a *Coxiella*-containing vacuole (CCV) [42, 44, 45].

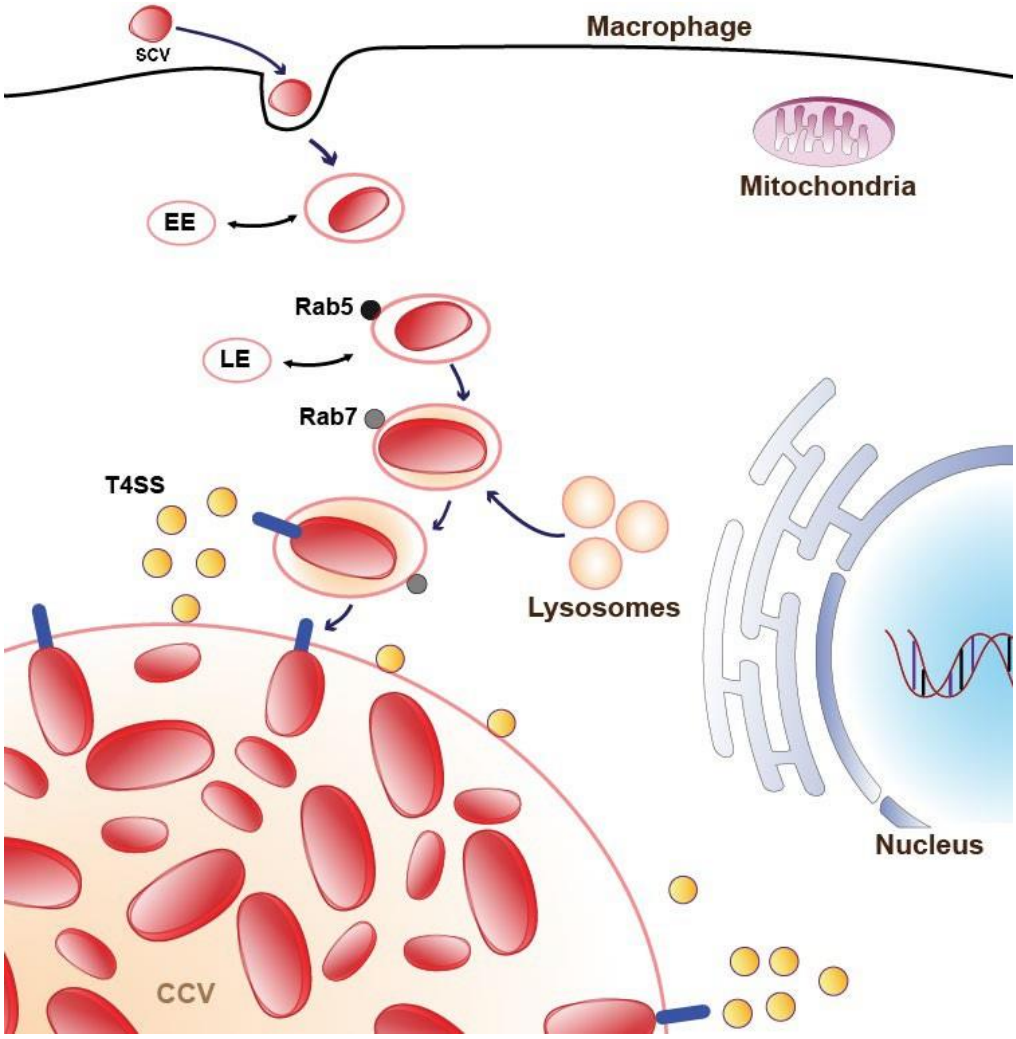

Figure 1.1 Biogenesis of the *Coxiella*-containing vacuole.

The SCV of *C. burnetii* gets internalised by a macrophage via phagocytosis. The newly formed phagosome will passively traffic through the host endocytic pathway, interacting with the early endosomes (EE) and late endosomes (LE) and eventually the lysosome. The acidic environment of the lysosome triggers *C. burnetii* to become metabolically active. *C. burnetii* utilises its type IV secretion system (T4SS), to inject effector proteins into host-cell cytoplasm to remodel the host cellular environment to facilitate intracellular replication. Due to the extreme fusogenicity of the mature *Coxiella*-containing vacuole (CCV), it grows to occupy most of the cytoplasmic space.

The vacuolar pH further reduces to 4.5 when the CCV fuses with lysosomes and it acquires lysosomal markers such as acid phosphatases, hydrolases, and Cathepsin D [42]. Once the bacteria reach the acidic environment, they become metabolically active and direct the remodeling of the CCV. The acidic luminal lysosomal environment induces the transition of *C. burnetii* SCVs to the metabolically active and replicative LCV form [84]. During this transition, a shift in virulence is observed and the CCV is modified by the pathogen to support bacterial replication [86]. Towards the end of the replicative cycle, CCVs contain a mixture of LCVs and SCVs [91]. Transformation of LCVs to SCVs occurs around 6 days post infection. Surprisingly, the host cell viability is not affected by this morphological transition as evident by the induction of pro-survival factors and inhibition of apoptotic signaling pathways [92, 93].

The mechanism by which *C. burnetii* survives the acidic confines of the CCV is poorly defined. In comparison to other medically important group of pathogens, the *C. burnetii* genome encodes mostly basic proteins having a pI of 8.25 [73]. This helps the pathogen in buffering the acidic confines of the CCV, thus helping it to flourish [94]. Bioinformatic analysis has also identified four Na^+/ K^+ exchangers and transporters for osmoprotectants that may help in combating oxidative and osmotic stress within the phagolysosome-like vacuole [73]. It was recently demonstrated that the mature CCV has a pH of ~5.2, higher than the pH of lysosomes, ~4.8 [94]. In this study, forcing further acidification of CCVs to pH ~4.8 resulted in bacterial lysis suggesting active regulation of the CCV pH by *C. burnetii* [94].

A genome-wide screen was performed to identify the host factors required for *C. burnetii* intracellular replication by using small interfering RNA (siRNA) [95]. This screen identified *STX17* (Syntaxin 17), a host factor required for the fusion of autophagosomes with lysosomes. Silencing expression of *STX17*, resulted in a robust multi-vacuolar phenotype and prevented the progression of autophagy [95]. Aside from Syntaxin 17, this study also showed an important role for the retromer complex, that is involved in the transmembrane receptor recycling from endosomes to the trans-Golgi network. This study also showed an interesting association between defects in the translocation of T4SS effectors resulting from silencing the host factors required for intracellular replication [95] .

1.11 Molecular pathogenesis of *C. burnetii*

1.11.1 Lipopolysaccharide phase variation

Lipopolysaccharides (LPS) are a class of macromolecules representing the main surface antigen of most Gram-negative bacteria and play an important role in host-pathogen interaction [96]. The LPS acts as a barrier to detergents, antibiotics and various proteins from the host [97]. The membrane composition of *C. burnetii* resembles that of several Gram-negative bacteria and there are surface, biochemical and structural differences between the two antigenic forms, virulent phase I and the avirulent phase II [98]. Phase I, isolated from sources of infection such as laboratory infected animals or naturally infected humans, has a complete LPS (containing full-length O-polysaccharide) and is highly infectious [99]. Phase II, lacks the capacity to synthesize O-antigen polysaccharide due to a spontaneous chromosomal deletion, or mutation, that leads to formation of

truncated LPS (lacks the O-polysaccharide) [21, 99, 100]. *C. burnetii* phase II is highly attenuated within *in vivo* models of infection [21, 99, 101]. LPS was thus the first virulence factor to be identified for *C. burnetii*.

This phase variation occurs spontaneously during serial passage of *C. burnetii* in cells or embryonated chicken eggs [99, 102]. The chromosomal deletion of the O - antigen polysaccharide of the well-characterised Nine Mile strain, makes it impossible for the phase II cells to revert to Phase I [99]. This non-pathogenic or avirulent NM phase II strain, RSA439, is indistinguishable from the virulent Phase I, RSA493, strain in tissue culture cell lines and is a safer laboratory model [103].

1.11.2 The role of secretion systems in *C. burnetii* pathogenesis

Bioinformatics analysis of the *C. burnetii* genome revealed the pathogen encodes for three secretion systems, namely, a type I secretion system (T1SS) [22], a type 2 secretion system (T2SS)-related pilus biogenesis machinery [104] and a type 4 secretion system (T4SS) [105]. The type I secretion system apparatus comprises of a specific outer membrane protein (OMP), an ABC (ATP-binding cassette transporter) protein and a membrane fusion protein (MFP). The *C. burnetii tolC* gene encodes for a protein that is homologous to the T1SS outer membrane channel protein. Function of TolC in *C. burnetii* is unknown, but it could possibly be involved in virulence and multidrug efflux as it is homologous to the well characterised *L. pneumophila* TolC [106-108]. In *L. pneumophila*, TolC is an essential protein required for the bacterial survival within the protistan host *Paramecium tetraurelia* [108]. Though *C. burnetii* is devoid of the archetypal model of the

type II secretion system, it encodes several genes that are homologous to the type IV pili assembly [109]. This suggests a functional similarity of the components of the secretion systems and evolutionary similarity [109].

The first whole-genome sequence of *C. burnetii*, identified a genetic locus encoding for a complete Type IVB Secretion System (T4SS) [73]. The T4SS is a multiprotein apparatus found in some proteobacteria that facilitates transport of effector molecules across bacterial and host cell membranes. It is ancestrally related to the conjugation Type IVA secretion system (T4ASS). The sequence analysis of *C. burnetii* RSA493 phase I strain presented major progress into the understanding of the pathogenesis and biology of this bacterial pathogen [73]. The sequencing also revealed a high degree of similarity to Dot/Icm T4SS of *L. pneumophila* [73]. The genome of *C. burnetii* encodes 25 *dot/icm* genes that were shown to be functionally analogous to *L. pneumophila* Dot/Icm components through complementation of *L. pneumophila* mutants with the respective *C. burnetii* genes [73, 110-112]. Bacterial DNA transfer has been well reported by the Dot/Icm T4SS of both *L. pneumophila and C. burnetii* [113, 114]. The Dot/Icm T4SS was originally shown to be essential for intracellular replication and survival of *L. pneumophila* by two independent research groups, thus leading to the dual naming of the system as Dot/Icm (defective organelle trafficking (Dot) and intracellular multiplication (Icm)) [115, 116]. A large number of subsequent studies have identified over 300 *L. pneumophila* proteins that are translocated through this apparatus, across the two bacterial membranes and the vacuole membrane to reach the host cell cytoplasm [117]. These bacterial effector proteins act to remodel the environment and create a replicative niche

for the pathogen [118, 119]. Dot-Icm-deficient *L. pneumophila* cannot replicate intracellularly and are destroyed by the host cell lysosome, as such this T4SS is considered an essential virulence factor *for L. pneumophila* [120].

Interestingly, the transposon mutant disrupting *icmL* first demonstrated that this T4SS is essential for intracellular replication of *C. burnetii* [121]. A further study by Beare et al in 2011, showed the requirement of T4SS apparatus for the formation of vacuoles within human macrophages [122]. The study illustrated the T4SS effectors being able to induce genetic complementation one day after infection [122]. Unlike *L. pneumophila*, the *C. burnetii dot/icm* mutants are not rapidly destroyed by the host cell. This surprising observation indicates that there are Dot/Icm independent traits of *C. burnetii* that allow it to survive in the lysosomal environment [122] (Figure 1.2).

L. pneumophila and *C. burnetii* are evolutionarily related and are also the only two human pathogens known to utilize the Dot/Icm Type IV Secretion System. *Piscirickettsia salmonis*, a fish bacterial pathogen, is also known to possesses the T4SS for achieving productive infection. [111, 123, 124]. *P. salmonis* utilises the T4SS to inhibit the phagosome-lysosome fusion in order to survive [125]. Given the ease with which *L. pneumophila* can be genetically manipulated in the laboratory, initial screening strategies for *C. burnetii* T4SS effectors involved using *L. pneumophila* as a surrogate model [121]. In an attempt to identify new effectors, random *C. burnetii* genomic DNA fragments were transcriptionally fused to an adenylate cyclase reporter and screened for the capacity to be translocated into the eukaryotic host cell. This screen led to

identification of new effectors that had no homology to the T4SS effectors from *L. pneumophila*.

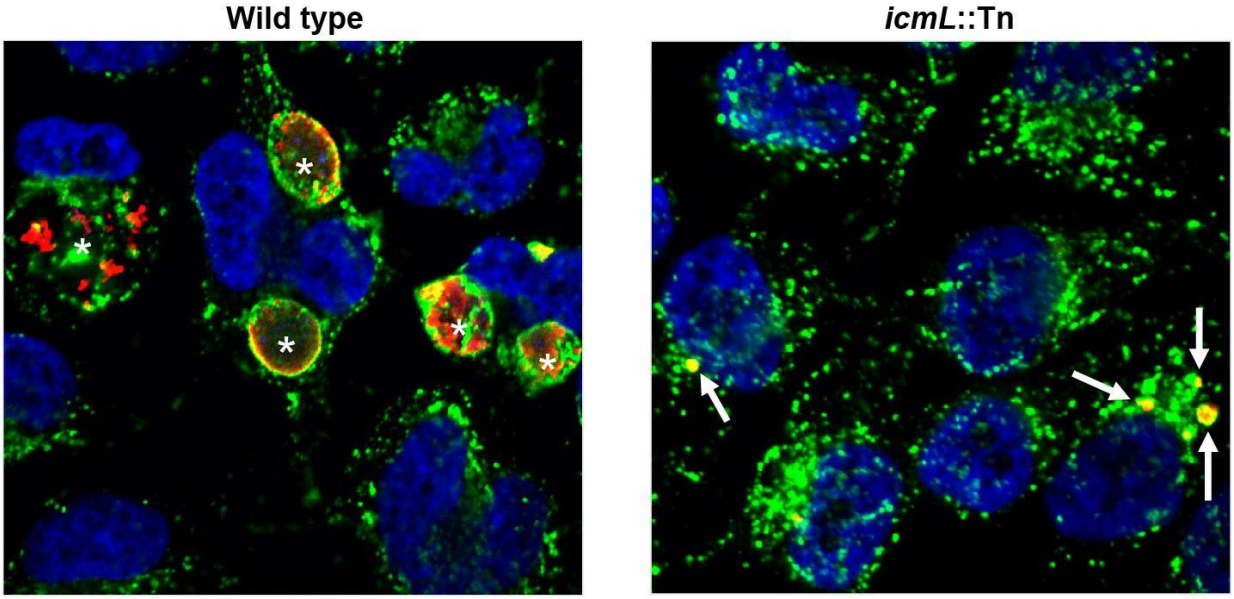

Figure 1.2 The importance of the *C. burnetii* Dot/Icm Type IV Secretion System for intracellular replication.

Human epithelial cells, infected with either wild type or *icmL*::Tn mutant for 3 days and stained with LAMP1, a lysosomal marker, *C. burnetii* (red) and nuclei stained using DAPI. In comparison to the wild type *C. burnetii*, disruption of the Dot/Icm type IV secretion system leads to no replication of the *icmL*::Tn mutant strain in the host cells. Through this secretion system, *C. burnetii* translocates approximately 150 effectors into the host cell.

* indicates CCV. Arrows indicate *icmL*::Tn mutant.

Despite both of these pathogens being dependent on the Dot/Icm T4SS for intracellular success, they establish very different intracellular replicative niches, where *C. burnetii* thrives within the acidic phagolysosome, *L. pneumophila* resides in a vacuole derived from the host endoplasmic reticulum (ER) [117]. Therefore, it makes sense that they activate their secretion systems at different times. *L. pneumophila* needs to rapidly remodel the phagosome to avoid endocytic fusion while *C. burnetii* only needs to start remodeling the vacuole once it is residing in a lysosome. These different intracellular niches reflect the need to modulate different host processes and therefore infer that they possess very different cohorts of effector proteins that target different host pathways [115, 116, 121].

1.11.3 Transcriptional regulation of the Dot/Icm system

Reporter assays have been used to probe the dynamics of effector translocation for both *L. pneumophila* and *C. burnetii.* Interestingly, *L. pneumophila* activates effector translocation as soon as it contacts a host cell [126]. In contrast, *C. burnetii* effector translocation is significantly delayed, with detection several hours post-infection [81, 121, 127]. Further investigation has shown that this reflects the Dot/Icm system being transcriptionally and functionally activated only once the bacteria reach the lysosomal environment [127]. A study by Newton et al., demonstrated the use of a reporter system consisting of a β-lactamase enzyme (BlaM) fused to *C. burnetii* effector proteins to study protein translocation of specific T4SS effectors. This study showed that translocation of Dot/Icm effector proteins required acidification and maturation of the CCV [127].

During *C. burnetii* infection, the transcription of the genes that encode for apparatus components of the T4SS is regulated by the PmrA/B two-component system [128, 129]. This two-component system is essential for intracellular replication as disruption of either gene leads to non-replicating bacteria [81, 130]. Transcriptional comparisons between WT and a *pmrA* mutant demonstrated that a subset of the T4SS effector proteins are also transcriptionally controlled by this system [130]. It was recently demonstrated that the *C. burnetii* PmrA/B TCS is activated by certain amino acids present in the lysosomes [131].

1.11.4 Dot/Icm effector identification

To date, approximately 150 effector proteins of *C. burnetii* have been identified, however the vast majority have not been functionally characterised. Several strategies have been employed to identify *C. burnetii* effectors including bioinformatic approaches, presence of a Dot/Icm C-terminal translocation signal, identification of eukaryotic-like domains, sequence similarity to known substrates, and presence of PmrA regulatory motifs encoded upstream of the candidate effector gene [121, 129, 130, 132, 133]. In a large-scale bioinformatic study by Chen et al in 2014, potential *C. burnetii* substrates were identified through *L. pneumophila* as a surrogate host [129]. Thus *C. burnetii* T4SS effectors that had paralogs to *L. pneumophila* substrates, harboring eukaryotic-like motifs, E-block motifs or containing PmrA recognition sites were identified [134, 135].

There are two commonly used reporter assays that allow demonstration of effector translocation. Both of these approaches rely on production of a fusion protein between

an enzyme that is selectively active in the host cytosol and the putative effector of interest [136, 137]. The commonly used reporter to examine effector translocation into mammalian cells is the calmodulin-activated adenylate cyclase, CyaA from *Bordetella pertussis*. After being translocated into the host cell by the Dot/Icm system, the Cya protein binds to calmodulin and converts adenosine triphosphate (ATP) to cyclic adenosine monophosphate (cAMP) which can then be quantified using an enzyme-linked immunosorbent assay [136-138]. The TEM-1 β-lactamase (BlaM) fluorescence-based system is another reporter system which provides both visual and quantitative means to measure translocation of *C. burnetii* effector proteins [136, 137].

The gene of interest is fused to TEM-1 β-lactamase (BlaM) on a reporter plasmid that provides constitutive expression. 24 hr post-infection, cells are loaded with the membrane permeable BlaM substrate that contains two fluorophores, coumarin and fluorescein moiety (Figure 1.3) [136, 137]. When there is no translocation of the effector, excitation at 410 nm results in a green fluorescence signal (520 nm) [136, 137]. If the BlaM-fusion protein is translocated into the host cell, the β-lactamase activity of the fusion protein will cleave the BlaM substrate, resulting in FRET disruption and a blue fluorescence signal (450 nm) after excitation at 410 nm [136, 137]. Both the green and blue fluorescence signals can be detected either visually or using a fluorescence plate reader to quantify effector translocation. [136, 137].

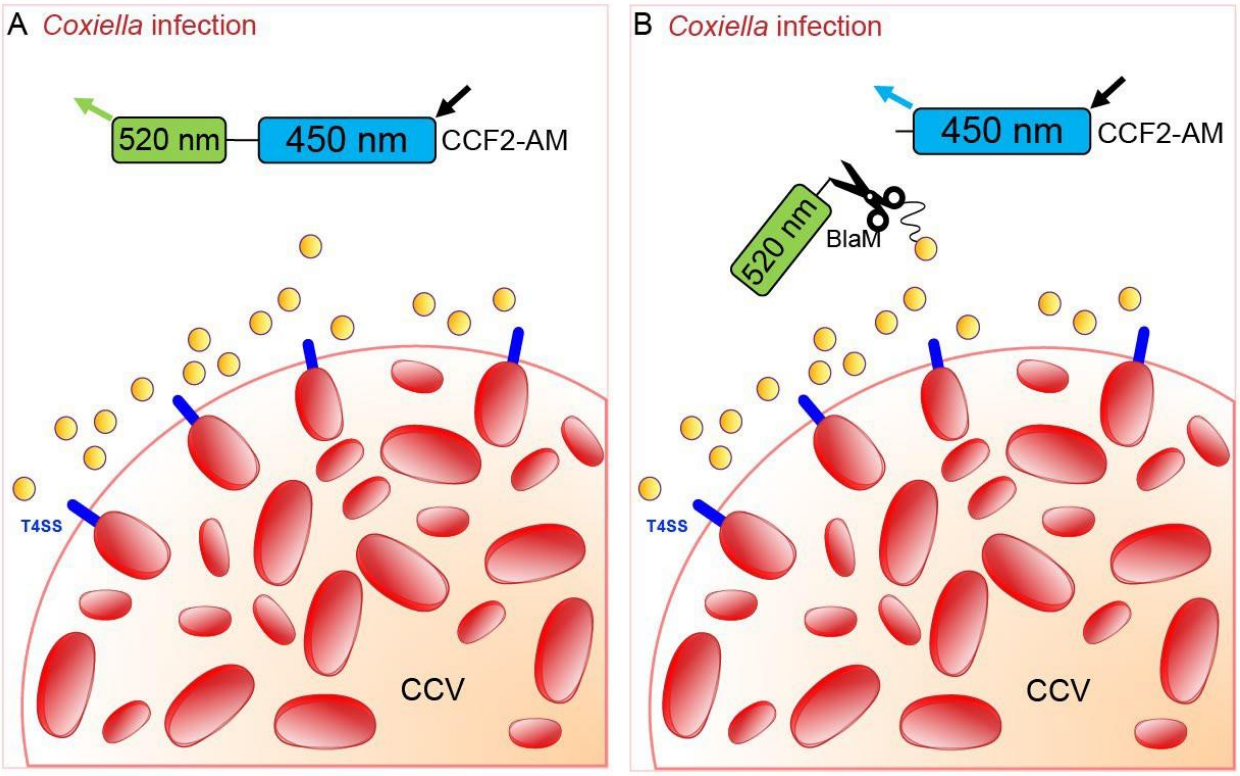

Figure 1.3 Mechanism of β-lactamase assay for quantifying *C. burnetii* host cell fusion

During *C. burnetii* infection, (A) in a translocation negative scenario, no translocation of the fusion protein results in FRET to fluorescein, observed as a green fluorescence signal (520 nm) upon excitation at 410 nm (B) In translocation positive scenario, the β-lactamase activity results in the cleavage of CCF2-AM resulting in a change in fluorescence profile. Excitation at 410 nm results in a blue fluorescence signal (450 nm) due to FRET disruption. BlaM is accessible to the cytoplasmic CCF2-AM substrate. CCF2-AM forms a FRET (fluorescence resonance energy transfer) pair as it is labelled with two fluorophores. A fluorescence plate reader detects both the green and blue fluorescence signal.

The initial screening strategies for *C. burnetii* T4SS effectors involved using *L. pneumophila* as a surrogate host [121]. Dot/Icm-dependent translocation of a few Ankyrin Repeat Homology Domain containing proteins from *C. burnetii* was demonstrated using the CyaA translocation assay in *L. pneumophila* [139]. As most T4SS effectors harbor a translocation signal at the carboxy terminal region of the protein, an unbiased screen was carried out to identify novel *C. burnetii* T4SS proteins effective in being able to deliver into the host cytosol using the Cya reporter. The Dot/Icm system was shown to be important, but specific translocation of any of the identified effectors was not demonstrated to be important for *C. burnetii* intracellular replication [121]. A bacterial two hybrid screen was undertaken to identify *C. burnetii* T4SS substrates interacting with DotF, a component of the T4SS apparatus. Thus identifying 25 ORFs that were further investigated for their ability to translocate into the host-cell via a *L. pneumophila* based Cya translocation assay [129].

1.11.5 Characterisation of *C. burnetii* Dot/Icm effectors

Most of the *C. burnetii* effectors that have been identified remain functionally undefined. However, some broad approaches have been undertaken to glean functional information about these novel proteins. A simple approach, that has been applied to nearly all predicted *C. burnetii* effectors, is to examine the subcellular localisation of ectopically expressed effectors in mammalian cells. This has identified many effectors that demonstrate specific localisation to different eukaryotic compartments including the nucleus, mitochondria, endoplasmic reticulum, and the Golgi apparatus [121, 132, 140]. This information may point to these effectors contributing to the host-pathogen interaction

at these specific subcellular compartments. However, investigation of the mitochondrial effector MceA has demonstrated that localisation of ectopically expressed protein can be deceiving [141]. Earlier studies demonstrated that ectopically expressed ^{3xFLAG}MceA (CBU0077) co-localised with LAMP1 indicating a likely lysosomal membrane localisation [142]. However, it was later shown that ^{3xFLAG}MceA, expressed and translocated by *C. burnetii*, very specifically localises to the mitochondrial outer membrane during *C. burnetii* infection [141].

Effector localisation at the ER or Golgi may indicate that these proteins interfere with protein or vesicular trafficking. For example, ectopically expressed CBU0635 localises to the Golgi and was demonstrated to cause a defect in exocytosis of SEAP (secreted alkaline phosphatase), suggesting that this effector might interfere with the exocytic pathway [121]. CBU1556 (CvpC), CBU1825 and CBUA0019 are the other effectors known to disrupt membrane trafficking by interfering with the host secretory pathway as demonstrated by SEAP activity [132].

Some effectors have been shown to localise to the nucleus where they may act to manipulate host DNA and/or influence host transcription [132]. Ectopically expressed CBU1314 localises to the nucleus and is known to associate with the host chromatin [143]. With the help of powerful techniques such as Chromatin Immunoprecipitation (ChIP) and deep sequencing, host genes associated with CBU1314 were identified. These host factors play important roles in cell signaling, modulation of host transcription and immune response [143]. Yet another subset of *C. burnetii* Dot/Icm effectors localise

to the CCV and are therefore named *Coxiella* vacuolar proteins (CvpA to CvpF) [144, 145]. The effector protein CvpA associates with host clathrin and subverts clathrin-mediated endocytosis, by physically interacting with AP-2, thus facilitating *C. burnetii* replication [146]. Deletions of each of these Cvp effectors has been shown to have an impact on intracellular replication of *C. burnetii* and CCV biogenesis suggesting localisation of multiple effectors to the CCV membrane promotes bacterial replication [144].

Several transposon mutagenesis screens have been conducted to identify genes that are important for the biogenesis of the CCV. CirA (*Coxiella* effector for intracellular replication) is a T4SS effector that stimulates the activity of the host Rho GTPases to promote CCV biogenesis implying its importance in the pathogenesis of *C. burnetii* [147]. Another screen to identify effectors required for the biogenesis of the CCV revealed the novel effector Cig57 as being required for optimal intracellular replication of *C. burnetii*. The transposon screen also identified another effector Cig2 (also known as CvpB) to be important for the homotypic fusion of CCV, thus revealing its requirement for the biogenesis of CCV [81]. Cig57 was also recently shown to co-opt clathrin-mediated trafficking by interacting with the clathrin-coated pit accessory protein FCHO2 [148]. Both Cig57 and CvpA mutants have intracellular replication defects, which means they act in non-redundant ways to recruit clathrin to the CCV membrane.

An independent study using transposon insertion sequencing technology (INSeq) identified *C. burnetii* effector mutants having deficiencies in the CCV biogenesis [80].

Together this recent body of research demonstrates that many of the *C. burnetii* effectors act in non-redundant ways to facilitate biogenesis of the CCV and intracellular replication of *C. burnetii*. This is in stark contrast to what has long been observed for the large *L. pneumophila* effector cohort where very few individual effectors have a measurable impact on intracellular replication of the pathogen.

Another study which showed that the Dot/Icm apparatus is essential for translocation of effectors in to host cell showed the successful use of transposons to disrupt the Dot/Icm system [121]. Martinez et al identified CBU1260 (OmpA) as having a role in bacterial entry of non-phagocytic cells using a high-content phenotypic transposon-mutagenesis screen. It was observed that transposon insertion disrupting *ompA* resulted in an entry defect [88]. It was also shown that OmpA mediates internalization of *C. burnetii*, and this was shown by the ability of beads coated with OmpA to enter non-phagocytic Vero cells [88].

1.11.5.1 Anti-apoptotic effectors

It is not surprising that some *C. burnetii* effectors interfere with cell death pathways to keep the host cell alive. Preventing host cell death is essential for the replication of the slow growing pathogen and for the maintenance of the large CCV. Ectopic expression of AnkG, CaeA and CaeB (*C. burnetii* anti-apoptotic effector) demonstrates that they all possess strong anti-apoptotic activity [139, 142, 149]. To inhibit pathogen-induced apoptosis, AnkG binds the host cell mitochondrial protein p32 [93, 150]. The protein appears to traffic from mitochondria into the nucleus, where the anti-apoptotic activity occurs. AnkG is also known to traffic to the nucleus through interaction with importins and

this interaction requires its anti-apoptotic activity [150, 151]. CaeB has an efficient anti-apoptotic activity and inhibits apoptosis at the mitochondria [152].

In comparison, CaeA has a weaker anti-apoptotic activity and there is limited data for the molecular mechanism of this CaeA-dependent block of cell death [142, 152]. In mammalian cells, the effector protein CaeA was shown to localise to the nucleus and was found to contain 2 nuclear localisation signals (NLS) [151]. CaeA expression also resulted in the up-regulation of an inhibitor of activated-caspase, survivin, a protein known to prevent apoptotic cell death [149]. When CaeA sequence from 25 different *C. burnetii* isolates was compared, a genetically variable EK (glutamic acid/lysine) repetition motif was identified that was essential for the anti-apoptotic activity [149]. To date there has been no mutant characterisation to determine the role of these proteins during infection and hence it is unclear whether they are functionally redundant or act at different times to keep the eukaryotic host alive. IcaA is another T4SS effector identified which when expressed, inhibits caspase-11 activation in primary mouse macrophages [153]. *C. burnetii icaA*$^{-}$ mutants failed to suppress inflammasome activation mediated by *L. pneumophila* infection [153]. It was thus demonstrated that *C. burnetii* inhibits the non-canonical activation of the NLRP3 inflammasome [153].

1.11.5.2 Effectors that influence vesicular trafficking

Host cell vesicular trafficking pathways are crucial for *C. burnetii* as they contribute to formation of the fusogenic CCV. This intracellular bacterial pathogen manipulates lysosomes, endosomes and autophagosomes via Dot/Icm T4SS effector proteins.

Endocytosis is a highly regulated and fundamental cellular process that occurs from the internalisation of plasma membrane and protein, and its organisation to distinct membrane-bound intracellular compartment. Clathrin-mediated endocytosis or receptor-mediated endocytosis is one of the mechanisms that is moderated by the protein complex clathrin. Clathrin heavy chain was identified to be enriched on the CCV and was shown to be important for *C. burnetii* intracellular replication and CCV biogenesis through autophagosome-vacuole fusion [146].

To date two T4SS effectors have been shown to interact with components of the clathrin trafficking machinery. CvpA (CBU0655) was identified as an effector that localises to clathrin-coated vesicles, the CCV and endosomes and interacts with AP-2 components [146]. Cig57 is another effector of *C. burnetii* that mediates vesicular trafficking by interacting with the endocytosis nucleator FCHO2 (FCH And Mu Domain Containing Endocytic Adaptor 2) [148]. Deletion of either of these effectors has a significant impact on the ability of *C. burnetii* to replicate intracellularly, demonstrating the importance of commandeering this trafficking pathway [81].

There is no role for clathrin during internalisation of *C. burnetii*. Latomanski and Newton, 2018, demonstrated the importance of clathrin heavy chain for interaction of CCV and autophagic vesicles [154]. Silencing expression of clathrin heavy chain results in the formation of CCVs unable to fuse with each other, a phenotype also observed when autophagy is blocked [154]. Absence of clathrin also resulted in the loss of LC3B from the CCVs [154]. Autophagosomes contributing to the formation and expansion of CCVs was

also shown to be dependent on clathrin in this study [154]. Thus the CCV was demonstrated as an important tool to provide a functional link between autophagy and clathrin [154].

1.12 Roles of host autophagy in CCV biogenesis

Autophagy/macroautophagy is a degradative cellular process that is activated as a host response to amino acid starvation and other stresses such as infections [155]. In the process, lipids, cellular proteins and other organelles are targeted to lysosomes for degradation [156]. Lysosomal destruction of autophagosomal contents facilitates maintenance of cellular homeostasis. Having multiple roles in innate immunity, autophagy is directly involved in removal of pathogens via 'xenophagy' [157].

Many intracellular bacterial pathogens such as *Mycobacterium tuberculosis*, *L. pneumophila*, *Shigella flexneri*, *Listeria monocytogenes*, *Streptococcus pyogens* and *Salmonella typhimurium* senses autophagic machinery as a cellular response during infection [158]. In canonical autophagy, p62 (sequestosome-1), an autophagy receptor and NDP52 (a 52 kDa nuclear dot protein) act as cytoplasmic sensors, binding LC3 and ubiquitinated substrates targeting bacteria for degradation. *M. tuberculosis* is known to replicate within macrophages by evading macroautophagy [159]. Likewise, the fate of *Listeria monocytogenes* is also controlled by canonical autophagy [160]. On the contrary, few bacteria such as *C. burnetii* and *Salmonella enterica* subsp. *enterica* serovar Typhimurum can survive within the autophagosome-like structure generated by non-canonical autophagy [81, 161, 162]. Several effectors of *L. pneumophila* act to facilitate

the pathogen evasion of autophagosomes and have been shown to block autophagy [162-165]. The *L. pneumophila* effector protein RavZ inhibits autophagy on the autophagosomal membrane by catalysing the irreversible delipidation of LC3 by cleavage of the amino terminal conjugation site thus blocking the progression of autophagosomes [162, 163].

Autophagy is an innate, cell autonomous antibacterial mechanism, and fascinatingly, *C. burnetii* is the only bacterial pathogen known to positively regulate autophagy for its efficient replication within the host cell [166, 167]. LC3 is a marker for autophagy. LC3-I (cytosolic form of LC3) is conjugated to phosphatidylethanolamine to form LC3-phosphatidylethanolamine conjugate LC3-II. LC3-I is found in the cytoplasm and LC3-II is present in the autophagosomal membrane compartments [168]. LC3-I to II conversion is an indication that there is autophagy induction [169]. A study indicated a defect in the intracellular replication of *C. burnetii* when autophagy was blocked using 3-MA (3-Methyl Adenine, a PI3K autophagy inhibitor) or wortmannin, another autophagy inhibitor [170].

Under normal conditions, when multiple *C. burnetii* infect the same cell, only one replicative CCV is formed due to the fusion of CCVs. The T4SS effector Cig2 has been identified as being important for the fusogenic properties of the CCV as mutation of the gene encoding Cig2 leads to a multi-CCV phenotype [81]. Interestingly, this phenotype is also observed during silencing of genes involved in autophagy [81]. This indicates that *C. burnetii* subverts the host autophagic pathway to promote homotypic fusion of CCVs and influences the maturation of the CCV [81, 171]. Subsequent functional analysis of

Cig2 demonstrated that this effector contributes to the CCV biogenesis by interacting with phosphoinositide's on the host cell membrane and manipulating phosphatidylinositol 3-phosphate [PI (3)P] metabolism [172]. As such Cig2 was demonstrated to maintain the CCV in an autolysosomal state of maturation. Interestingly, using the *Galleria mellonella* model of *C. burnetii* infection demonstrated that loss of Cig2 appears to increase the host tolerance to infection [171]. Taken together this data demonstrates the importance of autophagy in the biogenesis of the CCV and subsequent infection outcome [169].

1.13 Mammalian control of lysosome biogenesis and autophagy

The degradative pathway, both endocytic and autophagic, is a highly dynamic system and plays an important role in eukaryotic cell adaptation to nutrient availability and defense against microbes. Defects in this pathway have been linked to lysosomal storage disorders and several neurodegenerative diseases [173]. It has also recently been demonstrated that a lysosome-to-nucleus signaling pathway helps in adapting to changes in nutrient availability through transcriptional control of autophagy and lysosome biogenesis [174]. Promoter analysis of several lysosomal genes revealed the binding site of the basic-helix-loop-helix/leucine zipper transcription factor (bHLH-LZ) which comprises of a 10-base pair motif (5'-GTCACGTGAC-3') located within 200 bp of the transcription start site [175, 176]. This has subsequently been classified as the **C**oordinated **L**ysosomal **E**xpression **A**nd **R**egulation (CLEAR) network. The CLEAR element consists of a E-box (CANNTG), recognised by the microphthalmia transcription factor (MiTF/TFE) subfamily, a basic helix-loop-helix (bHLH) leucine-zipper family of transcription factors [177]. In humans, the MiTF/TFE family is comprised of four different

transcription factors, namely TFEB, TFE3, MiTF and TFEC [178]. TFEB and TFE3 have been found to be expressed in various cell types. MITF is primarily expressed in macrophages, mast cells, B cells, NK cells, mast cells, osteoclasts, and cardiomyocytes [179]. The role of TFEC is not very well defined, however it was found to be predominantly expressed in myelogenous cells [179].

Transcription **F**actor **EB** (TFEB) was identified to be involved in the regulation of lysosomal biogenesis through control of the CLEAR network [180]. ChIP-seq data confirmed the direct binding of TFEB to CLEAR elements thus identifying it as the first master regulator of lysosomal biogenesis [181, 182]. TFEB also binds to the promoters of approximately 400 genes implicated in lysosome-related processes, such as phagocytosis, endocytosis and autophagy [181, 183, 184]. TFEB is normally localised at the lysosomal membrane but mobilises into the nucleus under starvation conditions or when lysosomal function is compromised [185-187]. TFEB nuclear localisation is initiated in response to nutrient deprivation, stimulating translocation to the nucleus where it forms homo-or heterooligomers with other members of the microphthalmia transcription factor (MiTF) subfamily resulting in upregulated expression of genes involved in autophagy and lysosome biogenesis [188].

Recent reports have shown the role of Transcription Factor Binding To IGHM Enhancer 3 (TFE3) in autophagy and that, similar to TFEB, it also regulates the expression of lysosomal genes by binding to CLEAR elements [189]. TFE3 plays an independent role in promoting the expression of lysosomal genes as observed in TFEB-depleted cells and

this is not dependent on TFEB [189]. Both TFEB and TFE3 induces the expression of a small subset of autophagy genes [183, 189, 190].

A more recent study has demonstrated that TFEB and TFE3 bind overlapping sets of promoters and both transcriptionally regulate expression of autophagic and lysosomal genes, thus functioning in a similar mechanism [191]. Nuclear translocation of these transcription factors is controlled by the mammalian target of rapamycin (mTOR) complex 1 [174, 192, 193]. During stress or starvation conditions, mTORC1 dissociates from the lysosomal calcium transporter Mucolipin-1 (MCOLN1) at the lysosomal membrane and is inactivated (Figure 1.4).

Simultaneously, calcium is transported from the lysosome to cytoplasm via MCOLN1 leading to activation of the phosphatase calcineurin [194]. Activated calcineurin dephosphorylates TFEB/TFE3 facilitating nuclear translocation and subsequent influence on transcription and human cell function. During normal growth conditions, TFEB is phosphorylated at Ser122, Ser142 and Ser211 and TFE3 at Ser321 in a mTORC1-dependent manner. [188, 195] (Figure 1.4). Phosphorylation promotes association of TFEB/TFE3 with 14-3-3 family proteins and retention in the cytosol [188]. Inhibition of mTORC1 induces dephosphorylation of TFEB/TFE3 by calcineurin resulting in dissociation of the TFEB/TFE3/14-3-3 complex, and rapid transport of TFEB/TFE3 to the nucleus where it increases transcription of CLEAR network genes [188].

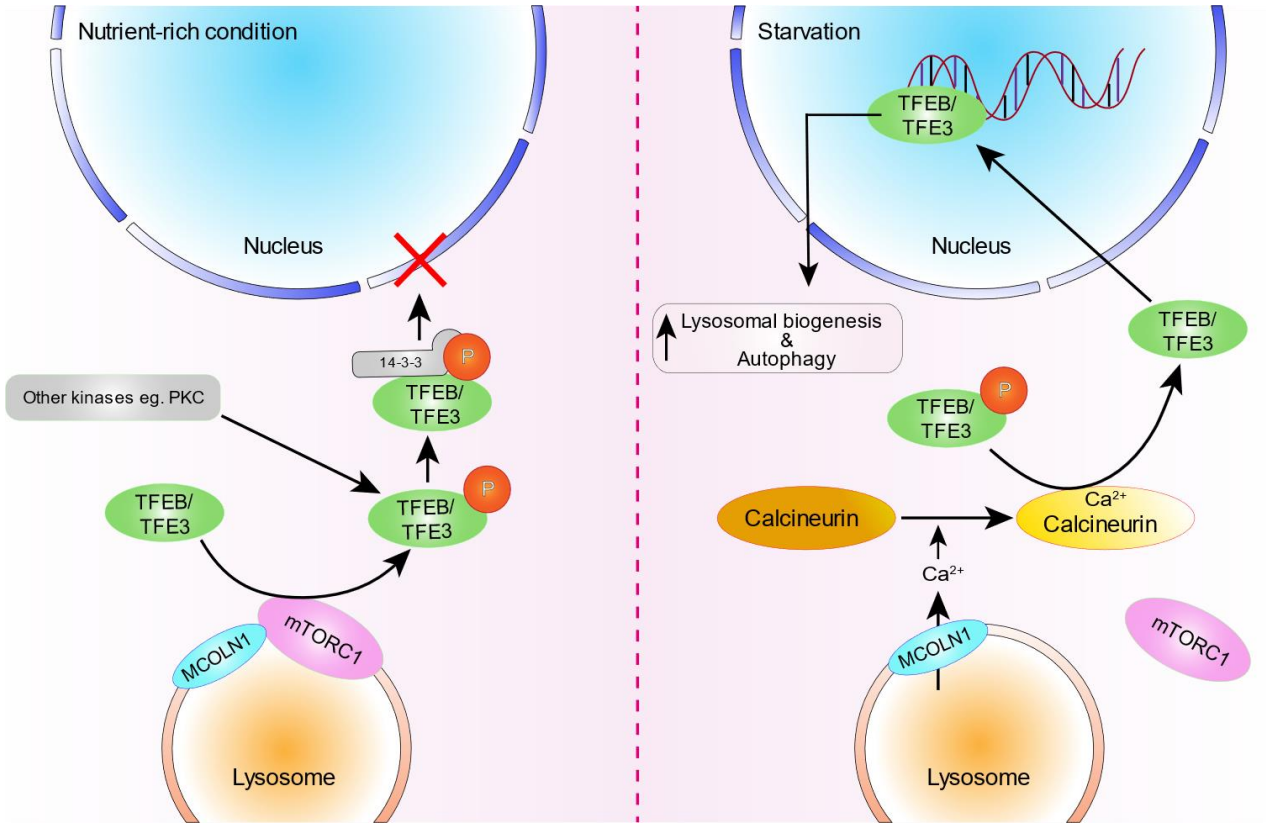

Figure 1.4 Control of TFEB/TFE3 activation

The lysosome-nuclear signaling axis controls lysosome biogenesis and autophagy in response to nutrient availability. Under healthy nutrient-rich conditions (left panel), active mTORC1 promotes the retention of TFEB/TFE3 in the cytosol by phosphorylation that facilitates interaction with 14-3-3 proteins. In contrast, under starvation conditions (right panel), Ca^{2+} is released from the lysosome via MCOLN1 activating phosphatase calcineurin. Activated Ca^{2+} calcineurin complex dephosphorylates TFEB/TFE3 mediating rapid translocation of TFEB/TFE3 into the nucleus thereby inducing increased production of proteins involved in lysosomal biogenesis and autophagy.

TFEB is also known to be phosphorylated by ERK2, a mitogen activated protein kinase 1 (MAPK1), which is part of the MAPK/ERK signaling pathway. ERK2 acts as a regulator for TFEB subcellular localisation by phosphorylation of TFEB at Ser142 site [181]. Evidence of ER stress resulting in TFEB/TFE3 nuclear translocation has also been defined [196]. This is shown to be mediated by the double-stranded RNA activated protein kinase (PRR) – like ER kinase (PERK) [188].

The transcriptional regulator of lysosomal biogenesis and autophagy, TFEB has been shown to play several roles in the host-pathogen interactions during a range of infections [183]. For example, it has been demonstrated that infection of macrophages with HIV results in an autophagic response through TLR8 (Human Toll-like receptor 8) and Beclin-1 (BECN1) dependent dephosphorylation of TFEB resulting in nuclear activation of TFEB [197]. This, transient autophagy activation is critical for viral replication. However, continued autophagy leads to viral degradation hence, upon establishment of HIV infection autophagy is inhibited [198]. This happens when Nef1, an anti-autophagic maturation factor activates MTORC1 through its interaction with BECN1 resulting in TFEB phosphorylation and cytosolic retention [188]. Thus, HIV infection modulates autophagy, through TFEB, in a temporal manner to promote replication and survival within the host.

The insect-borne and protozoan parasite *Trypanosoma cruzi*, the causative agent of Chagas disease, utilises the surface glycoprotein gp82, to induce inactivation of mTOR, thus inducing nuclear translocation of TFEB and increased host lysosomal biogenesis [190]. This leads to the accumulation of lysosomes near the edges of the host cells and

results in entry of the parasite into the host cell [191, 192]. Thus, TFEB enhances the host cell invasion of this protozoan parasite.

M. tuberculosis has been shown to modify TFEB by downregulating its expression, and replicate within a Mycobacterium phagosomal compartment, suggesting there are less lysosomes and the bacteria are less likely to be degraded [183]. This is achieved by the production of specific micro RNAs, *Mir33,* and *Mir33**, that directly target several genes involved in autophagy and lysosomal biogenesis. These specific micro RNAs also reduces TFEB mRNA levels through AMP-activated protein kinase (AMPK) [189]. Thus, by repressing autophagy, *Mir33,* and *Mir33** promote intracellular replication of *M. tuberculosis.*

The Gram-negative opportunistic bacterial pathogen, *Acinetobacter baumannii*, which is mostly associated with hospital-acquired infections, requires TFEB for bacterial pathogenesis. This was demonstrated by infection of human lung epithelial cells with *A. baumannii* leading to the activation of TFEB. Further, silencing of TFEB led to a decrease in *A. baumannii* internalisation in A549 cells [193]. Additional examples of TFEB modulation by bacterial pathogens was demonstrated by *Salmonella enterica,* serovar Typhimurium (*S*. Typhimurium) and *Staphylococcus aureus*. It was observed that the evolutionarily conserved phospholipase C - Phospho Kinase D (PLC-PKD) pathway, was indispensable for activation of TFEB in *Caenorhabditis elegans* infected with *S*. Typhimurium and mouse macrophages infected with *S. aureus* [199]. A theoretical model has been established in which mouse macrophages infected with *S*. Typhimurium

activate Gαq, a family of heteromeric G protein alpha subunit known to activate G protein signalling pathway [199]. The activation of Gαq is most likely via an unidentified G-protein-coupled receptor Gαq which activates PLC [199]. PLC activates PKD by generating diacylglycerol (DAG) that is in turn required for the activation of TFEB [199]. Thus, by enhancing the function of lysosomes, TFEB can in turn increase the capacity of macrophages to clear intracellular bacterial pathogen. This shows the positive regulation of TFEB during infection dependent on the evolutionarily conserved PLC-PKD pathway. These examples demonstrate that this host process can be either beneficial or detrimental to different pathogen. Some pathogens can control the autophagy-lysosome signaling axis to its advantage, but other pathogens can be cleared through the action of TFEB.

The potential role of TFEB/TFE3 activation is increased cellular clearance of foreign materials. This is extremely crucial for human health since defects in lysosomal biogenesis and autophagy has been associated with diseases such as lysosomal storage disorders (LSD), neurodegenerative diseases, and even in many cancers [185, 200]. A recent study using animal models for neurodegenerative diseases have demonstrated the role of lysosomal-autophagic pathway and its impact on LSD and common neurodegenerative diseases [201]. It was observed that, in mouse models of Parkinson's disease, pharmacological and genetic activation of TFEB/TFE3 helps block disease progression [202].

1.14 Thesis aims

The zoonotic disease agent *C. burnetii* causes human Q fever by invading and replicating within host alveolar macrophages. *C. burnetii* unlike other bacterial pathogens survive and replicates within a bacterially modified lysosome. Given the autolysosomal nature and significant size of the CCV, we hypothesised an increase in the expression of genes involved in lysosomal biogenesis during *C. burnetii* infection. Therefore, we wanted to understand whether the transcription factors, TFEB and TFE3 that regulate the expression of lysosomal biogenesis and autophagy, contributed to the pathogenesis of *C. burnetii*.

The specific aims of the thesis were:

1) Chapter 3 aimed at understanding the host and pathogen interactions of *C. burnetii*. To examine changes to the host proteome during infection of THP-1 cells, a SILAC based proteomics approach was undertaken. The role of host transcription factors TFEB and TFE3 was analysed. Further, the host transcription factors TFEB and TFE3 were silenced either individually or together to study the impact of gene function on the intracellular replication of *C. burnetii* and biogenesis of CCV.

2) Chapter 4 aimed to identify *C. burnetii* effector proteins that modulate TFEB. For this, an immunofluorescence screen was undertaken, where examination of the impact of 151 putative *C. burnetii* T4SS effector proteins resulted in the identification of CBU1701 and CBU2016 as capable of inducing nuclear localisation of TFEB. In order to understand the

role of these proteins in the nuclear localisation of TFEB, cell lines with inducible expression of ^{3xFLAG}CBU1701 and ^{3xFLAG}CBU2016 were generated and a whole cell proteomic analysis was undertaken.

3) The final results chapter aimed at understanding the importance of these effector proteins in the intracellular replication of *C. burnetii*. For this, mutant strains of *cbu1701* and *cbu2016* were generated and initial characterisation of the role of these proteins during infection was carried out.

Chapter 2

Materials and Methods

2.1 Chemicals and reagents

The chemicals and reagents used in this study were purchased from Sigma-Aldrich (MO, USA), Merck (Darmstadt, Germany), Chem Supply (Australia) or Amresco (OH, USA), Bio - Strategy Pty Ltd (Australia) unless specified. Antibiotics were acquired from Sigma-Aldrich, or Boehringer Ingelheim (Germany) and tissue culture media components were obtained from Thermo Fisher Scientific Australia Pty Ltd.

2.2 Bacterial strains

The bacterial strains used in this study are listed in Table 2. 1**.**

2.2.1 Culturing condition for *Escherichia coli*

All *E. coli* strains were cultivated at 37 °C in Luria-Bertani (LB) medium (Appendix), supplemented with ampicillin (100 µg/mL), kanamycin (50 µg/mL), chloramphenicol (25 µg/mL) or tetracycline (125 µg/mL) when necessary. The liquid cultures were cultivated at 37 °C with agitation unless otherwise stated. LB was either liquid or supplemented with 1.5% agar to account for plate cultivation.

2.2.2 Cultivation of *Coxiella burnetii*

C. burnetii Nine Mile Phase II, strain RSA439, clone 4 and the derivative strains were cultured axenically in acidified citrate cysteine media 2 (ACCM-2) (Appendix) [71] [70]. The cultivation that required the use of arginine biosynthesis selection were carried out in

ACCM-D dropout [72], lacking arginine supplemented with 0.75 mM citrulline at 37 °C with 5% CO_2 and 2.5% O_2 for 7 days. When required, chloramphenicol and/or kanamycin were added to ACCM-2 or ACCM-D lacking arginine at 3 µg/mL and 375 µg/mL, respectively.

Table 2. 1 Lists of bacterial strains used in this study.

Bacterial Strain	Description of the strain	Reference
***E. coli* DH5α**	*supE44 DlacU169 (f80 lacZDM15) hsdR17 recA1 endA1 gyrA96thi-relA1*	Clontech
***C. burnetii* Nine Mile Phase II RSA439 (NMII)**	Plaque purified *C. burnetii* Nine Mile phase II (NMII), strain RSA439 clone 4. Referred to throughout as wildtype (WT)	Ted Hackstadt, NIH, USA
***C. burnetii* expressing mCherry**	*C. burnetii* transposon mutant where the mCherry encoding transposon has inserted into an intergenic region allowing detection of *C. burnetii* fluorescence in infected HeLa cells.	[127]
***C. burnetii icmL::*Tn**	Transposon interrupted *icmL* in WT *C. burnetii*	[121]
***C. burnetii cbu1701::*Tn**	Transposon interrupted *cbu1701*	This study, [81]

C. burnetii Δcbu2016	WT *C. burnetii* strain with *cbu2016* replaced with Kan^R cassette controlled by a *C. burnetii* constitutive promoter 1169^P	This study
***C. burnetii Δcbu2016 cbu1701*::Tn**	*cbu1701*::Tn with deletion of *cbu2016*	This study

2.3 Molecular Biology Techniques

2.3.1 Recombinant DNA techniques

Plasmids used in this study are listed in Table 2. 2

Table 2. 2 Plasmids used in this study.

Name	Description	Antibiotic selection	Reference
pcDNA4/TO-3×FLAG (pFLAG)	Mammalian expression vector encoding a 3×FLAG epitope upstream of a multiple cloning site (MCS)	Amp	Clontech, Roy Laboratory, Yale University, [121]
pFLAG-cbu1701	pFLAG with full-length *cbu1701* cloned into *Bam*HI and *Eco*RI restriction sites for eukaryotic expression	Amp	This study

pFLAG-cbu1701$^{1-159}$	pFLAG with *cbu1701* N-terminal region cloned into *Bam*HI and *Eco*RI restriction sites for eukaryotic expression	Amp	This study
pFLAG-cbu2016	pFLAG with full-length *cbu2016* cloned into *Bam*HI and *Eco*RI restriction sites for eukaryotic expression	Amp	This study
pJB-CAT-BlaM	*C. burnetii* expression vector for constitutive expression of BlaM	Cm	[79]
pJB-CAT-BlaM-MceA	pJB-CAT-BlaM-MceA used as a positive control for translocation assay	Cm	[121, 127]
pJB-CAT-BlaM-*cbu1701*	*cbu1701* cloned into *Sal*I sites of pJB-CAT-BlaM to create a transcriptional fusion of BlaM and *cbu1701*	Cm	This study
pJB-CAT-BlaM-*cbu1701*$^{435-468}$	*cbu1701*$^{435-468}$ cloned into *Sal*I sites of pJB-CAT-BlaM to create a transcriptional fusion of BlaM and *cbu1701*$^{435-468}$	Cm	This study

pFTRE_3G_puro	Empty vector for lentiviral stable cell line production	Amp	A gift from John Silke's laboratory, WEHI
pCMV-VSV-G	Plasmid encoding for envelope protein for lentiviral production and MuLV retroviral particle. To be used in conjunction with a packaging plasmid such as pCMV-dR8.2 dvpr	Amp	Plasmid # 8454, Addgene
pCMV-dR8.2 dvpr	Plasmid for 2nd generation lentiviral packaging. To be used in conjunction with pCMV-VSV-G	Amp	Plasmid # 8455, Addgene,
pFTRE-3G-$^{3\times FLAG}$ *cbu1701*	*cbu1701* cloned into *Bam*HI restriction enzyme site of pFTRE-3G vector to be used for lentiviral stable cell line production	Amp	This study
pFTRE-3G-$^{3\times FLAG}$ *cbu1701*	*cbu2016* cloned into *Bam*HI restriction enzyme site	Amp	This study

	pFTRE-3G vector to be used for lentiviral stable cell line production		
pJC-CAT	Suicide vector for *C. burnetii* gene deletion encoding for *sacB*	Cm	[79]
pJC-CAT:: *cbu2016*-5'3'-Kan	Approximately 2000 bp upstream (U) and downstream (D) of *cbu2016* cloned into *Bam*HI and *Sal*I sites of pJC-CAT. Kan cassette cloned into *Not*I site between the two inserts.	Kan and Cm	This study

2.3.1.1 Oligonucleotides

Oligonucleotides used in this study are listed in Table 2. 3.

Restriction endonucleases sites in the oligonucleotides are underlined. Oligonucleotides were used at a 10 µM working concentration and synthesised commercially by Sigma-Aldrich.

Table 2. 3 Oligonucleotides used in this study.

#	Oligonucleotide F - forward and R – reverse	Sequence details (5'-3') *restriction enzyme sites are underlined	Reference
1	F for pcDNA4/TO-^{3xFLAG}CBU1701. *Bam*HI	GACGGATCCATGCATCGCAACTTAGAAGA	This study
2	R for pcDNA4/TO-^{3xFLAG}CBU1701. *Eco*RI	GACGAATTCCTAAGGATCAAGTAAAGGGG	This study
3	F for pcDNA4/TO-^{3xFLAG}CBU2016. *Bam*HI	AAGGATCCATGGTGGTTATGCTAGAAGAC	This study
4	R for pcDNA4/TO-^{3xFLAG}CBU2016. *Xho*I	AACTCGAGTTAGGGATCGAAGCCGGAG	This study
5	F to amplify *cbu1701* for cloning into pJB vectors. *Sal*I	AAGTCGACATGCATCGCAACTTAGAAGAAA	This study
6	R to amplify *cbu1701* for cloning into pJB vectors. *Sal*I	AAGTCGACTTAAGGATCAAGTAAAGGGGTA	This study
7	F to amplify *cbu1701* for cloning into pFTRE. *Bgl*II	AAAGATCTATGGACTACAAAGACCATGAC	This study
8	R to amplify *cbu1701* for cloning into pFTRE. *Bgl*II	AAAGATCTTTAAGGATCAAGTAAAGGGGTA	This study

9	R to amplify *cbu2016* for cloning pFTRE. *Bgl*II. Used with #7	GCAGATCTTTAGGGATCGAAGCCGGAGGAT	This study
10	F to amplify 2000 bp upstream of *cbu2016* for cloning into pJC-CAT. *Sac*I	AAGAGCTCTCATGCTGAATAAGGACATAAGCATGT	This study
11	R to amplify 2000 bp upstream of *cbu2016* for cloning into pJC-CAT. *Not*1	GAGCTACTTAGAACAGCCGATTTTGTGCGGCCGCCCCTCGGCCTAACGTTATTCAA	This study
12	F to amplify 2000 bp downstream of *cbu2016* for cloning into pJC-CAT. *Not*1	TTGAATAACGTTAGGCCGAGGGGCGGCCGCACAAAATCGGCTGTTCTAAGTAGCTC	This study
13	R to amplify 2000 bp downstream of *cbu2016* for cloning into pJC-CAT. *Sal*I	AAGTCGACGTAGATTCGCTCCATGACCATCA	This study
14	F 2100 bp upstream of *cbu2016* for knock out mutant screening	TAAGAACAGTCTTATTTATGTTTACGCG	This study
15	R 2100 bp downstream of *cbu2016* for knock out mutant screening	ATTTCGACACCATATTCCGCTAACT	This study
16	5' outfiring primer for Kan^R cassette, to confirm	CGGACAGGTCGGTCTTGACAAAA	This study

	replacement of *cbu2016* with Kan^R cassette in *Δcbu2016* derivatives		
17	3' outfiring primer for Kan^R cassette, to confirm replacement of *cbu2016* with Kan^R cassette in *Δcbu2016* derivatives	GATGGAAGCCGGTCTTGTCGAT	This study
18	F *cbu2016* gene-specific to confirm knockout.	AAGAATTCATGGTGGTTATGCTA GAAGACGAAA	This study
19	R *cbu2016* gene-specific to confirm knockout.	AAGGATCCTTAGGGATCGAAGCC GGAGGATT	This study
20	F *cbu1701* gene-specific to confirm transposon mutant.	GACGGATCCATGCATCGCAACTT AGAAGA	This study
21	R *cbu1701* gene-specific to confirm transposon mutant.	GACGAATTCCTAAGGATCAAGTA AAGGGG	This study
22	F *ompA*-specific qPCR quantification of *C. burnetii* genome equivalents	CAGAGCCGGGAGTCAAGCT	[203]
23	R *ompA*-specific qPCR quantification of *C. burnetii* genome equivalents	CTGAGTAGGAGATTTGAATCGC	[203]
24	F for TPP1 qRT-PCR	GATCCCAGCTCTCCTCAATACG	[204]

25	R for TPP1 qRT-PCR	GCCATTTTTGCACCGTGTG	[204]
26	F for LAMP1 qRT-PCR	ACGTTACAGCGTCCAGCTCAT	[204]
27	R for LAMP1 qRT-PCR	TCTTTGGAGCTCGCATTGG	[204]
28	F for CTSF qRT-PCR	ACAGAGGAGGAGTTCCGCACTA	[204]
29	R for CTSF qRT-PCR	GCTTGCTTCATCTTGTTGCCA	[204]
30	F for MCOLN1 qRT-PCR	TTGCTCTCTGCCAGCGGTACTA	[204]
31	R for MCOLN1 qRT-PCR	GCAGTCAGTAACCACCATCGGA	[204]
32	F for HOXA9 qRT-PCR	CCCCCATCGATCCCAATAA	[204]
33	R for HOXA9 qRT-PCR	CCCTGGTGAGGTACATGTTGAA	[204]
34	F for TPP1 qRT-PCR	GATCCCAGCTCTCCTCAATACG	[204]

2.3.1.2 Polymerase Chain Reaction

GeneAmp PCR system 2400 thermal cycle (Applied Biosystems, USA) or Bio-Rad T100™ Thermal Cycler (Life Science Research) machines were used to run all PCR's. Each PCR reaction of a final volume of 50 µL contained 100 ng template DNA, 0.2 µM each of forward and reverse oligonucleotides, 250 µM dNTPs, 1 µL Pfu Ultra II Fusion HS DNA Polymerase and 1X Pfu Ultra II Reaction Buffer. The reaction mix was subjected to thermal cycles as per the manufacturer's recommendation.

2.3.1.3 Colony PCR to screen for positive transformants

Colony PCR was performed following *E. coli* transformation to screen for plasmids containing the desired insert. Individual colonies were suspended in a 10 µL PCR reaction

mixture comprising of 1X GoTaq® Green Master Mix (Promega, USA) or MyTaq (Bioline, Australia) and 0.2 µM each of forward and reverse oligonucleotide. Colony PCR was carried out using conditions as per manufacturer's instructions.

2.3.1.4 Agarose Gel Electrophoresis

To separate and/or purify DNA fragments following PCR, colony PCR or restriction digestion, agarose gel electrophoresis was performed. 1% (w/v) molecular grade agarose (Bioline) was dissolved in 1X Tris acetate EDTA (TAE) buffer (Appendix) supplemented with 0.01% SYBR Safe DNA gel stain (Thermo Fisher Scientific). To allow the DNA samples to run in agarose gels, prior to loading, samples were mixed with 6X purple gel loading dye (New England BioLabs, USA) except for GoTaq® and MyTaq® PCR products. DNA electrophoresis was performed at 105 V for 35 minutes. A 1 kb DNA ladder (NEB) was used as a reference size standard alongside DNA samples. Gel Box Documentation System (Syngene, UK) was used to visualise and image DNA.

2.3.1.5 Purification of DNA from agarose gel

Following visualisation of DNA using the Safe Imager Transilluminator (Thermo Fisher). Desired DNA bands were excised from the agarose gel using a clean scalpel blade and collected into a sterile microfuge tube. ISOLATE II PCR and Gel Kit (Bioline) was used to purify DNA according to the manufacturer's protocol and DNA was eluted in 30 µL of nuclease-free water (Qiagen).

2.3.1.6 Restriction digestion and ligation of DNA fragments

Restriction enzyme digestions were performed using enzymes and buffers from NEB (Maryland, USA) and Promega, according to manufacturer's instructions. Digestion reaction mixture comprised of 1 to 20 µg of DNA, one tenth reaction volume of 10X restriction buffer and 5 to 10 units of restriction enzyme. Reactions were made up to the final volume of 30 µL with dH_2O and incubated at 37 °C for 3 hours.

Each DNA ligation mixture consisted of 1X T4 DNA Ligase buffer (New England BioLabs), 1 unit of T4 DNA Ligase (NEB), in 10 µL volume with a vector: insert DNA ratio of 1:3 or 1:5, incubated at either at room temperature for 30 minutes or at 4 °C overnight.

2.3.1.7 DNA Sequencing

300 ng of dsDNA and 1 µL of 10 µM oligonucleotide in a 15 µL reaction volume was sent to the Australian Genome Research Facility (AGRF) for sequencing and run on a capillary electrophoresis sequencing machine. Result analysis was performed using the program Sequencher (Gene Codes Corporation, USA).

2.3.2 Transformation

2.3.2.1 Chemically competent *E. coli*

For transformation, *E. coli* DH5α were made chemically competent. *E. coli* DH5α were streak diluted on a LB agar plate and incubated at 37 ºC overnight. For a starter culture, a single bacterial colony was picked and inoculated into 10 mL LB liquid medium, that

was cultivated overnight with shaking at 37 ºC. From this starter culture, 1 mL was sub-cultured into 100 mL Super Optimal Broth (SOB) (Appendix), grown overnight with agitation at 37 ºC to reach an optical density at 600 nm (OD_{600}) between 0.4-0.8 (approximately 3-4 hours). These cells were then chilled on ice for 10 minutes prior to harvesting by centrifugation at 3,220 *x g* for 15 minutes at 4 ºC. Resuspension of the cell pellet was performed in 4 mL chilled TB (transformation buffer) (Appendix) with the addition of 0.3 mL of DMSO. These competent cells were then divided into single-use 50 µL aliquots, snap-frozen in a dry ice-ethanol bath for long-term storage at – 80 ºC.

2.3.2.2 Chemical transformation of *E. coli*

Introduction of plasmids into chemically competent *E. coli* DH5α was achieved using the heat-shock method. 100-200 ng of plasmid DNA or a ligation mixture was mixed with 50 µL of chemically competent *E. coli* on ice for 30 minutes. Heat shock at 42 ºC for 60 seconds was performed, after which the cells were incubated on ice for 2 minutes prior to the recovery step. Cells were recovered by addition of 950 µL of Super Optimal broth with Catabolite repression (SOC) medium (Appendix) at 37 ºC with agitation for 1 hour. For selection of transformants, *E. coli* were plated on LB agar supplemented with appropriate antibiotics and incubated overnight at 37 ºC.

2.3.2.3 Electroporation of *C. burnetii*

Axenically cultured *C. burnetii* were transformed by electroporation of plasmid DNA as previously described [121]. In brief, 20 ml axenically grown *C. burnetii* were pelleted by

centrifugation at 3,220 *x g*, 4 °C for 15 minutes and resuspended in 10 mL ice-cold 10% glycerol. *C. burnetii* were pelleted again using the same conditions as above and resuspended in 50 µL ice-cold 10% glycerol. 10 µg of plasmid DNA was added to a pre-chilled electroporation cuvette and mixed with the bacteria that were then electroporated at 1.8 kV, 500 Ω, 25 µF for 7 to 13 milliseconds. Electroporated *C. burnetii* were resuspended in 950 µL Roswell Park Memorial Institute (RPMI) GlutaMAX™ Media (RPMI; Gibco) containing 10% fetal bovine serum (FBS; Gibco). 200 µL of the bacterial suspension was added to 3 mL ACCM-2 in a 6-well plate. Cells were recovered for 24 h at 37 °C with 5% CO_2 and 2.5% O_2 before kanamycin or chloramphenicol was added at the appropriate concentration for selection. *C. burnetii* transformants were incubated for a total of 4 days; then, 100 µL of the culture was plated on antibiotic-containing ACCM-2 agarose. A soft agarose overlay method was used to allow the cultivation of *C. burnetii* within semi-solid media. The bottom solid medium base consisted of 1% ACCM-agarose and the top layer mixed the transformed *C. burnetii* with 0.5% ACCM-agarose. 6 to 7 days post-incubation single isolated colonies were picked and expanded in liquid ACCM-2 medium under continual antibiotic selection.

2.4 Eukaryotic cell lines

HeLa human cervical epithelial cells (CCL-2; American Type Culture Collection (ATCC)), HeLa derivatives engineered to express ^{3xFLAG}CBU1701 (HeLa ^{3xFLAG}CBU1701) or ^{3xFLAG}CBU2016 (HeLa ^{3xFLAG}CBU2016), HeLa TFEB-GFP stable cells (a kind gift from Shawn Ferguson, Yale University) and HEK293T cells (human embryonic kidney 293 cells expressing the SV40 large T antigen; ATCC) were cultured in Dulbecco's Modified

Eagle's Media GlutaMAX™ (DMEM; Gibco) supplemented with 10% heat-inactivated FBS at 37 °C with 5% CO_2. THP-1 (Tamm-Horsfall Protein 1) human monocytic cells (ATCC) were cultured in RPMI supplemented with 10% heat-inactivated FBS at 37 °C with 5% CO_2. HEK293T and HeLa cells were passaged when cells reached 80 to 90% confluency. HEK293T has the tendency to detach upon reaching confluency and was gently pipetted against the side of the flasks to break clusters and obtain a single-cell-suspension before resuspending into fresh media. HeLa cells were detached from flasks with 1 ml 0.05% Trypsin-EDTA (Gibco, Life Technologies) per 75 cm^2, then resuspended with 10 volumes of DMEM + 10% FBS. THP-1 cells were gently pipetted up and down several times to ensure that clumps were dispersed and further diluted in fresh media. The best cell model to use would be human alveolar macrophage which are not easily accessible. Additionally, using primary cells precludes, or significantly complicates, the ability to genetically manipulate the host cell. Therefore, HeLa cells, which are easy to cultivate and manipulate were used

2.5 Transfection of eukaryotic cell lines

HeLa CCL2 cells were seeded at a density of 1 x 10^5 cells per well in a 24-well tissue culture tray (Corning Inc, NY, USA) containing 12 mm sterile glass coverslips. This was then incubated for 24 h at 37 °C, 5% CO_2 to obtain an adherent monolayer. Post incubation, cells were transfected with the desired plasmid DNA, using Lipofectamine 3000 (Invitrogen, Thermo Fisher Scientific, USA) for up to 16 h following the manufacturer's protocol. In brief, the reagent, P3000™ was diluted 1/25 in Opti-MEM™ (Life Technologies, Thermo Fischer Scientific) containing 250 ng plasmid DNA.

Lipofectamine 3000 was diluted 1/25 in Opti-MEM™ separately. Post incubation for 20 minutes at room temperature, the two solutions were mixed. In a dropwise manner, the combined mixture was added to the cells and mixed gently. The cells were then incubated at 37 °C, 5% CO_2 for desired time periods.

2.6 siRNA treatment of HeLa cells

For siRNA-mediated gene silencing of TFEB and TFE3 in HeLa cells, cells were reverse transfected with small-interfering RNA (siRNA) siGenome SMARTpools (Dharmacon, GE Life Sciences, USA) against human TFEB, TFE3 or ON-TARGETplus non-targeting (OTP-NT) using DharmaFECT-1 (Dharmacon, GE Life Sciences). Cells were seeded at a density of 2.5 x 10^5 in 24-well plates with a final concentration of 40 nM siRNA. For the double knockdown of TFEB and TFE3, cells were transfected using 40 nM of each siRNA pool. 24-hour post-transfection the media was changed, and cells incubated for a further two days. Transfected cells were then infected with *C. burnetii* at a multiplicity of infection (MOI) of 100 for 4 hours, washed once with PBS and media replaced with DMEM containing 5% FBS. This timepoint was designated day 0. Samples for immunoblotting were collected by resuspending them in SDS-PAGE sample buffer at 1, 3- and 5-days post transfection. Samples were processed for *C. burnetii* genome quantification at day 0, 3 and 5 as described in section 2.13.2. At three days post-infection, duplicate samples were fixed and processed for immunofluorescence as described in section 2.9.

2.7 Extraction of RNA

RNA was extracted from infected adherent human epithelial cells using the following method. Samples from duplicate wells were washed once with 500 µL phosphate buffered saline (PBS). Homogenisation was performed using 500 µL TRIsure added to each well. Samples were collected by scraping the well surface and collected into microfuge tubes. This was incubated at room temperature (RT) for 10 mins and then placed on ice. For

phase separation, samples were incubated at room temperature for 5 mins followed by addition of 200 µL chloroform and shaken vigorously for 15 secs. Samples were incubated at RT for 2-3 mins and centrifuged at 10,000 x *g* for 15 mins at 4 °C. The upper aqueous phase, containing RNA, was collected into a new tube without disrupting the interphase. RNA was precipitated by addition of 500 µL cold isopropanol and the samples were incubated for 60 mins at -20 °C. Samples were precipitated by centrifugation at 10,000 x *g* for 10 mins at 4 °C. Post precipitation, supernatant was removed and the RNA pellet was washed with 1 mL 75% ethanol made up with Diethyl pyrocarbonate (DEPC) treated distilled water and then allowed to dry. To resuspend RNA, 10 µL DEPC treated distilled H_2O was added. Samples were then placed at 60 °C for 5 mins. NanoDrop® spectrophotometer was used to quantify the RNA concentration and A_{260}/A_{280} ratio was adjusted to a concentration of 2.0.

DNase removal step was carried out using the Ambion DNase treatment and removal kit according to the manufacturers protocol. BioRad iScript cDNA synthesis kit was used for reverse transcription of 4 µg RNA according to manufacturer's guidelines. qPCR was performed using Bioline SensiFast SYBR No-ROX kit using 18S rRNA as a control transcript.

2.8 Protein Biochemistry

2.8.1 Sodium dodecyl sulfate–polyacrylamide gel electrophoresis and Immunoblotting

Samples were resuspended in SDS-PAGE sample buffer (Appendix) and boiled at 95 °C for 5 mins before being loaded on 4-12% NuPAGE Bis-Tris gels (Life Technologies Pty Ltd, Australia) with either 2-[N-morpholino]ethanesulfonic acid (MES) or 3-(N-morpholino) propanesulfonic acid (MOPS) running buffer (Life Technologies). Separated proteins were transferred to nitrocellulose membranes using the iBlot2 system (Life Technologies). Membranes were blocked in 5% skim milk in Tris-buffered saline with 0.1% Tween-20 (TBST) (Appendix) (Thermo Fisher Scientific) for at least 1 hour at room temperature. If required, the blocking buffer was washed off with TBS or PBS 0.1% Tween-20 three times for 10 minutes.

Primary antibodies were diluted in 5% BSA (bovine serum albumin fraction V, Sigma Aldrich) in TBST and incubated with the membranes overnight. Secondary antibodies were diluted in TBST containing 5% skim milk (SM) and incubated with the membranes for approximately 1 hour. Membranes were washed between the antibody steps as for blocking buffer and before the use of Clarity Western ECL Reagents (BioRad) and MF-ChemiBIS, version 3.2 (DNR Bio-Imaging Systems, Ltd.) to develop the blots. Blots were exposed for between 10 secs and 1 min and were assessed with Gel Capture, version 7.0.18 software (DNR Bio-Imaging Systems, Ltd.) to ensure band detection was within the linear range.

2.8.2 Antibodies

The working concentrations of all antibodies used in this study are listed in Table 2. 4. All antibodies were diluted in TBST containing 5% SM or 5% BSA for immunoblotting. Antibodies for use in immunofluorescence (IF) were diluted in PBS (Appendix) with 0.05% saponin and 2% BSA.

Table 2. 4 Antibodies used in this study.

Antibody	Dilution		Diluent	Host/ Clonality	Manufacturer
	Immuno-blotting	IF			
Anti-Mouse IgG Alexa Fluor® 468	N/A	1:2,000	5 % BSA	Goat/ Polyclonal	Thermo Fischer Scientific
Anti-Mouse IgG Alexa Fluor® 568	N/A	1:2,000	5 % BSA	Goat/ Polyclonal	Thermo Fischer Scientific
Anti-Mouse IgG Alexa Fluor® 488	N/A	1:2,000	5 % BSA	Goat/ Polyclonal	Thermo Fischer Scientific

Anti-Mouse IgG Alexa Fluor® 588	N/A	1:2,000	5 % BSA	Goat/ Polyclonal	Thermo Fischer Scientific
Anti-β-actin	1:5,000	N/A	5 % SM	Mouse/ Monoclonal	Sigma-Aldrich
Anti-BlaM	1:1500	N/A	5 % SM	Mouse/ Monoclonal	QED Bioscience, Australia
Anti-*C. burnetii*	N/A	1:10,000	2 % BSA	Rabbit/ Polyclonal	A kind gift from Roy Laboratory, Yale University
Anti-FLAG	N/A	1:2,000	5 % SM	Mouse/ Monoclonal	Sigma-Aldrich
Anti-Mouse IgG Horse radish peroxidase (HRP) – linked	1:3,000	N/A	5 % SM	Goat/ Polyclonal	Perkin Elmer, USA
Anti-rabbit IgG, HRP-linked	1:3,000	N/A	5 % SM	Goat/ Polyclonal	Perkin Elmer

Anti-Histone H3	1: 2000	N/A	5 % BSA	Rabbit/ Monoclonal	Cell signalling Technology, USA
Anti-LAMP-1	1:1,000	1: 250	5 % BSA	Mouse/ Monoclonal	Developmental Studies Hybridoma Bank, USA
Anti-TFEB	1: 1,000	1: 100	5 % BSA	Rabbit/ Polyclonal	Cell signalling Technology, USA
Anti-TFE3	1: 1,000	1: 100	5 % BSA	Rabbit/ Polyclonal	Sigma Aldrich
Anti-Tubulin	1: 1,000	N/A	5 % BSA	Mouse/ Monoclonal	Santa-Cruz Biotechnology, USA
Anti-TPP-1	1: 100	N/A	3% SM + 0.1% Tween-20 TBS	Mouse/ Monoclonal	Santa-Cruz Biotechnology

2.8.3 Preparation of protein lysates for proteomic analysis

Stable cells lines were treated with 20 ng/µL of doxycycline for 48 h before being washed three times in ice-cold PBS, to remove residual media. Cells were placed on a bed of ice,

1ml of ice cold guanidine hydrochloride (GdmCl) lysis buffer (6M GdmCl, 100 mM Tris (pH 8.0), 10 mM tris(2-carboxyethyl) phosphine and 40 mM 2-chloroacetamide (CAA)) containing protease inhibitors (cOmplete™ EDTA-free protease inhibitor cocktail, Roche) added and lysate collected by cell scrapping. Lysates were boiled at 95 °C with shaking on ThermoMixer for 10 minutes to shear DNA, inactivate proteases/ phosphatases and ensures all the material is solubilised.

Lysates were then allowed to cool on ice for 10 minutes. 10 µL of the cooled lysate was used to determine protein concentration using a BCA kit (Pierce). 1000 µg of each lysate was cleaned by acetone precipitation by adjusting the final volume of sample to 200 µL then adding 800 µL of ice-cold acetone in 1.5 ml eppendorf tubes. Samples could precipitate overnight at -20 ºC, precipitated protein collected by centrifugation at 6000 *x g* for 15 min at 0 ºC and acetone removed. To ensure complete removal of possible contaminates a second round of acetone precipitation was undertaken by resuspending protein pellets in 80 % ice-cold acetone and allowing precipitation at -20 ºC for at least 4 hours. Post incubation, samples were collected by centrifugation at 6000 *x g* for 15min, 0 ºC to remove residual acetone and then allowed to air dry.

2.8.4 Digestion and peptide clean-up of proteome samples

Dried protein pellets were resuspended in resuspension buffer (6M Urea, 2M Thiourea, 100 mM Ammonium bicarbonate) and then reduced for 1 hour at room temperature with freshly prepared DTT (final concentration 10 mM). Samples were subsequently alkylated by the addition of chloroacetamide (final concentration 40 mM) in the dark for 1 hour.

Alkylation was halted and excess chloroacetamide quenched by the addition of DTT (50 mM final concentration) and incubation for 15 min at RT. Reduced/alkylated samples were digested for 3 hours with Lys-C (1/200 (w/w); Wako Lab Chemicals) at 25 °C before being diluted 1 in 4 with ammonium bicarbonate (100 mM; Sigma) and digested overnight with trypsin (1/50 (w/w); Promega) at 25 °C.

Digested peptides were then acidified by the addition of formic acid (final concentration 2%; Sigma) and desalted using tC18 Sep-Pak Waters Corporation according to the manufacturer's instructions. Briefly, tC18 Sep-Pak were conditioned by washing with 10 column bed volumes of Buffer B (80% acetonitrile, 0.1% formic acid) then 20 column bed volumes of Buffer A* (2% acetonitrile, 0.1% trifluoroacetic acid). Acidified samples were loaded onto the column and then the column washed with a further 20 column bed volumes of Buffer A*. Peptides were eluted with 10 column bed volumes of Buffer B and dried down for analysis by LC-MS. Prior to loading, samples were reconstituted in MS running buffer (2% acetonitrile, 0.1% trifluoroacetic acid) to a concentration of 0.5 µg/µL of which 2 µg was loaded for analysis.

2.8.5 LC-MS and Label-free proteomic analysis

Samples were analysed by LC-MS on an Q-exactive™ plus mass spectrometer (ThermoFisher Scientific) coupled to a Dionex Ultimate 3000 Ultra-Performance Liquid Chromatography (ThermoFisher Scientific) using a two-column chromatography set up composed of a PepMap100 C18 20 mm x 75 µm trap and a PepMap C18 500 mm x 75 µm analytical column (Thermo Fisher Scientific). Samples were concentrated at 5 µL/min

onto the trap column for 5 minutes prior to the initiation of the analytical separation which was performed at 300 nl/min. Analysis separation was undertaken by altering the composition of Buffer B from 3% to 30% over 160 min then from 30% to 40% over 7 min, 40% to 90% over 5 min, holding at 90% for 5 minutes then dropped to 3% Buffer B over 3 min with the column then equilibrated by holding at 3% Buffer B for 5 min. Experiments were acquired using Data Dependent Acquisition with a top 15 method where MS1 scans were acquired at 70k resolution with a m/z range of 350 – 1400 (automatic gain control (AGC) set to 3 x 10^6 or a maximum injection time of 50 ms) followed by 15 MS2 scans. MS2 scans were acquired using high-energy collision dissociation fragmentation with a stepped normalised collision energy of 25, 30, 35 resolution of 17.5k and an AGC of 5 x 10^5 or a maximum injection time of 80 ms.

LC-MS data files were analysed using the MaxQuant platform (version 1.5.3.30 [67]) searching against the Human Proteome (Uniprot accession: UP000005640), ^{3xFLAG}CBU1701, ^{3xFLAG}CBU2016, and a database containing common contaminants. Carbamidomethylation of cysteine was set as a fixed modification and oxidation of methionine and acetylation of protein N-termini set as variable modifications. Searches were performed with trypsin cleavage specificity allowing 2 miscleavage events with a maximum false discovery rate (FDR) of 1.0% set for protein and peptide identifications. To enhance the identification of peptides between samples the Match Between Runs option was enabled with a precursor match window set to 2 minutes and an alignment window of 10 minutes. To enabled comparison of samples by label-free quantitation MaxLFQ within MaxQuant [130] was enabled. The resulting protein group output was

processed within the Perseus (v1.4.0.6) [205] analysis environment to remove reverse matches and common protein contaminates prior. For LFQ comparisons missing values were imputed using Perseus and visualized using ggplot in R. The mass spectrometry proteomics data for the stable cell lines have been deposited to the Proteome Xchange Consortium via the PRIDE [206] partner repository with the dataset identifier PXD016598 and can be accessed using the login: reviewer64337@ebi.ac.uk Password: QH1GAcC9.

2.9 Immunofluorescence staining and Confocal microscopy

The following steps were carried out at room temperature. HeLa and THP-1 cells that were seeded onto glass coverslips, post various treatments, were fixed with 4% paraformaldehyde (Sigma-Aldrich) in PBS for 20 minutes, followed by three washes in PBS for 5 mins each. Fixed cells were then permeabilised and blocked in blocking buffer (PBS with 2% BSA and 0.05% saponin) for 1 hour, before they were immunostained in primary antibodies for one hour at RT or overnight at 4 °C. Prior to immunostaining using secondary antibodies, coverslips were subjected to 3 washes in PBS for 5 minutes per wash. Refer to

Table 2. 4 for the concentrations of antibodies used for immunofluorescence. Both primary and secondary antibodies were diluted in blocking buffer. Following secondary antibody incubation, the coverslips were incubated with 4′,6-diamidino-2-phenylindole (DAPI) diluted 1:10,000 in PBS for 5 minutes, followed by 2 washes in PBS for 5 minutes per wash. Coverslips were mounted with ProLong Gold Antifade Mountant (Thermo

Fisher Scientific) onto glass microscope slides (Livingstone, Australia) and stored at 4 °C until analysis by confocal microscopy.

2.9.1 Visualisation of immunofluoresence images using Confocal microscopy

Confocal microscope images were acquired using Zeiss LSM700 laser confocal microscope (Zeiss, Germany). Images were processed using FIJI (https://imagej.nih.gov/ij/).

2.10 Stable cell lines

2.10.1 Constructs and viral particle production

HeLa cells expressing ^{3xFLAG}CBU1701 or ^{3xFLAG}CBU2016 under the control of a doxycycline inducible promoter were engineered using lentiviral transduction. 7.5 µg each of pFTRE-3G-^{3xFLAG}CBU1701 or pFTRE-3G-FLAG-^{3xFLAG}CBU2016 was transfected using FuGENE6 (Promega) into HEK293T cell monolayers seeded in a 10 cm dish. The transfection was done in combination with 2.5 µg pCMV-VSV-G and 3.5 µg of pCMV-dR8.2dvpr. This was incubated at 37 ºC for 24 h, following which the media was replaced with DMEM containing 10% FCS and incubated for another 48 h. 2.5 ml of 1 x 10^5 cells/ml of HeLa cells were seeded into a 6-well plate and incubated for 24h. The virus was harvested from the HEK293T cells 48 h post transfection using a syringe and the supernatant and was filtered using a 0.45 µm PES (polyethrsulfone) filter. 2 ml of the viral supernatant was then added onto the HeLa CCL2 monolayer along with polybrene (5

mg/ml) at a 1:1000 dilution. The plates were then spun at 500 x *g* for 1 hour at RT and incubated at 37 °C overnight. Media was replaced every 24 h (DMEM with 10% FCS containing 5 µg/mL puromycin) until all susceptible cells had died and puromycin resistant cells replicated to confluency. Puromycin selection was maintained until all the cells were dead in control wells. The expression of ^{3xFLAG}CBU1701 and ^{3xFLAG}CBU2016 was confirmed by immunoblot of cell lysate following induction of expression using 20 ng/mL of doxycycline. Aliquots of stable cell lines positive by immunoblotting were stored long term in liquid nitrogen.

2.10.2 Clonal selection (Fluorescence-activated cell sorting)

In order to ensure clonal selection of stable cell lines, a confluent T75 flask of puromycin resistant cells was washed twice with PBS and trypsinised as described in section 2.4. These cells were resuspended in 10 mL DMEM + 10% FCS and collected into a 15 mL tube and pelleted at 800 x *g* for 5 minutes. The cells were resuspended in 10 mL of FACS buffer (Appendix). In duplicate, 1mL of the resuspended solution was transferred into a FACS vial (Falcon® Round-Bottom Polystyrene Tubes, Corning). Prior to sorting, cells were stained using 2 µg/mL propidium iodide, a viability dye, and filtered using a 0.45 µm filter to remove any clumps or debris. Post sorting, cells were spotted onto 96-well plates containing DMEM + 20 % FCS with 1% penicillin-streptomycin (10,000 U/mL) (GIBCO™). The plates were incubated at 37 ºC with 5% CO_2, with media replaced every 2 days. Wells containing replicating cells were monitored until the cells became confluent. These cells were then expanded gradually. Once a confluent 6-well plate was obtained, the cells were then processed for immunoblotting to confirm the positive clonal isolate. Post confirmation

of the positive clones, at least four independent clonal isolates were stored in liquid nitrogen for future use.

2.11 Subcellular fractionation of ^{3xFLAG}CBU1701 and ^{3xFLAG}CBU2016 stable cells lines

Subcellular fractionation of HeLa ^{3xFLAG}CBU1701 and ^{3xFLAG}CBU2016 stable cells lines was carried out, to monitor localisation of ^{3xFLAG}CBU1701 and ^{3xFLAG}CBU2016 and to determine the localisation of host transcription factors TFEB and TFE3 upon induction of effector expression. All samples were kept on ice throughout the procedure and centrifugations were performed at 4 ºC. Briefly, cells were plated at a density of 5 x 10^5 cells/dish in a 100 mm dish. The next day, effector expression was induced by addition of 20 ng/ml doxycycline for 48 hours. At the end of incubation, cells were washed twice using ice-cold PBS and trypsinised according to section 2.4. A total of 1 x 10^6 cells was lysed in the presence of 500 µL cytoplasmic extraction buffer (Appendix). The cells were lysed by gently inverting every 5 minutes on ice for 15 minutes. The homogenate was spun for 15 minutes at 2000 x *g* and 250 µL of the supernatant containing cytosolic and membrane content was collected into a fresh microfuge tube. The nuclear pellet was washed three times with the cytoplasmic extraction buffer and resuspended in 0.1 ml of high-salt nuclear extraction buffer (Appendix). The suspension was then sonicated three times for 3 secs at low output to shear the gDNA using Sonicator Ultrasonic Processor, Misonix, Inc., USA. The suspension was maintained on ice between each sonication pulse. The homogenate was spun at 4 °C for 5 min at 10,000 x *g* and approximately 90

µL of the nuclear extract was collected into a microfuge tube. The cytoplasmic and nuclear protein extracts were subsequently analysed by immunoblotting with various antibodies.

2.12 Genetic manipulation of *C. burnetii*

cbu1701::Tn transposon mutant, identified within a large library of *C. burnetii* transposon mutants, was clonally isolated as described previously [80]. *cbu1701* is disrupted with a transposon that is inserted 1023 bp downstream of the start codon, thus making a non-functional *cbu1701::*Tn mutant.

Deletion of *C. burnetii* effector protein, *cbu2016* was achieved using the published homologous recombination protocol [79]. This targeted gene deletion approach was employed to delete *cbu2016* in both *C. burnetii* NMII and *cbu1701*::Tn strains. A suicide plasmid, pJC-CAT::CBU2016-5'3'-Kan, encoding approximately 2000 bp upstream and downstream regions of *cbu2016* flanking a kanamycin resistance cassette was constructed. The plasmid contained a chloramphenicol acetyltransferase (*cat)* and *Bacillus subtillis sacB* (*sacB*) gene cassette driven by *C. burnetii* promoter 1169^{P}. This plasmid was then introduced by electroporation into the wild type *C. burnetii* and *cbu1701*::Tn strains as described above (Section 2.3.2.3). Positive transformants for the generation of double knockout strains were selected by culturing the bacteria in ACCM-2 supplemented with 3 µg/mL chloramphenicol and 350 µg/mL kanamycin and routinely passaged every 7 days for 28 days with a 1:120 ratio. This was followed by PCR to verify chromosomal integration of the suicide plasmid using specific oligonucleotides,16-19 and 18-17 listed in Table 2. 3. For PCR, 1 ml of the *C. burnetii* culture was pelleted, at 10,000

x g for 20 minutes at room temperature and resuspended in 30 µL of PBS. 3 µL of the resuspended *C. burnetii* culture was used as the template for the PCR. The positive transformants, were then further subcultured in ACCM-2 containing 1% sucrose, for 4 days to excise the suicide plasmid. Transformants were then passaged by culturing in ACCM-2 supplemented with 3 µg/mL chloramphenicol and 350 µg/mL kanamycin and clonally isolated by picking individual colonies grown in ACCM-2 agarose as described previously in section 2.3.2.3. The deletion of *cbu2016* in *cbu1701*::Tn and WT was verified using oligonucleotides specified in Table 2. 3.

2.13 Infections with *C. burnetii*

2.13.1 PicoGreen to quantify *C. burnetii* Genome Equivalents

To quantify axenically cultivated *C. burnetii*, the Quant-iT PicoGreen dsDNA Assay Kit (Thermo Fischer Scientific) was used according to the manufacturer's instruction.

2.13.2 Quantitative PCR (qPCR) for enumeration of genome equivalents of *C. burnetii*

qPCR was used to enumerate *C. burnetii* genome equivalents. For this, infected cells were lysed in sterile distilled H_2O and collected. Lysed samples were pelleted to obtain the *C. burnetii* and mammalian cell debris before being resuspended in 100 µL of sterile H_2O. *C. burnetii* genomic DNA was extracted using the Quick-DNA^{TM} Miniprep Kit (Zymo Research), and bacterial genome equivalents were enumerated by qPCR using *ompA*

specific oligonucleotides (see Table 2. 3) and genomic DNA at known concentrations [203].

5 µL of purified *C. burnetii* gDNA or a known concentration of *C. burnetii* gDNA standard, SensiFAST™ SYBR® No-ROX (Bioline) and 1 µM each of *ompA*-specific oligonucleotides (Table 2.3) in a final volume of 20 µL was used to perform qPCR. The following thermal cycling conditions: 50 °C for 2 minutes, followed by 95 °C for 10 minutes before 45 cycles of 95 °C for 1 second, 60 °C for 20 seconds were used to perform qPCR on a MX3005P qPCR system (Agilent Technologies, USA). This step was followed by 95 °C for 1 minute, 55 °C for 30 seconds, and 95 °C for 30 seconds. Data analysis was carried out using the Quant Studio 7 software. The standard curve to calculate the number of *C. burnetii* genomic copies was constructed by qPCR containing the known concentrations of *C. burnetii* gDNA standards ranging from 10^5 to 10^9.

2.14 Effector translocation reporter assay

pJB-CAT-BlaM-*cbu1701* and pJB-CAT-BlaM-*cbu1701*$^{435\text{-}468}$ plasmid constructs were generated by introducing the full length and C-terminal regions of CBU1701 into the *Sal*I site of pJB-CAT-BlaM that has the constitutive CBU1169 promoter driving the expression of the BlaM fusion protein [122, 208]. These plasmids were electroporated into *C. burnetii* NMII and *icmL*::Tn strains according to section 2.3.2.3. Post electroporation and cultivation on ACCM-2 agarose, the colonies were picked using a P-200 pipette. To facilitate removal of colonies, a wide orifice pipette tip was used. Each agarose plug was added to ACCM-2 media to allow expansion of colony population. Expression of BlaM

fusion proteins by transformant *C. burnetii* was confirmed by western blot using anti-BlaM and positive transformants were stocked for later use. For the translocation assay, HeLa CCL2 cells were seeded at a density of 5 x 10^4 cells/well into a black clear bottom 96 well tray (Corning Incorporated, Corning NY). Various *C. burnetii* strains were used to infect HeLa monolayers at the specified MOI and the infection proceeded until the desired time point. Infected cells were then loaded with the fluorescent substrate CCF2-AM, using the Live Blazer FRET B/G kit (Invitrogen) with 0.1M probenecid, and incubated in the dark for 2 h at room temperature. Fluorescence was quantified using CLARIOstar® Microplate reader (BMG LABTECH), with an excitation of 410 nm and emission at 450 nm and 520 nm. The ratio of 450 nm to 520 nm (blue to green) was calculated following background subtraction and expressed relative to the uninfected cells.

2.15 Statistics

Data graphs were generated using GraphPad Prism version 7.03. All graphs display mean ± SD. An unpaired, two-tailed student t-test was used for comparison between two groups. p values less than 0.05 was considered significant.

For detailed methods that relate only to Chapter 3 please refer to the materials and methods section within this chapter.

Chapter 3

Biogenesis of the spacious *Coxiella*–containing vacuole depends on the host transcription factors TFEB and TFE3

3.1 Synopsis

Coxiella burnetii is a Gram-negative obligate intracellular bacterial pathogen and the etiological agent of the zoonotic infection Q fever. In humans, *C. burnetii* infections often result in asymptomatic infection, or may present as an acute disease such as hepatitis, pneumonia, or self-limited influenza-like illness. The severe manifestation of chronic Q fever is endocarditis observed in approximately 2% of acute Q fever patients. Upon internalisation by macrophages, this obligate intracellular bacterial pathogen replicates inside the lysosome derived *Coxiella*-containing vacuole (CCV). *C. burnetii* directs the massive expansion of the CCV to accommodate the replicating pathogen while still maintaining the hydrolytic and acidic nature of the host lysosome. Formation of this replicative vacuole involves many host and bacterial proteins. The Dot/Icm type 4 secretion system (T4SS) is a critical virulence factor essential for intracellular replication of *C. burnetii*. Showing similarity to the *L. pneumophilla* T4SS, this apparatus translocates approximately 150 bacterial effector proteins into the host cell modulating various cellular processes. While the presence of some of these effectors have been shown to be important for intracellular replication, their individual biochemical functions are poorly defined. Studies have demonstrated that *C. burnetii* effectors can influence important eukaryotic processes including vesicular traffic, autophagy, and cell death signalling.

In order to develop an understanding of the impact *C. burnetii* has on infected THP-1 cells, SILAC based proteomics was performed to examine changes in the host proteome during infection. Many changes were observed when comparing uninfected cells with *C. burnetii* infected cells for 3 days. Of particular interest, infection of THP-1 macrophage-

like cells with *C. burnetii* showed an increase in the abundance of many proteins involved in host cell autophagy and lysosomal biogenesis. This led to the hypothesis that the host transcription factor's TFEB and TFE3, might be involved in the regulation of a network of genes involved in autophagy and lysosomal biogenesis. Upon infection of both epithelial and phagocytic cell lines with *C. burnetii*, at different stages post-infection, TFEB and TFE3 were activated as demonstrated by their trafficking from cytoplasm into the nucleus. This could be demonstrated to be dependent on the *C. burnetii* T4SS, as inhibition of bacterial translation using chloramphenicol, or infection of cells lines with a Dot/Icm-deficient mutant, did not induce nuclear translocation of TFEB or TFE3. Indeed, treatment with chloramphenicol effectively induced the transport of these proteins back into the cytoplasm indicating that *C. burnetii* is actively inducing the nuclear localisation of these transcription factors. We silenced expression of the host transcription factors TFEB and TFE3, either singly or in tandem. There was a reduction in the size of the CCV, and we do not see reduced replication in the absence of TFEB and TFE3. This was significant when both the transcription factors were silenced together, suggesting that these transcription factors play an important role in the formation and expansion of CCV (Figure 3.2).

3.1.1 Research objectives

To create a large lysosome-derived CCV, *C. burnetii* subverts host cell-signalling pathways expanding the lysosomal network to create a massive lysosome-derived replicative vacuole. Our non-biased proteomics data of macrophage cells with *C. burnetii*, revealed a host proteome change of proteins involved in autophagy and biosynthesis of the lysosomes. We thus hypothesized that activation of the transcriptional regulators of autophagy and lysosomal biogenesis, TFEB and TFE3, respectively may be an important way in which the host cell can support *C. burnetii* replication.

The key aims for this part of the thesis were:

a) Create a proteomic map of changes that occur during *C. burnetii* infection of macrophage-like cells.

b) Investigate the localisation and activation state of TFEB and TFE3 throughout *C. burnetii* infection of epithelial and macrophage-like cells.

c) Investigate the role of the *C. burnetii* type IV secretion system in the nuclear localisation of TFEB and TFE3.

d) Examine the importance of TFEB and TFE3 individually or together in the intracellular success of *C. burnetii*.

This chapter includes a journal article published by Infection and Immunity in 2019 and additional supporting data that was not included in the publication. The article contains data which supports the hypothesis that the host transcription factors, TFEB and TFE3, play a crucial role in the formation of the CCV.

All the co-authors have given permission for the article to be included in this Thesis in an un-modified form, from the published version.

3.2 Publication

Biogenesis of the spacious *Coxiella*-containing vacuole depends on host transcription factors TFEB and TFE3. *Infection and Immunity.*

Padmanabhan B, Fielden LF, Hachani A, Newton P, Thomas DR, Cho HJ, Khoo CA, Stojanovski D, Roy CR, Scott NE, and Newton HJ (2019).

Published December 9, 2019. https://www.ncbi.nlm.nih.gov/pubmed/31818957
PMID: 31818957

Contributions of each author to this publication are:

BP: conceptualisation, data curation, formal analysis, investigation, methodology, validation, visualisation, writing original draft, review, and editing

LFF: data curation, formal analysis, investigation, methodology, visualisation, writing review and editing

AH: formal analysis, methodology, writing review and editing

PN: data curation, writing review and editing

DT: data curation, writing review and editing

CHJ: methodology, software development, writing review and editing

CAK: data curation, methodology, writing review and editing

DS: funding acquisition, resources, project administration, supervision, writing review and editing

CRR: conceptualisation, funding acquisition, writing review, and editing

NES: funding acquisition, formal analysis, methodology, visualisation, project administration, supervision, writing review and editing

HJN: conceptualisation, data curation, formal analysis, funding acquisition, methodology, project administration, supervision, resources, visualisation, writing original draft, review, and editing.

AMERICAN SOCIETY FOR MICROBIOLOGY | Infection and Immunity®

CELLULAR MICROBIOLOGY:
PATHOGEN-HOST CELL MOLECULAR INTERACTIONS

Biogenesis of the Spacious *Coxiella*-Containing Vacuole Depends on Host Transcription Factors TFEB and TFE3

Bhavna Padmanabhan,[a] Laura F. Fielden,[a,b,c] Abderrahman Hachani,[a] Patrice Newton,[a] David R. Thomas,[a] Hyun-Jung Cho,[d] Chen Ai Khoo,[a] Diana Stojanovski,[b,c] Craig R. Roy,[e] Nichollas E. Scott,[a] Hayley J. Newton[a]

[a]Department of Microbiology and Immunology, University of Melbourne at the Peter Doherty Institute for Infection and Immunity, Melbourne, VIC, Australia
[b]Department of Biochemistry and Molecular Biology, The University of Melbourne, Melbourne, VIC, Australia
[c]Bio21 Molecular Science and Biotechnology Institute, The University of Melbourne, Melbourne, VIC, Australia
[d]Biological Optical Microscopy Platform, The University of Melbourne, Parkville, VIC, Australia
[e]Department of Microbial Pathogenesis, Yale University School of Medicine, New Haven, Connecticut, USA

ABSTRACT *Coxiella burnetii* is an obligate intracellular bacterial pathogen that replicates inside the lysosome-derived *Coxiella*-containing vacuole (CCV). To establish this unique niche, *C. burnetii* requires the Dot/Icm type IV secretion system (T4SS) to translocate a cohort of effector proteins into the host cell, which modulate multiple cellular processes. To characterize the host-pathogen interactions that occur during *C. burnetii* infection, stable-isotope labeling by amino acids in cell culture (SILAC)-based proteomics was used to identify changes in the host proteome during infection of a human-derived macrophage cell line. These data revealed that the abundances of many proteins involved in host cell autophagy and lysosome biogenesis were increased in infected cells. Thus, the role of the host transcription factors TFEB and TFE3, which regulate the expression of a network of genes involved in autophagy and lysosomal biogenesis, were examined in the context of *C. burnetii* infection. During infection with *C. burnetii*, both TFEB and TFE3 were activated, as demonstrated by the transport of these proteins from the cytoplasm into the nucleus. The nuclear translocation of these transcription factors was shown to be dependent on the T4SS, as a Dot/Icm mutant showed reduced nuclear translocation of TFEB and TFE3. This was supported by the observation that blocking bacterial translation with chloramphenicol resulted in the movement of TFEB and TFE3 back into the cytoplasm. Silencing of the TFEB and TFE3 genes, alone or in combination, significantly reduced the size of the CCV, which indicates that these host transcription factors facilitate the expansion and maintenance of the organelle that supports *C. burnetii* intracellular replication.

KEYWORDS *Coxiella burnetii*, SILAC, TFE3, TFEB, autophagy, host-pathogen interactions, lysosome biogenesis

Coxiella burnetii is a Gram-negative obligate intracellular pathogenic bacterium and the causative agent of Q (query) fever, a life-threatening zoonosis (1, 2). The clinical presentation of infection is quite varied, ranging from acute influenza-like symptoms to debilitating chronic illness, such as hepatitis or endocarditis, with significant mortality (2).

Human alveolar macrophages are the primary targets of *C. burnetii* (3). Following internalization, *C. burnetii* transits through the endolysosomal pathway. Once the pathogen reaches the acidic lysosomal environment, *C. burnetii* becomes metabolically active and begins remodeling the vacuolar environment to support its replication. This bacterially modified spacious and unique replicative niche is termed the *Coxiella*-containing vacuole (CCV) (4). The Dot/Icm type IVB secretion system (T4SS) is essential

Citation Padmanabhan B, Fielden LF, Hachani A, Newton P, Thomas DR, Cho H-J, Khoo CA, Stojanovski D, Roy CR, Scott NE, Newton HJ. 2020. Biogenesis of the spacious *Coxiella*-containing vacuole depends on host transcription factors TFEB and TFE3. Infect Immun 88:e00534-19. https://doi.org/10.1128/IAI.00534-19.

Editor Guy H. Palmer, Washington State University

Address correspondence to Hayley J. Newton, hnewton@unimelb.edu.au.

Received 11 July 2019
Returned for modification 1 August 2019
Accepted 13 November 2019
Accepted manuscript posted online 9 December 2019
Published 20 February 2020

for intracellular replication and biogenesis of the CCV (5, 6). This secretion system translocates over 130 bacterial effector proteins into the host cytoplasm, where they modulate various cellular processes (7). To date, the functional roles of very few of these effectors have been defined.

The CCV is highly fusogenic and merges with endocytic vesicles, other CCVs, and autophagosomes to create a large organelle that will rapidly occupy much of the host cell's cytoplasmic space. The CCV is positive for lysosomal markers, including lysosome-associated membrane glycoproteins, CD63, the vacuolar ATPase, and cathepsin D (8–10). More recent findings have demonstrated that the CCV remains in an autolysosomal state of maturation, with autophagosome-CCV fusion contributing to CCV biogenesis (11, 12). In agreement with this, the internal pH of the mature CCV was recently shown to be slightly elevated from the normal lysosomal pH (13).

Degradative membrane transport pathways, both endocytic and autophagic, are highly dynamic systems that play important roles in eukaryotic cell adaptation to nutrient availability and defense against microbes (14). The transcription factors TFEB and TFE3 are bona fide master transcriptional regulators of lysosomal biogenesis, facilitating the expression of many genes implicated in lysosome-related processes, including phagocytosis and autophagy (15, 16). When present in the nucleus, TFEB and TFE3 form homo- or heterodimers that specifically bind to CLEAR (coordinated lysosomal expression and regulation) elements to induce the transcription of genes critical for autophagosome and lysosome biogenesis (17, 18).

The activation of TFEB and/or TFE3 is controlled by a multifaceted lysosome-to-nucleus signaling pathway. Under nutrient-rich conditions, TFEB/TFE3 is phosphorylated by active mammalian/mechanistic target of rapamycin complex 1 (mTORC1) at the lysosomal membrane (19–21). The phosphorylation of TFEB/TFE3 promotes interactions with 14-3-3 proteins, leading to their retention in the cytoplasm (20, 21). Under nutrient-limited conditions, mTORC1 dissociates from the lysosome and is inactivated. Calcium is released from the lysosome into the cytoplasm via the lysosomal calcium channel mucolipin-1 (MCOLN1) (also known as TRPML1), leading to the localized activation of the phosphatase calcineurin (22). Activated calcineurin dephosphorylates TFEB and TFE3, facilitating their nuclear translocation and subsequent influence on the cellular transcriptional profile (22).

Because *C. burnetii* creates a large lysosome-derived vacuole that subverts the host autophagy pathway, we hypothesized that TFEB and TFE3 activation may be an important element of infection. In support of this idea, an unbiased analysis of the host proteome during infection demonstrated a significant increase in the abundance of many proteins within the CLEAR network and that the activation of the transcription factors TFEB and TFE3 during *C. burnetii* infection is important for CCV biogenesis.

RESULTS

***C. burnetii* infection leads to a host cell proteome shift that supports increased lysosome biogenesis.** To gain insight into the human host cell response to *C. burnetii* infection, quantitative proteomics using stable-isotope labeling by amino acids in cell culture (SILAC) was employed to examine changes to the host proteome of human macrophage-like THP-1 cells during infection. Labeled and differentiated THP-1 cells were infected with *C. burnetii* expressing mCherry for 3 days, allowing CCV establishment and intracellular replication. To ensure that all cells were infected, cells were sorted for mCherry fluorescence prior to mixing with mock-sorted uninfected cells. Proteins were digested and analyzed by mass spectrometry, identifying a total of 5,112 proteins at a 1% false discovery rate (FDR), with 83% (4,266) of these proteins being derived from the host proteome and 846 being derived from *C. burnetii* (see Table S1 in the supplemental material). Of the 4,266 host proteins, 851 were altered in abundance when comparing infected to uninfected cells, as determined by a one-sample *t* test with a Benjamini-Hochberg multiple-hypothesis correction of 5%, leading to a significance cutoff of a >1.85 $-\log_{10}(P \text{ value})$ (47). Analysis of these altered proteins using Fisher's exact enrichment analysis of protein-associated gene ontology (GO)

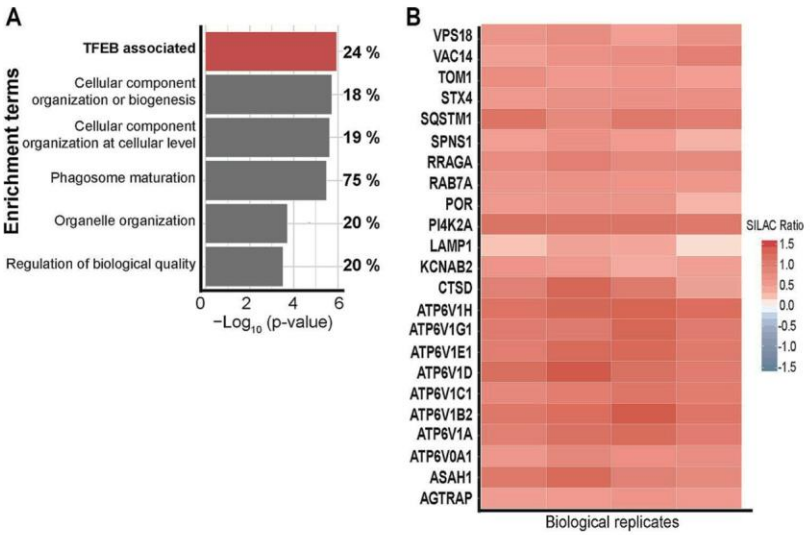

FIG 1 *C. burnetii* infection leads to a host cell proteome shift that supports increased lysosome biogenesis. (A) GO-based enrichment of proteins involved in various biological processes analyzed using Fisher's exact enrichment analysis. Percentages represent the proportions of proteins enriched in each category compared to the observable proteome. (B) Heat map of proteins with TFEB-associated gene expression. Color represents the SILAC ratio for each of four biological replicates, where red represents an increase in *C. burnetii*-infected THP-1 cells.

terms identified significant enrichment of proteins involved in "phagosome maturation" (15 out of 20 proteins identified; 75%), "cellular component organization or biogenesis" (228 out of 1,257 proteins identified; 18%), and "organelle organization" (128 out of 653 proteins identified; 20%) (Fig. 1A and Table S2). Importantly, 24% (60 of the 252) of the proteins regulated by TFEB (23) were significantly altered upon infection with *C. burnetii* (Fig. 1A). The SILAC ratios revealed significant increases in proteins within the TFEB/TFE3 regulatory network, which were consistent across all four biological replicates (Fig. 1B), including many components of the vacuolar ATPase and the autophagy receptor Sequestosome 1 (SQSTM1), which has previously been shown to be increased in abundance during *C. burnetii* infection (12, 24). This proteomics-based analysis demonstrated that 3 days after infection with *C. burnetii*, the abundances of proteins associated with lysosomal biogenesis were increased.

Nuclear translocation of TFEB-GFP during *C. burnetii* infection of HeLa TFEB-GFP cells. Given the increased abundance of proteins involved in lysosome biogenesis and autophagy observed during *C. burnetii* infection, the nuclear translocation of TFEB was examined. The subcellular localization of TFEB-green fluorescent protein (GFP) was monitored in uninfected HeLa cells and compared to that in cells infected with *C. burnetii* for 1, 3, or 5 days. In uninfected cells, the majority of the TFEB-GFP was retained within the cytoplasm (Fig. 2A). Cells infected with *C. burnetii* for 1 day (24 h) showed a similar cytoplasmic TFEB-GFP distribution. In contrast, at 3 and 5 days postinfection, when *C. burnetii* was replicating within the CCV, TFEB-GFP nuclear translocation was observed (Fig. 2). The nuclear translocation of TFEB-GFP was quantified by calculating the nuclear-to-cytoplasmic ratio of the TFEB-GFP ratio. This ratio was quantified for at least 30 cells under each experimental condition for each of three independent biological replicates. Regardless of individual cell variability (Fig. 2B), a consistent increase in the nuclear/cytoplasmic TFEB-GFP signal was observed at days 3 and 5 of *C. burnetii* infection (Fig. 2C). By day 5 postinfection, this increase was equivalent to that in uninfected cells treated with chloroquine (CQ), a lysosomotropic agent that induces TFEB nuclear translocation by causing lysosomal stress (20) (Fig. 2).

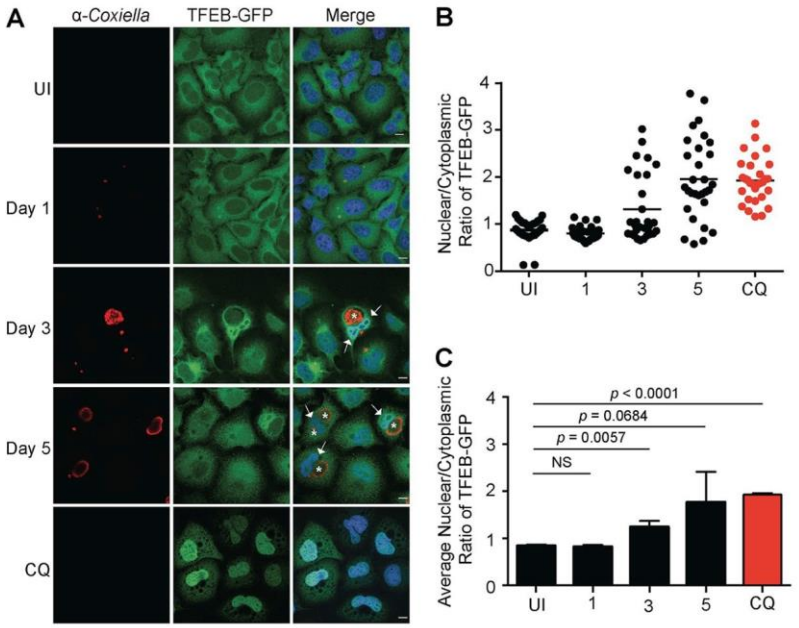

FIG 2 Nuclear translocation of TFEB-GFP during *C. burnetii* infection of HeLa TFEB-GFP cells. (A) Representative confocal images of HeLa TFEB-GFP cells that were uninfected (UI); infected for 1, 3, or 5 days with *C. burnetii* NMII at an MOI of 100; or treated for 24 h with 50 μ,g/ml chloroquine (CQ). Following infection and/or treatment, cells were fixed and immunolabeled with anti-*C. burnetii* (red), and nuclei were stained with DAPI (blue). White arrows and asterisks denote TFEB nuclear translocation and CCVs, respectively. Bars, 10 μ,m. (B) Representative nuclear/cytoplasmic ratios of TFEB-GFP from 30 uninfected, infected, or treated cells at the time points indicated. (C) Average nuclear/cytoplasmic ratios of TFEB-GFP from three biological replicates. The means and SD for each time point are presented. An unpaired two-tailed *t* test was used to determine the statistical significance between samples. NS, not significant.

***C. burnetii* infection induces nuclear translocation of endogenous TFEB.** To discount the potential impact of TFEB overexpression on its nuclear translocation during *C. burnetii* infection, the localization of endogenous TFEB was examined. HeLa cells (Fig. 3A) and differentiated THP-1 cells (Fig. 3B) were fixed and stained with anti-TFEB and anti-*C. burnetii* antibodies under the following conditions: uninfected, treated with CQ for 24 h, or infected with *C. burnetii* for 3 or 5 days. Consistent with our previous findings, TFEB was observed to be enriched within the nucleus 3 and 5 days after infection with *C. burnetii* in both cell lines (Fig. 3). The anti-TFEB antibody demonstrated significant cross-reactivity with *C. burnetii*, hampering the possibility of quantifying the nuclear/cytoplasmic intensity of TFEB during infection. Visual observation confirms that TFEB is recruited into the host cell nucleus during *C. burnetii* infection, which may account for the increased production of host proteins that contribute to lysosome biogenesis and autophagy observed in our SILAC studies.

Endogenous nuclear translocation of TFE3 is induced during *C. burnetii* infection. Given that both TFEB and TFE3 upregulate the expression of genes involved in lysosomal biogenesis and autophagy, the subcellular localization of TFE3 during *C. burnetii* infection was also examined. HeLa cells (Fig. 4A) and differentiated THP-1 cells (Fig. 4B) were infected with *C. burnetii* for 1, 3, and 5 days before being fixed and stained with anti-TFE3 and anti-*C. burnetii*. These samples were compared to uninfected cells that remained untreated or were treated with CQ for 24 h. As expected, in uninfected cells, the majority of TFE3 was present in the cytoplasm. TFE3 was observed to translocate into the host cell nucleus throughout the course of infection. The nuclear/cytoplasmic intensity of TFE3 was calculated for at least 30 HeLa cells under

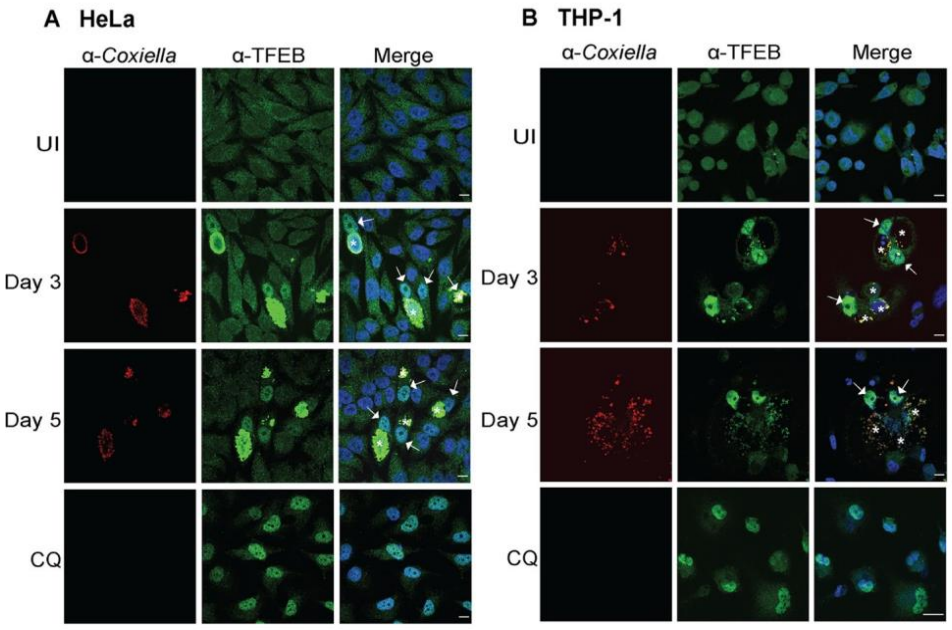

FIG 3 *C. burnetii* infection induces nuclear translocation of endogenous TFEB. (A) Representative immunofluorescence images of HeLa CCL2 cells that were uninfected, infected with *C. burnetii* NMII at an MOI of 100 for 3 or 5 days, or treated using 50 μ,g/ml chloroquine (CQ) for 24 h. (B) Differentiated THP-1 macrophage cells were uninfected, infected with *C. burnetii* NMII at an MOI of 100 for 3 or 5 days, or treated using 50 μ,g/ml CQ for 24 h. Cells after infection and upon treatment were fixed for immunolabeling with antibodies against *C. burnetii* (red) and TFEB (green), and nuclei were stained with DAPI (blue). Bars, 10 μ,m. White arrows and asterisks denote endogenous TFEB nuclear translocation and CCVs, respectively.

each experimental condition (Fig. 4C) for each of three independent experiments (Fig. 4D). A statistically significant increase in nuclear TFE3 was observed from day 1 postinfection, compared to uninfected cells, and this ratio increased at day 3 and day 5 postinfection, approaching the TFE3 nuclear translocation observed with CQ treatment (Fig. 4D). These results demonstrate that TFE3, in addition to TFEB, is actively recruited into the host nucleus during *C. burnetii* infection. Interestingly, TFE3 nuclear localization was observed at an earlier stage of infection than TFEB.

Nuclear localization of TFEB-GFP and TFE3 during *C. burnetii* infection is Dot/Icm dependent and reversed upon inhibition of bacterial protein translation. To determine whether the nuclear translocation of TFEB and TFE3 is driven by *C. burnetii*, the localization of these host proteins was visualized in HeLa cells infected for 3 days with Dot/Icm-deficient *C. burnetii*. *C. burnetii* with a disrupted T4SS did not induce the nuclear translocation of TFEB-GFP or TFE3 3 days after infection of HeLa cells (Fig. 5). In order to account for the absence of replication of this *C. burnetii* mutant, a 10-fold-increased multiplicity of infection (MOI) of *C. burnetii icmL*::Tn (6) was included, but there was still no observable increase in the nuclear-to-cytoplasmic ratio of TFEB-GFP (Fig. 5A and C) or TFE3 (Fig. 5B and D).

In order to examine whether the sustained nuclear localization of TFEB-GFP and TFE3 required *C. burnetii* activity, HeLa cells infected with *C. burnetii* for 3 days, to induce the nuclear translocation of TFEB-GFP and TFE3, were treated with 10 μ,g/ml of chloramphenicol for 8 h (Fig. 5). Chloramphenicol blocks bacterial protein synthesis and has previously been used to demonstrate the importance of *C. burnetii* protein synthesis during infection (6, 25). Similar to the results seen with Dot/Icm-deficient *C. burnetii*, blocking of bacterial protein translation with chloramphenicol led to a loss of nuclear TFEB-GFP and TFE3. Quantification of the ratio of nuclear to cytoplasmic signals

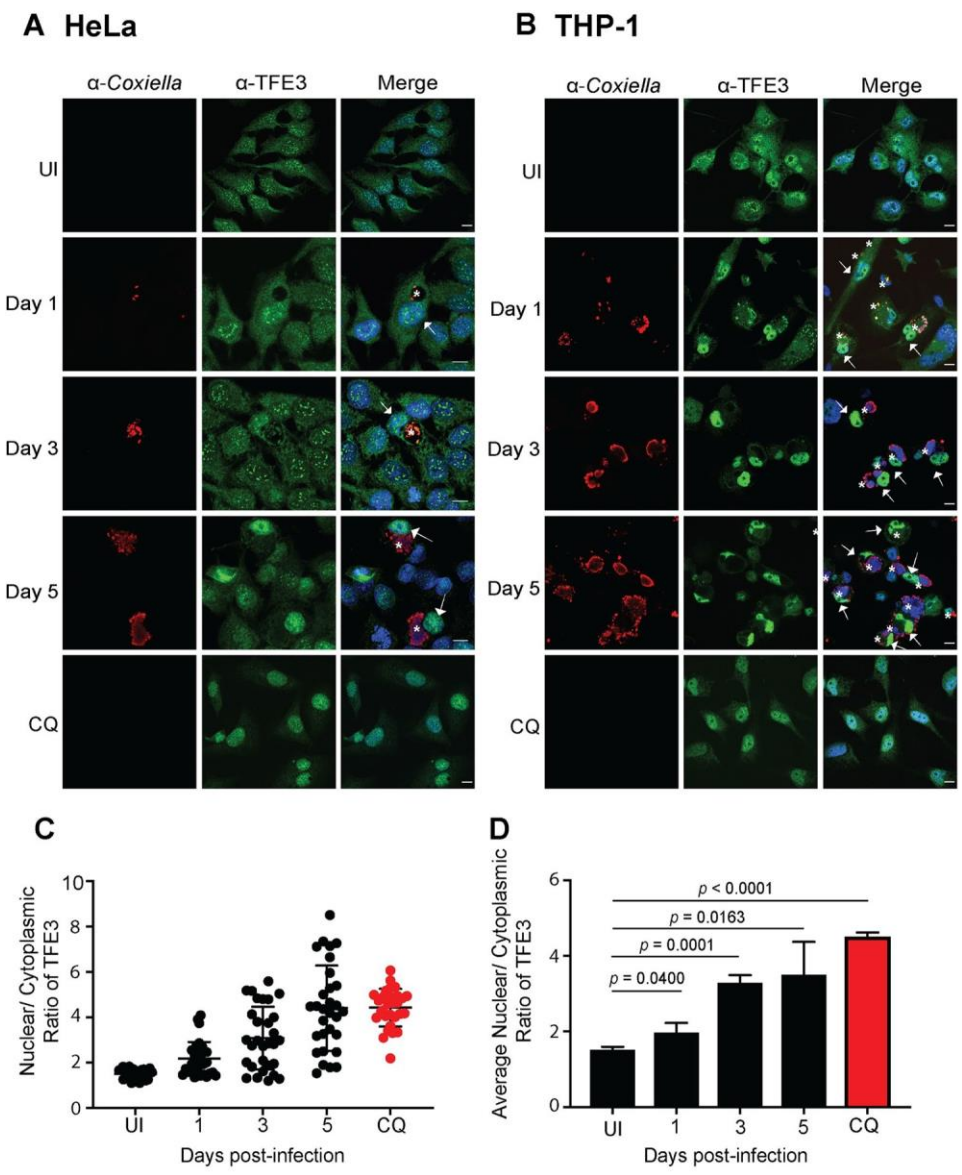

FIG 4 *C. burnetii* infection induces nuclear translocation of endogenous TFE3. (A and B) Representative confocal images of HeLa CCL2 cells (A) or THP-1 cells (B) that were uninfected or infected with *C. burnetii* NMII at an MOI of 100 for 1, 3, or 5 days. After infection or following chloroquine (CQ) treatment, cells were fixed and immunolabeled with antibodies against *C. burnetii* (red) and TFE3 (green), and nuclei were stained with DAPI (blue). White arrows and asterisks denote endogenous TFE3 nuclear translocation and CCVs, respectively. Bars, 10 μ,m. (C) Representative nuclear/cytoplasmic ratios of endogenous TFE3 from 30 uninfected, infected, or treated HeLa CCL2 cells at the time points indicated. (D) Average nuclear/cytoplasmic ratios of endogenous TFE3 in HeLa CCL2 cells from three independent experiments. The means and SD for each time point are presented. An unpaired two-tailed *t* test was used to determine the statistical significance between samples.

was confirmed by immunofluorescence microscopy (Fig. 5C and D). Together, these data indicate that the sustained nuclear localization of TFEB-GFP and TFE3 during *C. burnetii* infection depends on bacterial protein synthesis and the activity of the Dot/Icm secretion system.

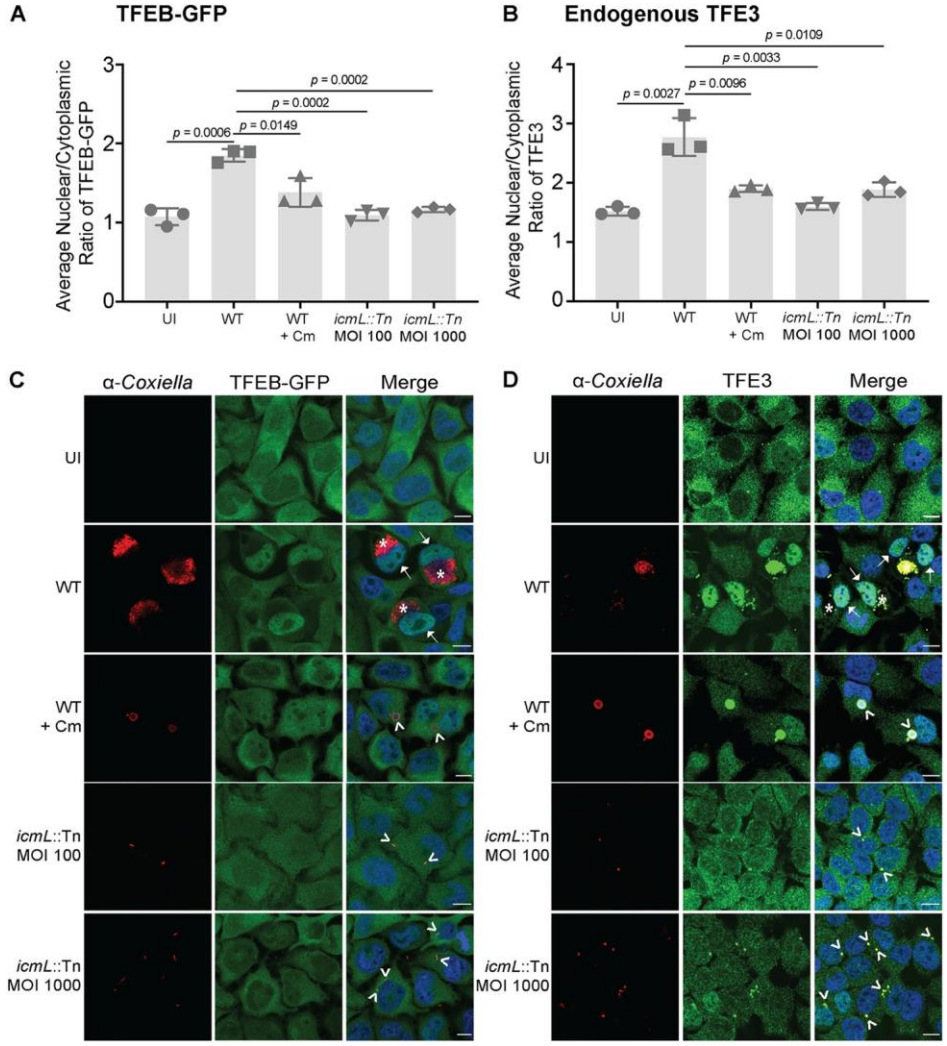

FIG 5 *C. burnetii* drives nuclear translocation of TFEB-GFP and TFE3. (A) HeLa cells constitutively expressing TFEB-GFP were infected with either wild-type (WT) *C. burnetii* or a Dot/Icm-deficient mutant (*icmL*::Tn) and treated as indicated before being fixed at 3 days postinfection and stained for *C. burnetii*. "Cm" refers to addition of chloramphenicol 8 h before fixation. The average nuclear/cytoplasmic ratio of TFEB-GFP was calculated from three independent experiments. (B) HeLa cells were infected as described above and stained for endogenous TFE3 and *C. burnetii* at 3 days postinfection. The average nuclear/cytoplasmic ratio of TFE3 was calculated from three independent experiments. In both scenarios, the signal ratio from a minimum of 30 individual cells was calculated under each condition tested in each independent experiment. The mean ratio for each independent experiment is shown, and the gray bar represents the average mean from the independent experiments. Error bars represent standard deviations. An unpaired two-tailed *t* test was used to determine statistical significance between WT infection and other samples, and *P* values of <0.05 are displayed. (C and D) Representative images of TFEB-GFP (C) and TFE3 (D). WT CCVs are labeled in the merged images with asterisks, and nucleus-localized TFEB-GFP or TFE3 is highlighted with an arrow. Collapsing CCVs and nonreplicating *C. burnetii* cells are indicated with arrowheads. Bars, 10 μ,m.

TFEB and TFE3 are important for vacuole biogenesis during *C. burnetii* infec- tion. The nuclear translocation of TFEB and TFE3 and the increase in the abundances of many proteins controlled by TFEB and TFE3 during *C. burnetii* infection call for a direct assessment of these transcription factors toward a productive *C. burnetii* infection. To examine the effects of these transcription factors on CCV biogenesis and the

replication of *C. burnetii*, small interfering RNA (siRNA) was used to silence the expression of TFEB or TFE3. HeLa cells were transfected with siRNA targeting TFEB (siTFEB) or TFE3 (siTFE3) or the OnTarget Plus nontargeting (OTP-NT) control (siOTP-NT). Reductions in TFEB and TFE3 were confirmed by immunoblotting lysates collected at 1, 3, and 5 days posttransfection (Fig. 6A). Two days after siRNA transfection, HeLa cells were infected with *C. burnetii*, and bacterial replication was measured by collecting cell lysates at 4 h (day 0), 3 days, and 5 days postinfection (corresponding to 2, 5, and 7 days posttransfection). Across 4 independent experiments, siTFEB treatment led to a small but significant ($P = 0.011$) reduction in *C. burnetii* replication (Fig. 6C). HeLa cells treated with siOTP-NT supported a fold change in *C. burnetii* genome equivalents of 205.00 ± 81.60 over 5 days, compared to 52.81 ± 18.81 for siTFEB treatment ($P = 0.011$). Gene silencing of TFE3 induced a similar trend toward less *C. burnetii* replication, with siOTP-NT control-treated cells supporting a fold change in *C. burnetii* genome equivalents of 272.24 ± 131.84 across 5 days, compared to 91.84 ± 58.12 for TFE3-silenced cells ($P = 0.055$) (Fig. 6D). At 3 days postinfection, samples were fixed and stained with anti-*Coxiella* and anti-lysosome-associated membrane protein 1 (LAMP1) to monitor CCV size upon the depletion of TFEB and TFE3 (Fig. 6F, G, and J). The microscopy analysis independently validated the functional impact of TFEB and TFE3 gene silencing, as significantly less LAMP1 was observed in gene-silenced cells (Fig. 6J and K). The sizes of the CCVs formed during gene silencing of TFEB or TFE3 were significantly reduced compared to those of vacuoles that formed with siOTP-NT treatment (Fig. 6F, G, and J). Figure 6F demonstrates the range of CCV sizes in individual host cells in one experiment, and Fig. 6G shows the average CCV sizes and standard deviations from three independent experiments. With siOTP-NT treatment, CCVs were 315.40 ± 30.95 μ,m^2, compared to 101.43 ± 6.04 μ,m^2 in the absence of TFEB ($P = 0.0003$) and 122.03 ± 7.21 μ,m^2 in the absence of TFE3 ($P = 0.0005$).

To determine whether TFEB and TFE3 act independently or have overlapping roles during *C. burnetii* infection of HeLa cells, double-knockdown experiments were performed. Here, the expression of both TFEB and TFE3 was silenced (Fig. 6B), and *C. burnetii* infection was compared to that in siOTP-NT control-treated cells. *C. burnetii* intracellular replication in the absence of both TFEB and TFE3 was comparable to that with siOTP-NT treatment (Fig. 6E). Even at 5 days postinfection, there was no observable difference in bacterial numbers ($n = 5$; $P = 0.6467$). However, in agreement with the silencing of either TFEB or TFE3, the CCV area was significantly impacted by the absence of both TFEB and TFE3 (Fig. 6H, I, and K). Consistent with previous measurements, the average CCV size 3 days after infection of siOTP-NT-treated HeLa cells was 236.41 ± 69.44 μ,m^2, compared to 53.80 ± 14.63 μ,m^2 for cells treated with both siTFEB and siTFE3 ($P = 0.0112$). These data demonstrate that TFEB and TFE3 contribute to the biogenesis of the normally spacious CCV.

DISCUSSION

Intracellular bacterial pathogens mediate complex interactions with eukaryotic host cells that similarly have evolved many strategies to recognize and respond to infection. Deciphering this arms race can inform our understanding of bacterial pathogenesis and reveal a novel understanding of eukaryotic cell function and dysfunction. Here, a SILAC-based proteomics approach was employed to capture a global snapshot of the host proteomic changes that occur during *C. burnetii* infection. This revealed a significant increase in many lysosomal proteins within the TFEB and TFE3 CLEAR regulatory network.

In support of previous findings, the SILAC experiments performed here demonstrated an increase in the abundance of the autophagy receptor SQSTM1 during *C. burnetii* infection (12, 24). A previous study showed the noncanonical recruitment of SQSTM1 to the CCV during infection, where it is proposed to act as a signaling molecule activating the Nrf2-Keap1 cytoprotective pathway (24). Rab7, a marker of late endosomes, showed a marked increase in abundance during infection with *C. burnetii*. As a key regulator of endocytic maturation and autophagosome-lysosome fusion, Rab7 is

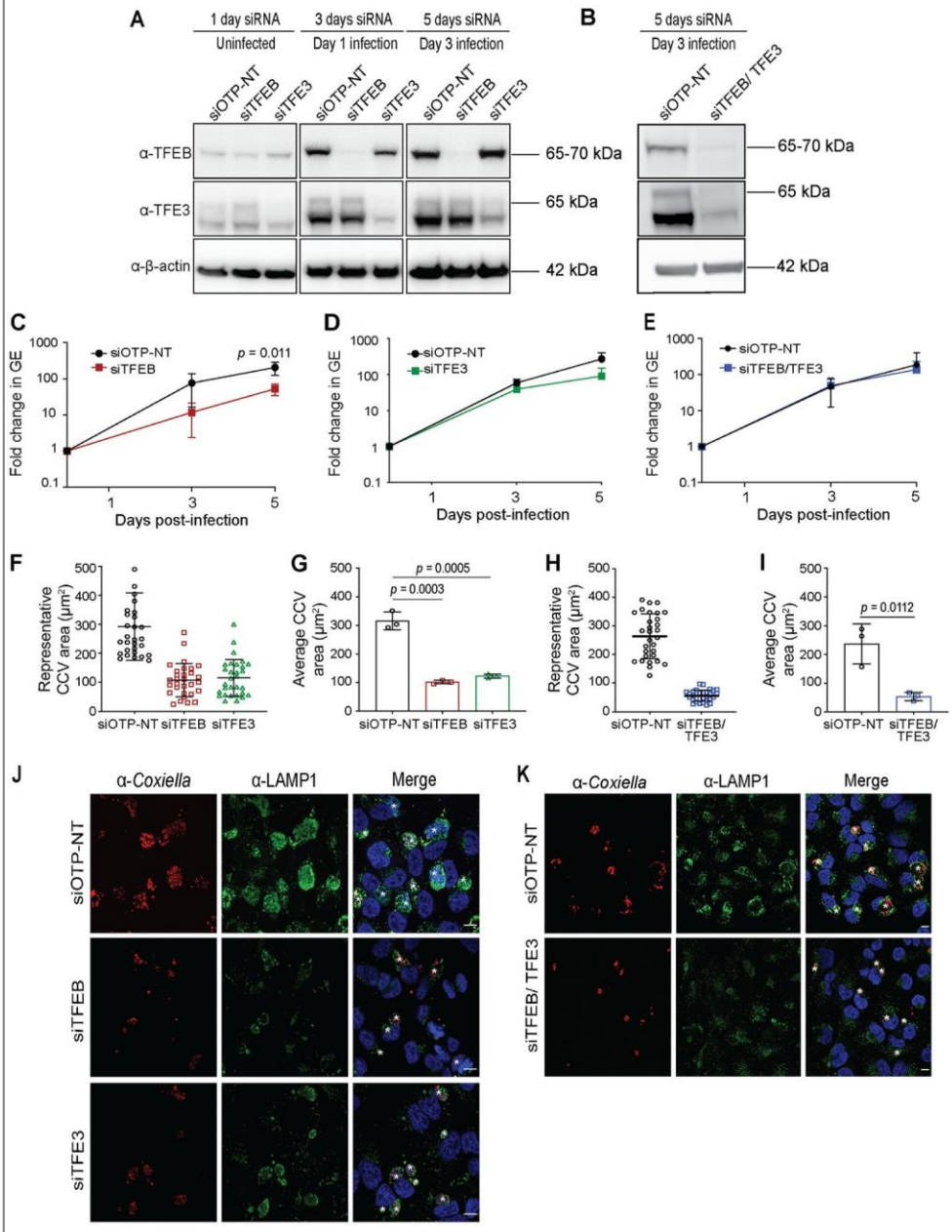

FIG 6 Functional importance of TFEB and TFE3 during *C. burnetii* infection. HeLa cells were transfected with nontargeting siRNA (siOTP-NT) or siRNA specifically targeting TFEB (siTFEB), TFE3 (siTFE3), or both siTFEB and siTFE3 (siTFEB/TFE3) and harvested at days 0, 3, and 5 days posttransfection. (A) Immunoblot analysis of whole-cell lysate showing the absence of TFEB and TFE3 with siTFEB and siTFE3 treatment. (B) Immunoblot analysis of whole-cell lysates showing the loss of both TFEB and TFE3 5 days after siTFEB/TFE3 treatment. *a-[3-*Actin was used as a loading control in both panels A and B. (C to E) siRNA-transfected HeLa cells were infected with *C. burnetii* at an MOI of 100, and intracellular replication was quantified by enumerating genome equivalents (GE) by qPCR at 0, 3, and 5 days postinfection. Nontargeting siRNA (siOTP-NT) treatment was compared to siTFEB (C), siTFE3 (D), and siTFEB/TFE3 (E) treatments. (F) CCV area measurement from 30 individual infected cells from one experiment showing variation in CCV size following siRNA treatments. (G) Quantification of the average CCV area from three biological replicates comparing siOTP-NT treatment with silencing of the expression of either TFEB or TFE3. (H) CCV area measurement from 30 individual infected cells from one experiment showing variation in CCV size

(Continued on next page)

required for the biogenesis of the CCV and the activation of the *C. burnetii* T4SS (26, 27). Additionally, the abundances of eight subunits of the vacuolar ATPase, the proton pump responsible for the acidification of the endocytic network, were increased during *C. burnetii* infection.

Examination of TFEB and TFE3 localization throughout infection demonstrated significant nuclear translocation of these host transcription factors. Interestingly, significant nuclear localization of TFE3 was detected at 1 day postinfection, and TFEB nuclear translocation was notable from 3 days postinfection, corresponding to CCV expansion and *C. burnetii* replication. This nuclear translocation of TFEB and TFE3 likely accounts for the increased abundance of CLEAR network proteins observed during *C. burnetii* infection.

In HeLa cells, the nuclear translocation of TFEB and TFE3 appears to be controlled by *C. burnetii*, as blocking bacterial translation with chloramphenicol leads to TFEB/TFE3 movement back into the cytoplasm. In support of this hypothesis, a Dot/Icm-deficient *C. burnetii* mutant was unable to induce the nuclear recruitment of TFEB and TFE3. Intriguingly, these data suggest that *C. burnetii* may encode Dot/Icm effectors that promote the activation of this signaling pathway to facilitate increased lysosomal biogenesis and autophagy.

To determine the impact of TFEB or TFE3 on *C. burnetii* infection, we used siRNA gene silencing in HeLa cells and measured the consequences for *C. burnetii* intracellular success. The loss of TFEB or TFE3 had a significant impact on CCV expansion but little impact on the intracellular replication of *C. burnetii*. The absence of both TFEB and TFE3 recapitulated a nonredundant role for these proteins in CCV expansion. Despite these host transcription factors not influencing bacterial replication, *C. burnetii* replication within a noncanonical, tightly bound CCV may have important downstream consequences for *C. burnetii* fitness that can be observed only in multicellular models of infection.

The findings reported here should be considered in the context of similar research published during the preparation of this article (28). In agreement with our findings, that study also demonstrated TFE3 nuclear translocation during *C. burnetii* infection of HeLa cells and reported that this may be linked to the observation that mTORC1 activity is inhibited during infection in a Dot/Icm-dependent manner (28). Knockout of both TFEB and TFE3 in RAW 264.6 macrophage-like cells also led to the production of smaller CCVs but, surprisingly, more *C. burnetii* replication across 3 days. This finding supports our observation that TFEB and TFE3 are important for the formation of the hallmark spacious CCV but are not necessary for bacterial replication. Interestingly, Larson et al. demonstrated that infection with Dot/Icm-deficient *C. burnetii* can also induce the nuclear translocation of TFE3 in HeLa cells (28). This TFE3 activation appears to be independent of mTORC1 inhibition and may represent a host response to bacterial infection independent of the pathogen-driven activation of this pathway that we observed here. Given the opposing findings presented here and by Larson et al., it will be interesting to explore whether any Dot/Icm effector proteins can, either directly or indirectly, influence the nuclear localization of TFEB and TFE3 and the activity of mTORC1.

Research into the relationship between other bacterial pathogens and TFEB has demonstrated that the activation of this pathway can have divergent consequences for different infections. *Acinetobacter baumannii*, a Gram-negative pathogen predominantly associated with hospital-acquired infections, induces the activation of TFEB in alveolar epithelial cells, and this promotes the internalization and intracellular success

FIG 6 Legend (Continued)
following treatment with either siOTP-NT or siTFEB/TFE3. (I) Quantification of the average CCV area from three biological replicates comparing siOTP-NT and siTFEB/TFE3 treatments. Error bars in panels F to I represent the SD. An unpaired two-tailed *t* test was used to determine statistical significance between siOTP-NT and the other siRNAs tested, and all *P* values of <0.05 are displayed. (J and K) Immunofluorescence images of HeLa cells depicting CCVs at 3 days postinfection. Cells were fixed and immunolabeled with antibodies against LAMP1 (green) and *C. burnetii* (red), and DNA was stained with DAPI (blue). White asterisks indicate CCVs. Bars, 10 μ,m.

of this pathogen (29). In contrast, TFEB activation during both *Staphylococcus aureus* and *Salmonella enterica* serovar Typhimurium infections is considered an important host response to infection (30–32). Interestingly, *Mycobacterium tuberculosis*, the causative agent of tuberculosis, has been shown to inhibit TFEB activation by inducing the increased expression of the host microRNA miR-33 (33).

To date, the factors that influence the host cell transcriptome during *C. burnetii* infection are not clearly understood. The proteomics data presented here reflect the complex interplay between host and bacterial signaling influences, both transcriptional and posttranscriptional. Not all TFEB/TFE3-regulated proteins demonstrate increased abundances during *C. burnetii* infection. Despite the observed nuclear translocation of TFEB and TFE3, there are other host and bacterial factors that contribute to the host transcriptome during infection. For example, the Nrf2-Keap1 antioxidant pathway, regulated by SQSTM1, was recently shown to be exploited by *C. burnetii* with the transcription factor Nrf2 present in the nucleus of infected cells (24). *C. burnetii* can influence host transcription through Dot/Icm effector proteins. *C. burnetii* has many effectors with the capacity to enter the host nucleus, including CaeA and AnkG, both of which possess antiapoptotic activity, and CBU1314, which has been shown to interact with chromatin and induce transcriptional changes when ectopically expressed in eukaryotic cells (34–36). Both host and bacterial factors may be acting in potentially cooperative and antagonistic manners to impact the host proteome profile defined here.

This research demonstrates that *C. burnetii* actively manipulates host cell transcription to promote autophagy and lysosomal biogenesis. The mechanism by which the Q fever pathogen controls this pathway is important for developing our understanding of the virulence strategies possessed by this emerging pathogen. Cumulative evidence suggests that the regulation of lysosomal biogenesis and autophagy by TFEB can influence important human diseases such as lysosomal storage disorders and neurodegenerative diseases (37). Thus, understanding how *C. burnetii* controls the lysosome-nucleus signaling axis may provide novel insights into understanding mammalian cell function and the mechanisms contributing to several important human disease states.

MATERIALS AND METHODS

Mammalian cell culture and *C. burnetii*. HeLa CCL2 and HeLa TFEB-GFP stable cells (a kind gift from Shawn Ferguson, Yale University) were maintained in Dulbecco's modified Eagle's medium (DMEM) with GlutaMAX (Gibco) supplemented with 10% heat-inactivated fetal bovine serum (FBS) at 37°C with 5% CO_2. THP-1 cells were maintained in RPMI 1640 supplemented with 10% FBS at 37°C with 5% CO_2. *C. burnetii* Nine Mile phase II (NMII) strain RSA439, clone 4, and *C. burnetii icmL*::Tn (6) were axenically cultured in liquid ACCM-2 (38) with chloramphenicol added at 3 μg/ml, when required, at 37°C with 5% CO_2 and 2.5% O_2 for 7 days.

***C. burnetii* infections.** HeLa cell lines were plated at a density of 5×10^4 cells/well into 24-well tissue culture plates 1 day prior to infection, with or without 10-mm glass coverslips. THP-1 cells were seeded into 24-well tissue culture plates at a density of 5×10^5 cells/well and treated with 10 nM phorbol 12-myristate 13-acetate (PMA) for 72 h to induce differentiation into adherent, macrophage-like cells. Axenically grown *C. burnetii* cells were quantified using the Quant-iT PicoGreen double-stranded DNA (dsDNA) assay kit (Thermo Fischer Scientific) according to the manufacturer's instructions. Sample values were compared to DNA standards of known concentrations, and quantification of *C. burnetii* genome equivalents was performed using the mass of the *Coxiella* genome (2.2×10^{-9} μg) to enumerate the multiplicity of infection (MOI). In all experiments, HeLa cells were infected with *C. burnetii* at an MOI of 100, and THP-1 cells were infected at an MOI of 25. Cells were incubated for 4 h at 37°C with 5% CO_2, washed once in phosphate-buffered saline (PBS), and further incubated in fresh DMEM with 5% FBS (HeLa cells) or RPMI 1640 with 10% FBS (THP-1 cells). At defined times postinfection, samples were either fixed with 4% paraformaldehyde (PFA) for microscopy analysis or lysed with H_2O and collected for *C. burnetii* genomic DNA quantification.

Western blot analysis. Samples for Western blotting were collected at the indicated time points throughout infection by resuspension in 2× SDS-PAGE sample buffer. Proteins were resolved using Bolt 4 to 12% Bis-Tris Plus gels (Thermo Fischer Scientific, Invitrogen) and transferred to nitrocellulose membranes using the iBlot 2 transfer system (Life Technologies, Thermo Fischer Scientific). Membranes were blocked using 5% skim milk in Tris-buffered saline containing 0.1% Tween 20 (TBST). The following antibodies were diluted in 5% bovine serum albumin (BSA) or skim milk in TBST and incubated with a nitrocellulose membrane at 4°C overnight: polyclonal anti-TFEB (1:1,000; Cell Signaling Technology), polyclonal anti-TFE3 (1:1,000; Sigma), monoclonal anti-β-actin AC-74 (1:5,000; Sigma), anti-mouse horseradish peroxidase (HRP) (1:3,000; Perkin Elmer), and anti-rabbit HRP (1:3,000; Perkin Elmer). Blots were

developed using Clarity Western ECL reagent (Bio-Rad) and exposed on an MF-ChemiBIS system, version 3.2 (DNR Bio-Imaging Systems, Ltd.). Immunoblots were analyzed using GelCapture software, version 7.0.18 (DNR Bio-Imaging Systems, Ltd.).

SILAC labeling and infection of the THP-1 cell line. SILAC labeling of undifferentiated THP-1 cells was performed as previously described (39, 40). Briefly, RPMI 1640 (Cambridge Isotope Laboratories, Inc.) lacking arginine and lysine was supplemented with 10% dialyzed FBS (Sigma). Arginine and lysine were added in either a light (L-arginine and L-lysine [Sigma] [Arg0; Lys0]) or heavy (L-[$^{13}C_6$, $^{15}N_4$]arginine and L-[$^{13}C_6$, $^{15}N_2$]lysine [Cambridge Isotope Laboratories] [Arg6; Lys4]) combination to final concentrations of 1.15 mM for arginine and 0.274 mM for lysine. THP-1 cells were split and passaged independently 5 times to allow for the incorporation of labeled amino acids into the cellular proteome. THP-1 cells were PMA differentiated 72 h prior to infection with *C. burnetii* expressing mCherry (5) at an MOI of 100. Cells were washed with PBS at 24 h postinfection to remove any extracellular bacteria and maintain infections within a 24-h window. Infected cells were incubated for a further 2 days prior to isolation and sorting for mCherry fluorescence using fluorescence-activated cell sorting (FACS). An equal number of uninfected cells were similarly counted via FACS and combined 1:1 with the infected cells. Cells were snap-frozen in liquid nitrogen prior to preparation for proteomic analysis.

Proteomics of whole-cell SILAC samples. Whole-cell SILAC samples were lysed in guanidine hydrochloride (GdHCl) lysis buffer [6 M GdHCl, 100 mM Tris (pH 8.0), 10 mM tris(2-carboxyethyl) phosphine, 40 mM 2-chloroacetamide (CAA)] at 95°C at 1,400 rpm (41). Lysates were cooled, and the protein concentration was determined using a bicinchoninic acid (BCA) kit (Pierce). A total of 50 to 100 μg of protein was acetone precipitated (4 volumes of acetone, 1 volume of water, and 1 volume of the sample) overnight at −20°C. Precipitated material was then pelleted at 16,000 × *g* for 10 min at 4°C and dried, to remove the remaining acetone, at 65°C. Pellets were resuspended in buffer containing 6 M urea, 2 M thiourea, and 10 mM dithiothreitol (DTT) and incubated at room temperature (RT) in the dark for 1 h to reduce disulfide bonds. Samples were then alkylated by the addition of 40 mM CAA and incubated for a further hour. Alkylation was halted by the addition of 20 mM DTT, and the samples were incubated at RT for 15 min. Samples were digested with endoproteinase Lys-C (1/200 [wt/wt]; Wako Lab Chemicals) for 4 h at RT before dilution with 20 mM ammonium bicarbonate and digestion with trypsin (1/50 [wt/wt]; Sigma) overnight at 25°C. Digested peptides were then acidified by the addition of 2% formic acid and desalted using homemade C_{18} (Empore C_{18}; Sigma) stage tips (42) before being dried down for analysis by liquid chromatography-mass spectrometry (LC-MS). Prior to loading, samples were reconstituted in MS running buffer (2% acetonitrile, 0.1% trifluoroacetic acid) to a concentration of 0.5 μg/μl, of which 2 μg was loaded for analysis.

Samples were analyzed by LC-MS on an Orbitrap Fusion Lumos Tribrid mass spectrometer (Thermo Fisher Scientific) coupled to a Dionex Ultimate 3000 ultraperformance liquid chromatography system (Thermo Fisher Scientific) using a two-column chromatography setup composed of a PepMap100 C_{18} 20-mm by 75-μm trap column and a PepMap C_{18} 500-mm by 75-μm analytical column (Thermo Fisher Scientific). Samples were concentrated at 5 μl/min onto the trap column for 5 min with buffer A (2% acetonitrile and 0.1% formic acid) prior to the initiation of analytical separation, which was performed at 300 nl/min. Liquid chromatography separation was undertaken by altering the composition of buffer B from 3% to 30% over 180 min and then from 30% to 40% over 7 min and 40% to 90% over 5 min, with holding at 90% for 5 min and then a drop to 3% buffer B (80% ACN and 0.1% formic acid) over 3 min, with the column then equilibrated by holding at 3% buffer B for 5 min. Data from experiments were acquired using data-dependent acquisition with a 120,000-resolution MS1 scan of a mass-to-charge (*m/z*) range of 400 to 1,600 (automatic gain control [AGC] set to 5×10^5 or a maximum injection time of 50 ms) acquired every 3 s, followed by MS2 scans. MS2 scans were acquired using high-energy collision dissociation fragmentation with a normalized collision energy of 35, a resolution of 15,000, and an AGC of 2×10^5 or a maximum injection time of 40 ms.

All raw files were analyzed using the MaxQuant platform (version 1.6.3.4), searching against the UniProt human and *C. burnetii* databases (UniProt accession numbers UP000005640 and UP000215556, respectively; downloaded July 2017) containing reviewed, canonical, and isoform variants and a database containing common contaminants generated by the Andromeda search engine (43). A multiplicity of 2 was used, denoting either the canonical amino acids (Arg0 and Lys0) or the SILAC amino acids (Arg6 and Lys4). Searches were performed with cysteine carbamidomethylation as a fixed modification and methionine oxidation and N-terminal acetylation as variable modifications. A false discovery rate (FDR) of 1% was applied as defined within the default parameters. "Re-quantify" and "match between runs" functions were enabled, with a match time window of 2 min. Unique and razor peptides were used for identification, with a minimum ratio count of 2. The "protein groups" output file was then imported into the Perseus platform (version 1.6.2.3) for further analysis (44). Identifications labeled by MaxQuant as "only identified by site," "potential contaminant," and "reverse hit" were removed, and the SILAC ratios were $\log_2$ transformed. Identifications were matched to human and *C. burnetii* annotation files (UniProt) using gene name identifiers. Mean $\log_2$-transformed heavy/light ratios and *P* values for each group were calculated using a single-sample two-sided *t* test. Proteins determined to be significantly altered between groups were assessed using Fisher's exact enrichment analysis to identify overrepresented GO terms. Both the determination of altered proteins and Fisher's exact enrichment analysis were subjected to multiple-hypothesis correction using Benjamini-Hochberg correction at an FDR of 5%. Data were exported into the R framework for visualization.

***C. burnetii* intracellular replication.** To enumerate *C. burnetii* genome equivalents by quantitative PCR (qPCR), infected cells were lysed in sterile distilled H_2O and collected. Lysed samples were pelleted to obtain the *C. burnetii* and mammalian cell debris before being resuspended in 100 μl of sterile H_2O.

C. burnetii genomic DNA was extracted using the Quick-DNA miniprep kit (Zymo Research), and bacterial genome equivalents were enumerated by qPCR using *ompA*-specific primers and comparison to reference samples (45).

Confocal microscopy. Immunofluorescence labeling was performed in TFEB-GFP stable cells to monitor TFEB nuclear localization. At the desired times postinfection, the cells were washed once with PBS and fixed with 4% (wt/vol) paraformaldehyde for 20 min at room temperature. The fixed cells were blocked and permeabilized using 0.05% saponin and 2% BSA in PBS, followed by staining using the following primary and secondary antibodies: rabbit polyclonal anti-*C. burnetii* (1:10,000; in-house [6]) and secondary antibody conjugated to Alexa Fluor 568 (1:2,000; Life Technologies). To monitor the endogenous nuclear translocation of TFEB and TFE3, cells were washed once with PBS, fixed with 4% PFA, and permeabilized with 0.2% Triton X-100 in PBS for 10 min at room temperature. This was followed by primary antibody staining in 10% FBS and 0.1% saponin for 1 h at RT with the following antibodies: rabbit polyclonal anti-TFEB (1:100; Cell Signaling) or rabbit polyclonal anti-TFE3 (1:200; Sigma), mouse monoclonal anti-LAMP1 (1:200; Developmental Studies Hybridoma Bank), and mouse anti-*C. burnetii* (1:1,000; in-house). Secondary antibodies conjugated to rabbit Alexa Fluor 488 (1:2,000; Invitrogen) and mouse Alexa Fluor 568 (1:2,000; Invitrogen) were used in the same blocking buffer. Antibody incubations were followed by PBS washes and incubation with 4′,6-diamidino-2-phenylindole (DAPI) (diluted 1:10,000 in PBS) to stain DNA. Coverslips were mounted using ProLong gold antifade mountant (Invitrogen). Images were acquired with a Zeiss LSM700 confocal laser scanning microscope (Zeiss, Germany) and processed using Fiji software (46).

siRNA gene silencing of TFEB and TFE3. For siRNA-mediated gene silencing of TFEB and TFE3 in HeLa cells, cells were reverse transfected with small interfering RNA (siRNA) siGenome SMARTpools (Dharmacon, GE Life Sciences) against human TFEB or TFE3 or OnTarget Plus nontargeting (OTP-NT) siRNA using DharmaFECT-1 (Dharmacon, GE Life Sciences). Cells were seeded at a density of 2.5×10^5 cells in 24-well plates with a final concentration of 40 nM siRNA. Cells treated with both siTFEB and siTFE3 were transfected with 40 nM each siRNA. At 24 h posttransfection, the medium was changed, and cells were incubated for a further 2 days. Transfected cells were then infected with *C. burnetii* at an MOI of 100 for 4 h and washed once with PBS, and the medium was replaced with DMEM containing 5% FBS. This time point was designated day 0. Samples for immunoblotting were collected by resuspending them in 2X SDS-PAGE sample buffer at 1, 3, and 5 days posttransfection. Cells were processed for *C. burnetii* genome quantification at days 0, 3, and 5 postinfection as described above. At 3 days postinfection, cells were fixed and processed for immunofluorescence as described above.

Quantification of the nuclear-to-cytoplasmic ratio. The nuclear-to-cytoplasmic ratios of TFEB and TFE3 were measured using Fiji (46). The image analysis workflow was semiautomated with a custom ImageJ macro where the microscope images were imported and the fluorescence intensity on the segmented nucleus and cytoplasm was measured automatically. The cytoplasm, nucleus, and infected area were segmented from TFEB/TFE3, DAPI, and infection channels, respectively. The segmentation threshold was determined from the background of each channel or by using the negative-control image and applied identically to every image. In noninfected cells, the applied threshold yielded no positive segmentation. The applied threshold was further checked by visual inspection and minimally adjusted, if necessary, prior to use for segmentation. Following segmentation, cells that were touching the boundary of the image were excluded. All complete cells were sorted based on infection status. For each cell, the mean intensity of cytoplasm and nucleus areas were measured, and the nucleus-to-cytoplasm ratio was calculated as nuclear mean intensity/cytoplasmic mean intensity.

Statistical analysis and quantification. Data graphs were generated using GraphPad Prism, version 7.03. All graphs display means ± standard deviations (SD). Unpaired two-tailed Student's *t* test was used for comparisons between two groups.

SUPPLEMENTAL MATERIAL

Supplemental material is available online only.

SUPPLEMENTAL FILE 1, XLSX file, 2.2 MB.

SUPPLEMENTAL FILE 2, XLSX file, 0.02 MB.

ACKNOWLEDGMENTS

This research was financially supported by NHMRC grant 1120344 awarded to H.J.N.; ARC grant DP180101298 awarded to H.J.N., D.S., and N.E.S.; and NIH grant R01AI114760 awarded to C.R.R. A.H. is supported by the H2020-MSCA-Global Fellowship, grant number 657766. B.P. is supported by a Melbourne International Research Scholarship and a Melbourne International Fee Remission Scholarship, The University of Melbourne. Confocal imaging was performed at the Biological Optical Microscopy Platform, The University of Melbourne (www.microscopy.unimelb.edu.au). We thank Shawn M. Ferguson, Yale University, for the TFEB-GFP stable HeLa cell line.

REFERENCES

1. Angelakis E, Raoult D. 2010. Q fever. Vet Microbiol 140:297–309. https://doi.org/10.1016/j.vetmic.2009.07.016.
2. Schneeberger PM, Wintenberger C, van der Hoek W, Stahl JP. 2014. Q fever in the Netherlands—2007-2010: what we learned from the largest outbreak ever. Med Mal Infect 44:339–353. https://doi.org/10.1016/j.medmal.2014.02.006.

3. Graham JG, MacDonald LJ, Hussain SK, Sharma UM, Kurten RC, Voth DE. 2013. Virulent Coxiella burnetii pathotypes productively infect primary human alveolar macrophages. Cell Microbiol 15:1012–1025. https://doi.org/10.1111/cmi.12096.
4. Newton HJ, Roy CR. 2011. The Coxiella burnetii Dot/Icm system creates a comfortable home through lysosomal renovation. mBio 2:e00226-11. https://doi.org/10.1128/mBio.00226-11.
5. Beare PA, Gilk SD, Larson CL, Hill J, Stead CM, Omsland A, Cockrell DC, Howe D, Voth DE, Heinzen RA. 2011. Dot/Icm type IVB secretion system requirements for Coxiella burnetii growth in human macrophages. mBio 2:e00175-11. https://doi.org/10.1128/mBio.00175-11.
6. Carey KL, Newton HJ, Luhrmann A, Roy CR. 2011. The Coxiella burnetii Dot/Icm system delivers a unique repertoire of type IV effectors into host cells and is required for intracellular replication. PLoS Pathog 7:e1002056. https://doi.org/10.1371/journal.ppat.1002056.
7. Luhrmann A, Newton HJ, Bonazzi M. 2017. Beginning to understand the role of the type IV secretion system effector proteins in Coxiella burnetii pathogenesis. Curr Top Microbiol Immunol 413:243–268. https://doi.org/10.1007/978-3-319-75241-9_10.
8. Heinzen RA, Scidmore MA, Rockey DD, Hackstadt T. 1996. Differential interaction with endocytic and exocytic pathways distinguish parasitophorous vacuoles of Coxiella burnetii and Chlamydia trachomatis. Infect Immun 64:796 –809.
9. Howe D, Mallavia LP. 2000. Coxiella burnetii exhibits morphological change and delays phagolysosomal fusion after internalization by J774A.1 cells. Infect Immun 68:3815–3821. https://doi.org/10.1128/iai.68.7.3815-3821.2000.
10. Howe D, Shannon JG, Winfree S, Dorward DW, Heinzen RA. 2010. Coxiella burnetii phase I and II variants replicate with similar kinetics in degradative phagolysosome-like compartments of human macrophages. Infect Immun 78:3465–3474. https://doi.org/10.1128/IAI.00406-10.
11. Kohler LJ, Reed SR, Sarraf SA, Arteaga DD, Newton HJ, Roy CR. 2016. Effector protein Cig2 decreases host tolerance of infection by directing constitutive fusion of autophagosomes with the Coxiella-containing vacuole. mBio 7:e01127-16. https://doi.org/10.1128/mBio.01127-16.
12. Latomanski EA, Newton HJ. 2018. Interaction between autophagic vesicles and the Coxiella-containing vacuole requires CLTC (clathrin heavy chain). Autophagy 14:1710 –1725. https://doi.org/10.1080/15548627.2018.1483806.
13. Mulye M, Samanta D, Winfree S, Heinzen RA, Gilk SD. 2017. Elevated cholesterol in the Coxiella burnetii intracellular niche is bacteriolytic. mBio 8:e02313-16. https://doi.org/10.1128/mBio.02313-16.
14. Onyenwoke RU, Brenman JE. 2015. Lysosomal storage diseases—regulating neurodegeneration. J Exp Neurosci 9:81–91. https://doi.org/10.4137/JEN.S25475.
15. Settembre C, Fraldi A, Medina DL, Ballabio A. 2013. Signals from the lysosome: a control centre for cellular clearance and energy metabolism. Nat Rev Mol Cell Biol 14:283–296. https://doi.org/10.1038/nrm3565.
16. Raben N, Puertollano R. 2016. TFEB and TFE3: linking lysosomes to cellular adaptation to stress. Annu Rev Cell Dev Biol 32:255–278. https://doi.org/10.1146/annurev-cellbio-111315-125407.
17. Sardiello M, Palmieri M, di Ronza A, Medina DL, Valenza M, Gennarino VA, Di Malta C, Donaudy F, Embrione V, Polishchuk RS, Banfi S, Parenti G, Cattaneo E, Ballabio A. 2009. A gene network regulating lysosomal biogenesis and function. Science 325:473– 477. https://doi.org/10.1126/science.1174447.
18. Martina JA, Diab HI, Lishu L, Jeong AL, Patange S, Raben N, Puertollano R. 2014. The nutrient-responsive transcription factor TFE3 promotes autophagy, lysosomal biogenesis, and clearance of cellular debris. Sci Signal 7:ra9. https://doi.org/10.1126/scisignal.2004754.
19. Settembre C, Zoncu R, Medina DL, Vetrini F, Erdin S, Erdin S, Huynh T, Ferron M, Karsenty G, Vellard MC, Facchinetti V, Sabatini DM, Ballabio A. 2012. A lysosome-to-nucleus signalling mechanism senses and regulates the lysosome via mTOR and TFEB. EMBO J 31:1095–1108. https://doi.org/10.1038/emboj.2012.32.
20. Roczniak-Ferguson A, Petit CS, Froehlich F, Qian S, Ky J, Angarola B, Walther TC, Ferguson SM. 2012. The transcription factor TFEB links mTORC1 signaling to transcriptional control of lysosome homeostasis. Sci Signal 5:ra42. https://doi.org/10.1126/scisignal.2002790.
21. Martina JA, Chen Y, Gucek M, Puertollano R. 2012. MTORC1 functions as a transcriptional regulator of autophagy by preventing nuclear transport of TFEB. Autophagy 8:903–914. https://doi.org/10.4161/auto.19653.
22. Medina DL, Di Paola S, Peluso I, Armani A, De Stefani D, Venditti R, Montefusco S, Scotto-Rosato A, Prezioso C, Forrester A, Settembre C, Wang WY, Gao Q, Xu HX, Sandri M, Rizzuto R, De Matteis MA, Ballabio A. 2015. Lysosomal calcium signalling regulates autophagy through calcineurin and TFEB. Nat Cell Biol 17:288 –299. https://doi.org/10.1038/ncb3114.
23. Palmieri M, Impey S, Kang H, di Ronza A, Pelz C, Sardiello M, Ballabio A. 2011. Characterization of the CLEAR network reveals an integrated control of cellular clearance pathways. Hum Mol Genet 20:3852–3866. https://doi.org/10.1093/hmg/ddr306.
24. Winchell CG, Dragan AL, Brann KR, Onyilagha FI, Kurten RC, Voth DE. 2018. Coxiella burnetii subverts p62/Sequestosome 1 and activates Nrf2 signaling in human macrophages. Infect Immun 86:e00608-17. https://doi.org/10.1128/IAI.00608-17.
25. Howe D, Melnicakova J, Barak I, Heinzen RA. 2003. Maturation of the Coxiella burnetii parasitophorous vacuole requires bacterial protein synthesis but not replication. Cell Microbiol 5:469–480. https://doi.org/10.1046/j.1462-5822.2003.00293.x.
26. Romano PS, Gutierrez MG, Beron W, Rabinovitch M, Colombo MI. 2007. The autophagic pathway is actively modulated by phase II Coxiella burnetii to efficiently replicate in the host cell. Cell Microbiol 9:891–909. https://doi.org/10.1111/j.1462-5822.2006.00838.x.
27. Newton HJ, McDonough JA, Roy CR. 2013. Effector protein translocation by the Coxiella burnetii Dot/Icm type IV secretion system requires endocytic maturation of the pathogen-occupied vacuole. PLoS One 8:e54566. https://doi.org/10.1371/journal.pone.0054566.
28. Larson CL, Sandoz KM, Cockrell DC, Heinzen RA. 2019. Noncanonical inhibition of mTORC1 by Coxiella burnetii promotes replication within a phagolysosome-like vacuole. mBio 10:e02816-18. https://doi.org/10.1128/mBio.02816-18.
29. Parra-Millan R, Guerrero-Gomez D, Ayerbe-Algaba R, Pachon-Ibanez ME, Miranda-Vizuete A, Pachon J, Smani Y. 2018. Intracellular trafficking and persistence of Acinetobacter baumannii requires transcription factor EB. mSphere 3:e00106-18. https://doi.org/10.1128/mSphere.00106-18.
30. Visvikis O, Ihuegbu N, Labed SA, Luhachack LG, Alves AF, Wollenberg AC, Stuart LM, Stormo GD, Irazoqui JE. 2014. Innate host defense requires TFEB-mediated transcription of cytoprotective and antimicrobial genes. Immunity 40:896 –909. https://doi.org/10.1016/j.immuni.2014.05.002.
31. Maurer K, Reyes-Robles T, Alonzo F, III, Durbin J, Torres VJ, Cadwell K. 2015. Autophagy mediates tolerance to Staphylococcus aureus alpha-toxin. Cell Host Microbe 17:429–440. https://doi.org/10.1016/j.chom.2015.03.001.
32. Najibi M, Labed SA, Visvikis O, Irazoqui JE. 2016. An evolutionarily conserved PLC-PKD-TFEB pathway for host defense. Cell Rep 15:1728 –1742. https://doi.org/10.1016/j.celrep.2016.04.052.
33. Ouimet M, Koster S, Sakowski E, Ramkhelawon B, van Solingen C, Oldebeken S, Karunakaran D, Portal-Celhay C, Sheedy FJ, Ray TD, Cecchini K, Zamore PD, Rayner KJ, Marcel YL, Philips JA, Moore KJ. 2016. Mycobacterium tuberculosis induces the miR-33 locus to reprogram autophagy and host lipid metabolism. Nat Immunol 17:677– 686. https://doi.org/10.1038/ni.3434.
34. Bisle S, Klingenbeck L, Borges V, Sobotta K, Schulze-Luehrmann J, Menge C, Heydel C, Gomes JP, Lührmann A. 2016. The inhibition of the apoptosis pathway by the Coxiella burnetii effector protein CaeA requires the EK repetition motif, but is independent of survivin. Virulence 7:400 – 412. https://doi.org/10.1080/21505594.2016.1139280.
35. Schafer W, Eckart RA, Schmid B, Cagkoylu H, Hof K, Muller YA, Amin B, Luhrmann A. 2017. Nuclear trafficking of the anti-apoptotic Coxiella burnetii effector protein AnkG requires binding to p32 and importin-alpha1. Cell Microbiol 19:e12634. https://doi.org/10.1111/cmi.12634.
36. Weber MM, Faris R, McLachlan J, Tellez A, Wright WU, Galvan G, Luo ZQ, Samuel JE. 2016. Modulation of the host transcriptome by Coxiella burnetii nuclear effector Cbu1314. Microbes Infect 18:336 –345. https://doi.org/10.1016/j.micinf.2016.01.003.
37. Bajaj L, Lotfi P, Pal R, Ronza AD, Sharma J, Sardiello M. 2019. Lysosome biogenesis in health and disease. J Neurochem 148:573–589. https://doi.org/10.1111/jnc.14564.
38. Omsland A, Beare PA, Hill J, Cockrell DC, Howe D, Hansen B, Samuel JE, Heinzen RA. 2011. Isolation from animal tissue and genetic transformation of Coxiella burnetii are facilitated by an improved axenic growth medium. Appl Environ Microbiol 77:3720 –3725. https://doi.org/10.1128/AEM.02826-10.
39. Stoehr G, Schaab C, Graumann J, Mann M. 2013. A SILAC-based approach identifies substrates of caspase-dependent cleavage upon TRAIL-

induced apoptosis. Mol Cell Proteomics 12:1436 –1450. https://doi.org/10.1074/mcp.M112.024679.
40. Scott NE, Rogers LD, Prudova A, Brown NF, Fortelny N, Overall CM, Foster LJ. 2017. Interactome disassembly during apoptosis occurs independent of caspase cleavage. Mol Syst Biol 13:906. https://doi.org/10.15252/msb.20167067.
41. Humphrey SJ, Azimifar SB, Mann M. 2015. High-throughput phosphoproteomics reveals in vivo insulin signaling dynamics. Nat Biotechnol 33:990 –995. https://doi.org/10.1038/nbt.3327.
42. Rappsilber J, Mann M, Ishihama Y. 2007. Protocol for micro-purification, enrichment, pre-fractionation and storage of peptides for proteomics using StageTips. Nat Protoc 2:1896–1906. https://doi.org/10.1038/nprot.2007.261.
43. Cox J, Mann M. 2008. MaxQuant enables high peptide identification rates, individualized p.p.b.-range mass accuracies and proteome-wide protein quantification. Nat Biotechnol 26:1367–1372. https://doi.org/10.1038/nbt.1511.
44. Tyanova S, Temu T, Sinitcyn P, Carlson A, Hein MY, Geiger T, Mann M, Cox J. 2016. The Perseus computational platform for comprehensive analysis of (prote)omics data. Nat Methods 13:731–740. https://doi.org/10.1038/nmeth.3901.
45. Jaton K, Peter O, Raoult D, Tissot JD, Greub G. 2013. Development of a high throughput PCR to detect Coxiella burnetii and its application in a diagnostic laboratory over a 7-year period. New Microbes New Infect 1:6 –12. https://doi.org/10.1002/2052-2975.8.
46. Schindelin J, Arganda-Carreras I, Frise E, Kaynig V, Longair M, Pietzsch T, Preibisch S, Rueden C, Saalfeld S, Schmid B, Tinevez JY, White DJ, Hartenstein V, Eliceiri K, Tomancak P, Cardona A. 2012. Fiji: an open-source platform for biological-image analysis. Nat Methods 9:676 – 682. https://doi.org/10.1038/nmeth.2019.
47. Benjamini Y, Hochberg Y. 1995. Controlling the false discovery rate: a practical and powerful approach to multiple testing. JR Statist Soc B 57:289 –300. https://www.jstor.org/stable/2346101.

3.3 Results

Human epithelial cells infected with *C. burnetii* resulted in upregulation of CLEAR network of genes.

In order to validate that *C. burnetii* infection leads to increased expression of genes in the CLEAR network, a subset of these genes was examined following infection of human epithelial cells. It was important to determine whether there was any host type specificity to this response as the original SILAC study was performed using THP-1 cells. However, much of the research examining TFEB localisation was performed using HeLa cells. RNA was extracted from either uninfected HeLa cells or HeLa cells persistently infected with *C. burnetii.* The transcript of the lysosomal and autophagy genes: TPP1, LAMP1, CTSF, MCOLN1, and the non-CLEAR control HOXA9 was measured using quantitative real time PCR and compared between uninfected and infected samples (Figure 3.1). A fold increase of 2 in case of TPP1 and LAMP1, approximately 1.8 fold increase of CTSF and MCOLN1 and a fold change of less than 1 was observed in the case of HOXA9. These results indicate, that as observed in THP1 cells, activation of TFEB during *C. burnetii* infection in human epithelial cells upregulation of CLEAR transcripts.

Expression of lysosomal proteins, TPP1 and LAMP1 was confirmed from HeLa CCL2 infected with *C. burnetii* at a multiplicity of infection of 100 at 1, 3 and 5 days post infection. A representative immunoblot from 3 independent biological replicates demonstrates an increase in the expression of LAMP1 and TPP1 in cells infected for 3 and 5 days. This western blot data confirms that the SILAC data obtained is not specific to macrophages

alone and that epithelial cells can also demonstrate an increase in CLEAR regulated proteins.

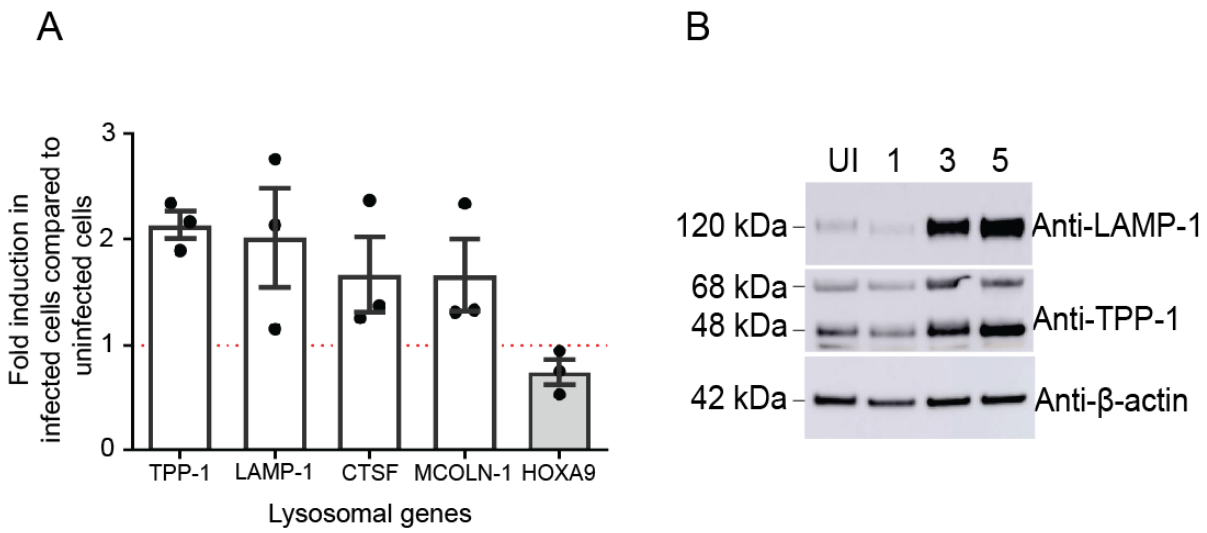

Figure 3.1 Upregulation of components of the CLEAR network in human epithelial cells infected with *C. burnetii*.

(A) Quantitative real time PCR (qRT-PCR) analysis demonstrating the expression of lysosomal and autophagy genes: TPP1, LAMP1, CTSF, MCOLN1, and HOXA9 (in grey, a non-CLEAR control) in persistently infected HeLa cells in comparison to uninfected cells. This data supports the likely activation of TFEB during *C. burnetii* infection of epithelial cells, n = 3.

(B) Expression of selected lysosomal proteins in human epithelial cells infected with *C. burnetii* (MOI, 100) throughout infection. Immunoblot analysis to determine the relative amounts of lysosomal proteins LAMP1 and TPP1 in human epithelial cells infected with *C. burnetii* at 1, 3 and 5 days post infection, in comparison to the uninfected HeLa cells (UI). Protein expression clearly demonstrates an increase in the relative abundance of LAMP1 and TPP1 as infection progresses. Immunoblot is representative of three independent biological replicates.

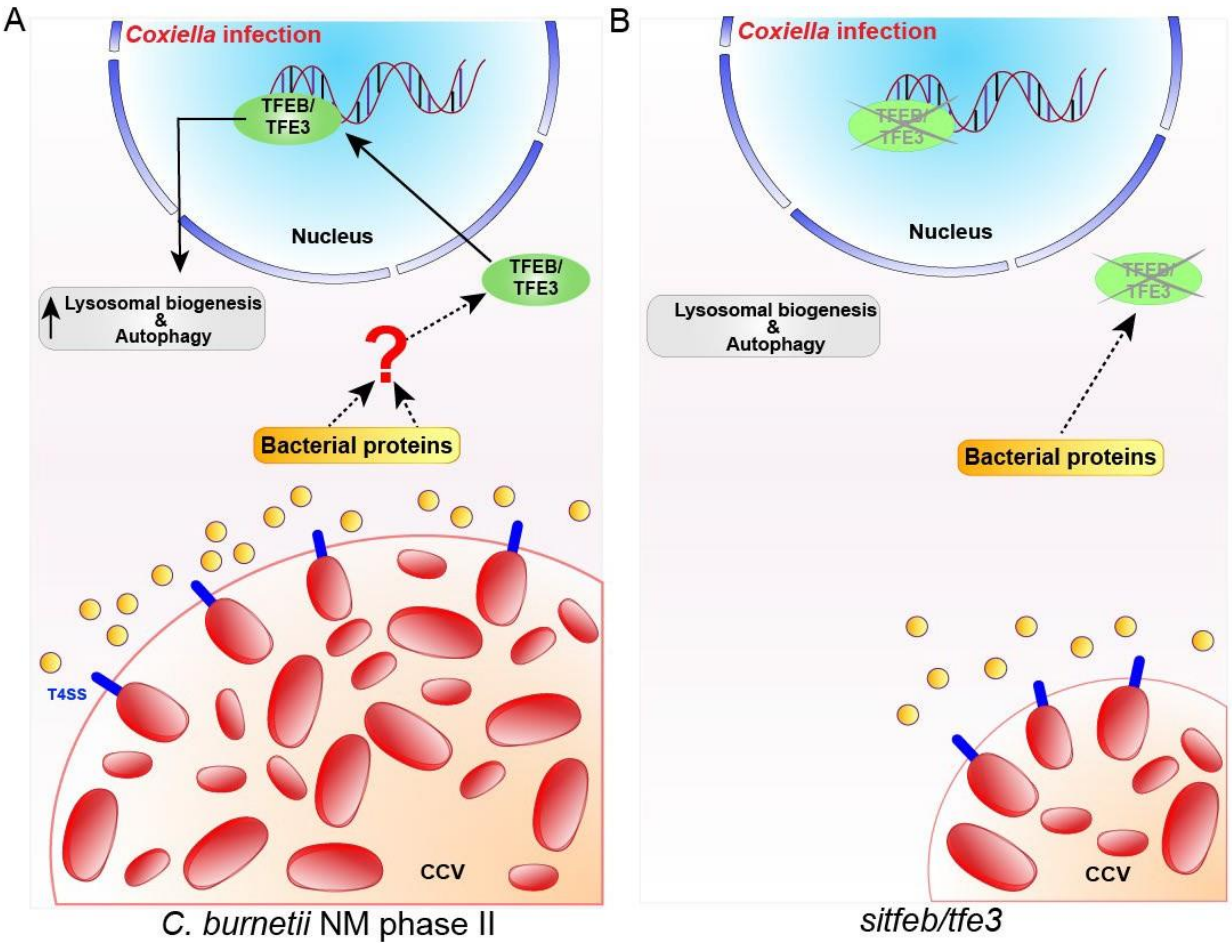

Figure 3.2 Schematic summary of Chapter 3 findings.

(A) The research presented in this Chapter indicates that during normal infection of human cells with *C. burnetii* NM phase II, there are bacterial effector proteins (in yellow) translocated out of CCV that facilitates nuclear localisation of TFEB/TFE3 (in green) subsequently inducing transcription of genes important for lysosome biogenesis and autophagy to support expansion of the CCV. (B) Silencing the host transcription factors TFEB and TFE3, results in a significant decrease in the size of CCV size, presumably due to reduced autophagy and lysosome biogenesis.

Chapter 4

Identification of *C. burnetii* effector proteins that modulate TFEB

4.1 Introduction

In order to replicate within a lysosome-like environment, *C. burnetii* utilises a type IV secretion system (T4SS) to inject approximately 150 effector proteins into the host cytosol [209]. In doing so, *C. burnetii*, subverts many host cellular processes and signaling pathways to establish itself as a successful intracellular pathogen [81, 121, 148, 210]. As demonstrated in Chapter 3 of this thesis, the transcriptional upregulation of lysosome biogenesis is an important aspect in the biogenesis of the CCV. The host transcription factors TFEB and TFE3 are responsible for upregulating expression of many factors important for lysosome biogenesis and autophagy [211, 212], and are also required for CCV expansion. The transcription factors TFEB and TFE3 not only play a role in lysosomal biogenesis and autophagy [175, 189, 191, 213], they are also involved in the regulation of multiple cellular processes and are also known to play an important role in innate immune responses [185, 214].

Data presented in Chapter 3 indicated that nuclear translocation of TFEB and TFE3 was dependent on *C. burnetii* and more specifically on the activity of the Dot/Icm T4SS. When bacterial protein synthesis was inhibited using chloramphenicol, nuclear translocation of TFEB/TFE3 was reversed. In human epithelial cells infected with Dot/Icm-deficient *C. burnetii*, nuclear localisation of TFEB and TFE3 was significantly reduced [121, 211, 215].

Cellular clearance of damaged debris is extremely crucial for human health since defects in lysosomal biogenesis and autophagy have been associated with diseases such as

lysosomal storage disorders (LSD) [216], neurodegenerative diseases [185, 217], and even in many cancers [213]. Several recent studies using animal models for neurodegenerative diseases have demonstrated the role of the lysosomal-autophagic pathway and its impact on significant human diseases such as Parkinson's disease (PD), Alzheimer's disease (AD) and Huntington's disease (HD) [201]. It was observed that pharmacological and genetic activation of TFEB helps block disease progression by increasing autophagic degradation [202]. As these transcription factors are global regulators of various cellular processes, the control of TFEB/TFE3 transcriptional activity is considered as a promising therapeutic tool for several significant human disease states [175, 218].

Our initial studies clearly indicate the importance of TFEB and TFE3 in the vacuolar expansion of *C. burnetii* [211]. Therefore, understanding the unique mechanisms employed by *C. burnetii* to manipulate lysosomal biogenesis and autophagy may provide important new insight into a range of human diseases with the possibility of revealing new physiological ways to intervene in the progression of significant human disease states.

Data presented in Chapter 3 demonstrated that TFEB and TFE3 contribute to the expansion of the CCV leading to the hypothesis that one or more T4SS effectors is responsible for the nuclear localisation of these transcription factors during *C. burnetii* infection. In order to identify *C. burnetii* effector proteins that contribute to nuclear localisation of these host transcription factors; an immunofluorescence screen was performed to examine the localisation of TFEB in the presence of individual *C. burnetii*

effectors. This chapter details the identification and characterisation of the previously uncharacterised *C. burnetii* putative effector proteins, CBU1701 and CBU2016, and their role in the nuclear localisation of TFEB and TFE3. Both novel *C. burnetii* proteins investigated in this study have been identified previously as putative effectors [132, 133]. To understand the function of these proteins, stable cell lines were engineered to allow doxycycline-inducible expression of each effector. When effector expression was induced, nuclear localisation of TFEB and TFE3 was observed using confocal microscopy. Expression of CBU1701 and CBU2016 resulted in a significant change in the host proteome as observed using an unbiased whole cell proteomics approach. However, surprisingly these changes did not directly correlate with TFEB activation suggesting TFEB nuclear localisation during expression of these proteins may be either an indirect process and/or uncoupled from activation of host transcription.

4.2 Results

4.2.1 Identification of *C. burnetii* T4SS effectors that induces nuclear translocation of HeLa TFEB-GFP

Following establishment of the replicative CCV, inhibition of bacterial protein synthesis using chloramphenicol reversed the nuclear localisation of TFEB-GFP [211]. In addition, infection with Dot/Icm-deficient *C. burnetii* did not induce nuclear localisation of TFEB. This prompted us to hypothesise that individual *C. burnetii* Dot/Icm effectors may stimulate the nuclear localisation of TFEB. In order to investigate this, we employed an immunofluorescence screen to identify *C. burnetii* effector proteins that induce nuclear localisation of TFEB-GFP. For this, genes of known or putative *C. burnetii* effectors, were cloned into the mammalian expression vector pcDNA-4 ^{TM}T/O to be expressed with an N-terminal 3xFLAG tag (as detailed in Table 4.1). These effector constructs were then individually transfected into HeLa TFEB-GFP cells for 16 hours. Post transfection, cells were fixed and stained for anti-FLAG to detect the effector proteins and the nuclei was visualised by staining with DAPI (Figure 4.1). Confocal microscopy was used to examine the effector expression and subsequent localisation of TFEB-GFP. A duplicate set of transfected cells were treated with 50 µg/mL chloroquine (CQ), a lysomotropic agent that alters the pH of the lysosomes, for 24 hours at 37 °C. Treatment with CQ induces translocation of TFEB-GFP from the cytoplasm into the nucleus, thus acting as a positive control for nuclear localisation of TFEB-GFP. Chloroquine treatment of transfected cells also gave us an opportunity to examine whether any *C. burnetii* effectors induced cytoplasmic retention of activated TFEB. As anticipated, the screen revealed that the majority of the effectors did not impact TFEB-GFP localisation.

Table 4.1 C. burnetii effectors used in the TFEB-GFP localisation screen.

ORF	OTHER NAME	EVIDENCE for T4SS translocation[A]	REFERENCE
CBU0012	-	BlaM-Lp (1 %)	[132]
CBU0021	Cig2, CetCb1, CvpB	BlaM-Cb and CyaA-Lp	[133], [81], [144]
CBU0041	CoxCC1, CirA	BlaM-Lp (70 %)	[129], [132]
CBU0062	Cem1	CyaA-Lp	[219]
CBU0069	AnkP	BlaM-Lp (1 %)	[132]
CBU0071	AnkP	CyaA-Lp	[220]
CBU0072	AnkA	CyaA-Lp	[139], [220]
CBU0077	MceA	BlaM-Cb, visualisation of native translocated protein using MceA specific antibody	[121], [141]
CBU0080	-	CyaA-Lp, BlaM-Lp (70 %)	[121], [132]
CBU0113	Cem2	BlaM-Lp (7 %)	[132], [219]
CBU0122	-	CyaA-Lp	[130]
CBU0129	CoxCC2, AnkI	BlaM-Lp (70 %)	[129], [132]
CBU0144/ 0145	AnkB	CyaA-Lp	[139], [220]

CBU0175	CoxK1	BlaM-Lp (20 %)	[129], [132]
CBU0183	-	BlaM-Lp (20 %)	[132]
CBU0201	AnkC	BlaM-Lp (1 %)	[132]
CBU0212	-	BlaM-Lp (10 %)	[132]
CBU0270	-	BlaM-Lp (1 %)	[132]
CBU0295	-	CyaA-Lp, BlaM-Lp (2 %)	[121], [132]
CBU0329	-	CyaA-Lp	[121]
CBU0344	-	BlaM-Lp (5 %)	[132]
CBU0372	-	BlaM-Lp (20 %)	[132]
CBU0375	-	BlaM-Lp (35 %)	[132]
CBU0376	-	BlaM-Lp (7 %)	[132]
CBU0388	CetCb2	BlaM-Lp (40 %)	[219], [132]
CBU0393	-	BlaM-Lp (1 %)	[132]
CBU0410	CoxCC3	BlaM-Lp (45 %)	[129], [132]
CBU0410	CoxCC3	BlaM-Lp (45 %)	[129], [132]
CBU0414	CoxH1	BlaM-Lp (45 %)	[129], [132]
CBU0425	CirB	CyaA-Lp, BlaM-Lp (90 %)	[121], [132]
CBU0447	AnkF	CyaA-Lp	[139], [220]
CBU0469	-	BlaM-Lp (1 %)	[132]
CBU0513	-	BlaM-Lp (20 %)	[132]
CBU0534	-	CyaA-Lp	[144]
CBU0590	-	BlaM-Lp (70 %)	[132]
CBU0606	-	BlaM-Lp (2 %)	[132]

CBU0626	CvpF	BlaM-Cb	[145]
CBU0635	-	CyaA-Lp	[121]
CBU0637	-	BlaM-Lp (1 %)	[132]
CBU0665	CvpA	BlaM-Lp (3 %)	[132], [146]
CBU0773	-	BlaM-Lp (5 %)	[132]
CBU0781	AnkG	CyaA-Lp	[139], [220]
CBU0794	CoxCC4	BlaM-Lp (80 %)	[129], [132]
CBU0801	RimI, CoxH2	BlaM-Lp (10 %)	[129], [132]
CBU0814	CoxU1	BlaM-Lp (10 %)	[129], [132]
CBU0881	CoxCC5	BlaM-Lp (80 %)	[129], [132]
CBU0885	CetCb4	BlaM-Lp (1 %)	[133], [132]
CBU0937	CoxDFB1, CirC	BlaM-Lp (2 %)	[129], [132]
CBU0978	Cem3	CyaA-Lp	[219]
CBU1025	AnkH	CyaA-Lp	[220]
CBU1045	CoxDFB2	BlaM-Lp (40 %)	[129], [132]
CBU1063	Cem4	CyaA-Lp	[219]
CBU1079	-	BlaM-Lp (5 %)	[132]
CBU1102	-	BlaM-Lp (70 %)	[132]
CBU1107	-	CyaA-Lp	[121]
CBU1108	-	CyaA-Lp	[121]
CBU1110	-	BlaM-Lp (40 %)	[132]

CBU1150	-	BlaM-Lp (1 %)	[132]
CBU1198	-	BlaM-Lp (75 %)	[132]
CBU1213	AnkI	CyaA-Lp	[220]
CBU1217	CoxU2	BlaM-Lp (10 %)	[129], [132]
CBU1253/ 1254	AnkJ	CyaA-Lp	[220]
CBU1314	CoxCC6	BlaM-Lp (2 %)	[129], [132]
CBU1335	-	BlaM-Lp	Unpublished data
CBU1370	Cem5	CyaA-Lp	[219]
CBU1379	CoxK2	BlaM-Lp (1 %)	[129], [132]
CBU1387	Cem6	CyaA-Lp	[219]
CBU1406	CoxDFB3	BlaM-Lp (40 %)	[129], [132]
CBU1409	Cem7	CyaA-Lp	[219]
CBU1425	CoxDFB4	BlaM-Lp (1 %)	[129], [132]
CBU1434	-	BlaM-Lp (1 %)	[132]
CBU1457	CoxTPR1	BlaM-Lp (2 %)	[129], [132]
CBU1460	CoxCC8, Cig44	BlaM-Lp (40 %)	[129], [132],[140]
CBU1461	CoxCC8	BlaM-Lp (2 %)	[129], [132]
CBU1485	-	BlaM-Lp	Unpublished data

CBU1493	-	BlaM-Lp	Unpublished data
CBU1524	CoxCC9, CaeA	CyaA-Lp, BlaM-Lp (10 %)	[129], [121], [152], [132]
CBU1525	-	CyaA-Lp	[121], [132]
CBU1530	-	CyaA-Lp	[130]
CBU1532	CaeB	CyaA-Lp	[121], [152]
CBU1543	CoxCC10, Cig49	BlaM-Lp (25 %)	[129], [132],[140]
CBU1556	CoxCC11, CvpC	BlaM-Lp (50 %)	[129], [132], [144]
CBU1566	-	BlaM-Lp (5 %)	[132]
CBU1569	CoxCC12	BlaM-Lp (90 %)	[129], [132]
CBU1576	-	BlaM-Lp (2 %)	[132]
CBU1594	-	BlaM-Lp (5 %)	[132]
CBU1599	CoxCC13	BlaM-Lp (10 %)	[129], [132]
CBU1607	-	BlaM-Lp (5 %)	[132]
CBU1614	-	CyaA-Lp	[130]
CBU1620	-	BlaM-Lp (90 %)	[132]
CBU1634a	Cem8	CyaA-Lp	[219]
CBU1636	CoxCC14	BlaM-Lp (1 %)	[129], [132]
CBU1639	-	BlaM-Lp (4 %)	[132]
CBU1665	-	BlaM-Lp (1 %)	[132]

CBU1676	Cem9	CyaA-Lp	[219], [144]
CBU1677	-	BlaM-Lp (5 %)	[132]
CBU1685	-	BlaM-Lp (1 %)	[132], [130]
CBU1686	CetCb5	Lifshitz scored	[133], [130]
CBU1724	CetCb6	Lifshitz scored	[133]
CBU1751	Cig57, CoxDFB5	BlaM-Lp (50 %)	[129], [132],[140]
CBU1752	-	CyaA-Lp	[130]
CBU1754	-	BlaM-Lp (2 %)	[132]
CBU1757	AnkM	CyaA-Lp	[220]
CBU1769	CoxH3	BlaM-Lp (1 %)	[129], [132]
CBU1776	-	CyaA-Lp	[121]
CBU1780	-	BlaM-Cb	[81]
CBU1789	-	BlaM-Lp (1 %)	[132]
CBU1790	-	BlaM-Lp (1 %)	[132]
CBU1794	Cem10	CyaA-Lp	[219]
CBU1818	Cem11, CvpD	CyaA-Lp	[219], [144]
CBU1819	-	CyaA-Lp	[144]
CBU1823	CoxH4, Cig61	BlaM-Lp (50 %)	[129], [121], [132], [140]
CBU1825	CoxDFB5	BlaM-Lp (50 %)	[129], [121], [132]

CBU1863	CvpE	CyaA-Lp	[144]
CBU1963	-	CyaA-Lp	[121]
CBU2007	Cem12	BlaM-Lp (90 %)	[132], [219]
CBU2013	Cem13	BlaM-Lp (50 %)	[132], [219]
CBU2016	-	BlaM-Lp (1 %)	[132]
CBU2028	-	BlaM-Lp (1 %)	[132]
CBU2052	CoxCC15, CirD	BlaM-Lp (90 %)	[129], [121], [132]
CBU2056	-	CyaA-Lp	[121]
CBU2059	CirE	BlaM-Lp (40 %)	[121], [132]
CBU2064	-	BlaM-Lp (1 %)	[132]
CBU2076	-	BlaM-Lp (1 %)	[132]
CBU2078	CoxFIC1	BlaM-Lp (10 %)	[129], [132]
CBUA0006	CpeA	CyaA-Lp	[122]
CBUA0013	CpeB	CyaA-Lp	[122]
CBUA0014	CpeC	BlaM-Lp (10 %)	[122], [132]
CBUA0015	CpeD	BlaM-Lp (90 %)	[122], [132]
CBUA0016	CpeE, CbhE	CyaA-Lp	[122]
CBUA0019	-	BlaM-Lp (1 %)	[132]
CBUA0020	-	BlaM-Lp (1 %)	[132]
CBUA0023	CpeF	CyaA-Lp	[122]
CBUK1130	AnkN	CyaA-Lp	[220]
CBUD1108	AnkO	CyaA-Lp	[220]

PUTATIVE EFFECTORS			
CBU0360	-	Lifshitz score = 6.55	[219]
CBU0584	-	Lifshitz scored = 5.69	[219]
CBU0602	-	Lifshitz scored = 6.39	[219]
CBU0879	-	Lifshitz scored = 10.81	[219]
CBU1209	-	Lifshitz scored = 5.78	[219]
CBU1263	-	Lifshitz scored = 5.31	[219]
CBU1298	-	Lifshitz scored = 8.57	[219]
CBU1334	-	Lifshitz scored = 6.48	[219]
CBU1452	-	Lifshitz scored = 10.13	[219]
CBU1533	-	Lifshitz scored = 5.03	[219]
CBU1560	-	Lifshitz scored = 6.35	[219]
CBU1619	-	Lifshitz scored = 7.07	[219]
CBU1693	-	Lifshitz scored = 5.89	[219]
CBU1701	-	Lifshitz scored = 5.19	[219]
CBU1806	-	Lifshitz scored = 5.04	[219]
CBU2050	-	Lifshitz scored = 5.00	[219]

[A] List of *C. burnetii* substrates identified or confirmed for translocation based on bioinformatics screen, *L. pneumophila* based adenylate cyclase translocation assay (CyaA-Lp), C. *burnetii* BlaM-based translocation assay (BlaM-Cb) or *L. pneumophila* BlaM-based translocation assay (BlaM-Lp).

[B] CBU1701 (in red), CBU2016 (in red) are the *C. burnetii* substrates identified in this TFEB-GFP screen demonstrated to induce nuclear localisation of TFEB. In order to show, not all *C. burnetii* proteins are involved in the nuclear translocation of TFEB-GFP, CBU2059 (in red) is shown in Figure 4.2 as a negative control for the screen.

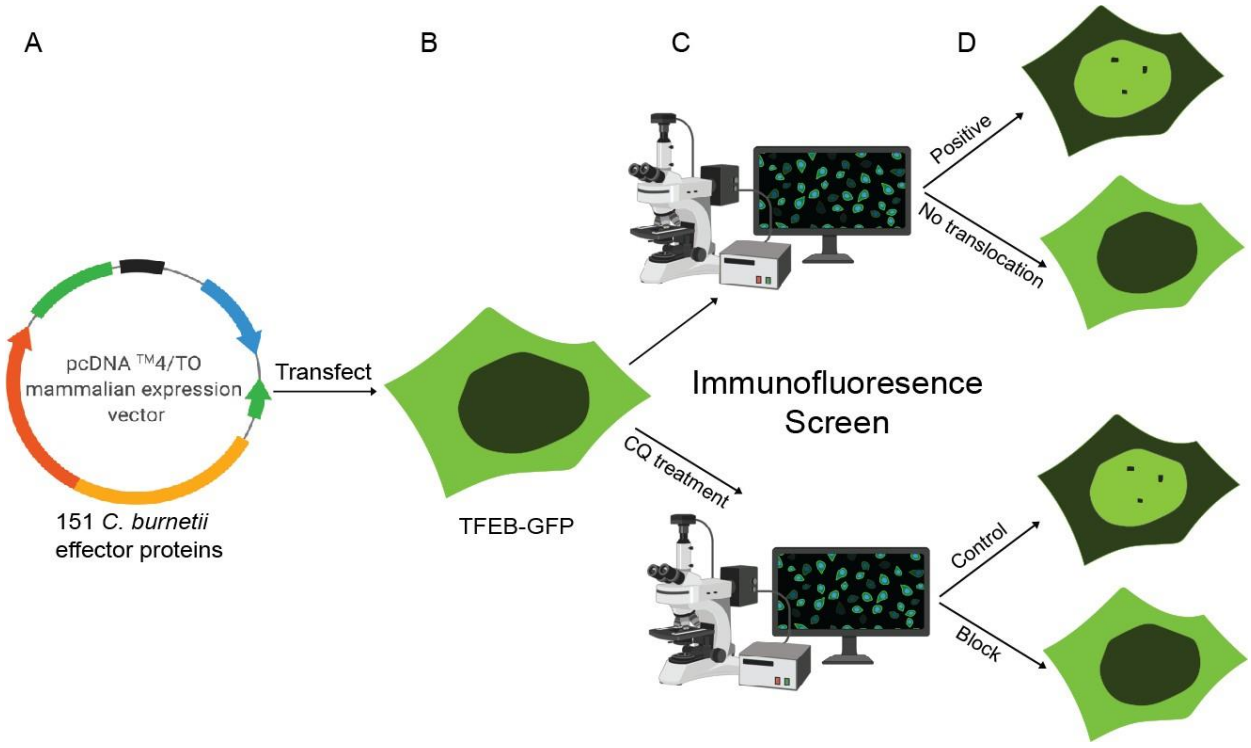

Figure 4.1 Schematic of immunofluorescence screen to identify *C. burnetii* effectors that influence TFEB localisation.

(A) 151 *C. burnetii* known or putative effector proteins (Table 4.1) were cloned into pcDNA ^{TM}4/TO mammalian expression vector for expression in eukaryotic cells with an N- terminal 3xFLAG tag. (B) Cloned *C. burnetii* effectors were individually transfected into HeLa TFEB-GFP cells and incubated for 24h before cells were fixed. Duplicate wells of transfected cells were treated with 50 µg/mL chloroquine (CQ), a positive control which drives nuclear translocation of TFEB, for 24 hours at 37 °C. The ability of *C. burnetii* proteins to block the nuclear translocation and activation of TFEB, can be determined upon treatment with CQ. (C) A confocal microscope (Confocal Zeiss LSM700) was used to visually screen for effectors that were (D) positive for nuclear translocation of TFEB or to demonstrate no nuclear translocation.

4.2.2 Ectopically expression of ^{3xFLAG}CBU1701 and ^{3xFLAG}CBU2016 confirms two potential *C. burnetii* effectors that induce nuclear translocation of TFEB

The immunofluorescence screen depicted in Figure 4.1 identified two putative *C. burnetii* effectors that appear to influence the localisation of TFEB-GFP. Figure 4.2 demonstrates that ^{3xFLAG}CBU1701 (Figure 4.2 A) and ^{3xFLAG}CBU2016 (Figure 4.2 B) were identified as putative effectors that, when ectopically expressed in HeLa cells, induce nuclear localisation of TFEB. ^{3xFLAG}CBU2059 (Figure 4.2 C) is included in this figure as an exemplar result for the remaining *C. burnetii* proteins that were screened in this process. None of the other 149 *C. burnetii* proteins altered the localisation of TFEB-GFP. Importantly, no *C. burnetii* effectors were observed that interfered with CQ induction of TFEB-GFP nuclear localisation.

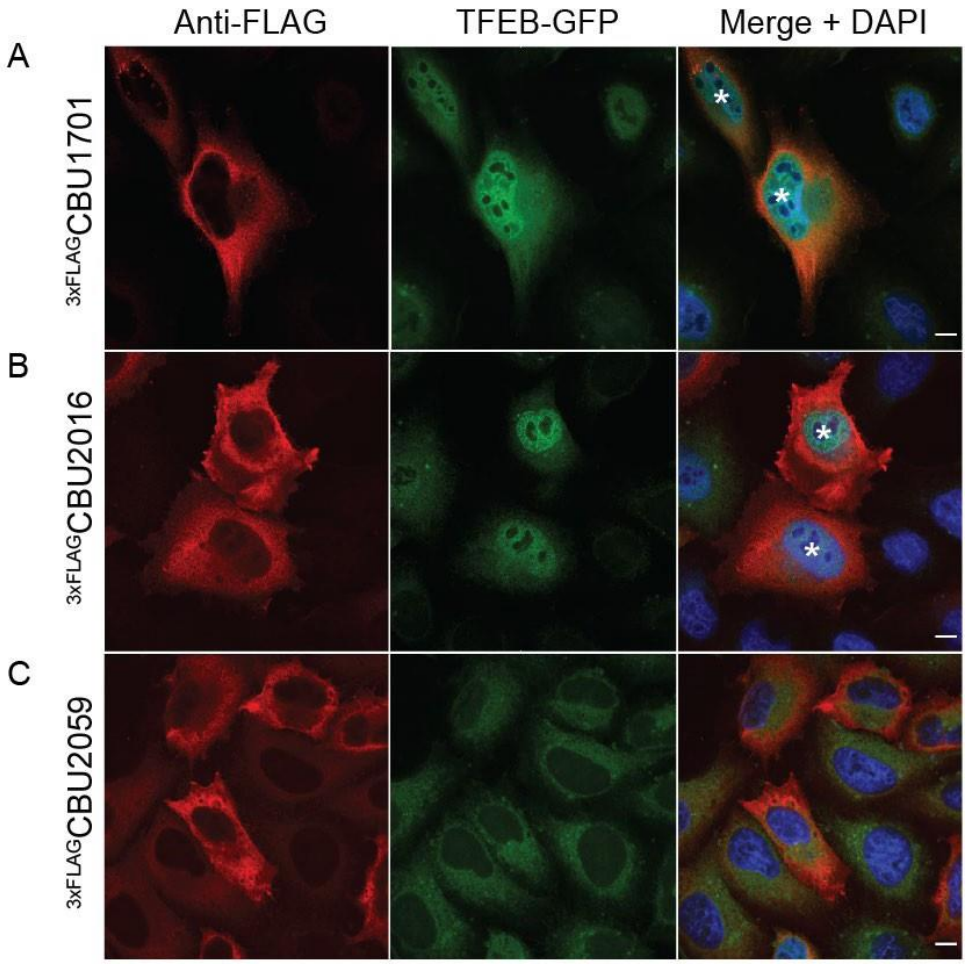

Figure 4.2 Ectopic expression of two *C. burnetii* putative effectors led to nuclear localisation of TFEB-GFP.

HeLa TFEB-GFP cells were transfected with 151 putative *C. burnetii* effectors and TFEB-GFP was monitored for altered localisation. Ectopic expression of (A) ^{3xFLAG}CBU1701 and (B) ^{3xFLAG}CBU2016 led to nuclear localisation of TFEB. (C) ^{3xFLAG}CBU2059 demonstrates the typical unaltered localisation of TFEB-GFP observed for expression of all other *C. burnetii* effectors. These confocal images are representative images of at least three biological replicates. 16 h post-transfection, cells were fixed and stained with anti-FLAG (red) and DAPI (nuclei). * indicates nuclear localisation of TFEB. Scale bars represent 10 µm.

4.2.3 Ectopic expression of full length and N-terminal region of ^{3xFLAG}CBU1701 in human epithelial cells

BLAST (Basic Local Alignment Search Tool) analysis (https://blast.ncbi.nlm.nih.gov/Blast.cgi) revealed that CBU1701 does not have any similarity to any other bacterial or non-bacterial protein nucleotide sequences. BLAST nucleotide suggested that CBU1701 has 100% conservation amongst all *C. burnetii* genomes.

The protein encoded by *cbu1701* is 52.082 kDa in length comprising of 468 amino acids. Bioinformatics analysis using TMHMM (Transmembrane Helices Hidden Markov Model) server version 2.0 (http://www.cbs.dtu.dk/services/TMHMM/), a programme that makes a prediction of the membrane-spanning regions and their orientation, revealed that there are 7 predicted transmembrane domains of CBU1701 encoded between amino acids 160 to 435 as depicted in Figure 4.3 A. The carboxy terminal region, from amino acid 419 to 468, of CBU1701 was found to have 98.20% identity to a region of a hypothetical ATPase from *C. burnetii* CbuG_Q212 strain and 73.53% identity to AAA family ATPase from *C. burnetii*. CBU1701 does not have an ATP binding motif and the amino-terminal half of CBU1701 does not have any homology to ATPase. The region that has high homology is not associated with the predicted ATPase activity so there is no evidence to suggest that CBU1701 has this activity.

To evaluate the subcellular localization of CBU1701, 3xFLAG tagged versions of full length, ^{3xFLAG}CBU1701, and the amino terminal region, ^{3xFLAG}CBU1701$^{1-159}$, were

ectopically expressed in HeLa cells. Figure 4.3 (A) shows the schematic representation of the full length (468 amino acid) protein, where the transmembrane domains are indicated in blue. The 159 amino acid, amino terminal region of this protein is also schematically represented. ^{3xFLAG}CBU1701 was found to be localised throughout the cytoplasm with a very strong peri-nuclear localisation pattern. This pattern of localisation was no longer observed for ^{3xFLAG}CBU1701$^{1-159}$ which lacks the predicted transmembrane domains. This truncated protein instead exhibited diffuse cytoplasmic localisation (Figure 4.3). The localisation for N terminal (CBU1701$^{1-159}$) seems to vary and no counterstaining using organelle marker was performed. Therefore, no further conclusion regarding the localisation of this truncation can be made.

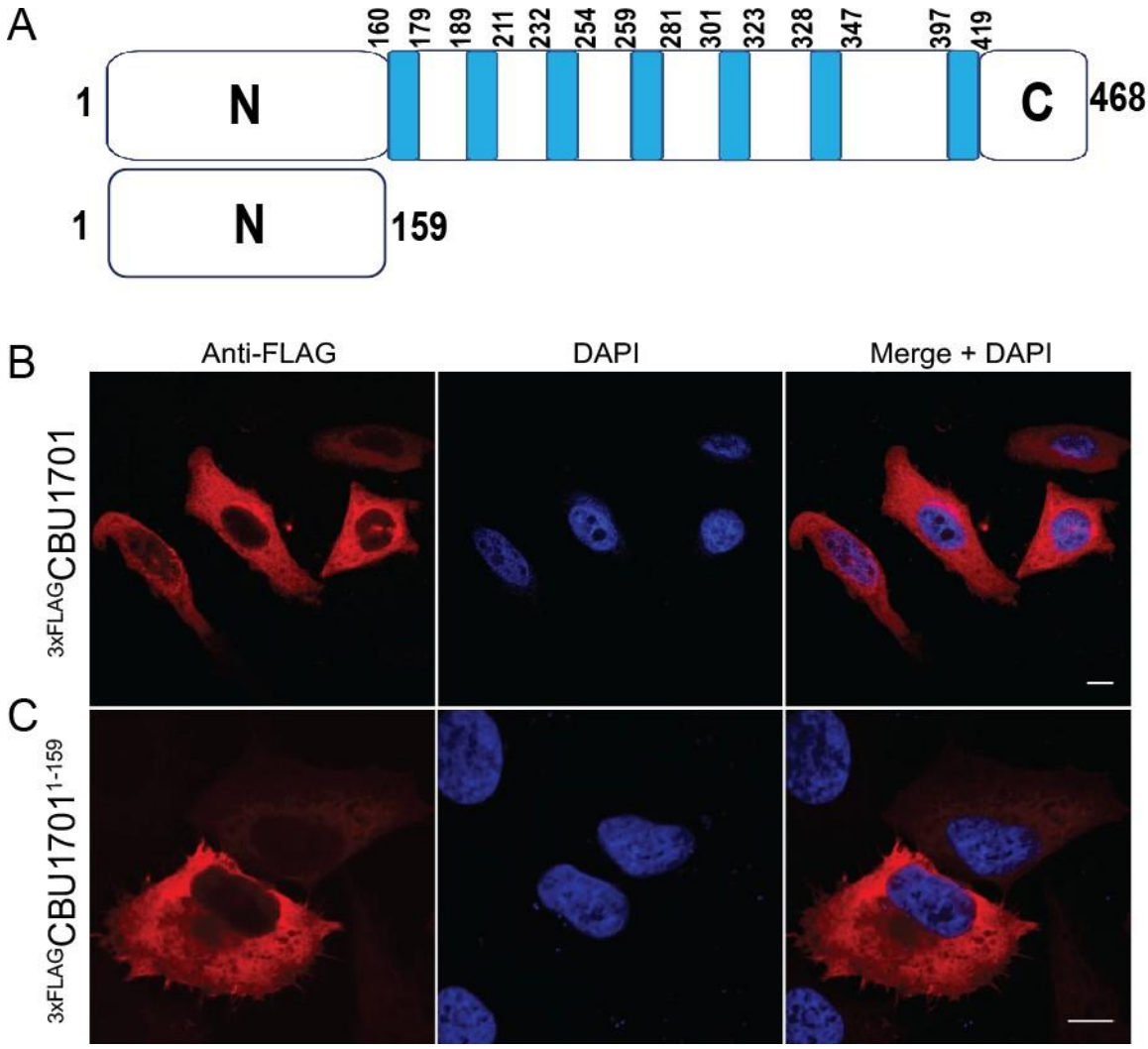

Figure 4.3 Subcellular localisation of full length and amino terminal region of ^{3xFLAG}CBU1701.

(A) Schematic representation of the full length (468 amino acids) and N-terminal region (159 amino acids) of CBU1701. Predicted transmembrane domains are displayed in blue in regions spanning residues from 160-419. (B) Representative confocal image of HeLa cells transfected with ^{3xFLAG}CBU1701 showed more accumulation of the protein near the nucleus and (C) localisation of ectopically expressed ^{3xFLAG}CBU1701$^{1-159}$ was observed uniformly through the cytoplasm. 16h post-transfection, cells were fixed and stained with anti-FLAG (red) and DAPI (nuclei). Scale bars 10 µm.

4.2.4 Representative co-localisation studies of full length and N-terminal region of ^{3xFLAG}CBU1701 with GFP-ATF6 in human epithelial cells to monitor ER localisation

Ectopic expression of ^{3xFLAG}CBU1701 resulted in enriched perinuclear signal indicating that the protein may at least partially be localised to the ER (endoplasmic reticulum). To examine this, co-localisation of ^{3xFLAG}CBU1701 and ^{3xFLAG}CBU1701$^{1-159}$ with GFP-ATF6 (amino terminally GFP tagged activated transcription factor 6) was determined using confocal microscopy. ATF6 is a membrane bound endoplasmic reticulum (ER) stress-regulated transcription factor and is involved in the regulation of ER stress response. This transcription factor is known to be involved in the unfolded protein response, a cellular response that results in the cleavage of ATF6 from ER when there is an accumulation of misfolded proteins [221]. Co-localisation studies using GFP-ATF6 suggested that ^{3xFLAG}CBU1701 at least partially co-localised with ATF6 protein in HeLa cells. However, this could be further validated in a more quantitative manner. To determine ER stress, western blot can be performed to look at the unfolded protein response. ^{3xFLAG}CBU1701$^{1-159}$ in-contrast, does not co-localise with the GFP-ATF6 construct (Figure 4.4).

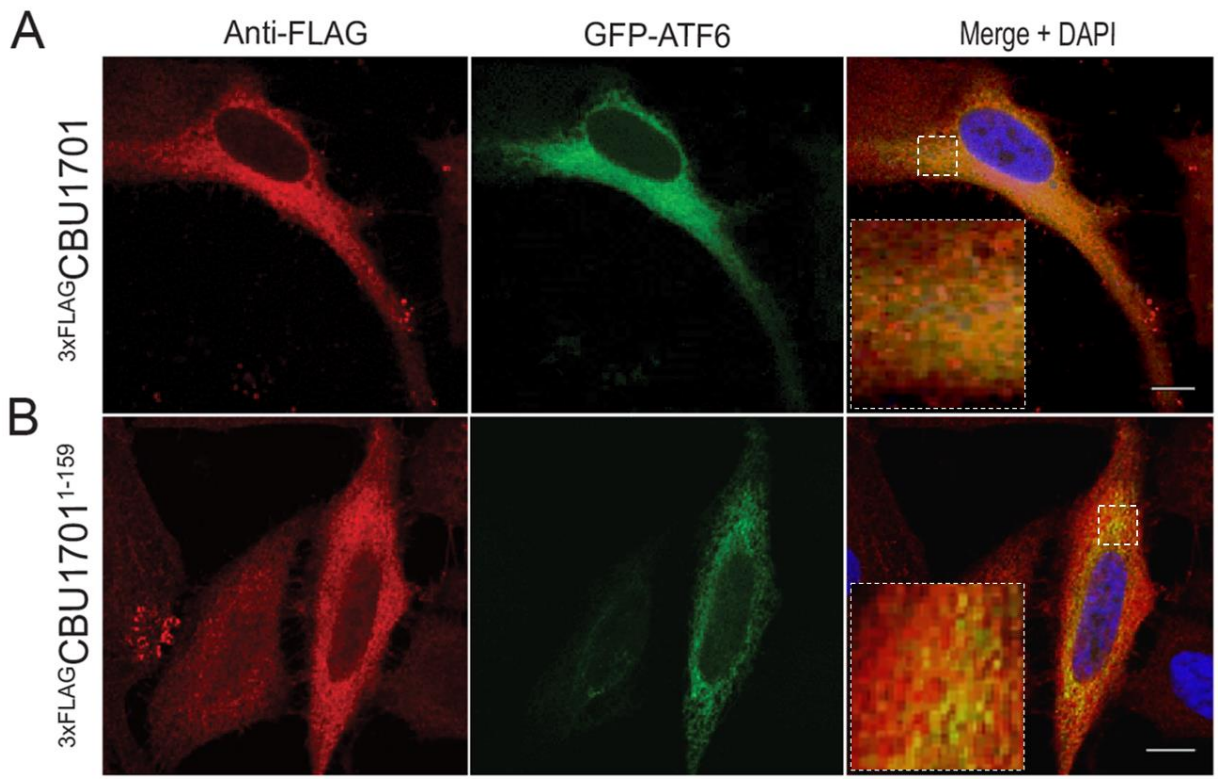

Figure 4.4 Co-localisation of full length and amino terminal region of ^{3xFLAG}CBU1701 with GFP-ATF6 to monitor ER localisation.

(A) Representative confocal images of co-transfection of HeLa cells with GFP-ATF6 and ^{3xFLAG}CBU1701 suggesting co-localisation. (B) No co-localisation was observed upon co-transfection of GFP-ATF6 and ^{3xFLAG}CBU1701$^{1-159}$. Upon transfection, cells were fixed and stained with anti-FLAG (red) and DAPI (nuclei). Scale bar 10 µm.

4.2.5 Examination of the impact of ^{3xFLAG}CBU1701$^{1-159}$ on TFEB localisation

In order to determine whether the amino terminal region of CBU1701 was sufficient to induce the nuclear translocation of TFEB, HeLa TFEB-GFP cells were transfected with 3xFLAG tagged CBU1701$^{1-159}$, expressed from pFLAG-CBU1701$^{1-159}$ and by the full-length protein expressed from pFLAG-CBU1701. As shown in Figure 4.5 (A), nuclear localisation of TFEB-GFP was observed upon ectopic expression using the full-length plasmid. No nuclear translocation of TFEB was observed upon ^{3xFLAG}CBU1701$^{1-159}$ expression (Figure 4.5 B).

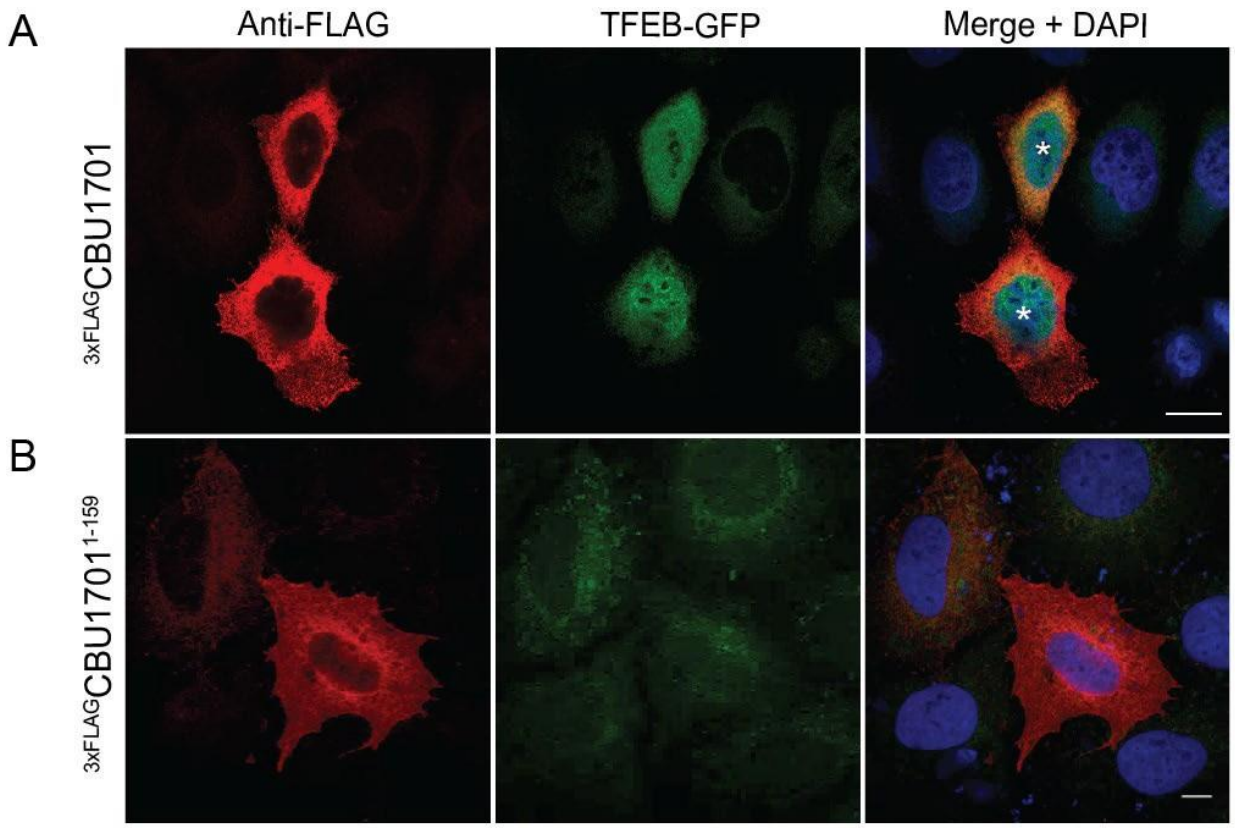

Figure 4.5 Localisation of ectopically expressed ^{3xFLAG}CBU1701 full length and amino terminal protein to monitor TFEB nuclear localisation.

Representative confocal images of HeLa TFEB-GFP cells transfected to express (A) ^{3xFLAG}CBU1701$^{1-159}$ showing TFEB-GFP nuclear translocation and (B) ^{3xFLAG}CBU1701$^{1-159}$ showing no nuclear translocation of TFEB-GFP. 16h post-transfection, cells were fixed and stained with anti-FLAG (red) and DAPI (nuclei). * indicates nuclear activation of TFEB. Scale bars represent 10 µm.

4.2.6 Investigation into the Dot/Icm-dependent translocation of CBU1701

A study by Lifshitz et al. 2013 used a hidden semi-Markov model (HSMM) bioinformatic screening approach to predict putative effectors of the Dot/Icm system. This approach was applied to the entire genome of multiple *Legionella* species, the genus *Rickettsiella* and *C. burnetii* with 44 *C. burnetii* proteins given the putative effector status [133]. The predictions were based on all 283 *L. pneumophila* known effectors and 1,000 non-effectors that served as a framework model. The final model consisted of only effectors having a really strong secretion signal and any effectors having a low-score were removed from the effector set. Any ORF from *Legionella, Coxiella* and *Rickettsia* having a score of more than 5 was considered a putative effector. Using this approach CBU1701 was indicated to be a likely Dot/Icm effector as it had a score of 5.19 [133].

To determine whether CBU1701 is a bona fide T4SS effector, CBU1701 was cloned into a reporter plasmid that facilitates the constitute expression of CBU1701 transcriptionally coupled to β-lactamase (BlaM) at the N-terminus. It has previously been shown that the carboxy (C) terminal region of T4SS effector proteins can be sufficient to drive translocation [127, 220]. Given the large number of transmembrane domains encoded by CBU1701, it seemed plausible that overexpression of this protein may impact its capacity for translocation. In order to circumvent this potential issue BlaM-CBU1701$^{435\text{-}468}$, encoding for just the C-terminal region after the transmembrane domains (Figure 4.3 (A)), was also generated. These plasmids were then introduced into wild-type *C. burnetii* and the *icmL*::Tn strain, to investigate Dot/Icm-dependent translocation of CBU1701.

Expression of the fusion proteins in wild-type and *icmL*::Tn were confirmed by immunoblot using anti-BlaM antibodies. The expected size of the full-length fusion protein is 81.1 kDa. However, western blots of *C. burnetii* lysate consistently showed truncated protein ranging in size from 29 kDa (BlaM alone) to 60 kDa (Figure 4.6). Expression of BlaM-CBU1701$^{435\text{-}468}$, resulted in a 32 kDa protein (3 kDa, C-terminus region of CBU1701 and 29 kDa, BlaM) as shown in Figure 4.6 (A). Immunoblot of the full length and C-terminal CBU1701 constructs using anti-BlaM antibodies resulted in truncated BlaM protein of 29 kDa. This cleavage is always seen to some extent but that is because the full-length protein is present in greater abundance, and this is not an issue. This apparent processing of BlaM-CBU1701 and BlaM-CBU1701$^{435\text{-}468}$ could have resulted in the loss of the translocation signal.

The translocation assay was carried out using the standardised assay developed in the laboratory [137]. Briefly, HeLa cells were infected with *C. burnetii* wild-type and *icmL*::Tn strains expressing BlaM-CBU1701 and BlaM-CBU1701$^{435\text{-}468}$ using a MOI (multiplicity of infection) of 100, 300 and 1000. BlaM-MceA was used as a positive control for the translocation assay [121, 127, 137]. In the BlaM-based translocation assay, CCF2-AM substrate containing two fluorophores (7-hydroxycoumarin and fluorescein) is linked by a β-lactam ring and is used to detect the delivery of BlaM into the host cell cytoplasm (Figure 1.3). Upon delivery of the BlaM-fusion protein into the host cell cytosol, β-lactamase activity of the protein cleaves the CCF2-AM molecule resulting in FRET disruption between the two fluorophores. This can be quantified using a fluorescence plate reader to excite samples at 410 nm that results in cleavage of CCF2-AM by BlaM leading to a

fluorescence emission at 520 nm (green) and 450 nm (blue). No BlaM translocation, due to absence of β-lactamase activity, results in no cleavage of CCF2-AM, resulting in a green signal (520 nm) upon excitation at 410 nm.

This assay revealed translocation of only MceA 24 hours post-infection, with a 450::520 nm signal ratio of 3.03 and less than 1.03 for *C. burnetii* WT expressing BlaM-CBU1701 and BlaM-CBU1701$^{435\text{-}468}$ as shown in Figure 4.6 (B). The 450::520 nm signal ratio was used to determine the translocation into the host cell cytoplasm of BlaM-MceA, BlaM-CBU1701 and BlaM-CBU1701$^{435\text{-}468}$. The results of this experiment could indicate one of the possible outcomes. It may be that the sensitivity of the plate reader-based assay is not enough to detect low frequency of translocation. Large scale studies that have screened for *C. burnetii* effectors have used this BlaM translocation assay with a visual readout rather than using a plate reader to detect the fluorescence emission shift. The translocation efficiency of many of the *C. burnetii* substrates was only 1% [132]. The fluorescence signal change, with only 1% of cells demonstrating the change can be detected visually but likely not through the plate reader approach employed here.

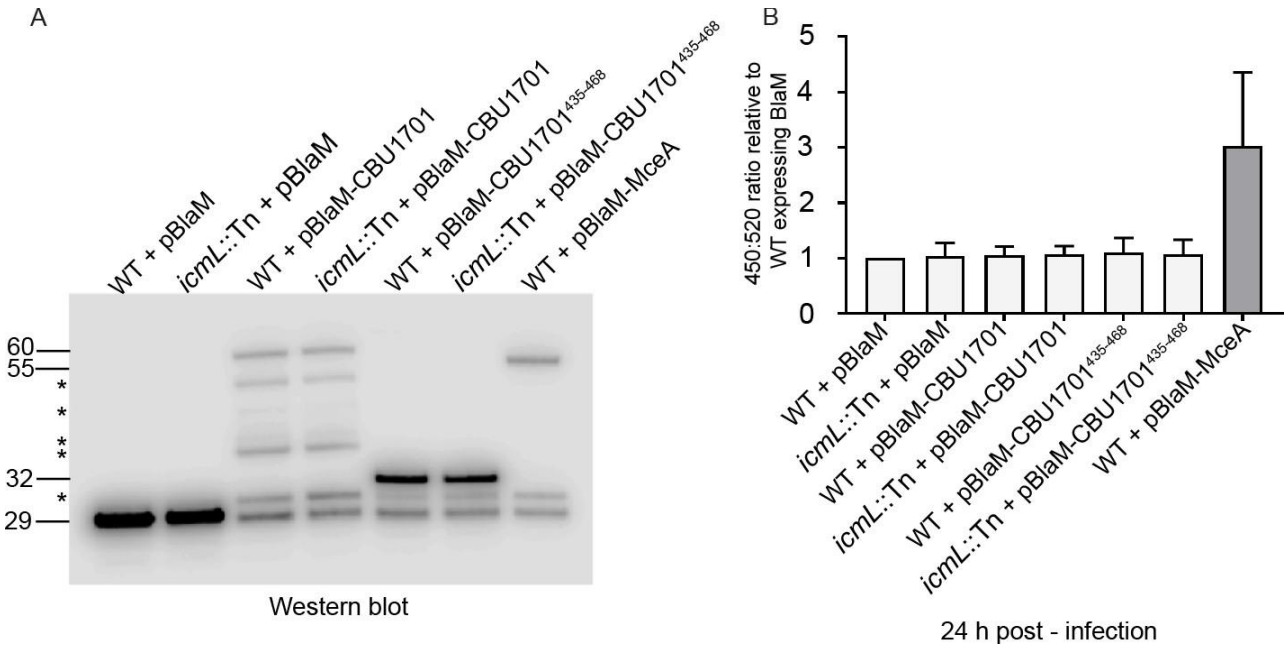

Figure 4.6 *C. burnetii* BlaM based translocation assay of CBU1701.

(A) Anti-BlaM immunoblot of lysates of *C. burnetii* WT and *icmL*::Tn strains carrying pJB- CAT-BlaM (BlaM) and BlaM-effector fusion constructs for CBU1701, CBU1701$^{435\text{-}468}$ and MceA. *C. burnetii* lysates were probed with anti-BlaM and the expression of BlaM (29kDa), BlaM-CBU1701 (breakdown bands between 29 and 60 kDa), BlaM-CBU1701$^{435\text{-}468}$ (32kDa) and BlaM-MceA (60kDa) was observed. Expression of the various proteins was consistent in both *C. burnetii* WT *and icmL*::Tn strain backgrounds. Asterisk (*) indicates breakdown bands. (B) Translocation of the various BlaM-fusion proteins 24 hours post-infection was determined by measuring the 450 nm/520 nm (fluorescence emission ratio). Results display the mean and standard deviation from three biological replicates relative to *C. burnetii* expressing BlaM alone. The data presented here is from infections with a MOI of 300, however similar results were observed using a MOI of 100 and 1000 (data not shown).

4.2.7 Characterisation of CBU2016, a Dot/Icm substrate

CBU2016 was identified as a T4SS effector by Weber et al. (2013), who reported no specific localisation pattern of ectopically expressed EGFP-CBU2016. This publication also indicated that transposon disruption of CBU2016 led to reduced intracellular replication and impaired CCV formation [132]. This study used a surrogate system in *L. pneumophila* to examine effector translocation. Using BlaM-CBU2016 expressing *L. pneumophila*, they were able to show 1% of cells to be translocation positive. Thus, providing evidence that CBU2016 is capable of Dot/Icm-dependent translocation [132]. In agreement with this report, our studies consistently showed that ectopic expression of ^{3xFLAG}CBU2016 in HeLa cells displays a non-specific cytoplasmic localisation as shown in Figure 4.7(A).

The protein encoded by *cbu2016* is 23.174 kDa comprising of 198 amino acid residues. The bioinformatics analysis using BLAST revealed no similarity to any bacterial or non-bacterial DNA or protein sequences. It was also found to be highly conserved amongst the sequenced *C. burnetii* strains and there are no homologs in non-*Coxiella* organisms. TMHMM server version 2.0 analysis revealed that there are no predicted transmembrane domains for this protein.

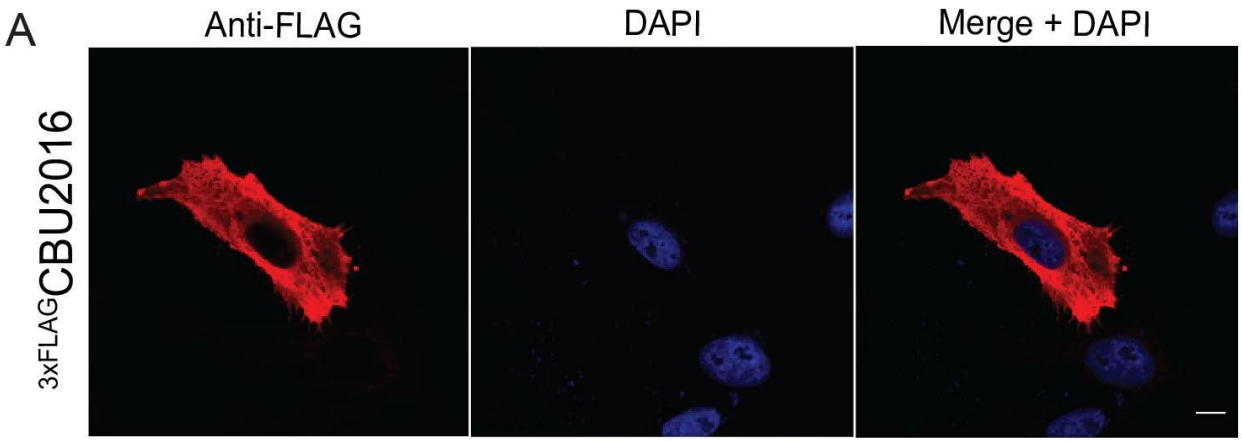

Figure 4.7 Localisation of ectopically expressed ^{3xFLAG}CBU2016 in HeLa cells.

(A) Localisation of ectopically expressed ^{3xFLAG}CBU2016 in HeLa cells. No specific pattern of localisation was observed with signal found throughout the cytoplasm but excluded from the nucleus. Confocal immunofluorescence image is a representative image from three biological replicates. 16h post-transfection, cells were fixed and stained with anti- FLAG (red) and DAPI (nuclei). Scale bar represents 10 µm.

4.2.8 Generation and validation of HeLa ^{3xFLAG}CBU1701 and ^{3xFLAG}CBU2016 doxycycline inducible stable cell lines.

In order to further investigate the impact of CBU1701 and CBU2016 on eukaryotic cell function, with a particular interest in TFEB and TFE3, HeLa cells were engineered to express ^{3xFLAG}CBU1701 or ^{3xFLAG}CBU2016 from a doxycycline inducible promoter. These genetically engineered stable cell lines, were sorted, using fluorescence-activated cell sorting (FACS), to generate a monoclonal cell line having uniform expression levels. The expression of these effector proteins was confirmed by western blot using FLAG antibodies (Figure 4.8 A and C). Upon confirming their expression, induction of these stable cell lines using various concentrations of doxycycline indicated that increasing the concentration of doxycycline did not alter the expression of ^{3xFLAG}CBU1701 or ^{3xFLAG}CBU2016.

Interestingly, ^{3xFLAG}CBU1701 consistently appeared as a truncated protein, similar to our observations *with C. burnetii* expression of BlaM-CBU1701 (Figure 4.6 A). The expected size of ^{3xFLAG}CBU1701 is 55 kDa and the truncated protein detected with FLAG antibody was 32 and 29 kDa. Together these data indicate possible cleavage of the C-terminus of CBU1701 both in bacteria and eukaryotic cells suggesting that the full-length protein is unstable and/or may undergo self-cleavage events. As predicted, a 26 kDa protein was observed by western using anti-FLAG antibodies for the ^{3xFLAG}CBU2016 stable cell line. When these stable cell lines were induced using 20 ng/µL of doxycycline and incubated for up to 72 hours, a gradual increase in the expression of protein was observed. This confirms the dose-dependent response for these stable cell lines (Figure 4.8 B and D).

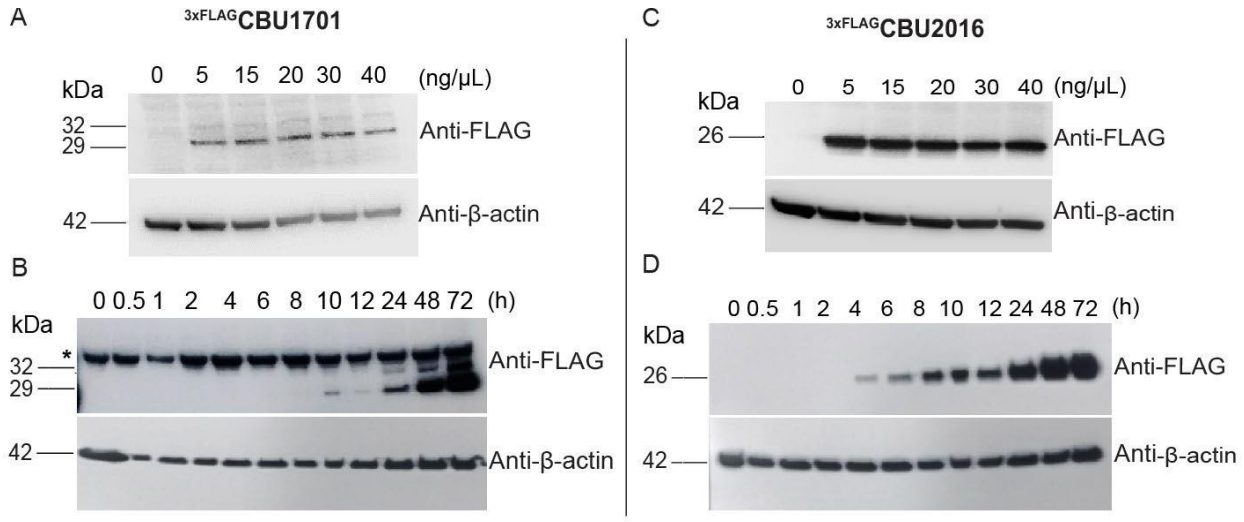

Figure 4.8 Stable cell line generation and validation of doxycycline-inducible expression of ^{3xFLAG}CBU1701 and ^{3xFLAG}CBU2016.

(A) Western blot of ^{3xFLAG}CBU1701 stable cell lines induced using 5, 15, 20, 30 and 40 ng/µl of doxycycline for 24 hours showing no dose dependent response. A truncated protein of 32 and 29 kDa was observed upon expression of CBU1701 stable cell line. Expected size of the fusion protein is 55 kDa. (B) Induction of ^{3xFLAG}CBU1701 stable cell lines using 20 ng/µL of doxycycline for 0.5, 1, 2, 4, 6, 8, 10, 12, 24, 48 and 72 hours shows an increase in the expression of ^{3xFLAG}CBU1701. (C) A 26 kDa protein showing no dose- dependent response across various doxycycline treatment tested was observed upon induction of ^{3xFLAG}CBU2016 stable cell line. (D) ^{3xFLAG}CBU2016 increased in abundance when stable cell lines were induced for increasing time with 20 ng/µL. Upon various treatments, equal amounts of lysate were loaded on SDS-PAGE and probed with anti- FLAG to look for the expression of ^{3xFLAG}CBU1701 and ^{3xFLAG}CBU2016. Anti-β-actin was used as a loading control and (*) asterisk indicates non-specific band.

4.2.9 Subcellular fractionation of ^{3xFLAG}CBU2016

Next, subcellular localisation of TFEB, upon induction of the ^{3xFLAG}CBU2016 stable cell line was investigated through cell fractionation [219]. For this, expression of ^{3xFLAG}CBU2016 was induced using 20 ng/µL of doxycycline for 48 hours and the cells were subjected to fractionation into cytoplasmic and nuclear components using the standardised protocol (section 2.11). Upon fractionation, the cytoplasmic and nuclear extracts was separated on SDS-PAGE to determine the localisation of TFEB upon expression of ^{3xFLAG}CBU2016. For immunoblotting, anti-FLAG antibodies were used to confirm the expression of ^{3xFLAG}CBU2016. As expected, based on immunofluorescence observations in Figure 4.7, this revealed a cytoplasmic localisation for ^{3xFLAG}CBU2016. Control antibodies were used to demonstrate clear separation of nuclear, anti-histone H3, and cytoplasmic, anti-Tubulin, compartments. Western blot using anti-TFEB revealed nuclear translocation of this transcription factor upon effector expression (Figure 4.9).

Sub-cellular fractionation of ^{3xFLAG}CBU2016 expressing cells confirmed our initial observation that this effector induces nuclear translocation of TFEB as shown in Figure 4.2. It was important to note that this key result was reproducible in the stable cell lines where the effector is expressed at lower levels than during transient expression. Cytoplasmic localisation of ^{3xFLAG}CBU2016 was also confirmed using anti-FLAG antibodies. Unfortunately, inconsistent results were obtained for sub-cellular fractionation of ^{3xFLAG}CBU1701 expressing cells.

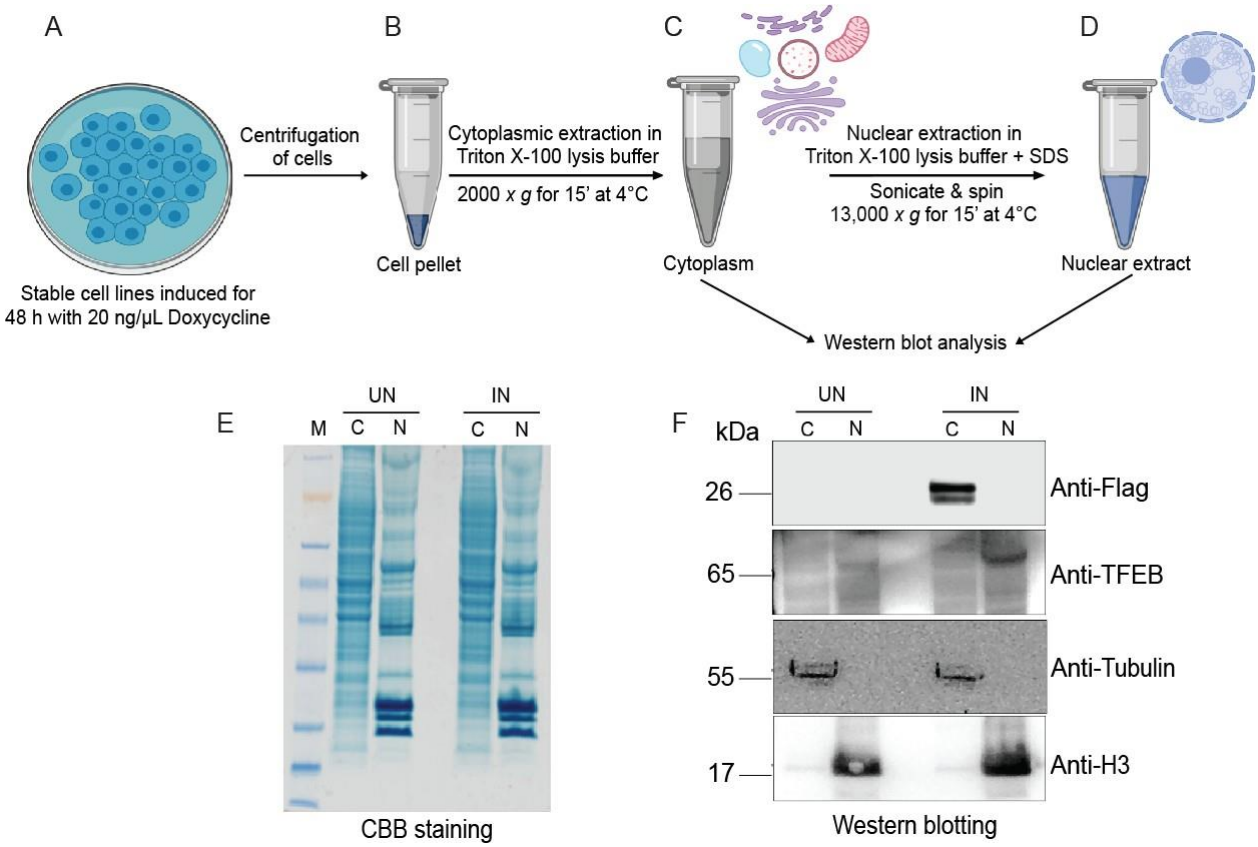

Figure 4.9 Subcellular fractionation of ^{3xFLAG}CBU2016.

(A) HeLa cells were treated with 20 ng/µL of doxycycline for 48 hours at 37 ºC, to induce expression of ^{3xFLAG}CBU2016. (B) Pools of uninduced and induced cells were collected in a microfuge tube and the cells were lysed in Triton X-100 lysis buffer before centrifugation to separate the cytoplasmic (soluble) fraction and the nuclear (insoluble) fraction. (C) The cytoplasmic fraction was collected and (D) the pellet was sonicated and lysed to obtain the nuclear content. (E) CBB (Coomassie Brilliant Blue) staining shows cytoplasmic and nuclear fractions in the uninduced (UN) and induced (IN) samples. (F) Equal amounts of cytoplasmic and nuclear fractions were separated by SDS-PAGE and probed using anti-FLAG, anti-TFEB, anti–Tubulin and anti–H3.

4.2.10 Nuclear translocation of TFEB and TFE3 upon expression of ^{3xFLAG}CBU1701 and ^{3xFLAG}CBU2016

As previously demonstrated, ectopic expression of these effectors induced nuclear localisation of TFEB-GFP (Figure 4.2). We were interested in validating the nuclear translocation of TFEB and TFE3 in its native state using ^{3xFLAG}CBU1701 and ^{3xFLAG}CBU2016 stable cell lines and not using overexpressed TFEB-GFP cells. The stable cell lines resulted in a low level of expression than the transient expression. Stable cell lines were treated using 20 ng/µL of doxycycline for 48 hours, to induce expression of ^{3xFLAG}CBU1701 and ^{3xFLAG}CBU2016, before the cells were fixed and stained using anti-TFEB (in green) or anti-TFE3 (in green), anti-FLAG (in red) and DAPI (nuclei). As shown in Figure 4.10 nuclear localisation of TFEB and TFE3 was observed upon expression of ^{3xFLAG}CBU1701 in comparison to the uninduced control 48 hours post induction (Figure 4.10 A and B). Similarly, upon induction of ^{3xFLAG}CBU2016 expression, nuclear localisation of TFEB and TFE3 was observed (Figure 4.10 C and D) validating the findings observed with subcellular fractionation (Figure 4.9). This data also demonstrates that CBU1701 can induce nuclear translocation of TFEB and TFE3, despite the cleavage events that have been observed.

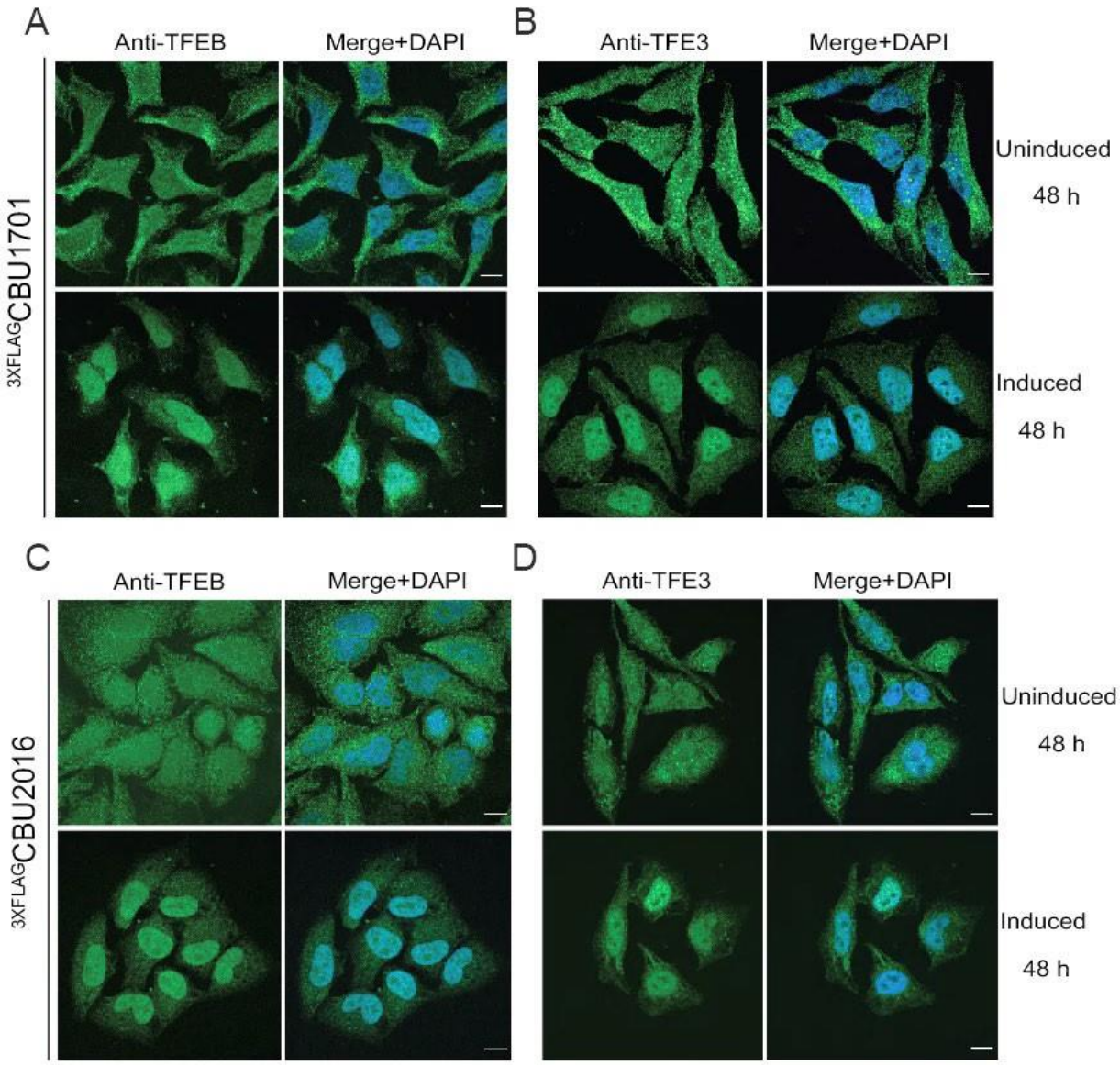
A
Anti-TFEB
Merge+DAPI
B
Anti-TFE3
Merge+DAPI
3XFLAGCBU1701
Uninduced
48 h
Induced
48 h
C
Anti-TFEB
Merge+DAPI
D
Anti-TFE3
Merge+DAPI
3XFLAGCBU2016
Uninduced
48 h
Induced
48 h

Figure 4.10 Visual examination of native TFEB and TFE3 localisation in HeLa cells stimulated to express ^{3xFLAG}CBU1701 or ^{3xFLAG}CBU2016.

(A and B) Representative confocal images of HeLa stable cell lines either uninduced for effector expression or induced for ^{3xFLAG}CBU1701 expression for 48 hours with 20 ng/µL of doxycycline. Following treatment, cells were fixed and stained with anti–TFEB (A, green) or anti–TFE3 (B, green), and DAPI (blue). (C) ^{3xFLAG}CBU2016 stable cells were also induced with 20 ng/µL of doxycycline for 48 hours, following which uninduced and induced cells were fixed and stained with anti–TFEB (green), (D) anti-TFE3 (green) and DAPI (nuclei). Scale bar represents 10 µm.

4.2.11 Non-biased examination of the impact of ^{3xFLAG}CBU1701 and ^{3xFLAG}CBU2016 expression on the human cell proteome

A global proteomics analysis was undertaken in order to take a non-biased approach towards understanding the impact of expression of ^{3xFLAG}CBU1701 and ^{3xFLAG}CBU2016 on human cells. Given the data presented here indicating that these effectors may stimulate expression of proteins involved in lysosome biogenesis and autophagy, through control of TFEB and TFE3, focus was paid to proteins within the CLEAR network. 5 independent replicates, each consisting of a sample with and without doxycycline treatment to induce expression of the FLAG-tagged effector, were processed for whole cell proteomics analysis. Western blot analysis using 300 ng of the independent samples, confirmed the expression of each of the *C. burnetii* proteins in the doxycycline treated samples. Upon confirmation of successful induction of effector expression, using anti-FLAG antibodies, whole cell proteome of HeLa cells expressing ^{3xFLAG}CBU1701 or ^{3xFLAG}CBU2016, and their non-expressing controls, were acetone precipitated. Western blot using anti-FLAG antibodies resulted in an expected protein size of 26 kDa protein in the case of ^{3xFLAG}CBU2016. However, breakdown bands of 32 kDa and 29 kDa protein band was observed in the case of ^{3xFLAG}CBU1701 likely due to the potential processing of the protein as previously observed. Protein was purified, digested with trypsin, and further processed for mass spectrometry analysis.

The analysis was performed using five independent biological replicates each for the uninduced condition, where there was no expression of ^{3xFLAG}CBU1701, and doxycycline induced conditions for ^{3xFLAG}CBU1701 expression (Figure 4.11). In the case

of ^{3xFLAG}CBU2016, analysis was performed using four uninduced (no effector expression) samples and five doxycycline induced (effector expressed) samples. Figure 4.12 represents a principal component analysis (PCA) plot for both ^{3xFLAG}CBU1701 and ^{3xFLAG}CBU2016 expressing cell lines. PCA is a statistical procedure which uses mathematical modelling to simplify the complex high-dimensional data into small clusters for the ease of analysis and visualization [223]. Each dot in the plot represents one biological replicate. The clustering of like samples indicates consistency among the biological replicates (Figure 4.12).

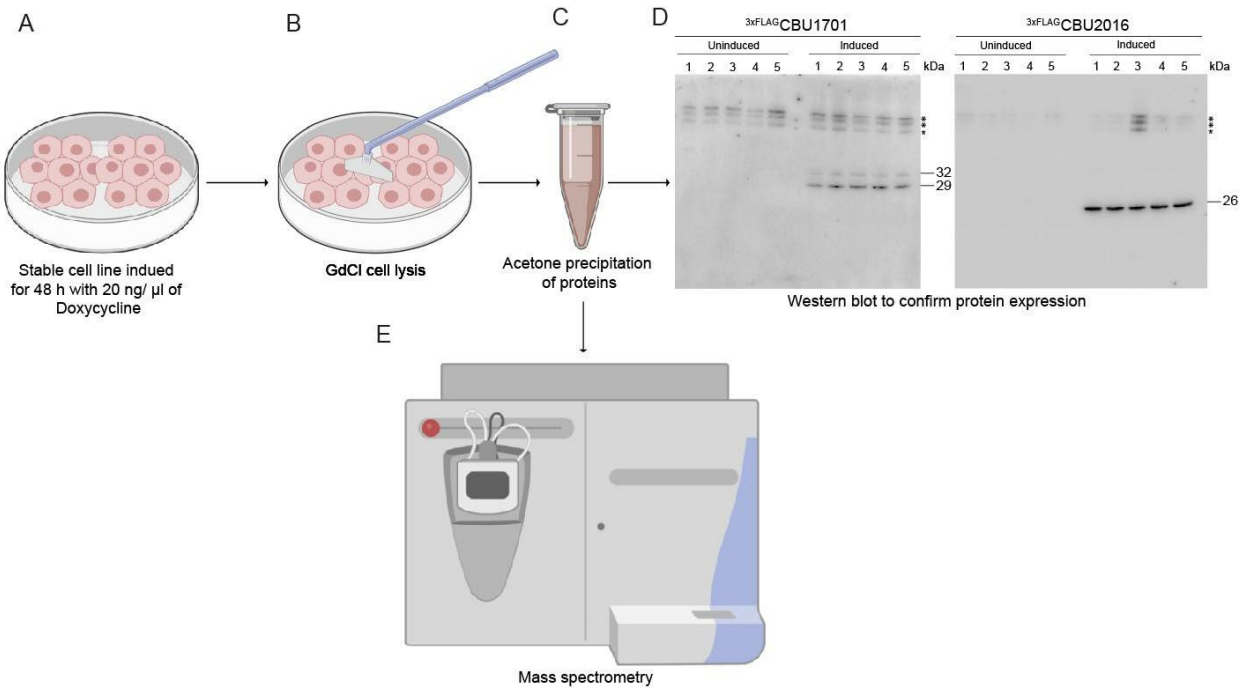

Figure 4.11 Schematic of experimental process for whole cell proteomics of stable cell lines.

(A) ^{3xFLAG}CBU1701 and ^{3xFLAG}CBU2016 stable cell lines were either left untreated or treated with 20 ng/µL of doxycycline for 48 hours. (B) Post-treatment, cells were washed using PBS and protein was collected using Guanidine hydrochloride (GdmCl) lysis buffer. (C) Protein was precipitated using acetone overnight at -20 ^{o}C. (D) Equal amount of protein quantified using BCA assay and was loaded onto SDS-PAGE to confirm the expression of protein using anti-FLAG antibodies. * indicates non-specific bands. (E) Protein was then prepared for mass spectrometry for further analysis.

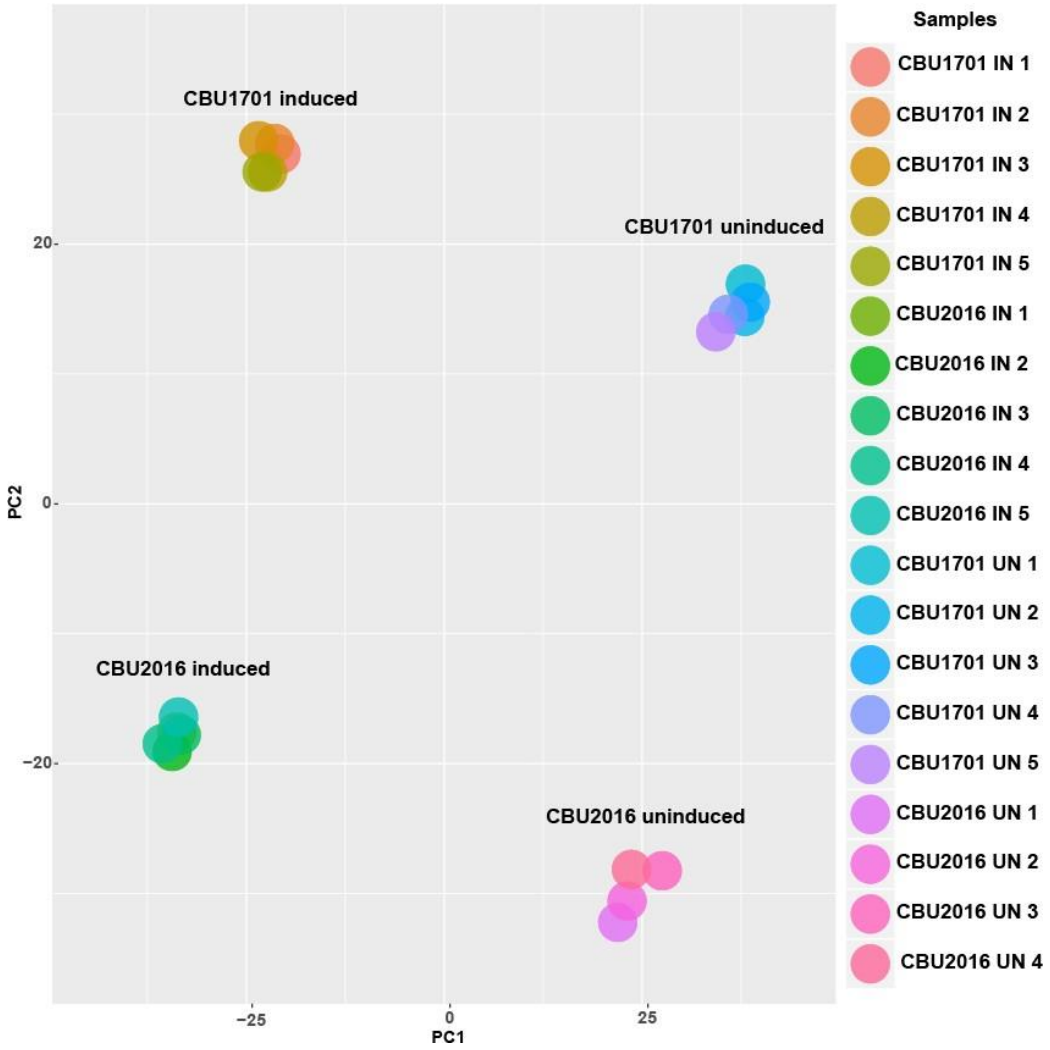

Figure 4.12 PCA plot demonstrating proteomic changes of HeLa cells in different conditions

The biplot represents proteome data labelled as dots for five biological replicates of ^{3xFLAG}CBU1701 induced (IN, protein expressed upon treatment using doxycycline) and uninduced (UN, no expression of protein) samples and five induced and four uninduced ^{3xFLAG}CBU2016 samples. The tight clustering suggests that each of the biological replicates are similar. PCA 1 and 2 dimensions, PC1 and PC2 respectively, clearly delineate between the two different cell types and the sample treatment.

4.2.12 Host proteome changes upon effector induction

Induction of ^{3xFLAG}CBU2016 expression led to a significant change in the abundance of 265 human proteins and expression of ^{3xFLAG}CBU1701 led to a significant change in the abundance of 251 proteins. These changes are summarised by the Venn diagram shown in Figure 4.13. There are changes that are significantly increased or decreased in abundance and of these, 73 proteins are common between the two. These common proteomic changes may indicate that there is a similar effect on the host proteome when these two effectors are expressed.

This dataset allowed closer inspection of the abundance of proteins that are transcriptionally controlled by TFEB. Using the TFEB regulated list generated by Palmieri et al., 303 proteins were classified as being influenced by TFEB activity. Surprisingly, few TFEB regulated proteins showed altered abundance upon expression of ^{3xFLAG}CBU1701 or ^{3xFLAG}CBU2016. Both ^{3xFLAG}CBU1701 and ^{3xFLAG}CBU2016 has 13 TFEB regulated proteins altered in abundance with 4 increased and 9 decreased in abundance. Of these, 5 proteins behave the same in both cell lines, 1 that is increased and 4 that are decreased in abundance. If CBU2016 or CBU1701 were directly impacting TFEB, and that was their primary function, then we expect to see a change to most, if not all of these proteins and their increase in abundance. This finding suggests that the TFEB nuclear localisation and TFEB transcription factor activity may be uncoupled in this situation. A pathway analysis as performed earlier in chapter 3 was not done as there were not a lot of changes. Future investigations using these results could start by looking at pathway analysis and connection between different proteins that change in abundance.

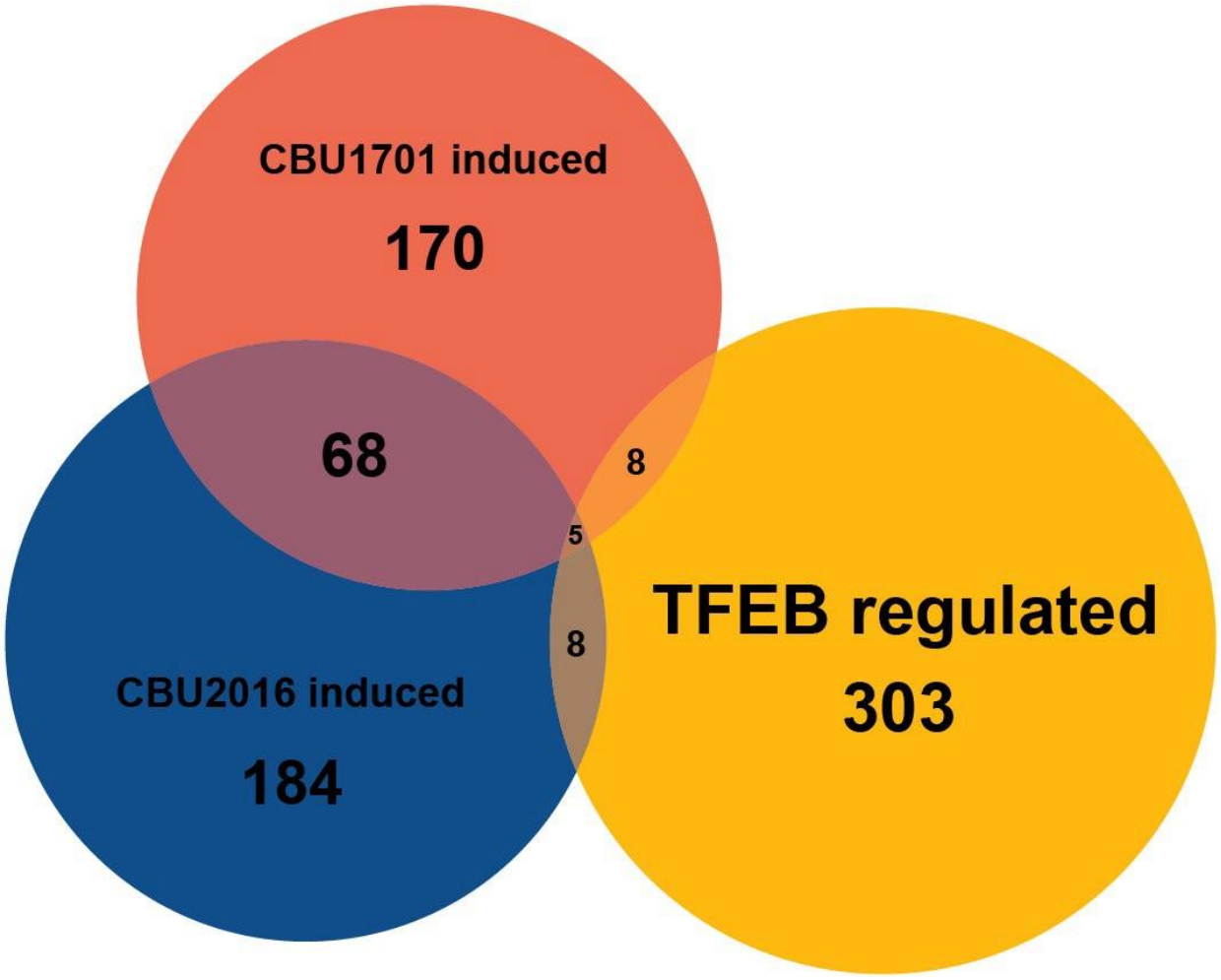

Figure 4.13 Venn diagram illustrating proteomic changes upon expression of ^{3xFLAG}CBU1701 and ^{3xFLAG}CBU2016.

Venn diagram illustrating significant changes in protein abundance upon the expression of ^{3xFLAG}CBU1701 and ^{3xFLAG}CBU2016 stable cell lines. Each circle represents a sample ID; ^{3xFLAG}CBU1701 induced, ^{3xFLAG} CBU2016 induced and TFEB regulated proteins used as input. The intersection refers to the proteins equally shared between the data sets. The overlap between all 3 data sets is also shown.

4.2.13 Proteomic changes induced by expression of ^{3xFLAG}CBU1701

Figure 4.14 is a volcano plot that highlights changes to TFEB regulated proteins upon expression of ^{3xFLAG}CBU1701. Red dots represent proteins whose expression has previously been shown to be influenced by TFEB [166, 171]. Grey dots indicate other protein change in response to ^{3xFLAG}CBU1701 expression. The TFEB-controlled protein details, fold change and *P* value of these changes are detailed in Table 4.2. Highlighted in blue are the proteins that are similarly increased or decreased in abundance upon the expression of ^{3xFLAG}CBU1701 and ^{3xFLAG}CBU2016.

Looking more broadly at the protein changes that occur when ^{3xFLAG}CBU1701 is present in eukaryotic cells, several very large and significant changes were observed. These are represented in the volcano plot shown in Figure 4.15. The fold change, *P* value and detail of various proteins that are changed in significant ways are listed in Table 4.3

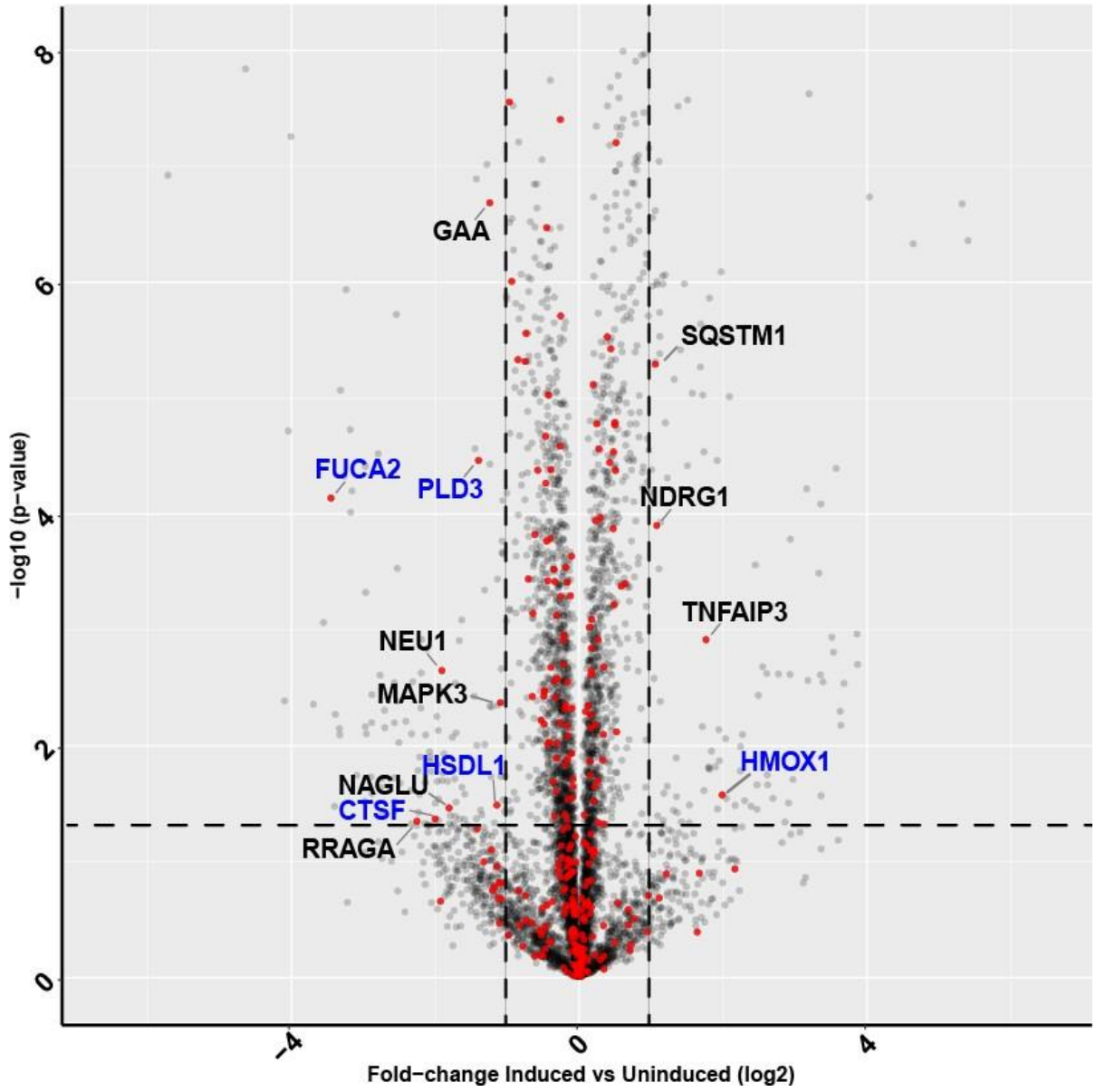
GAA
SQSTM1
FUCA2
PLD3
NDRG1
TNFAIP3
NEU1
MAPK3
HSDL1
HMOX1
NAGLU
CTSF
RRAGA
−log10 (p−value)
Fold−change Induced vs Uninduced (log2)
8
6
4
2
0
−4
0
4

Figure 4.14 Volcano plot showing changes in TFEB-regulated proteins upon induction of ^{3xFLAG}CBU1701.

Volcano plot showing proteomics data of 13 TFEB regulated proteins that significantly change in abundance with 4 increased and 9 decreased in abundance upon ^{3xFLAG}CBU1701 expression. The protein expression ratio (fold change) of ^{3xFLAG}CBU1701 induced (expression) vs uninduced (no expression) was plotted against the – log10 (*P* value) calculated by t-test. The horizontal dotted line shows where *P* = 0.05. Proteins above this line and outside the vertical dotted lines showed a statistically significant fold change greater than or less than -1. Proteins that have been previously shown to be influenced by TFEB are represented by red dots. TFEB-regulated proteins that show a significant change in abundance are labelled in black. Highlighted in blue are the proteins that are increased or decreased similarly in abundance upon ^{3xFLAG}CBU1701 and ^{3xFLAG}CBU2016 expression. Detailed information of the significant proteins identified is represented in the Table 4.2.

Table 4.2 TFEB-regulated proteins that demonstrate a significant change in abundance in response to expression of ^{3xFLAG}CBU1701.

Protein similarly increased or decreased in abundance upon ^{3xFLAG}CBU1701 and ^{3xFLAG}CBU2016 expression are highlighted in blue.

PROTEIN	PROTEIN NAME	FOLD CHANGE	*P* VALUE
HMOX1	Heme oxygenase 1	1.986	2.65E-02
TNFAIP3	Tumor necrosis factor alpha-induced protein 3	1.761	1.21E-03
NDRG1	Protein encoded by the N-myc downregulated gene family	1.077	1.26E-04
SQSTM1	Sequestosome-1	1.056	5.10E-06
MAPK3	Mitogen-activated protein kinase 3	-1.094	4.24E-03
HSDL1	Inactive hydroxysteroid dehydrogenase-like protein 1	-1.143	3.25E-02
GAA	Glycosylphosphatidylinositol anchor attachment 1 protein	-1.242	2.06E-07
PLD3	Phospholipase D3	-1.398	5.35E-03
NAGLU	Alpha-N-acetylglucosaminidase	-1.807	3.44E-02
NEU1	Sialidase-1	-1.907	2.24E-03
CTSF	Cathepsin F	-2.001	4.27E-02
RRAGA	Ras-related GTP-binding protein A	-2.252	4.47E-02
FUCA2	Plasma alpha-L-fucosidase	-3.447	7.28E-05

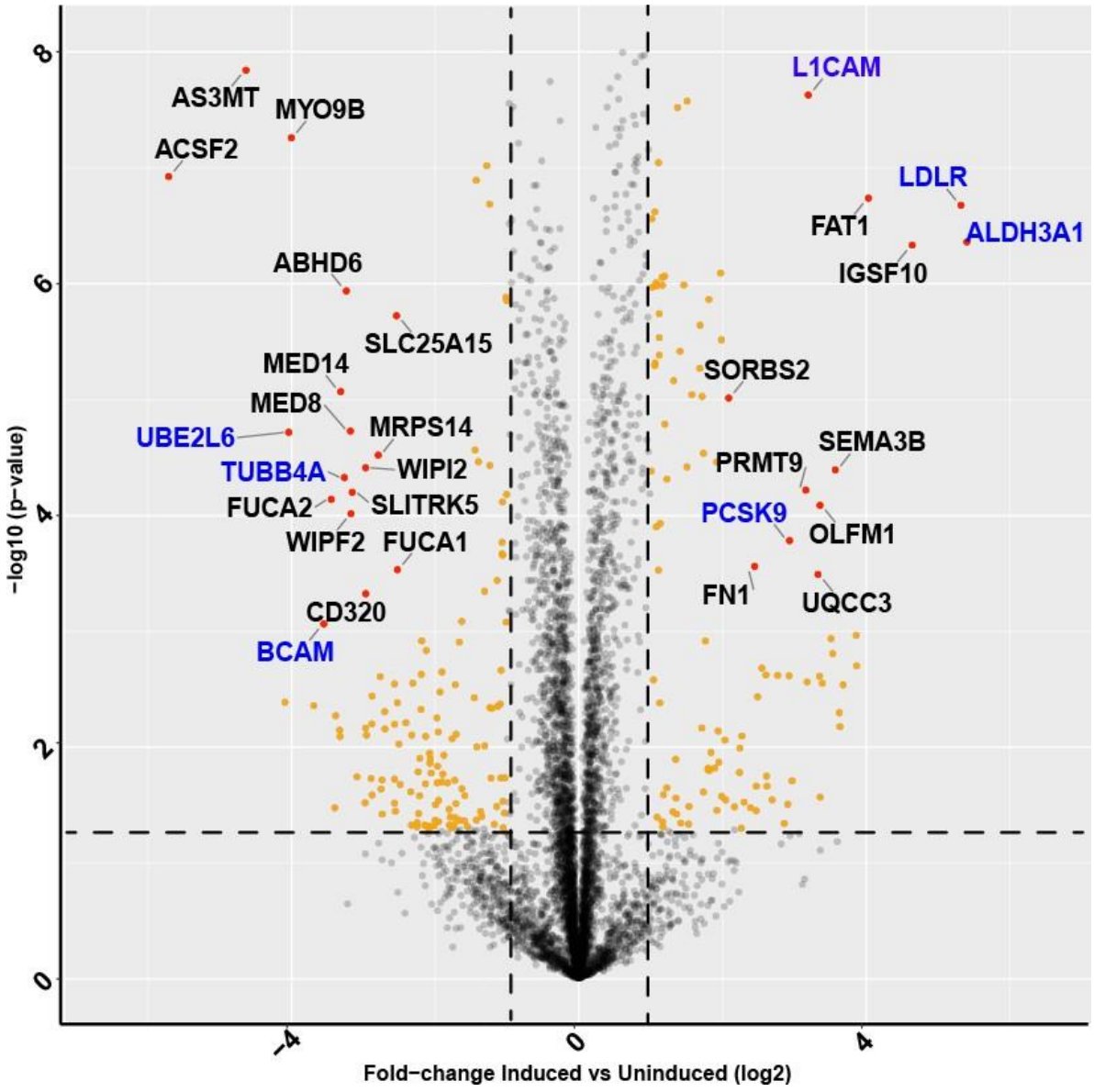
L1CAM
AS3MT
MYO9B
ACSF2
LDLR
FAT1
ALDH3A1
IGSF10
ABHD6
SLC25A15
MED14
SORBS2
MED8
MRPS14
UBE2L6
SEMA3B
PRMT9
TUBB4A
WIPI2
FUCA2
SLITRK5
PCSK9
OLFM1
WIPF2
FUCA1
FN1
UQCC3
CD320
BCAM
−log10 (p−value)
Fold−change Induced vs Uninduced (log2)

Figure 4.15 Volcano plot showing the significant protein changes upon expression of ^{3xFLAG}CBU1701

Volcano plot showing global proteome data for changes in the host proteome upon induction of ^{3xFLAG}CBU1701 expression. The x-axis shows induced/uninduced in fold change and Y-axis shows – log10 (*P* value) calculated by t-test. The plot is colored such that proteins having a fold change of less than 1 and/or not significant changes in abundance are shown as grey dots. Orange dots are proteins having a fold change of over one-fold. Those proteins labelled and represented by red dots represent host proteins that change upon ^{3xFLAG}CBU1701 expression, with a fold change greater than 2 and *P* value less than 0.001. Proteins commonly altered upon expression of ^{3xFLAG}CBU1701 and ^{3xFLAG}CBU2016 are labelled in blue. Detailed information of the significantly changed proteins is represented in Table 4.3, which includes the fold change and significance across the 5 replicates. The dashed horizontal line shows where *P* = 0. 05 and the two vertical dashed lines indicate a one-fold change in protein abundance.

Table 4.3 Table detailing significant change in proteome in response to expression of ^{3xFLAG}CBU1701.

These are proteins with a fold change greater than 2 and *P* value less than 0.001.

PROTEIN	PROTEIN NAME	FOLD CHANGE	*P* VALUE
ALDH3A1	Aldehyde dehydrogenase	5.400	4.37E-07
LDLR	Low-density lipoprotein receptor	5.318	2.11E-07
IGSF10	Immunoglobulin superfamily member 10	4.639	4.66E-07
FAT1	Protocadherin Fat 1	4.031	1.83E-07
SEMA3B	Semaphorin-3B	3.568	4.04E-05
OLFM1	Noelin	3.356	8.18E-05
UQCC3	Ubiquinol-cytochrome-c reductase complex	3.328	3.23E-04
L1CAM	Neural cell adhesion molecule L1	3.192	2.36E-08
PRMT9	Protein arginine N-methyltransferase 9	3.158	6.06E-05
PCSK9	Proprotein convertase subtilisin/kexin type 9	2.932	1.65E-04
FN1	Fibronectins	2.446	2.75E-04
SORBS2	Sorbin and SH3 domain-containing protein 2	2.085	9.71E-06
FUCA2	Plasma alpha-L-fucosidase	-2.356	7.28E-05
FUCA1	Tissue alpha-L-fucosidase	-2.526	2.94E-04
SLC25A15	Mitochondrial ornithine transporter 1	-2.538	1.90E-06

MRPS14	28S ribosomal protein S14, mitochondrial	-2.793	3.02E-05
CD320	CD320 antigen	-2.965	4.74E-04
WIPI2	WD repeat domain phosphoinositide-interacting protein 2	-2.968	3.88E-05
SLITRK5	SLIT and NTRK-like protein 5	-3.155	6.31E-05
WIPF2	WAS/WASL-interacting protein family member 2	-3.172	9.66E-05
MED8	Mediator of RNA polymerase II transcription subunit 8	-3.180	1.87E-05
ABHD6	Monoacylglycerol lipase	-3.237	1.16E-06
TUBB4A	Tubulin beta-4A chain	-3.264	4.71E-05
MED14	Mediator of RNA polymerase II transcription subunit 14	-3.315	8.55E-06
BCAM	Basal cell adhesion molecule	-3.550	8.63E-04
MYO9B	Myosins	-4.002	5.53E-08
UBE2L6	Ubiquitin/ISG15-conjugating enzyme E2 L6	-4.039	1.92E-05
AS3MT	Arsenite methyltransferase	-4.633	1.44E-08
ACSF2	Medium-chain acyl-CoA ligase, mitochondrial	-5.710	1.19E-07

4.2.14 Proteomic changes induced by expression of ^{3xFLAG}CBU2016

The volcano plot represented in Figure 4.16 highlights the proteomic changes upon expression of ^{3xFLAG}CBU2016. The TFEB regulated proteins that show a significant change in abundance are indicated as red dots. Proteins that are not differentially expressed with or without the expression of ^{3xFLAG}CBU2016 are indicated as grey dots. The protein details, fold change and *P* value of these proteins are detailed in Table 4.4. Highlighted in blue are the proteins that are similarly increased or decreased in abundance upon the expression of ^{3xFLAG}CBU1701 and ^{3xFLAG}CBU2016.

The Volcano plot shown in Figure 4.17 highlights altered protein significantly increased or decreased in abundance upon expression of ^{3xFLAG}CBU2016 in eukaryotic host cells. The fold change, *P* value and detail of various proteins that are changed in significant ways are listed in Table 4.5.

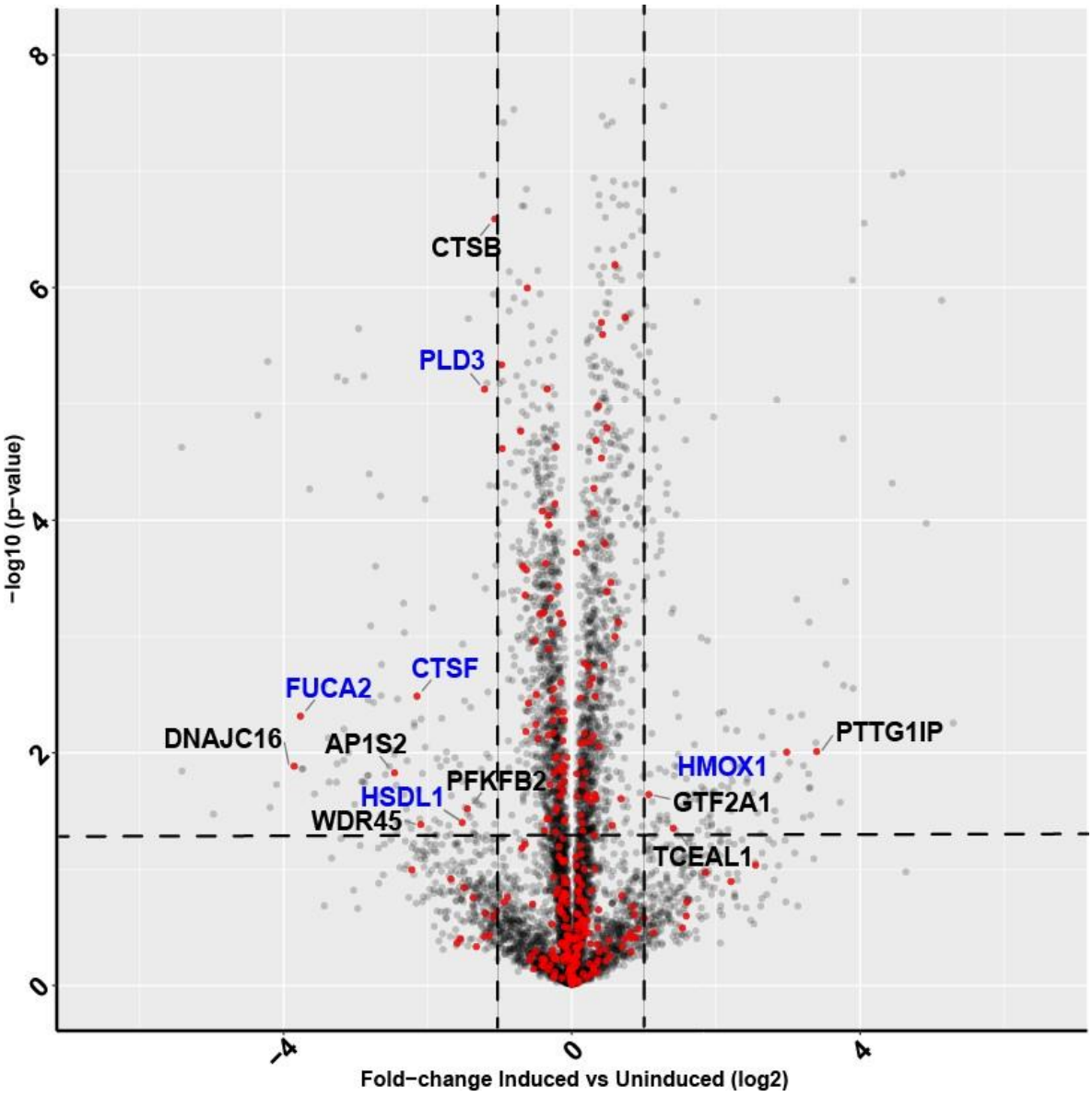
CTSB
PLD3
CTSF
FUCA2
DNAJC16
AP1S2
PFKFB2
HSDL1
WDR45
HMOX1
GTF2A1
PTTG1IP
TCEAL1
−log10 (p−value)
Fold−change Induced vs Uninduced (log2)

Figure 4.16 Volcano plot showing changes in the TFEB-regulated proteins upon induction of ^{3xFLAG}CBU2016.

Volcano plot showing proteomics data of altered proteins upon ^{3xFLAG}CBU2016 expression. The protein expression ratio (fold change) of ^{3xFLAG}CBU2016 induced (expression) vs uninduced (no expression) was plotted against the – log10 (*P* value) calculated by t-test. The horizontal dotted line shows where *P* = 0.05. Proteins above these lines and outside the vertical dotted lines showed a statistically significant fold change greater than 1 or less than -1. Proteins that have been previously shown to be influenced by TFEB are shown in red dots. TFEB-regulated proteins that show a significant change in abundance are labelled in black. TFEB-regulated proteins that are similarly increased or decreased in abundance upon expression of ^{3xFLAG}CBU2016 and ^{3xFLAG}CBU1701 are highlighted in blue Detailed information of the significant proteins identified is represented in the Table 4.4.

Table 4.4 TFEB-regulated proteins showing a significant change in abundance in response to expression of ^{3xFLAG}CBU2016.

Highlighted in blue are proteins that are similarly increased or decreased in abundance upon ^{3xFLAG}CBU2016 and ^{3xFLAG}CBU1701 expression.

PROTEIN	PROTEIN NAME	FOLD CHANGE	*P* VALUE
PTTG1IP	Pituitary tumor-transforming gene 1 protein-interacting protein	3.397	9.76E-03
HMOX1	Heme oxygenase 1	2.980	9.89E-03
TCEAL1	Transcription elongation factor A protein-like 1	1.406	4.45E-02
GTF2A1	Transcription initiation factor IIA subunit 1	1.067	2.28E-02
WDR45	WD repeat domain phosphoinositide-interacting protein 3	-0.003	9.82E-01
PLD3	5'-3' exonuclease PLD3	-0.964	7.48E-06
CTSB	Cathepsin B	-1.068	2.57E-07
PFKB2	6-phosphofructo-2-kinase	-1.450	3.03E-02
HSDL1	Inactive hydroxysteroid dehydrogenase-like protein 1	-1.522	3.98E-02
CTSF	Cathepsin F	-2.150	3.26E-03
AP1S2	AP-1 complex subunit sigma-2	-2.461	1.49E-02
FUCA2	Plasma alpha-L-fucosidase	-3.766	4.84E-03
DNAJC16	DnaJ homolog subfamily C member 16	-3.854	1.31E-02

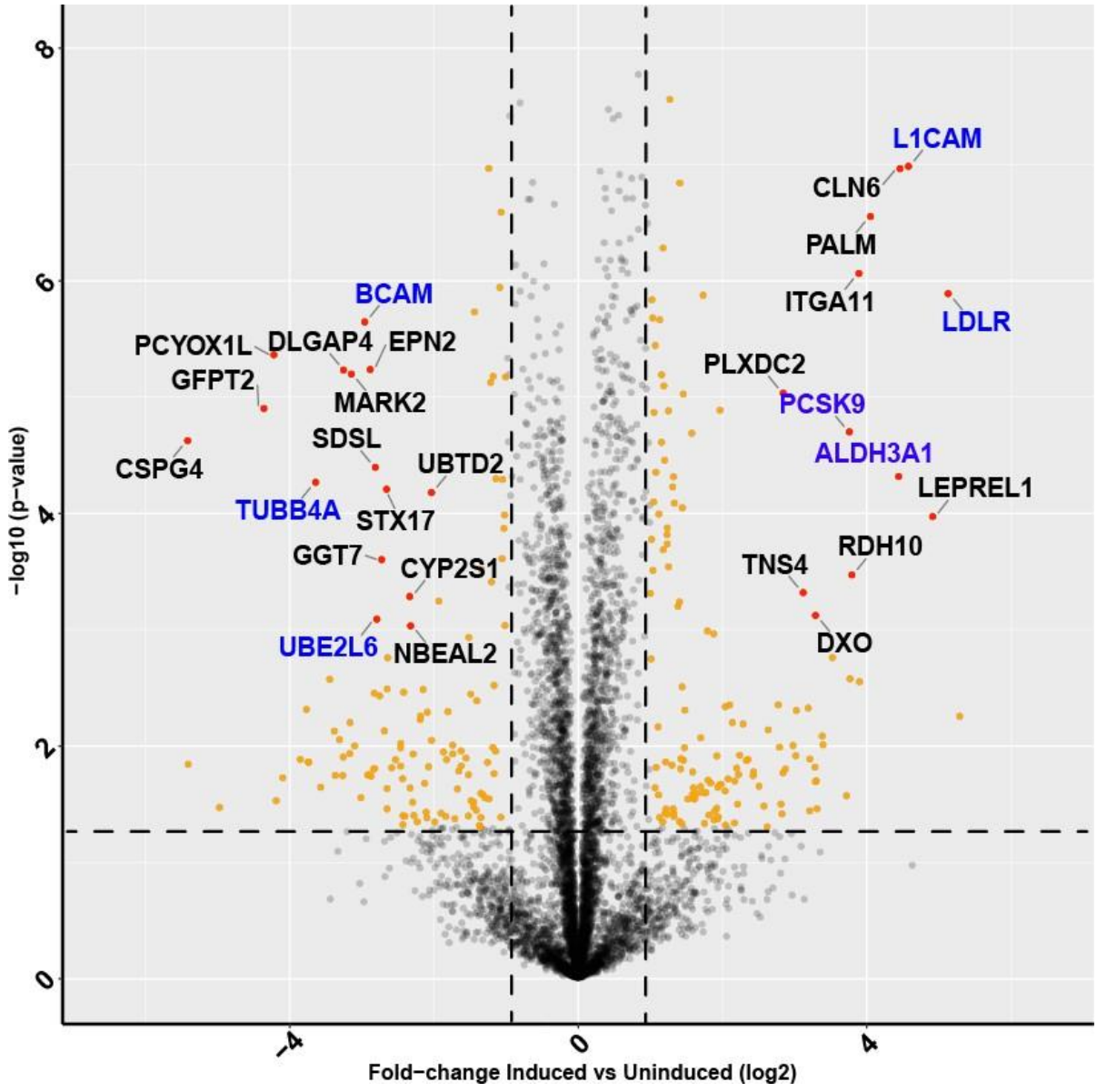
L1CAM
CLN6
PALM
ITGA11
LDLR
BCAM
PCYOX1L
DLGAP4
EPN2
GFPT2
MARK2
PLXDC2
PCSK9
SDSL
ALDH3A1
CSPG4
UBTD2
LEPREL1
TUBB4A
STX17
RDH10
GGT7
CYP2S1
TNS4
UBE2L6
NBEAL2
DXO
−log10 (p−value)
Fold−change Induced vs Uninduced (log2)

Figure 4.17 Volcano plot showing most significant/ substantial changes in the total proteome upon expression of ^{3xFLAG}CBU2016.

Volcano plot showing total proteome changes upon induction of ^{3xFLAG}CBU2016 expression. The x-axis shows induced/uninduced fold change and Y -axis shows – log10 of the *P* value. The plot is colored such that proteins having a fold change of less than 1 are shown as grey dots. Orange dots are proteins having a significant fold change of over one-fold. Altered host proteins are colored with the most pronounced changes colored in red and labelled greater than 2-fold change in abundance and with a *P* value less than 0.001. Proteins commonly altered upon expression of ^{3xFLAG}CBU1701 and ^{3xFLAG}CBU2016 are labelled in blue. Detailed information of the most significant proteins identified (red dots) is represented in the Table 4.5, which includes the fold change and significance across the various replicates. The dashed horizontal line shows where *P* = 0. 05, and the two vertical dashed lines indicate a one-fold change of protein abundance.

Table 4.5 Table showing significant protein changes in response to expression of ^{3xFLAG}CBU2016.

PROTEIN	PROTEIN NAME	FOLD CHANGE	*P* VALUE
LDLR	Low-density lipoprotein receptor	5.131	1.29E-06
LEPREL1	Prolyl 3-hydroxylase 2	4.917	1.06E-04
L1CAM	Neural cell adhesion molecule L1	4.580	1.04E-07
CLN6	Ceroid-lipofuscinosis neuronal protein 6	4.464	1.08E-07
ALDH3A1	Aldehyde dehydrogenase	4.445	4.81E-05
PALM	Paralemmin-1	4.054	2.80E-07
ITGA11	Integrin alpha-11	3.894	8.63E-07
RDH10	Retinol dehydrogenase 10	3.796	3.38E-04
PCSK9	Proprotein convertase subtilisin/kexin type 9	3.761	1.99E-05
DXO	Decapping and exoribonuclease protein	3.292	7.53E-04
TNS4	Tensin-4	3.121	4.79E-04
PLXDC2	Plexin domain-containing protein 2	2.845	9.23E-06
UBTD2	Ubiquitin domain-containing protein 2	-2.034	6.61E-05
NBEAL2	Neurobeachin-like protein 2	-2.324	9.26E-04
CYP2S1	Cytochrome P450 2S1	-2.336	5.18E-04
STX17	Syntaxin-17	-2.657	6.18E-05
GGT7	Glutathione hydrolase 7	-2.725	2.49E-04
UBE2L6	Ubiquitin/ISG15-conjugating enzyme E2 L6 protein	-2.792	8.11E-04

SDSL	Serine dehydratase-like	-2.812	4.01E-05
EPN2	Epsin-2	-2.884	5.78E-06
BCAM	Basal cell adhesion molecule	-2.960	2.26E-06
MARK2	Serine/threonine-protein kinase	-3.145	6.32E-06
DLGAP4	Disks large-associated protein 4	-3.254	5.85E-06
TUBB4A	Tubulin beta-4A chain	-3.640	5.40E-05
PCYOX1L	Prenylcysteine oxidase-like	-4.220	4.32E-06
GFPT2	Glutamine--fructose-6-phosphate aminotransferase (isomerizing) 2	-4.358	1.25E-05
CSPG4	Chondroitin sulfate proteoglycan 4	-5.415	2.37E-05

4.3 Discussion

In order to multiply within the CCV, *C. burnetii* utilises the Dot/Icm Type IVB Secretion System (T4SS). Using this secretion system, the bacterium translocates approximately 150 bacterial effector proteins into the host cell cytoplasm. The effector proteins deployed by *C. burnetii* are known to manipulate several important eukaryotic pathways such as endocytic and autophagic vesicular trafficking that are required for establishing the replicative niche.

Data presented in Chapter 3 of this thesis demonstrated that the host transcription factors TFEB and TFE3 are translocated into the nucleus during *C. burnetii* infection. This nuclear localisation of TFEB/TFE3 was reversed following treatment to block bacterial protein synthesis. These results suggest that *C. burnetii* is driving nuclear translocation of TFEB/TFE3 and this process is dependent on the T4SS. Based on this hypothesis, we attempted to identify the effectors involved in the nuclear translocation of TFEB. A comprehensive visual immunofluorescence screen was employed using 151 *C. burnetii* putative or known effectors. These effectors were cloned into a mammalian expression vector for expression in eukaryotic cells with a N-terminal 3xFLAG-tag. Transfection of these effectors individually into the HeLa TFEB-GFP stable cell line, resulted in the identification of ^{3xFLAG}CBU1701 and ^{3xFLAG}CBU2016 as two putative effectors that induce nuclear localisation TFEB (Figure 4.2). Importantly, these were the only two effectors, out of 151 that were tested, observed to induce nuclear translocation of TFEB.

However, there are some important caveats associated with this screen that may mean that not all TFEB influencing effectors were identified. A previous study showed that ectopic expression of a bacterial effector does not always correlate with effector localisation during infection [141]. Based on localisation of ectopically expressed protein, the *C. burnetii* effector protein MceA was observed to co-localise with LAMP1 suggesting lysosomal localisation [81]. Interestingly, ^{3xFLAG}MceA expressed by *C. burnetii* was later shown to localise to the mitochondrial outer membrane during *C. burnetii* infection and this was validated by MceA specific antibodies that showed mitochondrial localisation of the native protein during infection [141]. This demonstrates the possibility of effector mis-localisation during ectopic expression. Such mis-localisation may render an effector unable to perform its normal function within the eukaryotic host cell. Additionally, in this setting, each of the effectors are grossly overexpressed, compared to their abundance during infection, which might lead to pleiotropic effects and identification of false positives. Additionally, recent data indicates that bacteria with a large cohort of effectors may have some effectors that function in concert or in opposition with others thereby representing an additional layer of post-translocation effector regulation that cannot be mimicked by ectopic expression of single effectors [224]. Thus, it could be possible that two or more effectors might work together to manipulate these host transcription factors.

The Dot/Icm effector proteins identified using this screen were not previously characterised. Our bioinformatic analysis shows that they are unique to *C. burnetii* and show no similarity to any bacterial or eukaryotic proteins. BLAST analysis for CBU1701

and CBU2016 indicated a very high degree of conservation amongst the various sequenced *C. burnetii* isolates.

CBU1701 is likely a membrane protein due to the predicted 7 transmembrane domains. ATF6 (activating transcription factor - 6), a stress regulated transmembrane transcription factor [225], changes localisation in response to ER stress. Our preliminary evidence suggests that CBU1701 does not lead to ER stress and this is unlikely to be the reason that we see TFEB nuclear localisation in response to expression of CBU1701. The contribution of the transcription factors TFEB/TFE3 and their nuclear translocation in response to endoplasmic reticulum cellular stress is very well investigated [196, 226]. Thus, it will be interesting to further validate the localisation of various domains of CBU1701 in the endoplasmic reticulum using anti–calnexin marker.

A machine learning based analysis led to the prediction that CBU1701 was a *C. burnetii* effector [133]. In order to validate this prediction, we used a reporter assay to demonstrate T4SS-dependent translocation of CBU1701. This approach was unable to demonstrate translocation of CBU1701. Immunoblot of the BlaM-CBU1701 fusion protein resulted in truncated, presumably processed, protein suggesting one reason why we do not observe any translocation for CBU1701. These results may also indicate that the protein is translocated at a very low efficiency, as has been reported for several other *C. burnetii* effectors [132]. The possible cleavage of CBU1701, in both eukaryotic and bacterial systems, complicates the characterisation of this protein and warrants further investigation. Important questions remain regarding whether the native protein is a bona

fide Dot/Icm effector and whether the protein undergoes cleavage events in the bacteria and/or in the host cell.

CBU2016 is comparatively a smaller protein of 23 kDa and does not having any localisation pattern within the cytoplasm. CBU2016 showed 1% translocation using a *L. pneumophila* TEM-1 β-lactamase translocation assay classifying it as a T4SS effector by Weber et. al [132].

To gain mechanistic insights into the activation of TFEB by CBU1701 and CBU2016 respectively, human epithelial cells were engineered to allow induced expression of 3xFLAG-tagged versions of these *C. burnetii* proteins. A global proteomics approach was undertaken to determine the dynamic effect ^{3xFLAG}CBU2016 and ^{3xFLAG}CBU1701 have on the human cell proteome. This data revealed many significant changes in protein abundance upon the expression of either of these effectors. Interestingly, both effectors induced similar changes to the host proteome suggesting that both proteins have a similar influence on host cell function. Surprisingly, we observed only a small proportion of TFEB regulated proteins were altered in abundance upon expression of either effector. This gives us an indication that, our initial observation that CBU1701 and CBU2016 induce nuclear translocation of TFEB might be an indirect observation. This finding also raises the interesting possibility that TFEB nuclear localisation does not necessarily result in upregulation of the CLEAR network and that there may be additional factors that influence TFEB activity once in the nucleus.

One of the most striking observations from these experiments was that some of the most significant protein changes were shared between these two effector proteins. L1CAM (L1 cell adhesion molecule protein), LDLR (low – density lipoprotein receptor), PCSK9 (proprotein convertase subtilisin/kexin type 9), and ALDH3A1 (Aldehyde Dehydrogenase 3 Family Member A1) were found to be significantly increased in abundance similarly upon expression of both effector proteins. A review of the literature on these human proteins indicates important relationships. PCSK9 is an enzyme, expressed in many cell types and tissues, that plays an important role in the regulation of cholesterol homeostasis [32, 227, 228]. LDLR binds to low-density lipoproteins (LDLs) and plays an important role in the removal of excess cholesterol from the liver where it is found in abundance, thus regulating the amount of cholesterol in the blood [229, 230]. PCSK9 binds to LDLR and targets it for lysosomal degradation within cells [231-233]. mTORC1 is known to regulate LDL receptor (LDLR) expression [234, 235]. This suggests the role of lysosomes in regulating the mTORC1–dependent balance between lipid uptake and lipid synthesis (Figure 4.18).

The importance of host lipids in *C. burnetii* infection has been previously well–studied wherein lipids have been shown to be essential for maintaining the acidic CCV and for its formation [79, 236, 237]. Several recent reports have shown the importance of cholesterol in CCV formation and bacterial replication, suggesting an important role for lipids in the pathogenesis of *C. burnetii* [90, 236, 237]. This also is a balancing act as too much cholesterol seems to be detrimental to the pathogen.

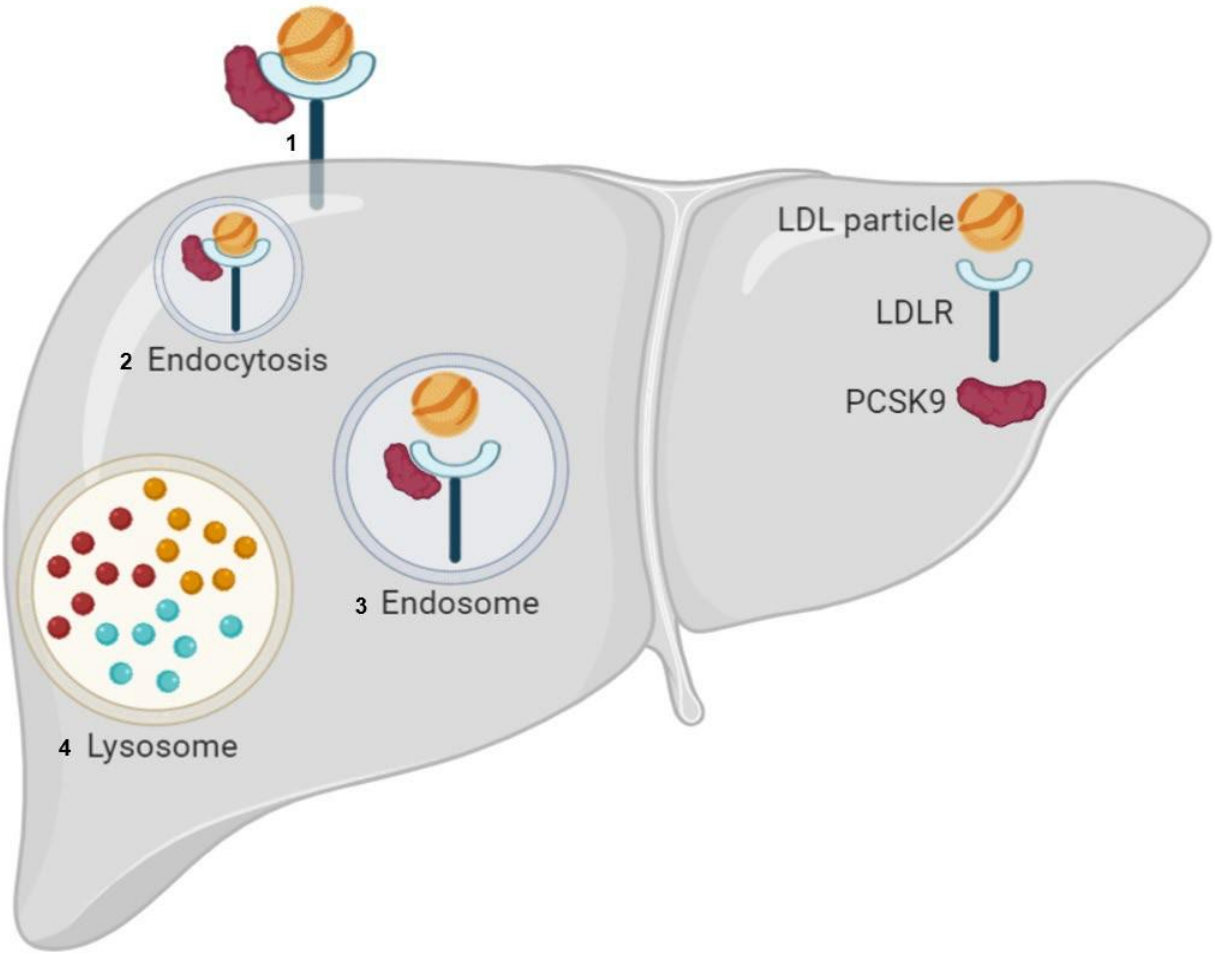

Figure 4.18 Mechanism of action of LDLR and PCSK9

1) PCSK9 binds to LDLR and upon internalisation (endocytosis) of the LDLR/PCKS9 complex (2). The complex gets internalised to undergo degradation in the lysosomes (3 and 4).

It has been demonstrated that the CCV is rich in cholesterol, and formation of CCV is prevented when cells are treated with inhibitors, suggesting these molecules are scavenged from the host and stored by the bacterial pathogens [61, 169]. The *C. burnetii* protein CBU1206 has been identified as an enzyme (sterol reductase) acting on cellular cholesterol during *C. burnetii* intracellular replication [238]. The mammalian lipid-binding protein, ORP1L (oxysterol-binding protein related-protein 1) has been shown to interact with the CCV in a T4SS-dependent manner and has been shown to be essential for the expansion of CCV [239].

The role of TFEB in lipid metabolism is also well studied as it has been demonstrated that a loss of the TFEB orthologue, *HLH-30*, in *Caenorhabditis elegans* resulted in decreased expression of enzymes required for lipid catabolism [240]. It will be interesting to investigate the role of *C. burnetii* putative effector CBU1701 and effector CBU2016 in the manipulation of host cell lipids which may further aid in our understanding *C. burnetii* pathogenesis.

To further characterise the two novel proteins, CBU1701 and CBU2016, that induce nuclear activation of TFEB and TFE3, various techniques can be employed by the tools generated in this study. This will lead to mechanistic understanding of how these effectors do manipulate lysosomal biogenesis and further have an impact in the infection of *C. burnetii*. For example, interacting partners of CBU1701 and CBU2016 can be identified using the stable cell lines expressing ^{3xFLAG}CBU1701 and ^{3xFLAG}CBU2016. This could be achieved by using anti-FLAG to immunoprecipitate the effector and any host

binding partners and identify these proteins via mass spectrometry. The potential targets could be further investigated using functional assays to determine their biological relevance during *C. burnetii* infection. Most bacterial effector proteins that have been thoroughly characterised are enzymes, so investigation into any potential modification of the host targets could yield an understanding of the biochemical function of these effectors [241].

Various signalling pathways can be assessed using these stable cell lines to determine the pathways that contribute to nuclear localisation of TFEB and TFE3 in this setting. As previously mentioned, since the host phosphatase, calcineurin is known to dephosphorylate TFEB/TFE3 and facilitate its nuclear translocation, we could demonstrate whether calcineurin is required for TFEB/TFE3 activation [242]. This could be done by treating the stable cell lines using FK506, a calcineurin inhibitor, and monitoring TFEB/TFE3 localisation by nuclear–cytoplasmic fractionation of ^{3xFLAG}CBU1701 and ^{3xFLAG}CBU2016 stable cell lines. Similarly, mTORC1 substrate phosphorylation status can also be monitored in these stable cell lines [189, 196]. This functional assay will give us insights into whether absence of mTORC1 activity is required for TFEB/TFE3 nuclear activation in the presence or absence of the stable cell lines. In a similar fashion, using specific kinase inhibitors to inhibit PKC and ERK2 we will be able to examine the role of these kinases in CBU1701 and CBU2016 induced nuclear localisation of TFEB and more broadly during *C. burnetii* infection [243].

To further determine whether autophagy is altered and there is more lysosome, LC3 lipidation or p62 turnover could have been monitored. The lysosomal functions could have been analysed using the well-established DQ BSA assay to look at proteolytic potentials of the lysosome. Autophagy can also be inhibited using 3-Methyladenine or wortmannin that inhibits type III PI-3K (phosphatidylinositol 3-kinases). Use of 3-MA results in inhibition of autophagy by blocking autophagosome formation. These chemicals can have pleiotropic effects such as cytotoxicity and can negatively impact cell growth and proliferation. Other approaches could involve the use of autophagy deficient cell lines like ATG5 knockout or silencing expression of Atg5 using RNA interference. This chapter described research towards understanding how *C. burnetii* effectors actively manipulate host cell transcription to promote autophagy and lysosome biogenesis. Understanding how *C. burnetii* controls the lysosome-signalling axis may provide novel insights into host-pathogen interactions and more broadly the mechanisms that contribute to important human disease states such as lysosomal storage disorders and neurodegenerative diseases.

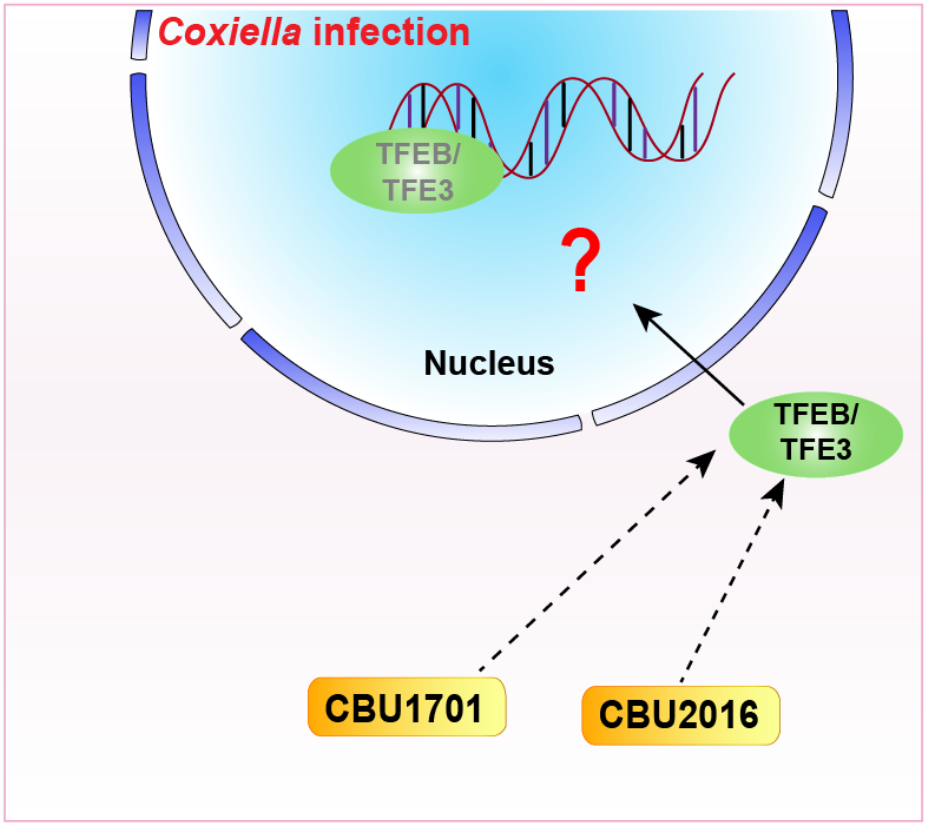

Figure 4.19 Summary of findings presented in Chapter 4.

An un-biased immunofluoresence screen using 151 *C. burnetii* proteins, identifies CBU1701 and CBU2016 to induce nuclear localisation of TFEB and TFE3. The proteomics data however proved that these proteins do not drive the expression of these genes, suggesting that TFEB localisation and its activity are uncoupled in this condition.

Chapter 5

Characterising the role of TFEB-modulating effector proteins during *C. burnetii* infection

5.1 Introduction

The research presented in this thesis has shown that *C. burnetii* manipulates TFEB/TFE3, promoting lysosomal biogenesis and autophagy, resulting in the expansion of the CCV [211]. This finding led to the hypothesis that *C. burnetii* drives activation of this lysosome-nuclear signalling axis through the novel actions of effector proteins and led to the identification of two putative *C. burnetii* proteins, CBU1701 and CBU2016, as potential novel regulators of this process.

Significant research has shown that lysosomal biogenesis is transcriptionally regulated by the transcription factors TFEB, TFE3, MITF and TFEC that make up the MiTF/TFE family [179]. These microphthalmia transcription factors are basic helix-loop-helix-leucine zipper (bHLH-Zip) family encoded regulators that bind as homo or heterodimers to E-box (CANNTG) element. TFEB and TFE3, which are the focus of this thesis, have a ubiquitous pattern of expression in many different cell lines. Expression of MITF is mostly found in macrophages, NK cells, B cells and TFEC is limited to myeloid cells such as monocytes, erythrocytes, platelets, or erythrocytes [179]. MiTF/TFE family regulators are known to transcriptionally control lysosomal biogenesis through various pathways [244].

Recent studies have highlighted the role of autophagy/lysosomal pathway, a highly dynamic system to be involved in the cellular adaptation to various stresses such as deprivation of nutrients, mitochondrial abnormalities, protein misfolding and infections by infectious agents [185]. Defects in the autophagosome-lysosome pathway have been highlighted in several human diseases such as Parkinson's disease (PD), Alzheimer's

disease, Neurodegenerative diseases, Huntington's disease, prions disease and in cancers [245]. This pathway is often hijacked by bacterial pathogens to regulate cellular survival, thus playing an important role in pathogenesis [246].

The clever intracellular bacterial pathogens have figured out ways to escape autophagy of the host in order to survive and multiply within the host. For example, *M. tuberculosis* H37Rv effector ESAT-6 and the virulence regulator PhoP target host Rab7 inhibiting the maturation of autophagosomes [247]. The effector Esx-1 from *M. marinum* targets the host mTORC-1 to block the autophagic-flux [248]. The *L. pneumophila* effector RavZ impedes autophagy catalysing irreversible delipidation of LC3, by cleaving amino terminal conjugation site thus blocking the progression of autophagosomes on the autophagosomal membrane [162]. *Listeria monocytogenes* autotransporter ActA catalyses actin polymerization, through interaction with Arp2/3, on the bacterial surface to escape autophagic recognition [160, 249]. These are some of the examples demonstrating how bacterial factors interact with the host autophagy machinery for the benefit of replication and survival within eukaryotic cell.

With the recent advancements in culturing *C. burnetii* in vitro [69], and subsequent development of genetic tools, potential effector proteins that could be influencing virulence of this pathogen have been identified. Thus far, there are approximately 150 effector proteins known to be encoded by *C. burnetii* and the role of the vast majority is not clearly defined [121, 129, 132, 133, 209, 250]. Multiple effectors have been linked to important cellular processes including inhibition of host cell apoptosis [93, 149],

redirecting host vesicular trafficking pathways [121, 132, 144, 146, 251-254] and influencing transcription of the host [143]. Most of these effectors are unique to *C. burnetii* having very low or no homology to other bacterial or eukaryotic proteins and are therefore predicted to possess novel biochemical functions that can uniquely modulate eukaryotic processes [121, 129].

The putative effector, CBU1701 and experimentally validated effector CBU2016 were identified in Chapter 4 as capable of inducing the nuclear localisation of TFEB and TFE3. Thus, functionally characterising the importance of these effectors, through production and analysis of mutant strains, will reveal their significance in *C. burnetii* intracellular replication and virulence.

With the findings in Chapter 3 that silencing of TFEB and TFE3 individually or together resulted in a remarkable reduction in the CCV size, we predicted that infection of HeLa CCL2 and THP-1 cell lines with *C. burnetii* lacking CBU1701 and/or CBU2016 would also have an impact on the expansion and maintenance of CCV that could in turn affect the replication of *C. burnetii*. However, the surprising findings in Chapter 4, that expression of these effectors had a minimal impact on the TFEB regulon, could suggest that these effectors may not influence CCV expansion analogous to the role of TFEB and TFE3 during infection. This chapter aimed to characterise the role of these effector proteins with an emphasis on strain generation and initial characterisation in the context of *C. burnetii* infection.

5.2 Results

5.2.1 Experimental process for production of *C. burnetii* effector mutants

To functionally characterise the role of CBU1701 and CBU2016 in *C. burnetii*, single and double knockout mutants were generated. Newton et al., 2014, created a *cbu1701*::Tn transposon mutant as part of a library of mutants that was used to identify novel factors that had an impact on the morphology of the CCV [81]. Deletion of *Δcbu2016* was achieved using the "loop in/loop out" inactivation strategy developed for *C. burnetii* (Figure 5.1) [130]. Deletion of *cbu2016*, was achieved in both wild-type and *cbu1701*::Tn strains using this knockout method.

Briefly, a suicide plasmid carrying the upstream and downstream regions of a target gene that allows for chromosomal integration via homologous recombination encoding a *sacB* counter selection marker, that allows the plasmid to come back out of the genome, is generated. This procedure facilitates generation of targeted mutants however is considerably time consuming with a mutant made in approximately 10 weeks if the procedure works optimally. Given the extensive time required to isolate *C. burnetii* deletion mutants, the thorough characterisation of these mutants is yet to be completed. However, this study has been able to begin to characterise the importance of these proteins during infection.

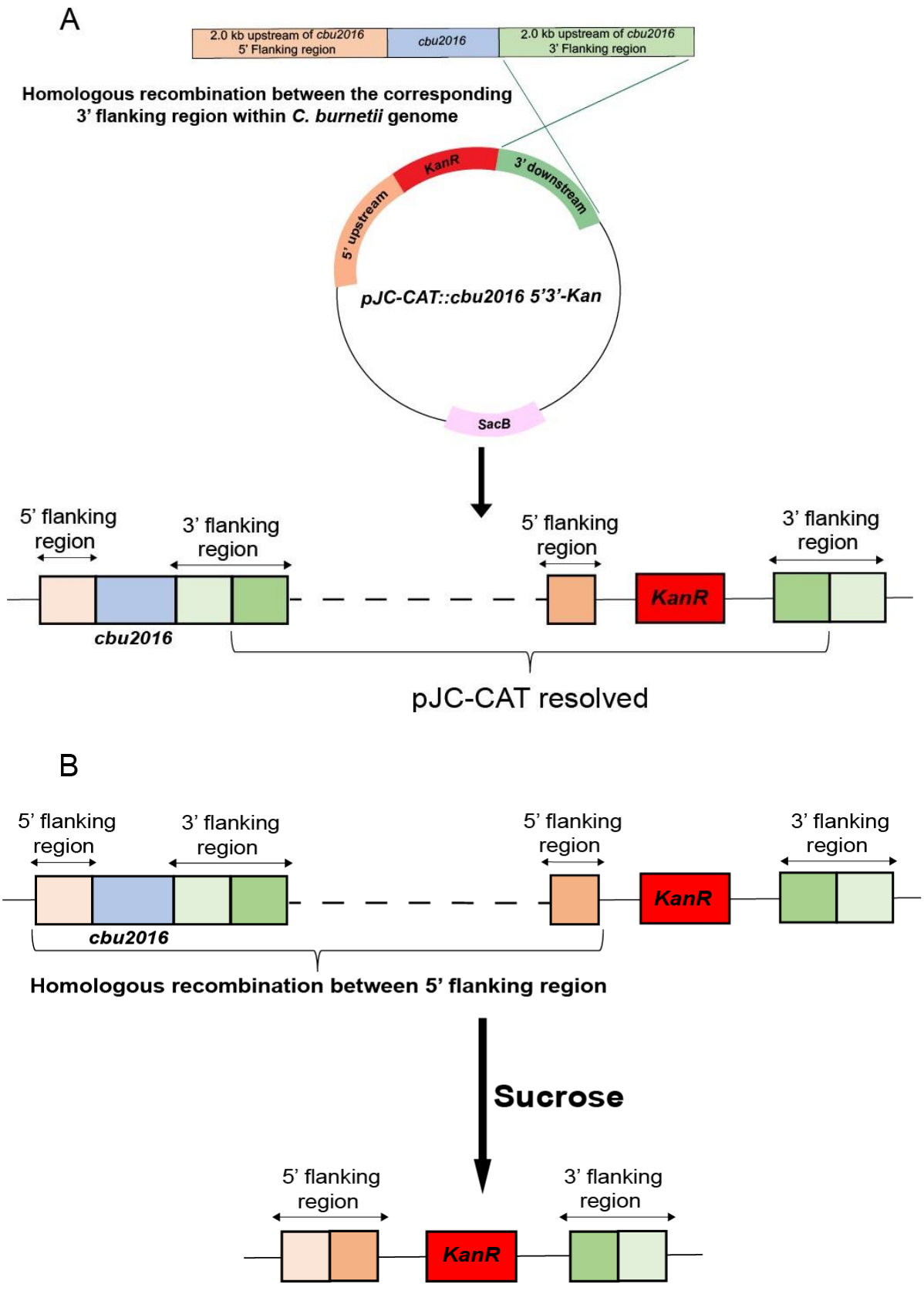
A
2.0 kb upstream of cbu2016 5' Flanking region
cbu2016
2.0 kb upstream of cbu2016 3' Flanking region
Homologous recombination between the corresponding 3' flanking region within C. burnetii genome
KanR
3' downstream
5' upstream
pJC-CAT::cbu2016 5'3'-Kan
SacB
5' flanking region
3' flanking region
5' flanking region
3' flanking region
KanR
cbu2016
pJC-CAT resolved
B
5' flanking region
3' flanking region
5' flanking region
3' flanking region
KanR
cbu2016
Homologous recombination between 5' flanking region
Sucrose
5' flanking region
3' flanking region
KanR

Figure 5.1 *cbu2016* knockout strategy

(A) pJC-CAT::*cbu2016* 5'3'-Kan knockout plasmid integration into the corresponding 3' region of the *C. burnetii* genome by homologous recombination between the 3' flanking region on the plasmid. The integration can also be mediated in the 5' flanking region (not shown).

(B) Second homologous recombination event between the flanking 5' region of the integrated plasmid and the reciprocal region within the *C. burnetii* genome. Selection in sucrose-containing media results in resolution of pJC-CAT::*cbu2016* 5'3'-Kan knockout plasmid without *cbu2016*, resulting in no change to the genome of *C. burnetii*. The gene of interest is replaced by the kanamycin cassette as a result of sucrose counter selection.

*cbu1701::*Tn was clonally isolated from a transposon mutant library [80, 81] (Figure 5.2). This strain contains a transposon 1023 bp from the start codon disrupting *cbu1701*. A non-functional *cbu1701::*Tn mutant is generated through transposon disruption. This is a "non-functional" mutant because the gene is disrupted such that the full length protein cannot be made, given that the translocation signal is usually within the C-terminal part of the protein. This means that even if a truncated N-terminal part of CBU1701 was produced, we could predict that it would lack the capacity for translocation. *cbu1701::*Tn mutant strain was confirmed using gene-specific primers 20 and 21 (Table 2. 3). *cbu1701* (1407 bp) was successfully PCR-amplified from WT gDNA but not from the *cbu1701::*Tn indicating disruption of *cbu1701* with a transposon insertion in the single and the double mutant strains.

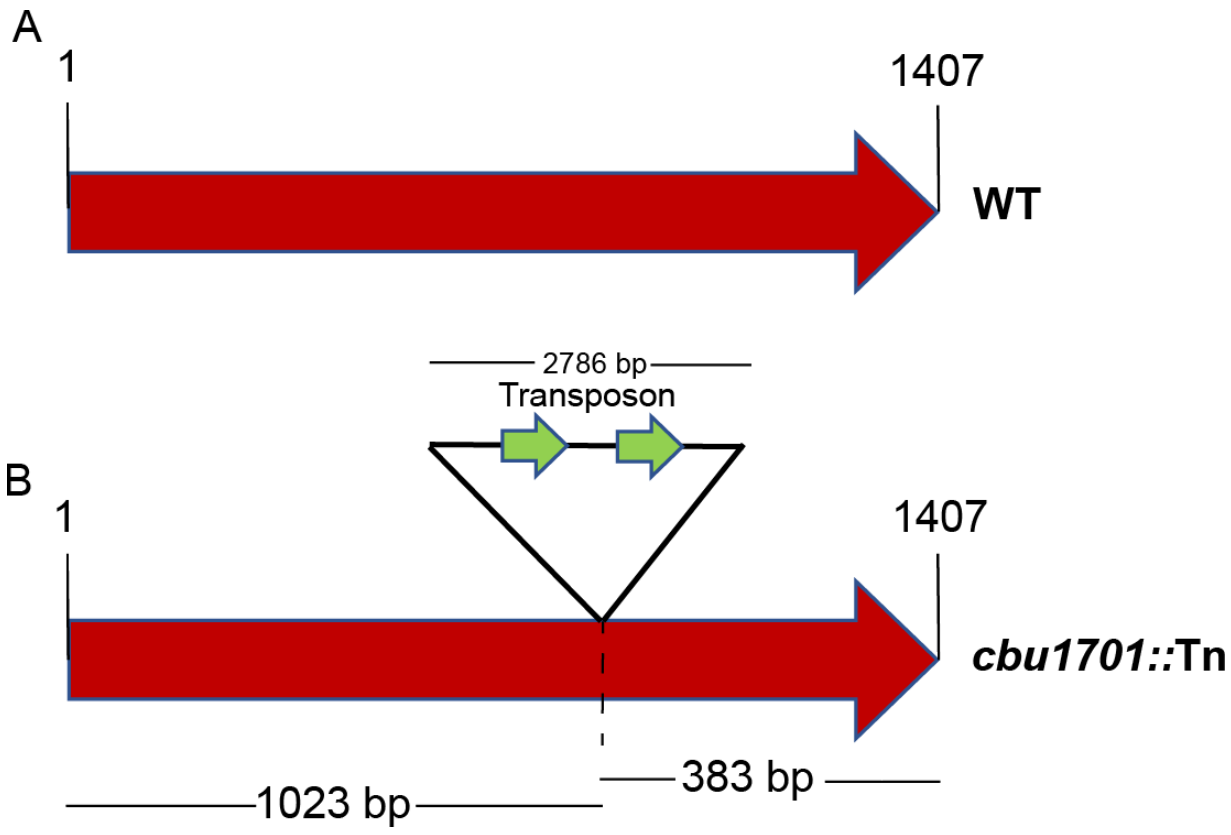

Figure 5.2 Schematics showing transposon insertion in *cbu1701*

(A) Schematic showing 1407 bp *C. burnetii cbu1701*. (B) The 2786 bp transposon is inserted 1023 bp from the start of *cbu1701*, resulting in gene disruption.

5.2.2 Targeted gene deletion in *C. burnetii*

Genetic manipulation of *C. burnetii* is a slow process with low efficiency. The primary integration of pJC- CAT::*cbu2016* 5'3'-Kan was achieved, but plasmid could not be resolved because of a mutation that was present in *sacB*. Hence, the first attempts to delete *cbu2016* were unsuccessful due to mutations within the plasmid. Therefore, the knockout plasmids for *cbu2016* were freshly constructed to generate mutant strains. Deletion of *cbu2016* was generated by the homologous recombination approach wherein *cbu2016* was replaced with a kanamycin resistance cassette [79]. This plasmid was introduced into WT and into *cbu1701::*Tn by electroporation to initiate the recombination process (Figure 5.1). Electroporation was followed by culturing and routinely passaging of these transformants for 28 days with the appropriate antibiotics. Initial recombination event showing successful chromosomal integration of the plasmid was confirmed by PCR. A second recombination event for achieving the knockout was achieved by sub-culturing transformants in the presence of sucrose as counter selection (Figure 5.1).

The sucrose counter selection for *cbu2016* knockout in the *cbu1701::*Tn background was done in the presence of chloramphenicol and kanamycin. This was essential as *cbu1701::*Tn required chloramphenicol selection and *Δcbu2016* was achieved by *cbu2016* replacement with a kanamycin resistance cassette following the excision of the suicide plasmid backbone. Double mutants were clonally isolated by picking individual colonies after subsequent expansion of the culture as detailed in section 2.12 [79]. Four independent double mutants were clonally isolated and further confirmed by PCR analysis.

Using gene-specific primers 18 and 19 (Table 2. 3), *cbu2016* (600 bp) was successfully PCR-amplified from WT gDNA but not from the *Δcbu2016* single and double mutants indicating the absence of *cbu2016* in the single and the double mutant strains. Successful PCR amplification from the *Δcbu2016 cbu1701*::Tn gDNA using primers 3 and 4, or 5 and 6, indicated the replacement of *cbu2016* with a kanamycin resistance cassette.

5.3 Infection of human epithelial cells with CBU1701 and CBU2016 mutant strains results in reduced replication.

Initial characterisation of the role of CBU1701 and CBU2016 during *C. burnetii* infection was performed by infecting human epithelial cells with *cbu1701*::Tn*, Δcbu2016* and Clone B (double mutant) strains and comparing these to the WT strain. This assay was performed using one clonal isolate for each of the mutants. Immunofluorescence imaging three days post–infection implied there may be a difference in the CCV size for *cbu1701*::Tn and *Δcbu2016* mutants in comparison to the WT. The *C. burnetii* double mutant strain Clone B immunofluorescence images also indicated a difference in the replication phenotype as shown in Figure 5.3. This data suggests a severe possible *C. burnetii* replication defect in the absence of both CBU1701 and CBU2016.

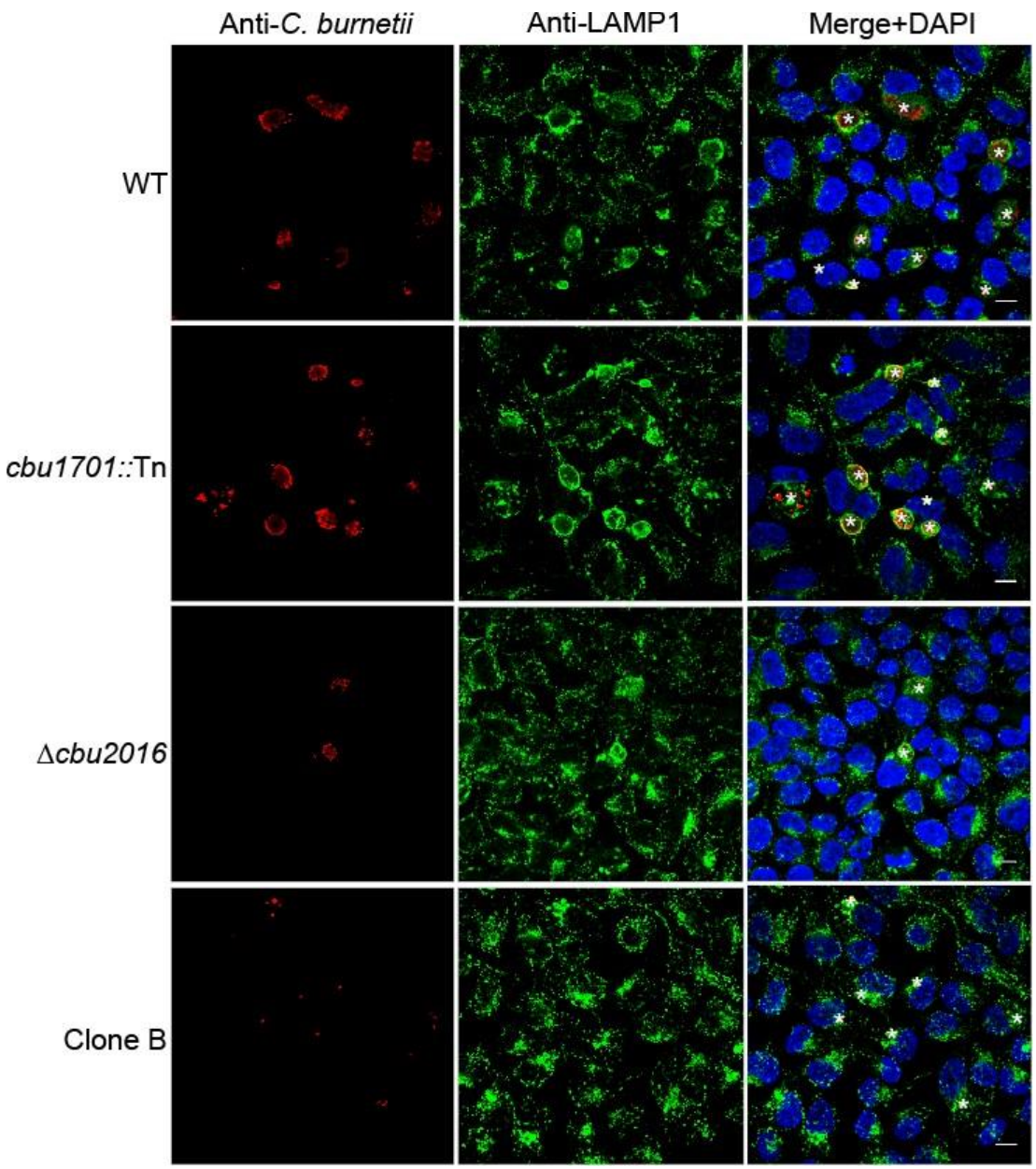

Figure 5.3 Infection of human epithelial cells using the CBU1701 and CBU2016 mutant strains results in reduced replication.

Representative confocal microscopy images of HeLa cells infected with WT, *cbu1701*::Tn, *Δcbu2016* and Clone B mutant strains for 3 days. Infected cells were fixed and stained with anti-*C. burnetii* (red), anti-LAMP1 (green) and DAPI (blue). * CCV. Scale bars, 10 µm.

5.3.1 Absence of CBU1701 and CBU2016 results in an intracellular replication defect.

To examine the requirement of CBU1701 and CBU2016 for *C. burnetii* intracellular replication, the replication of various *C. burnetii* mutant strains were examined in HeLa cells. Quantitative PCR (qPCR) was employed to perform intracellular replication curves of the various *C. burnetii* strains at days 0, 1, 3, 5- and 7-days post–infection (Figure 5.4 (A)). Data obtained from two replicates for two different clonal isolates of *cbu1701*::Tn tested displayed a slight replication defect in comparison to WT. This data indicated a possible reduction in the replication of the *cbu1701*::Tn mutant. However further replicates would be required to determine whether this difference is statistically significant.

A more severe replication defect was observed for two clonally isolated mutant strains of *Δcbu2016*. This mutant phenotype obtained for *Δcbu2016* corelates to the phenotype reported by Weber et al [132]. Surprisingly, the two independent clonal isolates of the double mutant strain demonstrated two very different replication defects (Figure 5.4). One of the double mutants phenocopied the CBU1701 mutant, Clone A, and the other isolate did not replicate intracellularly, Clone B, analogous to the Dot/Icm-deficient *icmL*::Tn strain. *C. burnetii icmL*::Tn did not show any replication as expected and acted as a negative control for *C. burnetii* replication.

CCV areas of the various mutants were quantified and compared to WT (Figure 5.4 B). This visual quantification was done at 3 days post–infection from two biological replicates.

The average CCV area measurement showed that the CCVs formed by the CBU1701 and CBU2016 single mutants were smaller in comparison to the parental strain. Additionally, the two clonal isolates of the double mutant strains displayed different CCV phenotypes, depicted in Figure 5.4 (B), that mirrored the replication results. Clone A (dark blue) replicated and showed CCVs similar in size to the CBU1701 mutant. In comparison clone B (light blue) showed no replication, similar to the Dot/Icm-deficient strain, and did not form spacious CCVs. The data shows the difference in the phenotypes displayed by the two independent double mutants. Taken together, this data suggests an important role for these proteins in both the intracellular replication of *C. burnetii* and CCV expansion.

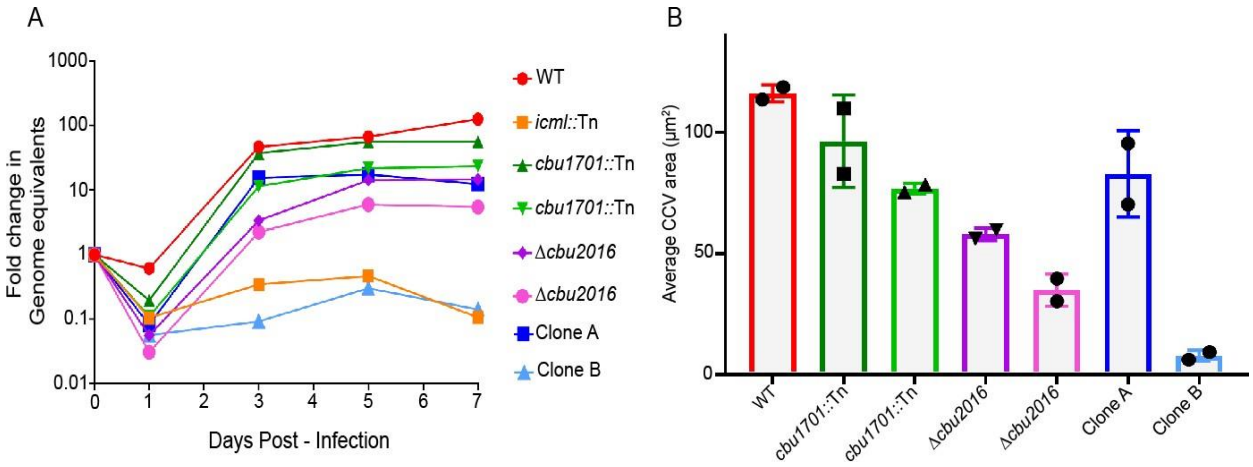

Figure 5.4 Loss of CBU1701 and CBU2016 impacts intracellular replication of *C. burnetii* and CCV expansion.

(A) HeLa cells were infected with WT, *icmL::*Tn and two clonal isolates of each of *cbu1701::*Tn, *Δcbu2016* and *Δcbu2016 cbu1701::*Tn (Clone A and Clone B). To determine the ability of various strains to replicate intracellularly, HeLa cells were infected at a MOI of 100, and cell lysates were harvested at days 0, 1, 3, 5 and 7 days post– infection. Replication curves were generated by calculating the fold change in genome equivalents of *C. burnetii* relative to Day 0. Graph represents the fold change in genome equivalents of a single experiment.

(B) The average CCV area from 30 different vacuoles for two biological replicates of HeLa cells infected with the indicated *C. burnetii* strains. The CCV area was quantified 3 days post–infected cells.

5.3.2 The localisation of TFEB-GFP depends on CBU2016 and CBU1701.

As previously described in Chapter 4, ectopic expression of *C. burnetii* effectors CBU1701 and CBU2016 induces nuclear localisation of TFEB. Therefore, in order to assess whether CBU1701 and CBU2016 mutant strains had a defect in the nuclear localisation of TFEB, *cbu1701*::Tn*, Δcbu2016* and Clone B (*Δcbu2016 cbu1701*::Tn) strains were used to infect HeLa TFEB-GFP stable cell lines at a MOI of 100. Immunofluorescence imaging three days post–infection resulted in nuclear localisation of TFEB in the case of WT and to a lesser extent for CBU1701 and CBU2016 single and double mutant strains (Figure 5.5 (A)). This observation was apparent when the nuclear/cytoplasmic ratio of TFEB–GFP was quantified using the N/C ratio quantification previously detailed in Chapter 3 [211]. As shown in Figure 5.5 (B), a decrease in the nuclear translocation of TFEB-GFP was observed in the *Δcbu2016* and Clone B strains, when quantified from a single experiment. The TFEB-GFP nuclear localisation during *cbu1701*::Tn infection was comparable to the WT strain.

This data suggests that *C. burnetii* requires both the effectors to induce nuclear localisation of TFEB-GFP. This initial quantification data supports preliminary replication data in indicating that *cbu2016* may be more critical than *cbu1701*. The average nuclear/cytoplasmic ratio for the double mutant was only quantitated from Clone B and may not be a true representation of the double mutant.

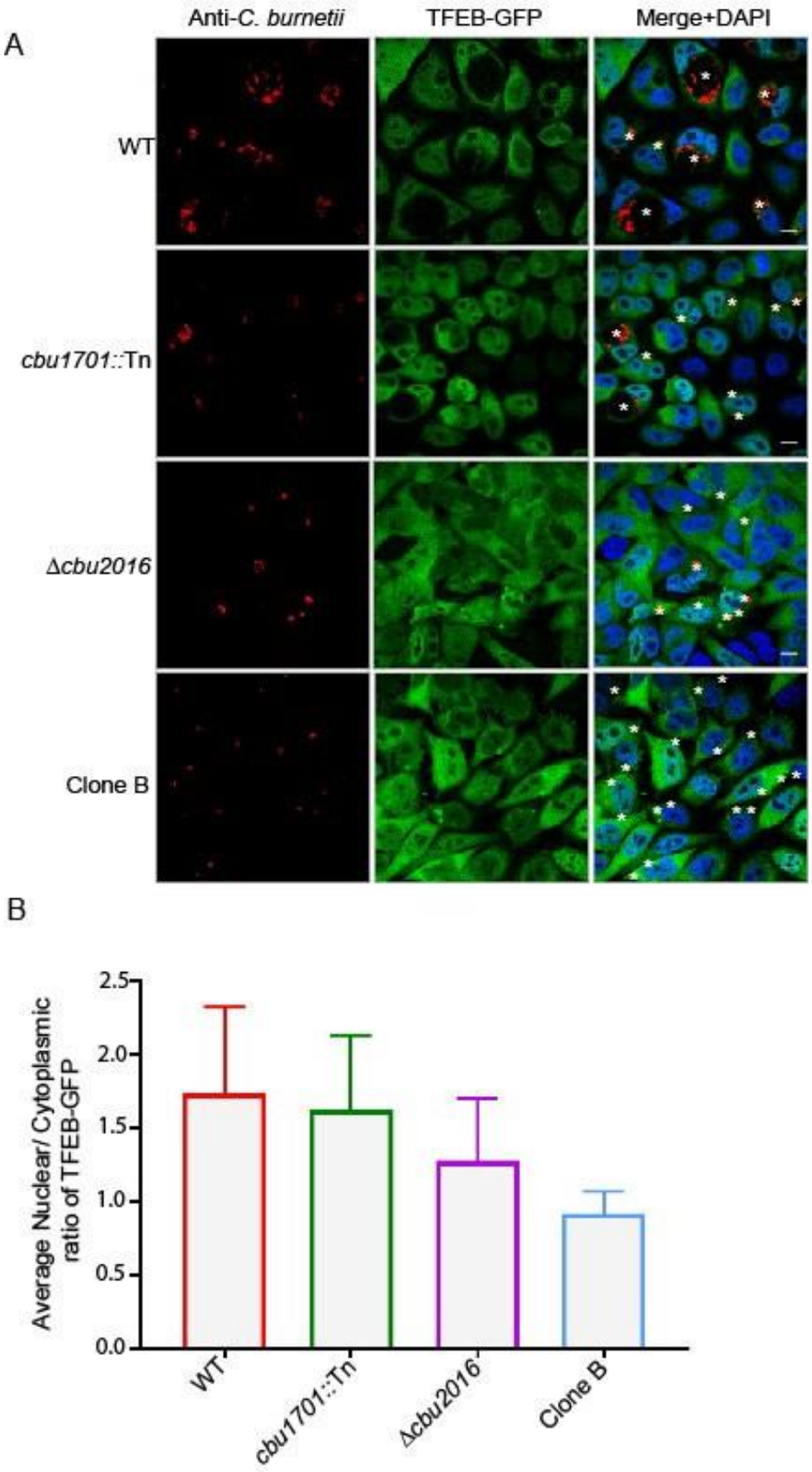
A
Anti-C. burnetii
TFEB-GFP
Merge+DAPI
WT
cbu1701::Tn
Δcbu2016
Clone B
B
Average Nuclear/ Cytoplasmic ratio of TFEB-GFP
2.5
2.0
1.5
1.0
0.5
0.0
WT
cbu1701::Tn
Δcbu2016
Clone B

Figure 5.5 Infection of TFEB-GFP cells using CBU1701 and CBU2016 mutant strains to monitor nuclear translocation of TFEB.

(A) Confocal microscopy images of HeLa TFEB–GFP cells infected for 3 days with WT, *cbu1701*::Tn, *Δcbu2016* and Clone B strains. Infected cells were fixed and stained with anti-*C. burnetii* (red) and DAPI (blue). * CCV. Scale bars, 10 μm.

(B) Average nuclear/cytoplasmic ratio (N/C ratio) of TFEB–GFP of 30 infected cells, from a single experiment for each of the single and double mutants tested as indicated.

5.3.3 Further investigation into the conflicting phenotypes observed by *Δcbu2016 cbu1701::*Tn double mutants.

The *C. burnetii* strain engineered to have *cbu1701* disrupted by a transposon and *cbu2016* replaced with a kanamycin resistance cassette had been previously confirmed through a series of PCRs. However, two independent clonal isolates of this double mutant displayed conflicting phenotypes in HeLa cells (Figure 5.4). These discrepancies were further examined with two additional isolated double mutants in HeLa cells.

Three days post–infection, cells were fixed and stained for LAMP-1 and *C. burnetii* to observe and quantify CCV size (Figure 5.6). WT resulted in large CCVs (average 200.56 μm^2) (Figure 5.6 (A)), whereas the newly tested clonal isolates (Clone C and Clone D) phenocopied the double mutants tested earlier Figure 5.6 (B and D)). Clone A had an average CCV size of 94.35 μm^2 and Clone B measured 3.68 μm^2. One of the double mutants (Clone C) produced a “small” CCV phenotype analogous to Clone A (67.79 μm^2) and the other mutant (Clone D) resulted in the “very small” CCV phenotype analogous to Clone B (3.40 μm^2) (Figure 5.6 (C and E)).

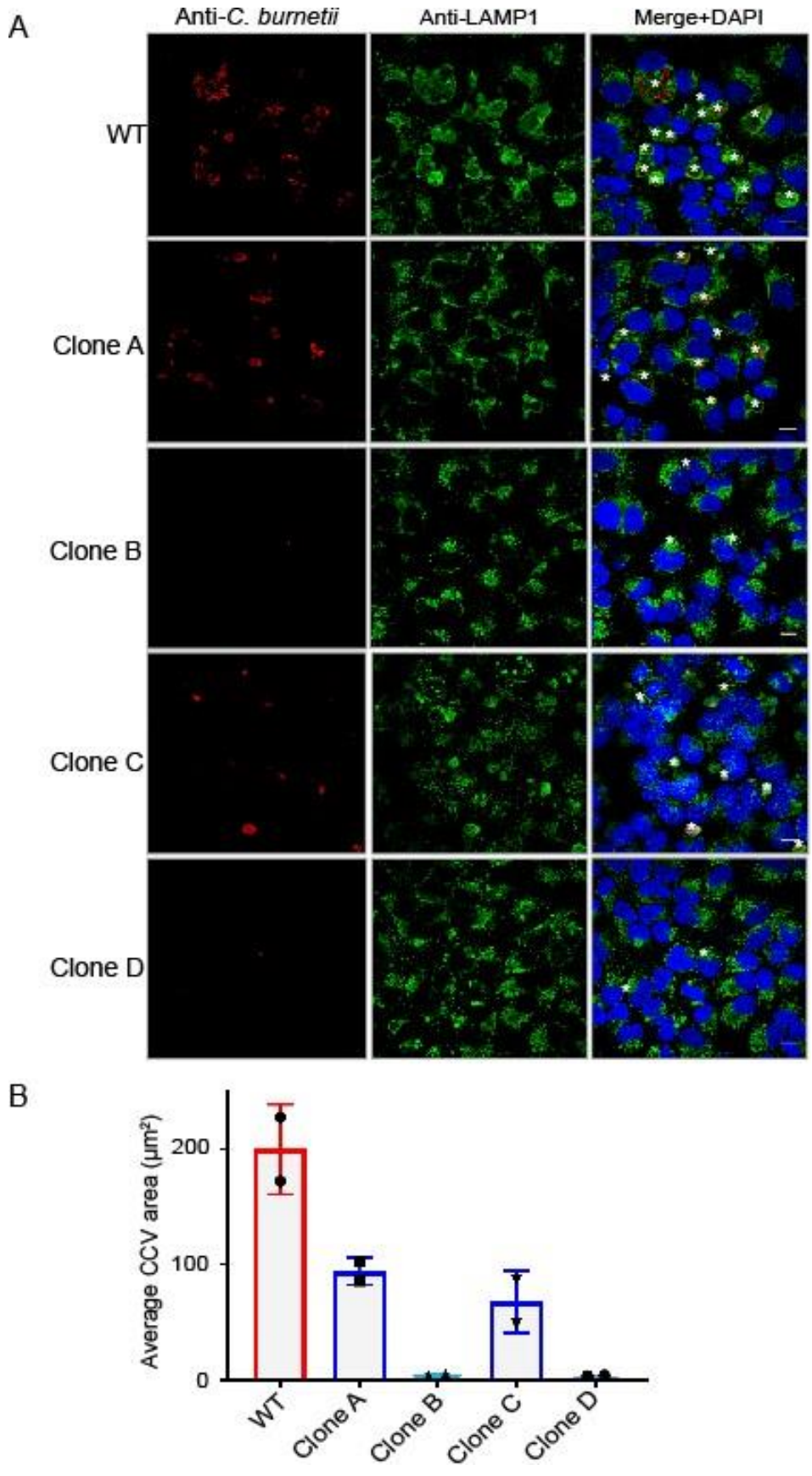
A
Anti-C. burnetii
Anti-LAMP1
Merge+DAPI
WT
Clone A
Clone B
Clone C
Clone D
B
Average CCV area (μm²)
200
100
0
WT
Clone A
Clone B
Clone C
Clone D

Figure 5.6 Comparison of multiple isolates of the CBU2016 CBU1701 double mutant in HeLa cells.

(A) Representative confocal microscopy images of HeLa cells infected for 3 days with WT, “small” CCV double mutant phenotype, Clone A and Clone C and “very small” CCV double mutant phenotype, Clone B and Clone D, respectively. Infected cells were fixed and stained with anti-*C. burnetii* (red), anti-LAMP1 (green) and DAPI (blue). * CCV. Scale bars, 10 µm.

(B) The average CCV area from two independent infections, quantified 3 days post– infection. CCV area was quantified from 30 different CCVs for two biological replicates of HeLa cells infected with the indicated *C. burnetii* strains.

5.3.4 Whole genome sequencing to confirm the CBU1701 and CBU2016 double mutant strains.

Given the phenotype discrepancies observed with independent isolates of the double mutant, whole genome sequencing was performed in order to both confirm the mutations and determine if any of the isolates possessed additional mutations that could explain the phenotypic differences. Genomic DNA was extracted from WT and from Clone A and Clone B of the *Δcbu2016 cbu1701*::Tn double mutant displaying the two different CCV phenotypes. Genomic DNA was processed for whole genome sequencing in collaboration with Dr Sacha Pidot and Professor Tim Stinear at the Doherty Applied Microbial Genomics Centre. Transposon insertion in *cbu1701* and replacement of *cbu2016* with a kanamycin resistance cassette was confirmed through this sequencing technique. Whole genome sequencing of these mutants suggested a 65 bp deletion towards the end of *cbu1877*, a gene predicted to encode an ATPase. This 65 bp deletion was observed in Clone B of the *Δcbu2016 cbu1701*::Tn double mutant strain. However, coverage of this region was also very low in Clone A.

Sanger sequencing was performed from a PCR using oligonucleotides to amplify the 65 bp region of *cbu1877* and this region was found completely conserved in all tested isolates. Thus, whole genome sequencing confirmed the *cbu1701* and *cbu2016* mutations but could not explain the difference in the phenotypes observed in the double mutant strains. Figure 5.7 shows a Clustal_W alignment which indicates that within this region the sequence was fully conserved.

Figure 5.7 Multiple sequence alignment of the double mutants with *C. burnetii* WT *cbu1877*.

Nucleotide sequence comparison of WT strain, double mutants Clones A and B in comparison to the 65 bp region of *C. burnetii cbu1877* reference genome (*C. burnetii* RSA 439 (red) to show the sequence similarities. Asterisk (*) indicate fully conserved residues.

5.3.5 Construction of a *C. burnetii* CBU1701::Tn complementation strain.

In order to establish whether the phenotypes reported in Section 5.3 could be attributed to the mutation of *cbu1701* and/or *cbu2016*, the *cbu1701* transposon mutant strain and the *Δcbu2016 cbu1701*::Tn double mutant strains were complemented with a constitutively expressed, plasmid encoded version of *cbu1701* with an N-terminal 3xFLAG epitope tag. This construct was engineered on the pJB-CAT::*argGH* backbone, that allows selection of genetic transformants through arginine auxotrophy [72]. In construction of the single and double mutant strains both chloramphenicol and kanamycin resistance were introduced into the bacteria. Thus, complementing these mutant strains using pArgGH–^{3xFLAG}CBU1701 would allow for a non-antibiotic based selection [72].

The expression of ^{3xFLAG}CBU1701 from pJB-CAT::*argGH* was confirmed by probing *E. coli* lysate carrying pArgGH–^{3xFLAG}CBU1701 with anti–FLAG antibodies (Figure 5.8 (A)). Truncated protein bands of approximately 38 kDa and 42 kDa were observed and the predicted size of ^{3xFLAG}CBU1701 is 55 kDa. As discussed previously in Chapter 4, ^{3xFLAG}CBU1701 was always found to be processed and different constructs do not demonstrate cleavage at exactly the same size indicating that it might be a stability issue rather than active cleavage of the protein. In comparison, the empty vector shows no FLAG reactive protein. Following this, the plasmid was electroporated into WT, *cbu1701*::Tn and Clones A and B of the double mutant. At least ten or more transformants were individually picked and recovered in ACCM–D (Acidified Cysteine Citrate Media supplemented with citrulline and lacking arginine). The non-antibiotic based selected

transformants were tested for ^{3xFLAG}CBU1701 expression in WT, *cbu1701*::Tn and *Δcbu2016 cbu1701*::Tn strains by immunoblotting using a FLAG antibody. Immunoblot data confirmed the expression of ^{3xFLAG}CBU1701 in the WT strain (Figure 5.8 (B)). The *cbu1701*::Tn and *Δcbu2016 cbu1701*::Tn strains carrying the pArgGH–^{3xFLAG}CBU1701 plasmid construct also expressed ^{3xFLAG}CBU1701 as observed by the immunoblot data (Figure 5.8 (C, D and E)). There was a difference in the banding pattern of CBU1701 as observed by immunoblot using anti–FLAG antibody. The expected size of ^{3xFLAG}CBU1701 is 55 kDa and truncated proteins of approximately 38 kDa and 42 kDa was observed. The same bands were observed upon expression of the plasmid in *E. coli*. Upon repeated complementation, expression of CBU1701 was not observed in the case of *Δcbu2016 cbu1701*::Tn double mutant strain, Clone A as shown in Figure 5.8 (E). The construct however is demonstrated to produce FLAG-tagged protein in the other *C. burnetii* strains. Further investigation would be required to understand why this strain was not obtained.

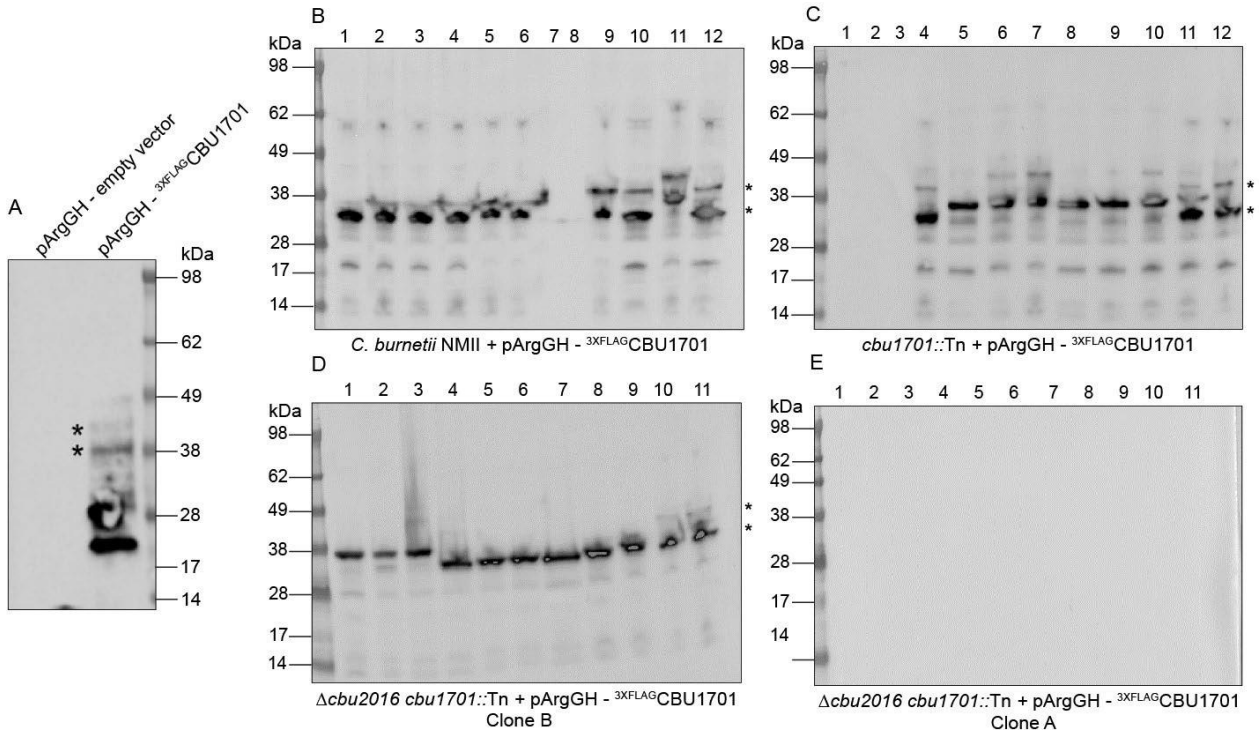

Figure 5.8 Immunoblot confirming complementation of strains with plasmid expressed ^{3xFLAG}CBU1701 in *C. burnetii*.

(A) Immunoblot of bacterial cell lysates using anti–FLAG antibodies confirming the expression of ^{3xFLAG}CBU1701 in *E. coli*. Empty vector shows no protein expression. (B) Immunoblot of ^{3xFLAG}CBU1701 complement strains (lanes 1 to 12) using anti–FLAG antibodies confirming the expression of ^{3xFLAG}CBU1701 in the WT background, (C) ^{3xFLAG}CBU1701 expression confirmation in *cbu1701*::Tn (lanes 1 to 12), (D) ^{3xFLAG}CBU1701 expression confirmation in *Δcbu2016 cbu1701::*Tn (Clone B), (lanes 1 to 11) and (E) no expression of ^{3xFLAG}CBU1701 was observed in the *Δcbu2016 cbu1701*::Tn (Clone A), (lanes 1 to 11) using anti–FLAG antibodies. Asterisk (*) indicates ^{3xFLAG}CBU1701 protein breakdown products.

5.3.6 Construction of a *C. burnetii* CBU2016 complementation strain.

As described in 5.3.5, complementation was performed by introduction of the expression plasmid pArgGH–^{3xFLAG}CBU2016. The expression of ^{3xFLAG}CBU2016 from pJB-CAT::*argGH* was confirmed by probing lysate of *E. coli* carrying this plasmid with anti–FLAG antibodies. The expected size of ^{3xFLAG}CBU2016 protein is 26 kDa and a band approximately 30 kDa was observed. The expression of CBU2016 with anti-FLAG antibodies was bigger than expected and this could be due to post-translational modification of CBU2016. The size discrepancy is small which is not uncommon for SDS-PAGE prediction of protein mass. The transformed empty vector did not have any protein expression (Figure 5.9 (A)). This construct was then electroporated into WT, *Δcbu2016* and clone A and clone B of the *Δcbu2016 cbu1701*::Tn double mutant. At least ten or more transformants were clonally isolated and recovered in ACCM–D (Acidified Cysteine Citrate Media supplemented with citrulline and missing arginine). The non-antibiotic based selected transformants were further tested for ^{3xFLAG}CBU2016 expression in the WT, *Δcbu2016* and *Δcbu2016 cbu1701*::Tn backgrounds by immunoblotting cell lysate with FLAG antibodies. Immunoblot data confirmed the expression of ^{3xFLAG}CBU2016 in the WT strain (Figure 5.9 (B)). The *Δcbu2016* and *Δcbu2016 cbu1701*::Tn strains were complemented by pArgGH–^{3xFLAG}CBU2016 as observed by the immunoblot data (Figure 5.9 (C, D and E)). Expression of ^{3xFLAG}CBU2016 was not observed in the case of *Δcbu2016 cbu1701*::Tn double mutant strain Clone A, upon repeated complementation, as shown in Figure 5.9 (E). Given the same observation as in the case of *cbu1701* complementation and the inability to work with either construct suggests there may be a problem with this strain needing additional investigation.

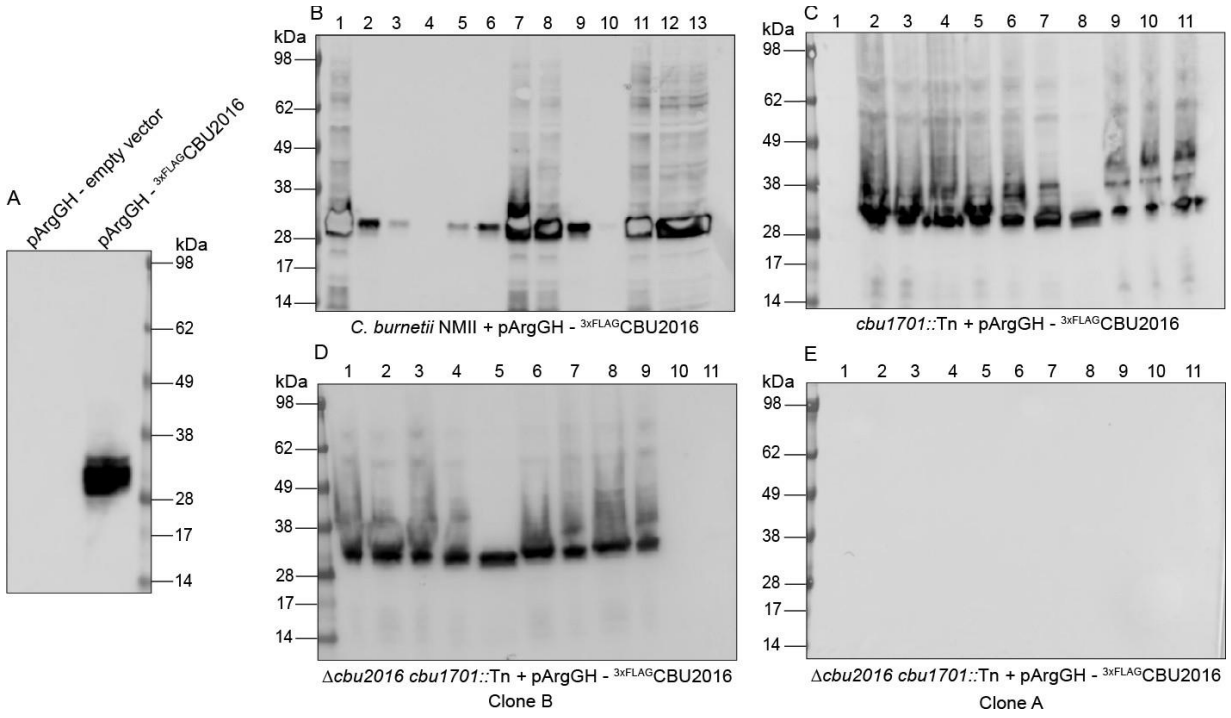

Figure 5.9 Immunoblot confirming the CBU2016 complement strains in *C. burnetii*.

(A) Immunoblot using anti–FLAG antibodies confirming the expression of ^{3xFLAG}CBU2016 in *E. coli*, thus confirming the protein expression from the plasmid. No expression of ^{3xFLAG}CBU2016 was observed in the empty vector transformed lane. (B) Immunoblot using anti–FLAG antibodies confirming the expression of ^{3xFLAG}CBU2016 in the WT background (lanes 1 to 13), (C) ^{3xFLAG}CBU2016 expression confirmation in single mutant strain *Δcbu2016*, (lanes 1 to 11) (D) ^{3xFLAG}CBU2016 expression confirmation in double mutant strain, Clone B, (lanes 1 to 11) and (E) no expression of ^{3xFLAG}CBU2016 was observed in the double mutant strain, Clone A (lanes 1 to 11).

5.4 Discussion

Chapter 4 of this thesis identified *C. burnetii* proteins CBU1701 and CBU2016 as two novel putative T4SS effectors that influence the localisation of TFEB and TFE3 (Figure 5.10 (A)). Curiously, our proteomic analysis did not demonstrate that this had a significant impact on upregulation of lysosomal biogenesis and autophagy. In order to determine how these effectors contribute to the intracellular replication and virulence of this pathogen *C. burnetii* lacking either CBU1701, CBU2016 or both proteins were engineered using the newly developed homologous recombination procedure [79, 130]. Using this recently developed, challenging and time-consuming technique, only a few laboratories in the world have reported successful gene deletion in *C. burnetii*. Fortunately, we had access to a transposon mutant disrupting *cbu1701* [80, 81] which was then used to create double mutants lacking both CBU1701 and CBU2016. Construction of these mutants took a considerable amount of time which unfortunately limited the subsequent characterisation of the strains.

These mutant strains were initially made to infect human epithelial cells to determine any noticeable phenotypic changes. Immunofluorescence observation indicated smaller CCVs for all the mutants, in comparison to the CCVs generated by the WT strain (Figure 5.10 (B)). To further investigate involvement of the effector proteins in the nuclear localisation of TFEB, HeLa TFEB-GFP cells were infected with CBU1701 and CBU2016 mutants and the nuclear to cytoplasmic ratio of TFEB-GFP was determined. These initial TFEB-GFP nuclear translocation assays indicated a reduction in the TFEB-GFP nuclear

translocation by the double mutant and *Δcbu2016* single mutant and to a lesser extent by *cbu1701*::Tn.

The initial infection studies were carried out using a single clonal isolate of the mutant strains. To increase the robustness of the data, two clonal isolates of each of the mutant strains were tested for their ability to produce a CCV and replicate intracellularly. An intracellular replication defect was observed for the *cbu1701*::Tn and *Δcbu2016* single mutant strains in comparison to the WT. *cbu1701*::Tn mutants displayed a slight replication defect in comparison to *Δcbu2016* mutant that showed a more severe replication defect (Figure 5.10 (B)). This phenotype is consistent with the *cbu2016* transposon mutant reported earlier by Weber et al [132]. Both of these phenotypes were consistent between the two independent mutant isolates that were tested, and the reduced replication phenotypes correlated with reduced CCV area quantification.

Upon infection of human epithelial cells using the two clonal isolates of the double mutant strain, one of the mutants displayed a phenotype similar to the *cbu1701*::Tn mutant and the other isolate displayed a phenotype analogous to the *icmL*::Tn phenotype. Two other clonal isolates of the double mutants were further tested to confirm the phenotype observed. To understand the distinctly different phenotype of different isolates of the double mutant, the genome sequence was analysed. However, no genetic changes were detected that could explain these divergent phenotypes. Future studies, using the complementation constructs engineered here, may be able to address these phenotype

discrepancies and confirm that the phenotypes observed in the single mutants can be attributed to the loss of CBU1701 or CBU2016.

The formation of smaller CCVs by these mutants was exciting given the findings in Chapter 3 that demonstrated a remarkable decrease in the CCV size upon silencing the transcription factors TFEB and TFE3. As there is no replication defect with the gene silencing of TFEB and TFE3, the replication defect seen for the mutants may add further evidence to the hypothesis that these effectors are not acting directly on TFEB but rather that this observation is an indirect outcome of these effectors functions. Extending these studies to both THP-1 macrophage-like cells and measuring virulence in the *Galleria mellonella* larvae model of infection will also increase our understanding of the importance of CBU1701 and CBU2016.

A comparative proteomics approach could be performed during infection with these mutants in comparison to the WT to determine changes in the abundance of TFEB controlled proteins. Using this approach, the role of TFEB signalling in these mutants could be further dissected. Given the findings in Chapter 4 that the effector proteins identified might be impacting TFEB localisation but not activity, a proteomics approach can be employed to address these questions in the future. Thus, using these various approaches we will be able to link the role of these effectors on *C. burnetii* virulence with their ability to manipulate the localisation of TFEB.

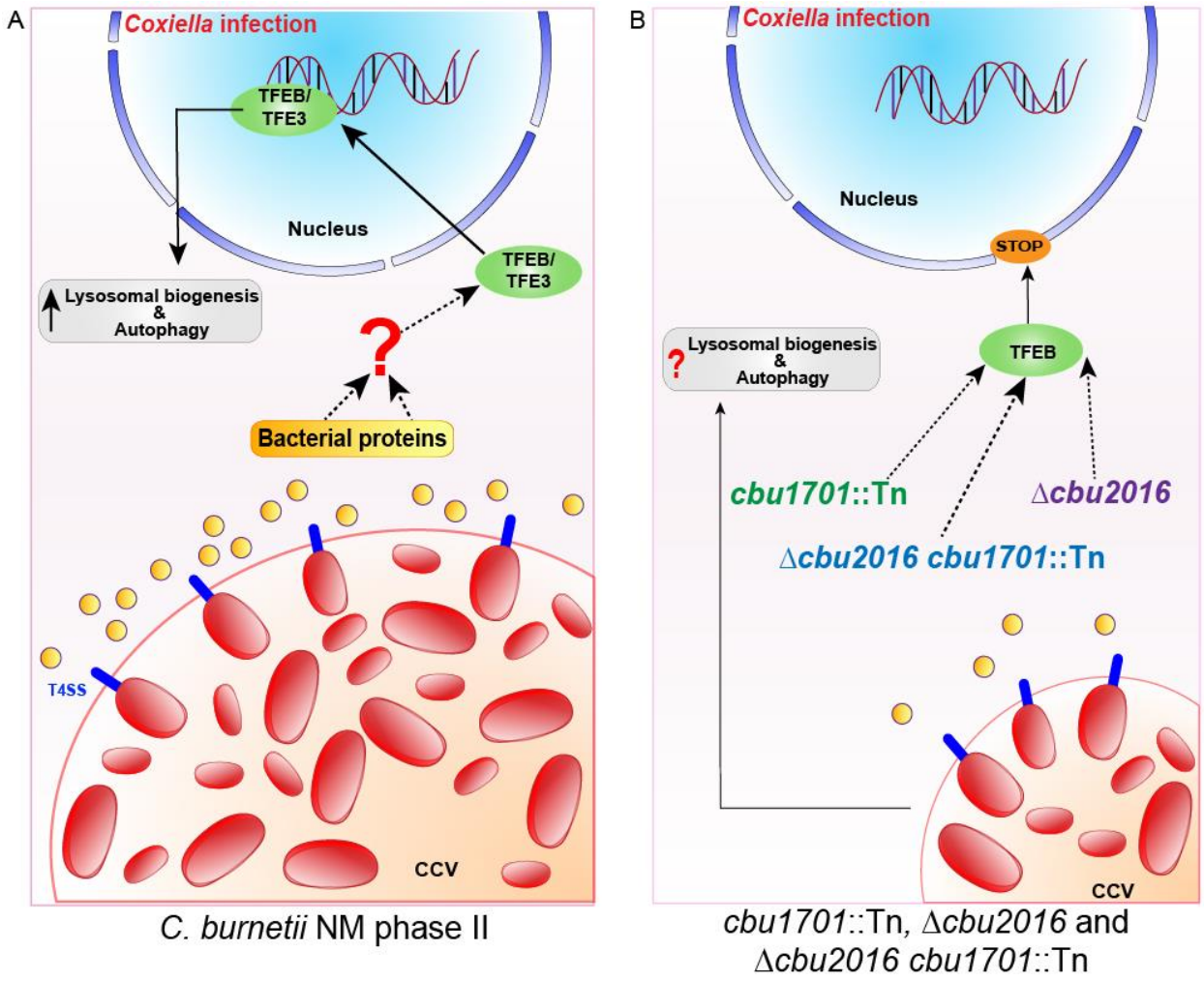

Figure 5.10 Summary of Chapter 5.

(A) In this chapter, construction of several important tools to address the importance of CBU1701 and CBU2016 during *C. burnetii* infection have been developed. (B) Each of the single and double mutant strains appears to have a replication defect and reduced CCV size. Based on our preliminary observation (Figure 5.5), TFEB can no longer localise to the nucleus, thus likely leading to reduced transcription of lysosomal biogenesis and autophagy.

Chapter 6

Perspective

Understanding how intracellular bacterial pathogens interact with the human host cell is a fascinating area of research. Bacterial pathogens have demonstrated sophisticated and novel mechanisms to fine tune many different eukaryotic processes and pathways to their advantage. Studying how bacterial virulence factors manipulate the host cell, will reveal important infection strategies used by the pathogen. Various cell biology processes and crucial pathways required for immune responses upon infection can be unraveled using host-pathogen communications. Such research not only informs us of what makes a successful intracellular pathogen but can also glean important insights into eukaryotic cell function and dysfunction.

A comprehensive example of this is the advances in understanding eukaryotic cytoskeletal dynamics that has been developed through study of the bacterial pathogens *Listeria monocytogenes* and *Shigella flexneri*. Both of these gastrointestinal pathogens invade human cells and use virulence factors to escape the phagosome and replicate in the cytoplasm. They commandeer the host cytoskeleton to facilitate movement and cell-to-cell spread without having to be exposed to the extracellular environment. IcsA is a *S. flexneri* specific actin-based motility factor required for actin tail formation and movement [255]. The unrelated *L. monocytogenes* requires ActA, present on the bacterial surface for actin-based motility [256]. Although these proteins have similar function, there are no sequence similarities between the sequences of these two proteins [257]. This shows that these two unrelated proteins have independently evolved the capacity to control cytoskeletal dynamics. These pathogens have been used as tools to identify and functionally characterise specific eukaryotic accessory proteins involved in actin

dynamics that are relevant during normal eukaryotic cell function and a range of human disease states.

Another example of how intracellular bacterial pathogens can teach us about human cell function is the manner in which different intracellular pathogens target Rab1. Rab1 is a small GTPase (guanosine triphosphatase), expressed in all mammalian cells that acts as a molecular switch regulating endocytic and membrane trafficking events between the endoplasmic reticulum (ER) and Golgi [258]. Rab1 not only plays a role in vesicular transport functions, but also plays a role in sensing of nutrient, and signaling movement of cells required for the maintenance of multicellular organelles and in the presentation of membrane and transmembrane receptors [259]. Rab1 expression deregulation results in a multitude of human diseases such as Parkinson's disease, cancers and disease of the heart muscles [260, 261].

The mechanisms of Rab1 manipulation by the intracellular bacterium*, L. pneumophila* are very well characterised. For example, the *L. pneumophila* T4SS effector protein DrrA/SidM interrupts the Rab1 mediated secretory transport to the Golgi activating Rab1 on plasma membrane organelles by competing with the native guanine-nucleotide exchange factors [262]. The DrrA is also known to AMPylate the switch II region of Rab1b, thereby restricting the access of DrrA to GTPase activating proteins, leading to Rab1b being constitutively active [263]. Another study identified the effector protein AnkX as being able to modify the function of Rab1 and Rab35 by a unique post-translational modification, phosphocholination [264]. *L. pneumophila* has also been shown to produce

T4SS effectors that reverse both of these post-translational modifications demonstrating likely spatial and temporal totally control of Rab1 activity. Discovery of such modifications has enabled the understanding of the mechanisms behind regulation of Rab proteins and the specific residues that can be manipulated to control activity.

Bacterial pathogens deploy virulence factors targeting the host cell giving rise to diseases. Studying intracellular pathogens can teach us about eukaryotic cell function or biology. The master regulatory gene, TFEB coordinates expression of membrane proteins, lysosomal proteins and genes involved in autophagy. This research project started based on the hypothesis that this transcription factor is a likely target of some intracellular pathogens and *C. burnetii* and may allow us to develop new insights into the signalling axis that controls lysosome biogenesis.

The disease Q fever, caused by the bacterial pathogen *C. burnetii*, is a neglected zoonosis. This infection is not only a major public health concern but poses a huge agricultural threat. Research done thus far has been able to reveal a lot about the mechanism of pathogenesis and the way in which this pathogen interacts with the eukaryotic host cell. However, the molecular details of these host-pathogen interactions and the functional significance of individual bacterial virulence factors are works in progress. Axenic cultivation has only been possible for just over 10 years. This was a significant breakthrough that facilitated the development of techniques to genetically manipulate the pathogen and identify important virulence determinants. Hence the field is still in its infancy and there is so much that is yet to be discovered.

Upon internalization through inhalation, *C. burnetii* infects alveolar macrophages. The bacteria traffics through the endocytic pathway forming the modified lysosome called the *Coxiella*-containing vacuole. The CCV has a very low pH and hydrolytic activity that supports bacterial replication. *C. burnetii* utilises the Dot/Icm T4SS to translocate approximately 150 bacterial proteins from within the CCV into the host cytosol to establish itself as a successful pathogen. *C. burnetii* for the spacious and distinctive vacuole formation utilises effector proteins in order to manipulate various pathways such as host-trafficking, autophagy, cholesterol biosynthesis and interaction with clathrin-coated vesicles, endocytic vesicles and autophagosomes. Yet, the exact mechanism of the host pathways and contributions of effector proteins towards the biogenesis of the CCV remains to be determined. Thus, future studies will involve elucidating how *C. burnetii* effectors modify the various host pathways and its specific components. This would unravel mechanisms behind host cellular processes also identifying *C. burnetii* effectors involved in this process.

In Chapter 3 of this thesis, the role of the host transcription factors, TFEB and TFE3, in the intracellular success of *C. burnetii* was deciphered. This research started with an unbiased SILAC-based proteomic analysis to identify changes in the host proteome during *C. burnetii* infection. This highlighted some key features of infected macrophages, including the increased abundance of many proteins involved in lysosomal biogenesis and autophagy. This led to the observed nuclear localisation of TFEB/TFE3, the key regulators of lysosomal biogenesis and autophagy, during *C. burnetii* infection of human epithelial cells. Further, infection of epithelial cells using *C. burnetii* lacking a functional

Dot/Icm system, validated the observation that nuclear localisation of TFEB was dependent on the T4SS. This was further demonstrated by treating the infected cells using chloramphenicol, that blocks bacterial protein synthesis. Silencing expression of these transcription factors resulted in a decrease in the expansion of the CCV indicating the requirement of TFEB/TFE3 in the biogenesis of the CCV.

The findings in Chapter 3 led to the hypothesis that nuclear localisation of TFEB/TFE3 is dependent on the *C. burnetii* T4SS and may be mediated by individual effector proteins translocated into the host cell via that system. Examining how effector proteins secreted by *C. burnetii* control the endolysosomal trafficking pathway will remarkably strengthen our understanding of the molecular mechanisms used by the bacterial pathogen. In order to investigate this, an unbiased immunofluorescence screen of TFEB localisation in the presence of approximately 150 putative effectors proteins was carried out as detailed in Chapter 4. The screen identified, CBU1701 and CBU2016 as two potential *C. burnetii* proteins capable of inducing nuclear localisation of TFEB. Cells were engineered to express each of these effectors under the control of a doxycycline inducible promoter. We observed that these effectors could induce nuclear activation of both TFEB and TFE3. A change in the host proteome upon induction of ^{3xFLAG}CBU1701 and ^{3xFLAG}CBU2016 was observed. Interestingly, the proteome data suggested a similar change or impact on the host proteome arising upon the expression of these two bacterial proteins. Some TEFB regulated proteins changed in abundance but not enough to suggest that either of these effectors directly modulate the TFEB regulon. This finding may suggest the association

between these effectors and TFEB is indirect and/or that the nuclear localisation and transcriptional activation activity of TFEB are uncoupled.

Chapter 5 involved production of mutant strains to dissect the contribution of CBU1701 and CBU2016 to *C. burnetii* intracellular success. Mutant strains were generated, with either transposon disruption or targeted gene knock out. Our preliminary data suggested a replication defect for *C. burnetii* lacking *cbu1701* and/or *cbu2016*. The CCV size was much smaller for the single and the double mutant strains in comparison to the wild-type strain. Initial characterisation revealed that nuclear localisation of TFEB-GFP depended on *cbu1701* and *cbu2016*. A defect in CCV biogenesis was observed upon infection of human epithelial cells using the mutant strains. The two different isolates of the double mutant strains showed conflicting phenotypes. However, whole genome sequencing was unable to explain the phenotypic difference of these strains. We were able to successfully generate the complement strains for these mutants. In the future, studies can be performed using the various tools generated, to determine whether these complement strains are able to rescue the phenotype observed in the absence of *cbu1701* and *cbu2016*.

TFEB/TFE3 was shown to be activated during *C. burnetii* infection. The two *C. burnetii* proteins identified to induce nuclear localisation of TFEB/TFE3 and the various reagents generated can be used to validate the mechanisms of TFEB modulation by *C. burnetii* using proteomics, biochemical and cell biology assays. And so, it will be interesting to determine the various signaling pathways resulting in TFEB nuclear localisation. During

the course of this research, Larson *et al*., published a similar study that showed nuclear localisation of TFE3 during *C. burnetii* infection. They further demonstrated the nuclear localisation of TFE3 by the T4SS mutants in comparison to this research that showed no TFEB/TFE3 nuclear localisation for T4SS-deficient *C. burnetii* [212]. Similar to the findings in this study, their work illustrated knock out of TFEB/TFE3 in RAW 264.6 macrophage-like cells resulted in a reduction in *C. burnetii* replication. Interestingly, they have further demonstrated that the nuclear localisation of TFE3 is not dependent on the inhibition of mTORC1. Thus, it will be interesting to examine whether the nuclear localisation of TFEB induced by the expression of ^{3xFLAG}CBU1701 and ^{3xFLAG}CBU2016 is dependent on activity of mTORC1 and their impact on the regulators of lysosomal biogenesis and autophagy.

The stable cell lines of the effectors identified in this study can be used to elucidate the mechanism by which these effectors control TFEB/TFE3 nuclear localisation. For example, in the presence or absence of the effector expression, we can determine whether mTORC1 has an effect on the nuclear localisation of TFEB/TFE3 by monitoring the activity of mTORC1. We could also perform immunoprecipitation experiments using ^{3xFLAG}CBU1701 and ^{3xFLAG}CBU2016 stable cell lines to determine whether these effectors interact with any components of mTORC1 and/or other eukaryotic proteins that may be involved in this signaling axis. Findings reported here indicate that *cbu1701* and *cbu2016* may not directly interfere with the lysosome-nuclear TFEB signaling axis. Which could also mean that there are other effectors responsible for the transcriptional activation presumably indirectly. The similar significant increase in proteins involved in cholesterol

transport may be worth pursuing to examine whether these effectors are influencing lipid transport during infection.

This study highlights how *C. burnetii* has developed various tactics to replicate and survive comfortably within the lysosome derived CCVs. However, the exact contributions of *C. burnetii* effector proteins and host pathways towards biogenesis of CCV still remains to be investigated. The fascinating pathogen *C. burnetii* within its lysosomal environment, interacts with autophagosomes, has a membrane that is enriched with cholesterol, is highly fusogenic and modifies the host trafficking system to form an expansive vacuole that support bacterial replication. This CCV biogenesis requires translocation of approximately 150 *C. burnetii* T4SS effector proteins into the host cytoplasm through the vacuole membrane. The research carried out in this thesis brings up the question of why *C. burnetii* mediates the formation of a large CCV and what are its implications on the biogenesis of the lysosomes. And whether understating the mechanisms behind how *C. burnetii* mediates CCV biogenesis can reveal novel ways in which lysosomal biogenesis in humans could be exploited. Thus *C. burnetii* can be used as a tool to uncover novel understanding of human lysosomal storage disorders, neurodegenerative diseases, and several cancers. Understanding how *C. burnetii* proteins mediate the activity of TFEB will inform us regarding the mechanisms behind the lysosome-nuclear signaling pathway. This would allow for the development of therapeutic interventions to control various human disease states modulated by lysosomal biogenesis

Bibliography

1. Angelakis, E. and D. Raoult, *Q Fever.* Vet Microbiol, 2010. **140**(3-4): p. 297-309.
2. Maurin, M. and D. Raoult, *Q fever.* Clin Microbiol Rev, 1999. **12**(4): p. 518-53.
3. Derrick, E.H., *"Q" fever, a new fever entity: clinical features, diagnosis and laboratory investigation.* Rev Infect Dis, 1983. **5**(4): p. 790-800.
4. Burnet, F.M. and M. Freeman, *Experimental studies on the virus of "Q" fever.* Rev Infect Dis, 1983. **5**(4): p. 800-8.
5. Dyer, R.J.P.h.r., *A Filter-Passing Infectious Agent isolated from Ticks. IV. Human Infection.* 1938. **53**(52).
6. Dyer, R.E., *Similarity of Australian "Q" Fever and a Disease Caused by an Infectious Agent Isolated from Ticks in Montana.* Public Health Reports (1896-1970), 1939. **54**(27): p. 1229-1237.
7. Tan, C.K. and L. Owens, *Infectivity, transmission and 16S rRNA sequencing of a rickettsia, Coxiella cheraxi sp. nov., from the freshwater crayfish Cherax quadricarinatus.* Dis Aquat Organ, 2000. **41**(2): p. 115-22.
8. Marrie, T.J., *Q fever - a review.* Can Vet J, 1990. **31**(8): p. 555-63.
9. Honarmand, H., *Q Fever: an old but still a poorly understood disease.* Interdiscip Perspect Infect Dis, 2012. **2012**: p. 131932.
10. Mori, M. and H.J. Roest, *Farming, Q fever and public health: agricultural practices and beyond.* Arch Public Health, 2018. **76**: p. 2.
11. Babudieri, B., *Q fever : a zoonosis.* Adv. Vet. Sci., 1959. **5**: p. 81-154.
12. Angelakis, E. and D. Raoult, *Emergence of q Fever.* Iran J Public Health, 2011. **40**(3): p. 1-18.
13. Anderson, A., et al., *Diagnosis and management of Q fever--United States, 2013: recommendations from CDC and the Q Fever Working Group.* MMWR Recomm Rep, 2013. **62**(RR-03): p. 1-30.
14. Cutler, S.J., M. Bouzid, and R.R. Cutler, *Q fever.* J Infect, 2007. **54**(4): p. 313-8.
15. Delsing, C.E., A. Warris, and C.P. Bleeker-Rovers, *Q fever: still more queries than answers.* Adv Exp Med Biol, 2011. **719**: p. 133-43.
16. Graham, J.G., et al., *Virulent Coxiella burnetii pathotypes productively infect primary human alveolar macrophages.* Cell Microbiol, 2013. **15**(6): p. 1012-25.
17. Scott, G.H. and J.C. Williams, *Susceptibility of Coxiella burnetii to chemical disinfectants.* Ann N Y Acad Sci, 1990. **590**: p. 291-6.
18. McCaul, T.F. and J.C. Williams, *Developmental cycle of Coxiella burnetii: structure and morphogenesis of vegetative and sporogenic differentiations.* J Bacteriol, 1981. **147**(3): p. 1063-76.
19. Rotz, L.D., et al., *Public health assessment of potential biological terrorism agents.* Emerg Infect Dis, 2002. **8**(2): p. 225-30.
20. Madariaga, M.G., et al., *Q fever: a biological weapon in your backyard.* Lancet Infect Dis, 2003. **3**(11): p. 709-21.
21. Moos, A. and T. Hackstadt, *Comparative virulence of intra- and interstrain lipopolysaccharide variants of Coxiella burnetii in the guinea pig model.* Infect Immun, 1987. **55**(5): p. 1144-50.

22. Beare, P.A., et al., *Comparative genomics reveal extensive transposon-mediated genomic plasticity and diversity among potential effector proteins within the genus Coxiella.* Infect Immun, 2009. **77**(2): p. 642-56.
23. Clark, N.J. and R.J. Soares Magalhaes, *Airborne geographical dispersal of Q fever from livestock holdings to human communities: a systematic review and critical appraisal of evidence.* BMC Infect Dis, 2018. **18**(1): p. 218.
24. Cornejo, J., et al., *Identification of Coxiella burnetii in Tank Raw Cow Milk: First Findings from Chile.* Vector Borne Zoonotic Dis, 2020. **20**(3): p. 228-230.
25. Hilbink, F., et al., *Q fever is absent from New Zealand.* Int J Epidemiol, 1993. **22**(5): p. 945-9.
26. Karakousis, P.C., M. Trucksis, and J.S. Dumler, *Chronic Q fever in the United States.* J Clin Microbiol, 2006. **44**(6): p. 2283-7.
27. Kampschreur, L.M., et al., *Chronic Q fever diagnosis- consensus guideline versus expert opinion.* Emerg Infect Dis, 2015. **21**(7): p. 1183-8.
28. Enserink, M., *Infectious diseases. Questions abound in Q-fever explosion in the Netherlands.* Science, 2010. **327**(5963): p. 266-7.
29. Barry, A.O., et al., *Impaired stimulation of p38alpha-MAPK/Vps41-HOPS by LPS from pathogenic Coxiella burnetii prevents trafficking to microbicidal phagolysosomes.* Cell Host Microbe, 2012. **12**(6): p. 751-63.
30. Wielders, C.C., et al., *Kinetics of antibody response to Coxiella burnetii infection (Q fever): Estimation of the seroresponse onset from antibody levels.* Epidemics, 2015. **13**: p. 37-43.
31. Arricau-Bouvery, N. and A. Rodolakis, *Is Q fever an emerging or re-emerging zoonosis?* Vet Res, 2005. **36**(3): p. 327-49.
32. Delsing, C.E., B.J. Kullberg, and C.P. Bleeker-Rovers, *Q fever in the Netherlands from 2007 to 2010.* Neth J Med, 2010. **68**(12): p. 382-7.
33. Kampschreur, L.M., et al., *Acute Q fever related in-hospital mortality in the Netherlands.* Neth J Med, 2010. **68**(12): p. 408-13.
34. van der Hoek, W., et al., *Epidemic Q fever in humans in the Netherlands.* Adv Exp Med Biol, 2012. **984**: p. 329-64.
35. Oliveira, R.D., et al., *Domestic sheep show average Coxiella burnetii seropositivity generations after a sheep-associated human Q fever outbreak and lack detectable shedding by placental, vaginal, and fecal routes.* PLoS One, 2017. **12**(11): p. e0188054.
36. Whelan, J., et al., *Q fever among culling workers, the Netherlands, 2009-2010.* Emerg Infect Dis, 2011. **17**(9): p. 1719-23.
37. Kopecny, L., et al., *Investigating Coxiella burnetii infection in a breeding cattery at the centre of a Q fever outbreak.* J Feline Med Surg, 2013. **15**(12): p. 1037-45.
38. Bond, K.A., et al., *One Health approach to controlling a Q fever outbreak on an Australian goat farm.* Epidemiol Infect, 2016. **144**(6): p. 1129-41.
39. Buckley, B., *Q fever epidemic in Victorian general practice.* Med J Aust, 1980. **1**(12): p. 593-5.
40. Gilroy, N., et al., *Abattoir-associated Q fever: a Q fever outbreak during a Q fever vaccination program.* Aust N Z J Public Health, 2001. **25**(4): p. 362-7.
41. *Q fever outbreak in an abattoir in Cooma, NSW.* Commun Dis Intell, 1998. **22**(10): p. 222.

42. Yohannes, K., et al., *Australia's notifiable diseases status, 2004, annual report of the National Notifiable Diseases Surveillance System.* Commun Dis Intell Q Rep, 2006. **30**(1): p. 1-79.
43. O'Connor, B.A., I.G. Tribe, and R. Givney, *A windyday in a sheep saleyard: an outbreak of Q fever in rural South Australia.* Epidemiol Infect, 2015. **143**(2): p. 391-8.
44. Wade, A.J., et al., *Q fever outbreak at a cosmetics supply factory.* Clin Infect Dis, 2006. **42**(7): p. e50-2.
45. Archer, B.N., et al., *Atypical outbreak of Q fever affecting low-risk residents of a remote rural town in New South Wales.* Commun Dis Intell Q Rep, 2017. **41**(2): p. E125-E133.
46. Archibald, J., *Disease in the dust: experiences of Q fever during drought in Australia.* Perspect Public Health, 2019. **139**(2): p. 77-78.
47. Bartelink, A.K., et al., *[Acute and chronic Q fever; epidemiology, symptoms, diagnosis and therapy of infection caused by Coxiella burnetii].* Ned Tijdschr Geneeskd, 2000. **144**(27): p. 1303-6.
48. Parker, N.R., J.H. Barralet, and A.M. Bell, *Q fever.* Lancet, 2006. **367**(9511): p. 679-88.
49. Fenollar, F., et al., *Risks factors and prevention of Q fever endocarditis.* Clin Infect Dis, 2001. **33**(3): p. 312-6.
50. Lacombe, V., et al., *Coxiella burnetii endocarditis as a possible cause of ANCA-associated vasculitis.* Rheumatology (Oxford), 2020.
51. Schneeberger, P.M., et al., *Real-time PCR with serum samples is indispensable for early diagnosis of acute Q fever.* Clin Vaccine Immunol, 2010. **17**(2): p. 286-90.
52. Klee, S.R., et al., *Highly sensitive real-time PCR for specific detection and quantification of Coxiella burnetii.* BMC Microbiol, 2006. **6**: p. 2.
53. Schneeberger, P.M., et al., *Q fever in the Netherlands - 2007-2010: what we learned from the largest outbreak ever.* Med Mal Infect, 2014. **44**(8): p. 339-53.
54. Million, M., et al., *Long-term outcome of Q fever endocarditis: a 26-year personal survey.* 2010. **10**(8): p. 527-535.
55. Raoult, D., et al., *Treatment of Q fever endocarditis: comparison of 2 regimens containing doxycycline and ofloxacin or hydroxychloroquine.* 1999. **159**(2): p. 167-173.
56. Raoult, D., et al., *Coxiella burnetii infection of a vascular prosthesis.* N Engl J Med, 1986. **315**(21): p. 1358-9.
57. Kersh, G.J., *Antimicrobial therapies for Q fever.* Expert Rev Anti Infect Ther, 2013. **11**(11): p. 1207-14.
58. Vanrompay, D., et al., *Antimicrobial Resistance in Chlamydiales, Rickettsia, Coxiella, and Other Intracellular Pathogens.* Microbiol Spectr, 2018. **6**(2).
59. Kermode, M., et al., *An economic evaluation of increased uptake in Q fever vaccination among meat and agricultural industry workers following implementation of the National Q Fever Management Program.* Aust N Z J Public Health, 2003. **27**(4): p. 390-8.
60. Zhang, G., et al., *Formalin-inactivated Coxiella burnetii phase I vaccine-induced protection depends on B cells to produce protective IgM and IgG.* Infect Immun, 2013. **81**(6): p. 2112-22.
61. Gidding, H.F., et al., *Australia's national Q fever vaccination program.* Vaccine, 2009. **27**(14): p. 2037-41.

62. O'Neill, T.J., J.M. Sargeant, and Z. Poljak, *The effectiveness of Coxiella burnetii vaccines in occupationally exposed populations: a systematic review and meta-analysis.* Zoonoses Public Health, 2014. **61**(2): p. 81-96.
63. Zhang, G. and J.E. Samuel, *Vaccines against Coxiella infection.* Expert Rev Vaccines, 2004. **3**(5): p. 577-84.
64. Hackstadt, T. and J.C. Williams, *pH dependence of the Coxiella burnetii glutamate transport system.* J Bacteriol, 1983. **154**(2): p. 598-603.
65. Hendrix, L. and L.P. Mallavia, *Active transport of proline by Coxiella burnetii.* J Gen Microbiol, 1984. **130**(11): p. 2857-63.
66. Kuley, R., et al., *Major differential gene regulation in Coxiella burnetii between in vivo and in vitro cultivation models.* BMC Genomics, 2015. **16**: p. 953.
67. Omsland, A., et al., *Sustained axenic metabolic activity by the obligate intracellular bacterium Coxiella burnetii.* J Bacteriol, 2008. **190**(9): p. 3203-12.
68. Sanchez, S.E., E. Vallejo-Esquerra, and A. Omsland, *Use of Axenic Culture Tools to Study Coxiella burnetii.* Curr Protoc Microbiol, 2018. **50**(1): p. e52.
69. Omsland, A., et al., *Host cell-free growth of the Q fever bacterium Coxiella burnetii.* Proc Natl Acad Sci U S A, 2009. **106**(11): p. 4430-4.
70. Omsland, A., et al., *Isolation from animal tissue and genetic transformation of Coxiella burnetii are facilitated by an improved axenic growth medium.* Appl Environ Microbiol, 2011. **77**(11): p. 3720-5.
71. Sandoz, K.M., et al., *Developmental transitions of Coxiella burnetii grown in axenic media.* J Microbiol Methods, 2014. **96**: p. 104-10.
72. Sandoz, K.M., et al., *Complementation of Arginine Auxotrophy for Genetic Transformation of Coxiella burnetii by Use of a Defined Axenic Medium.* Appl Environ Microbiol, 2016. **82**(10): p. 3042-51.
73. Seshadri, R., et al., *Complete genome sequence of the Q-fever pathogen Coxiella burnetii.* Proc Natl Acad Sci U S A, 2003. **100**(9): p. 5455-60.
74. Hemsley, C.M., et al., *Extensive genome analysis of Coxiella burnetii reveals limited evolution within genomic groups.* BMC Genomics, 2019. **20**(1): p. 441.
75. Maturana, P., et al., *Refining the plasmid-encoded type IV secretion system substrate repertoire of Coxiella burnetii.* J Bacteriol, 2013. **195**(14): p. 3269-76.
76. Voth, D.E., et al., *The Coxiella burnetii cryptic plasmid is enriched in genes encoding type IV secretion system substrates.* J Bacteriol, 2011. **193**(7): p. 1493-503.
77. Suhan, M.L., S.-Y. Chen, and H.A.J.J.o.b. Thompson, *Transformation of Coxiella burnetii to ampicillin resistance.* 1996. **178**(9): p. 2701-2708.
78. Beare, P.A., et al., *Characterization of a Coxiella burnetii ftsZ mutant generated by Himar1 transposon mutagenesis.* 2009. **191**(5): p. 1369-1381.
79. Beare, P.A., et al., *Two systems for targeted gene deletion in Coxiella burnetii.* 2012. **78**(13): p. 4580-4589.
80. Crabill, E., et al., *Dot/Icm-Translocated Proteins Important for Biogenesis of the Coxiella burnetii-Containing Vacuole Identified by Screening of an Effector Mutant Sublibrary.* Infect Immun, 2018. **86**(4).

81. Newton, H.J., et al., *A screen of Coxiella burnetii mutants reveals important roles for Dot/Icm effectors and host autophagy in vacuole biogenesis.* PLoS Pathog, 2014. **10**(7): p. e1004286.
82. Minnick, M.F. and R. Raghavan, *Developmental biology of Coxiella burnetii.* Adv Exp Med Biol, 2012. **984**: p. 231-48.
83. van Schaik, E.J., et al., *Molecular pathogenesis of the obligate intracellular bacterium Coxiella burnetii.* Nat Rev Microbiol, 2013. **11**(8): p. 561-73.
84. Coleman, S.A., et al., *Temporal analysis of Coxiella burnetii morphological differentiation.* J Bacteriol, 2004. **186**(21): p. 7344-52.
85. Sandoz, K.M., et al., *Transcriptional Profiling of Coxiella burnetii Reveals Extensive Cell Wall Remodeling in the Small Cell Variant Developmental Form.* PLoS One, 2016. **11**(2): p. e0149957.
86. Moffatt, J.H., P. Newton, and H.J. Newton, *Coxiella burnetii: turning hostility into a home.* Cell Microbiol, 2015. **17**(5): p. 621-31.
87. Moormeier, D.E., et al., *Coxiella burnetii RpoS Regulates Genes Involved in Morphological Differentiation and Intracellular Growth.* J Bacteriol, 2019. **201**(8).
88. Martinez, E., et al., *Identification of OmpA, a Coxiella burnetii protein involved in host cell invasion, by multi-phenotypic high-content screening.* PLoS Pathog, 2014. **10**(3): p. e1004013.
89. Coleman, S.A., et al., *Proteome and antigen profiling of Coxiella burnetii developmental forms.* 2007. **75**(1): p. 290-298.
90. Samanta, D. and S.D. Gilk, *Measuring pH of the Coxiella burnetii Parasitophorous Vacuole.* Curr Protoc Microbiol, 2017. **47**: p. 6C 3 1-6C 3 11.
91. Howe, D. and L.P. Mallavia, *Coxiella burnetii exhibits morphological change and delays phagolysosomal fusion after internalization by J774A.1 cells.* Infect Immun, 2000. **68**(7): p. 3815-21.
92. Voth, D.E., D. Howe, and R.A. Heinzen, *Coxiella burnetii inhibits apoptosis in human THP-1 cells and monkey primary alveolar macrophages.* Infect Immun, 2007. **75**(9): p. 4263-71.
93. Luhrmann, A., et al., *Inhibition of pathogen-induced apoptosis by a Coxiella burnetii type IV effector protein.* Proc Natl Acad Sci U S A, 2010. **107**(44): p. 18997-9001.
94. Samanta, D., et al., *Coxiella burnetii Type 4B Secretion System-dependent manipulation of endolysosomal maturation is required for bacterial growth.* PLoS Pathog, 2019. **15**(12): p. e1007855.
95. McDonough, J.A., et al., *Host pathways important for Coxiella burnetii infection revealed by genome-wide RNA interference screening.* mBio, 2013. **4**(1): p. e00606-12.
96. Maldonado, R.F., I. Sa-Correia, and M.A. Valvano, *Lipopolysaccharide modification in Gram-negative bacteria during chronic infection.* FEMS Microbiol Rev, 2016. **40**(4): p. 480-93.
97. Bertani, B. and N. Ruiz, *Function and Biogenesis of Lipopolysaccharides.* EcoSal Plus, 2018. **8**(1).
98. Amano, K. and J.C. Williams, *Sensitivity of Coxiella burnetii peptidoglycan to lysozyme hydrolysis and correlation of sacculus rigidity with peptidoglycan-associated proteins.* J Bacteriol, 1984. **160**(3): p. 989-93.

99. Beare, P.A., et al., *Genetic mechanisms of Coxiella burnetii lipopolysaccharide phase variation.* PLoS Pathog, 2018. **14**(3): p. e1006922.
100. van Schaik, E.J., et al., *The SCID Mouse Model for Identifying Virulence Determinants in Coxiella burnetii.* Front Cell Infect Microbiol, 2017. **7**: p. 25.
101. Hoover, T., et al., *Chromosomal DNA deletions explain phenotypic characteristics of two antigenic variants, phase II and RSA 514 (crazy), of the Coxiella burnetii nine mile strain.* 2002. **70**(12): p. 6726-6733.
102. Hotta, A., et al., *Phase variation analysis of Coxiella burnetii during serial passage in cell culture by use of monoclonal antibodies.* Infect Immun, 2002. **70**(8): p. 4747-9.
103. Howe, D., et al., *Coxiella burnetii phase I and II variants replicate with similar kinetics in degradative phagolysosome-like compartments of human macrophages.* Infect Immun, 2010. **78**(8): p. 3465-74.
104. Peabody, C.R., et al., *Type II protein secretion and its relationship to bacterial type IV pili and archaeal flagella.* 2003. **149**(11): p. 3051-3072.
105. Sexton, J.A. and J.P.J.T. Vogel, *Type IVB secretion by intracellular pathogens.* 2002. **3**(3): p. 178-185.
106. Ferhat, M., et al., *The TolC protein of Legionella pneumophila plays a major role in multi-drug resistance and the early steps of host invasion.* PLoS One, 2009. **4**(11): p. e7732.
107. McDonough, J.A., H.J. Newton, and C.R. Roy, *Coxiella burnetii secretion systems.* Adv Exp Med Biol, 2012. **984**: p. 171-97.
108. Nishida, T., et al., *Crucial Role of Legionella pneumophila TolC in the Inhibition of Cellular Trafficking in the Protistan Host Paramecium tetraurelia.* Front Microbiol, 2018. **9**: p. 800.
109. Stead, C.M., et al., *Sec-mediated secretion by Coxiella burnetii.* BMC Microbiol, 2013. **13**: p. 222.
110. Feldman, M., et al., *Coevolution between nonhomologous but functionally similar proteins and their conserved partners in the Legionella pathogenesis system.* Proc Natl Acad Sci U S A, 2005. **102**(34): p. 12206-11.
111. Zamboni, D.S., et al., *Coxiella burnetii express type IV secretion system proteins that function similarly to components of the Legionella pneumophila Dot/Icm system.* Mol Microbiol, 2003. **49**(4): p. 965-76.
112. Zusman, T., G. Yerushalmi, and G. Segal, *Functional similarities between the icm/dot pathogenesis systems of Coxiella burnetii and Legionella pneumophila.* Infect Immun, 2003. **71**(7): p. 3714-23.
113. Nagai, H. and T. Kubori, *Type IVB Secretion Systems of Legionella and Other Gram-Negative Bacteria.* Front Microbiol, 2011. **2**: p. 136.
114. Voth, D.E., L.J. Broederdorf, and J.G. Graham, *Bacterial Type IV secretion systems: versatile virulence machines.* Future Microbiol, 2012. **7**(2): p. 241-57.
115. Vogel, J.P., et al., *Conjugative transfer by the virulence system of Legionella pneumophila.* Science, 1998. **279**(5352): p. 873-6.
116. Segal, G., M. Purcell, and H.A. Shuman, *Host cell killing and bacterial conjugation require overlapping sets of genes within a 22-kb region of the Legionella pneumophila genome.* Proc Natl Acad Sci U S A, 1998. **95**(4): p. 1669-74.
117. Hubber, A. and C.R. Roy, *Modulation of host cell function by Legionella pneumophila type IV effectors.* Annu Rev Cell Dev Biol, 2010. **26**: p. 261-83.

118. Chandran Darbari, V. and G. Waksman, *Structural Biology of Bacterial Type IV Secretion Systems.* Annu Rev Biochem, 2015. **84**: p. 603-29.
119. Kubori, T., et al., *Native structure of a type IV secretion system core complex essential for Legionella pathogenesis.* Proc Natl Acad Sci U S A, 2014. **111**(32): p. 11804-9.
120. Zink, S.D., et al., *The Dot/Icm type IV secretion system of Legionella pneumophila is essential for the induction of apoptosis in human macrophages.* Infect Immun, 2002. **70**(3): p. 1657-63.
121. Carey, K.L., et al., *The Coxiella burnetii Dot/Icm system delivers a unique repertoire of type IV effectors into host cells and is required for intracellular replication.* PLoS Pathog, 2011. **7**(5): p. e1002056.
122. Beare, P.A., et al., *Dot/Icm type IVB secretion system requirements for Coxiella burnetii growth in human macrophages.* mBio, 2011. **2**(4): p. e00175-11.
123. Christie, P.J. and J.P. Vogel, *Bacterial type IV secretion: conjugation systems adapted to deliver effector molecules to host cells.* Trends Microbiol, 2000. **8**(8): p. 354-60.
124. Mancilla, M., et al., *The mutagenesis of a type IV secretion system locus of Piscirickettsia salmonis leads to the attenuation of the pathogen in Atlantic salmon, Salmo salar.* J Fish Dis, 2018. **41**(4): p. 625-634.
125. Gomez, F.A., et al., *Evidence of the presence of a functional Dot/Icm type IV-B secretion system in the fish bacterial pathogen Piscirickettsia salmonis.* PLoS One, 2013. **8**(1): p. e54934.
126. Wood, R.E., et al., *Dot/Icm Effector Translocation by Legionella longbeachae Creates a Replicative Vacuole Similar to That of Legionella pneumophila despite Translocation of Distinct Effector Repertoires.* Infect Immun, 2015. **83**(10): p. 4081-92.
127. Newton, H.J., J.A. McDonough, and C.R. Roy, *Effector protein translocation by the Coxiella burnetii Dot/Icm type IV secretion system requires endocytic maturation of the pathogen-occupied vacuole.* PLoS One, 2013. **8**(1): p. e54566.
128. Ghosal, D., et al., *Molecular architecture, polar targeting and biogenesis of the Legionella Dot/Icm T4SS.* Nat Microbiol, 2019. **4**(7): p. 1173-1182.
129. Chen, C., et al., *Large-scale identification and translocation of type IV secretion substrates by Coxiella burnetii.* Proc Natl Acad Sci U S A, 2010. **107**(50): p. 21755-60.
130. Beare, P.A., et al., *Essential role for the response regulator PmrA in Coxiella burnetii type 4B secretion and colonization of mammalian host cells.* J Bacteriol, 2014. **196**(11): p. 1925-40.
131. Newton, P., et al., *Lysosomal degradation products induce Coxiella burnetii virulence.* Proc Natl Acad Sci U S A, 2020. **117**(12): p. 6801-6810.
132. Weber, M.M., et al., *Identification of Coxiella burnetii type IV secretion substrates required for intracellular replication and Coxiella-containing vacuole formation.* J Bacteriol, 2013. **195**(17): p. 3914-24.
133. Lifshitz, Z., et al., *Computational modeling and experimental validation of the Legionella and Coxiella virulence-related type-IVB secretion signal.* Proc Natl Acad Sci U S A, 2013. **110**(8): p. E707-15.
134. Huang, L., et al., *The E Block motif is associated with Legionella pneumophila translocated substrates.* Cell Microbiol, 2011. **13**(2): p. 227-45.

135. Zusman, T., et al., *The response regulator PmrA is a major regulator of the icm/dot type IV secretion system in Legionella pneumophila and Coxiella burnetii.* Mol Microbiol, 2007. **63**(5): p. 1508-23.
136. Charpentier, X. and E. Oswald, *Identification of the secretion and translocation domain of the enteropathogenic and enterohemorrhagic Escherichia coli effector Cif, using TEM-1 beta-lactamase as a new fluorescence-based reporter.* J Bacteriol, 2004. **186**(16): p. 5486-95.
137. Newton, P., E.A. Latomanski, and H.J. Newton, *Applying Fluorescence Resonance Energy Transfer (FRET) to Examine Effector Translocation Efficiency by Coxiella burnetii during siRNA Silencing.* J Vis Exp, 2016(113).
138. Chakravarthy, S., B. Huot, and B.H. Kvitko, *Effector Translocation: Cya Reporter Assay.* Methods Mol Biol, 2017. **1615**: p. 473-487.
139. Pan, X., et al., *Ankyrin repeat proteins comprise a diverse family of bacterial type IV effectors.* Science, 2008. **320**(5883): p. 1651-4.
140. Wallqvist, A., et al., *Mechanisms of action of Coxiella burnetii effectors inferred from host-pathogen protein interactions.* PLoS One, 2017. **12**(11): p. e0188071.
141. Fielden, L.F., et al., *A Farnesylated Coxiella burnetii Effector Forms a Multimeric Complex at the Mitochondrial Outer Membrane during Infection.* Infect Immun, 2017. **85**(5).
142. Rodriguez-Escudero, M., et al., *Studying Coxiella burnetii Type IV Substrates in the Yeast Saccharomyces cerevisiae: Focus on Subcellular Localization and Protein Aggregation.* PLoS One, 2016. **11**(1): p. e0148032.
143. Weber, M.M., et al., *Modulation of the host transcriptome by Coxiella burnetii nuclear effector Cbu1314.* Microbes Infect, 2016. **18**(5): p. 336-45.
144. Larson, C.L., et al., *Coxiella burnetii effector proteins that localize to the parasitophorous vacuole membrane promote intracellular replication.* Infect Immun, 2015. **83**(2): p. 661-70.
145. Siadous, F.A., et al., *Coxiella effector protein CvpF subverts RAB26-dependent autophagy to promote vacuole biogenesis and virulence.* Autophagy, 2020: p. 1-17.
146. Larson, C.L., et al., *Coxiella burnetii effector protein subverts clathrin-mediated vesicular trafficking for pathogen vacuole biogenesis.* Proc Natl Acad Sci U S A, 2013. **110**(49): p. E4770-9.
147. Weber, M.M., et al., *The Type IV Secretion System Effector Protein CirA Stimulates the GTPase Activity of RhoA and Is Required for Virulence in a Mouse Model of Coxiella burnetii Infection.* Infect Immun, 2016. **84**(9): p. 2524-33.
148. Latomanski, E.A., et al., *The Effector Cig57 Hijacks FCHO-Mediated Vesicular Trafficking to Facilitate Intracellular Replication of Coxiella burnetii.* PLoS Pathog, 2016. **12**(12): p. e1006101.
149. Bisle, S., et al., *The inhibition of the apoptosis pathway by the Coxiella burnetii effector protein CaeA requires the EK repetition motif, but is independent of survivin.* Virulence, 2016. **7**(4): p. 400-12.
150. Eckart, R.A., et al., *Antiapoptotic activity of Coxiella burnetii effector protein AnkG is controlled by p32-dependent trafficking.* Infect Immun, 2014. **82**(7): p. 2763-71.
151. Schafer, W., et al., *Nuclear trafficking of the anti-apoptotic Coxiella burnetii effector protein AnkG requires binding to p32 and Importin-alpha1.* Cell Microbiol, 2017. **19**(1).

152. Klingenbeck, L., et al., *The Coxiella burnetii type IV secretion system substrate CaeB inhibits intrinsic apoptosis at the mitochondrial level.* Cell Microbiol, 2013. **15**(4): p. 675-87.
153. Cunha, L.D., et al., *Inhibition of inflammasome activation by Coxiella burnetii type IV secretion system effector IcaA.* Nat Commun, 2015. **6**: p. 10205.
154. Latomanski, E.A. and H.J. Newton, *Interaction between autophagic vesicles and the Coxiella-containing vacuole requires CLTC (clathrin heavy chain).* Autophagy, 2018. **14**(10): p. 1710-1725.
155. He, C. and D.J. Klionsky, *Regulation mechanisms and signaling pathways of autophagy.* Annu Rev Genet, 2009. **43**: p. 67-93.
156. Settembre, C. and A. Ballabio, *Lysosome: regulator of lipid degradation pathways.* Trends Cell Biol, 2014. **24**(12): p. 743-50.
157. Wang, Z. and C. Li, *Xenophagy in innate immunity: A battle between host and pathogen.* Dev Comp Immunol, 2020. **109**: p. 103693.
158. Siqueira, M.D.S., R.M. Ribeiro, and L.H. Travassos, *Autophagy and Its Interaction With Intracellular Bacterial Pathogens.* Front Immunol, 2018. **9**: p. 935.
159. Bento, C.F., N. Empadinhas, and V. Mendes, *Autophagy in the fight against tuberculosis.* DNA Cell Biol, 2015. **34**(4): p. 228-42.
160. Yoshikawa, Y., et al., *Listeria monocytogenes ActA-mediated escape from autophagic recognition.* Nat Cell Biol, 2009. **11**(10): p. 1233-40.
161. Zheng, Y.T., et al., *The adaptor protein p62/SQSTM1 targets invading bacteria to the autophagy pathway.* J Immunol, 2009. **183**(9): p. 5909-16.
162. Choy, A., et al., *The Legionella effector RavZ inhibits host autophagy through irreversible Atg8 deconjugation.* Science, 2012. **338**(6110): p. 1072-6.
163. Yang, A., S. Pantoom, and Y.W. Wu, *Elucidation of the anti-autophagy mechanism of the Legionella effector RavZ using semisynthetic LC3 proteins.* Elife, 2017. **6**.
164. Kubori, T., et al., *Legionella RavZ Plays a Role in Preventing Ubiquitin Recruitment to Bacteria-Containing Vacuoles.* Front Cell Infect Microbiol, 2017. **7**: p. 384.
165. Horenkamp, F.A., et al., *The Legionella Anti-autophagy Effector RavZ Targets the Autophagosome via PI3P- and Curvature-Sensing Motifs.* Dev Cell, 2015. **34**(5): p. 569-76.
166. Colombo, M.I., M.G. Gutierrez, and P.S. Romano, *The two faces of autophagy: Coxiella and Mycobacterium.* Autophagy, 2006. **2**(3): p. 162-4.
167. Campoy, E. and M.I. Colombo, *Autophagy in intracellular bacterial infection.* Biochim Biophys Acta, 2009. **1793**(9): p. 1465-77.
168. Kabeya, Y., et al., *LC3, a mammalian homologue of yeast Apg8p, is localized in autophagosome membranes after processing.* EMBO J, 2000. **19**(21): p. 5720-8.
169. Gutierrez, M.G., et al., *Autophagy induction favours the generation and maturation of the Coxiella-replicative vacuoles.* Cell Microbiol, 2005. **7**(7): p. 981-93.
170. Beron, W., et al., *Coxiella burnetii localizes in a Rab7-labeled compartment with autophagic characteristics.* Infect Immun, 2002. **70**(10): p. 5816-21.
171. Kohler, L.J., et al., *Effector Protein Cig2 Decreases Host Tolerance of Infection by Directing Constitutive Fusion of Autophagosomes with the Coxiella-Containing Vacuole.* MBio, 2016. **7**(4).

172. Martinez, E., et al., *Coxiella burnetii effector CvpB modulates phosphoinositide metabolism for optimal vacuole development.* Proc Natl Acad Sci U S A, 2016. **113**(23): p. E3260-9.
173. Onyenwoke, R.U. and J.E. Brenman, *Lysosomal Storage Diseases-Regulating Neurodegeneration.* J Exp Neurosci, 2015. **9**(Suppl 2): p. 81-91.
174. Settembre, C., et al., *A lysosome-to-nucleus signalling mechanism senses and regulates the lysosome via mTOR and TFEB.* EMBO J, 2012. **31**(5): p. 1095-108.
175. Napolitano, G. and A. Ballabio, *TFEB at a glance.* J Cell Sci, 2016. **129**(13): p. 2475-81.
176. Yamanaka, T., et al., *Genome-wide analyses in neuronal cells reveal that upstream transcription factors regulate lysosomal gene expression.* FEBS J, 2016. **283**(6): p. 1077-87.
177. Sardiello, M. and A. Ballabio, *Lysosomal enhancement: a CLEAR answer to cellular degradative needs.* Cell Cycle, 2009. **8**(24): p. 4021-2.
178. Kuiper, R.P., et al., *Regulation of the MiTF/TFE bHLH-LZ transcription factors through restricted spatial expression and alternative splicing of functional domains.* Nucleic Acids Res, 2004. **32**(8): p. 2315-22.
179. Martina, J.A., et al., *Novel roles for the MiTF/TFE family of transcription factors in organelle biogenesis, nutrient sensing, and energy homeostasis.* Cell Mol Life Sci, 2014. **71**(13): p. 2483-97.
180. Fisher, D.E., et al., *TFEB has DNA-binding and oligomerization properties of a unique helix-loop-helix/leucine-zipper family.* Genes Dev, 1991. **5**(12A): p. 2342-52.
181. Sardiello, M., *Transcription factor EB: from master coordinator of lysosomal pathways to candidate therapeutic target in degenerative storage diseases.* Ann N Y Acad Sci, 2016. **1371**(1): p. 3-14.
182. Palmieri, M., et al., *Characterization of the CLEAR network reveals an integrated control of cellular clearance pathways.* Hum Mol Genet, 2011. **20**(19): p. 3852-66.
183. Settembre, C. and A. Ballabio, *TFEB regulates autophagy: an integrated coordination of cellular degradation and recycling processes.* Autophagy, 2011. **7**(11): p. 1379-81.
184. Settembre, C., et al., *TFEB links autophagy to lysosomal biogenesis.* Science, 2011. **332**(6036): p. 1429-33.
185. Raben, N. and R. Puertollano, *TFEB and TFE3: Linking Lysosomes to Cellular Adaptation to Stress.* Annu Rev Cell Dev Biol, 2016. **32**: p. 255-278.
186. Li, L., et al., *A TFEB nuclear export signal integrates amino acid supply and glucose availability.* Nat Commun, 2018. **9**(1): p. 2685.
187. Roczniak-Ferguson, A., et al., *The transcription factor TFEB links mTORC1 signaling to transcriptional control of lysosome homeostasis.* Sci Signal, 2012. **5**(228): p. ra42.
188. Martina, J.A., et al., *MTORC1 functions as a transcriptional regulator of autophagy by preventing nuclear transport of TFEB.* Autophagy, 2012. **8**(6): p. 903-14.
189. Martina, J.A., et al., *The nutrient-responsive transcription factor TFE3 promotes autophagy, lysosomal biogenesis, and clearance of cellular debris.* Sci Signal, 2014. **7**(309): p. ra9.
190. Hershey, C.L. and D.E. Fisher, *Mitf and Tfe3: members of a b-HLH-ZIP transcription factor family essential for osteoclast development and function.* Bone, 2004. **34**(4): p. 689-96.

191. Pastore, N., et al., *TFEB and TFE3 cooperate in the regulation of the innate immune response in activated macrophages.* Autophagy, 2016. **12**(8): p. 1240-58.
192. Pena-Llopis, S., et al., *Regulation of TFEB and V-ATPases by mTORC1.* EMBO J, 2011. **30**(16): p. 3242-58.
193. Pena-Llopis, S. and J. Brugarolas, *TFEB, a novel mTORC1 effector implicated in lysosome biogenesis, endocytosis and autophagy.* Cell Cycle, 2011. **10**(23): p. 3987-8.
194. Medina, D.L., et al., *Lysosomal calcium signalling regulates autophagy through calcineurin and TFEB.* Nat Cell Biol, 2015. **17**(3): p. 288-99.
195. Puertollano, R., et al., *The complex relationship between TFEB transcription factor phosphorylation and subcellular localization.* EMBO J, 2018. **37**(11).
196. Martina, J.A., et al., *TFEB and TFE3 are novel components of the integrated stress response.* EMBO J, 2016. **35**(5): p. 479-95.
197. Campbell, G.R., et al., *Human Immunodeficiency Virus Type 1 Nef Inhibits Autophagy through Transcription Factor EB Sequestration.* PLoS Pathog, 2015. **11**(6): p. e1005018.
198. Dinkins, C., J. Arko-Mensah, and V. Deretic, *Autophagy and HIV.* Semin Cell Dev Biol, 2010. **21**(7): p. 712-8.
199. Najibi, M., et al., *An Evolutionarily Conserved PLC-PKD-TFEB Pathway for Host Defense.* Cell Rep, 2016. **15**(8): p. 1728-42.
200. Martina, J.A. and R. Puertollano, *TFEB and TFE3: The art of multi-tasking under stress conditions.* Transcription, 2017. **8**(1): p. 48-54.
201. Martini-Stoica, H., et al., *The Autophagy-Lysosomal Pathway in Neurodegeneration: A TFEB Perspective.* Trends Neurosci, 2016. **39**(4): p. 221-234.
202. Kilpatrick, K., et al., *Genetic and chemical activation of TFEB mediates clearance of aggregated alpha-synuclein.* PLoS One, 2015. **10**(3): p. e0120819.
203. Jaton, K., et al., *Development of a high throughput PCR to detect Coxiella burnetii and its application in a diagnostic laboratory over a 7-year period.* New Microbes New Infect, 2013. **1**(1): p. 6-12.
204. Sardiello, M., et al., *A gene network regulating lysosomal biogenesis and function.* Science, 2009. **325**(5939): p. 473-7.
205. Tyanova, S., et al., *Visualization of LC-MS/MS proteomics data in MaxQuant.* Proteomics, 2015. **15**(8): p. 1453-6.
206. Vizcaino, J.A., et al., *2016 update of the PRIDE database and its related tools.* Nucleic Acids Res, 2016. **44**(D1): p. D447-56.
207. Schindelin, J., et al., *Fiji: an open-source platform for biological-image analysis.* Nat Methods, 2012. **9**(7): p. 676-82.
208. Beare, P.A., et al., *Advances in genetic manipulation of obligate intracellular bacterial pathogens.* Front Microbiol, 2011. **2**: p. 97.
209. Luhrmann, A., H.J. Newton, and M. Bonazzi, *Beginning to Understand the Role of the Type IV Secretion System Effector Proteins in Coxiella burnetii Pathogenesis.* Curr Top Microbiol Immunol, 2017. **413**: p. 243-268.
210. Kohler, L.J., et al., *Erratum for Kohler et al., Effector Protein Cig2 Decreases Host Tolerance of Infection by Directing Constitutive Fusion of Autophagosomes with the Coxiella-Containing Vacuole.* mBio, 2016. **7**(5).

211. Padmanabhan, B., et al., *Biogenesis of the spacious Coxiella-containing vacuole depends on host transcription factors TFEB and TFE3.* Infect Immun, 2019.
212. Larson, C.L., et al., *Noncanonical Inhibition of mTORC1 by Coxiella burnetii Promotes Replication within a Phagolysosome-Like Vacuole.* MBio, 2019. **10**(1).
213. Brady, O.A., et al., *The transcription factors TFE3 and TFEB amplify p53 dependent transcriptional programs in response to DNA damage.* Elife, 2018. **7**.
214. Brady, O.A., J.A. Martina, and R. Puertollano, *Emerging roles for TFEB in the immune response and inflammation.* Autophagy, 2018. **14**(2): p. 181-189.
215. Howe, D., et al., *Maturation of the Coxiella burnetii parasitophorous vacuole requires bacterial protein synthesis but not replication.* Cell Microbiol, 2003. **5**(7): p. 469-80.
216. Lieberman, A.P., et al., *Autophagy in lysosomal storage disorders.* Autophagy, 2012. **8**(5): p. 719-30.
217. Torra, A., et al., *Overexpression of TFEB Drives a Pleiotropic Neurotrophic Effect and Prevents Parkinson's Disease-Related Neurodegeneration.* Mol Ther, 2018. **26**(6): p. 1552-1567.
218. Di Malta, C., L. Cinque, and C. Settembre, *Transcriptional Regulation of Autophagy: Mechanisms and Diseases.* Front Cell Dev Biol, 2019. **7**: p. 114.
219. Lifshitz, Z., et al., *Identification of novel Coxiella burnetii Icm/Dot effectors and genetic analysis of their involvement in modulating a mitogen-activated protein kinase pathway.* Infect Immun, 2014. **82**(9): p. 3740-52.
220. Voth, D.E., et al., *The Coxiella burnetii ankyrin repeat domain-containing protein family is heterogeneous, with C-terminal truncations that influence Dot/Icm-mediated secretion.* J Bacteriol, 2009. **191**(13): p. 4232-42.
221. Nadanaka, S., et al., *Activation of mammalian unfolded protein response is compatible with the quality control system operating in the endoplasmic reticulum.* Mol Biol Cell, 2004. **15**(6): p. 2537-48.
222. Medina, D.L., C. Settembre, and A. Ballabio, *Methods to Monitor and Manipulate TFEB Activity During Autophagy.* Methods Enzymol, 2017. **588**: p. 61-78.
223. Jolliffe, I.T. and J. Cadima, *Principal component analysis: a review and recent developments.* Philos Trans A Math Phys Eng Sci, 2016. **374**(2065): p. 20150202.
224. Urbanus, M.L., et al., *Diverse mechanisms of metaeffector activity in an intracellular bacterial pathogen, Legionella pneumophila.* Mol Syst Biol, 2016. **12**(12): p. 893.
225. Hillary, R.F. and U. FitzGerald, *A lifetime of stress: ATF6in development and homeostasis.* J Biomed Sci, 2018. **25**(1): p. 48.
226. Nabar, N.R. and J.H. Kehrl, *The Transcription Factor EB Links Cellular Stress to the Immune Response.* Yale J Biol Med, 2017. **90**(2): p. 301-315.
227. Ferri, N., *Proprotein convertase subtilisin/kexin type 9: from the discovery to the development of new therapies for cardiovascular diseases.* Scientifica (Cairo), 2012. **2012**: p. 927352.
228. Picard, C., et al., *Proprotein convertase subtilisin/kexin type 9 (PCSK9) in Alzheimer's disease: A genetic and proteomic multi-cohort study.* PLoS One, 2019. **14**(8): p. e0220254.
229. von Duvillard, S.P., *Lipids and lipoproteins in diet and exercise. Introduction.* Med Sci Sports Exerc, 1997. **29**(11): p. 1414-5.

230. Shapiro, M.D., H. Tavori, and S. Fazio, *PCSK9: From Basic Science Discoveries to Clinical Trials.* Circ Res, 2018. **122**(10): p. 1420-1438.
231. Lagace, T.A., *PCSK9 and LDLR degradation: regulatory mechanisms in circulation and in cells.* Curr Opin Lipidol, 2014. **25**(5): p. 387-93.
232. Poirier, S., et al., *Trafficking Dynamics of PCSK9-Induced LDLR Degradation: Focus on Human PCSK9 Mutations and C-Terminal Domain.* PLoS One, 2016. **11**(6): p. e0157230.
233. Xiao, J., et al., *PCSK9: A new participant in lipophagy in regulating atherosclerosis?* Clin Chim Acta, 2019. **495**: p. 358-364.
234. Filippakis, H., et al., *Lysosomal regulation of cholesterol homeostasis in tuberous sclerosis complex is mediated via NPC1 and LDL-R.* Oncotarget, 2017. **8**(24): p. 38099-38112.
235. Yang, H.X., et al., *Cholesterol in LDL receptor recycling and degradation.* Clin Chim Acta, 2020. **500**: p. 81-86.
236. Wang, T., et al., *Lipid A Has Significance for Optimal Growth of Coxiella burnetii in Macrophage-Like THP-1 Cells and to a Lesser Extent in Axenic Media and Non-phagocytic Cells.* Front Cell Infect Microbiol, 2018. **8**: p. 192.
237. Mulye, M., B. Zapata, and S.D. Gilk, *Altering lipid droplet homeostasis affects Coxiella burnetii intracellular growth.* PLoS One, 2018. **13**(2): p. e0192215.
238. Gilk, S.D., P.A. Beare, and R.A. Heinzen, *Coxiella burnetii expresses a functional Delta24 sterol reductase.* J Bacteriol, 2010. **192**(23): p. 6154-9.
239. Justis, A.V., et al., *Interactions between the Coxiella burnetii parasitophorous vacuole and the endoplasmic reticulum involve the host protein ORP1L.* Cell Microbiol, 2017. **19**(1).
240. Settembre, C., et al., *TFEB controls cellular lipid metabolism through a starvation-induced autoregulatory loop.* Nat Cell Biol, 2013. **15**(6): p. 647-58.
241. Popa, C.M., M. Tabuchi, and M. Valls, *Modification of Bacterial Effector Proteins Inside Eukaryotic Host Cells.* Front Cell Infect Microbiol, 2016. **6**: p. 73.
242. Di Paola, S. and D.L. Medina, *Ca(2+)-Dependent Regulation of TFEB and Lysosomal Function.* Methods Mol Biol, 2019. **1925**: p. 145-155.
243. El-Houjeiri, L., et al., *The Transcription Factors TFEB and TFE3 Link the FLCN-AMPK Signaling Axis to Innate Immune Response and Pathogen Resistance.* Cell Rep, 2019. **26**(13): p. 3613-3628 e6.
244. Yang, M., et al., *Emerging roles and regulation of MiT/TFE transcriptional factors.* Cell Commun Signal, 2018. **16**(1): p. 31.
245. Frake, R.A., et al., *Autophagy and neurodegeneration.* J Clin Invest, 2015. **125**(1): p. 65-74.
246. Vural, A., et al., *Activator of G-Protein Signaling 3-Induced Lysosomal Biogenesis Limits Macrophage Intracellular Bacterial Infection.* J Immunol, 2016. **196**(2): p. 846-56.
247. Chandra, P., et al., *Mycobacterium tuberculosis Inhibits RAB7 Recruitment to Selectively Modulate Autophagy Flux in Macrophages.* Sci Rep, 2015. **5**: p. 16320.
248. Cardenal-Munoz, E., et al., *Mycobacterium marinum antagonistically induces an autophagic response while repressing the autophagic flux in a TORC1- and ESX-1-dependent manner.* PLoS Pathog, 2017. **13**(4): p. e1006344.
249. Welch, M.D., A. Iwamatsu, and T.J. Mitchison, *Actin polymerization is induced by Arp2/3 protein complex at the surface of Listeria monocytogenes.* Nature, 1997. **385**(6613): p. 265-9.

250. Larson, C.L., et al., *Right on Q: genetics begin to unravel Coxiella burnetii host cell interactions.* Future Microbiol, 2016. **11**: p. 919-39.
251. Campoy, E.M., M.E. Mansilla, and M.I. Colombo, *Endocytic SNAREs are involved in optimal Coxiella burnetii vacuole development.* Cell Microbiol, 2013. **15**(6): p. 922-41.
252. Fielden, L.F., et al., *Targeting mitochondria: how intravacuolar bacterial pathogens manipulate mitochondria.* Cell Tissue Res, 2017. **367**(1): p. 141-154.
253. Graham, J.G., et al., *Identification of ElpA, a Coxiella burnetii pathotype-specific Dot/Icm type IV secretion system substrate.* Infect Immun, 2015. **83**(3): p. 1190-8.
254. Pryor, P.R., et al., *Combinatorial SNARE complexes with VAMP7 or VAMP8 define different late endocytic fusion events.* EMBO Rep, 2004. **5**(6): p. 590-5.
255. Goldberg, M.B. and J.A. Theriot, *Shigella flexneri surface protein IcsA is sufficient to direct actin-based motility.* Proc Natl Acad Sci U S A, 1995. **92**(14): p. 6572-6.
256. Kocks, C., et al., *L. monocytogenes-induced actin assembly requires the actA gene product, a surface protein.* Cell, 1992. **68**(3): p. 521-31.
257. Kocks, C., et al., *The unrelated surface proteins ActA of Listeria monocytogenes and IcsA of Shigella flexneri are sufficient to confer actin-based motility on Listeria innocua and Escherichia coli respectively.* Mol Microbiol, 1995. **18**(3): p. 413-23.
258. Hutagalung, A.H. and P.J. Novick, *Role of Rab GTPases in membrane traffic and cell physiology.* Physiol Rev, 2011. **91**(1): p. 119-49.
259. Yang, X.Z., et al., *Rab1 in cell signaling, cancer and other diseases.* Oncogene, 2016. **35**(44): p. 5699-5704.
260. Guadagno, N.A. and C. Progida, *Rab GTPases: Switching to Human Diseases.* Cells, 2019. **8**(8).
261. Gopal Krishnan, P.D., et al., *Rab GTPases: Emerging Oncogenes and Tumor Suppressive Regulators for the Editing of Survival Pathways in Cancer.* Cancers (Basel), 2020. **12**(2).
262. Murata, T., et al., *The Legionella pneumophila effector protein DrrA is a Rab1 guanine nucleotide-exchange factor.* Nat Cell Biol, 2006. **8**(9): p. 971-7.
263. Muller, M.P., et al., *The Legionella effector protein DrrA AMPylates the membrane traffic regulator Rab1b.* Science, 2010. **329**(5994): p. 946-9.
264. Mukherjee, S., et al., *Modulation of Rab GTPase function by a protein phosphocholine transferase.* Nature, 2011. **477**(7362): p. 103-6.

Appendix

APPENDIX: Recipes for media, buffers, and reagents.

GROWTH MEDIUM

Acidified citrate cysteine medium 2 (ACCM-2)

Bacto-neopeptone	0.1 mg/mL
$CaCl_2*2H_2O$	17.4 µM
Casamino acids	2.5 mg/mL
Citric acid	0.80 mM
$FeSO_4*7H_2O$	2 µM
KH_2PO_4	0.74 mM
L-cysteine	1.5 mM
Methyl-β-cyclodextrin	1 mg/mL
$MgCl_2*2H_2O$	0.2 mM
NaCl	24.9 mM
Roswell Park Memorial Institute Medium (RPMI)	12.5% (v/v)
Sodium citrate tribasic dihydrate	3.2 mM
Bacto-neopeptone	0.1 mg/mL
$CaCl_2*2H_2O$	17.4 µM
Casamino acids	2.5 mg/mL
Citric acid	0.80 mM
$FeSO_4*7H_2O$	2 µM
KH_2PO_4	0.74 mM

Adjusted to pH 4.75 by 10 M NaOH and filter sterilised before use

Luria-Bertani (LB) liquid medium

Yeast extract	0.5% (w/v)
Tryptone	1% (w/v)
NaCl	1% (w/v)

For **LB Agar plates**, supplement LB liquid medium with 1.5% (w/v) Agar.

Super Optimal Broth (SOB)

Yeast extract	0.5% (w/v)
Tryptone	2% (v/v)
NaCl	10 mM
KCl	2.5 mM

Super Optimal broth with Catabolite repression medium (SOC)

Yeast extract	0.5% (w/v)
Tryptone	2% (v/v)
NaCl	10 mM
$MgSO_4$	10 mM
$MgCl_2$	10 mM
KCl	2.5 mM
40% Glucose	40% 20 mM

BUFFERS AND REAGENTS

The following buffers and reagents were made in deionised water.

Cytoplasmic extraction buffer

Tris-HCl (pH-7.5)	50mM
Triton – X – 100	0.5%
NaCl	137.5 mM
Glycerol	10%
EDTA	5 mM
PMSF	1 mM
Sodium orthovanadate	1 mM
NaF	1 mM

Fluorescence-activated cell sorting (FACS) Buffer

FCS	2%
BSA	0.1%
EDTA	5 mM
KCl	2.7 mM
PBS	

Nuclear extraction buffer

Tris-HCl (pH-7.5)	50mM
Triton – X – 100	0.5%
SDS	0.5%
NaCl	137.5 mM
Glycerol	10%
EDTA	5 mM
PMSF	1 mM
Sodium orthovanadate	1 mM
NaF	1 mM

Phosphate-buffered saline (PBS)

NaCl	2.7 mM
Na_2HPO_4	10 mM
KH_2PO_4	1.8 mM
KCl	2.7 mM

2x SDS-PAGE sample buffer

Bromophenol blue	0.001% (w/v)
β-mercaptoethanol	1% (v/v)
SDS	1% (w/v)
Tris	0.75% (w/v)
Glycerol	10% (v/v)

50x TAE buffer

Glacial acetic acid	17.5% (v/v)
EDTA	0.05 M
Tris	0.2 M

For 1x (TAE) buffer, dilute from 50x TAE

Tris-buffered saline with 0.1% Tween-20 (TBST)

NaCl 150 mM	150 mM
Tris-HCl (pH 8.0) 200 mM	200 mM
Tween-20	0.1% (v/v)

TB (transformation buffer)

KCl	250 mM
$CaCl_2*2H_2O$	15 mM
PIPES	10 mM

Adjusted to pH 6.7 and filter sterilised before use.

Abbreviations

List of abbreviations

x g	Number of Times the Gravitational Force
ACCM	Acidified Citrate Cysteine Medium
ATCC	American Type Culture Collection
ATG	Autophagy-Related Protein
Amp	Ampicillin
BSA	Bovine Serum Albumin
CCV	*Coxiella*-containing Vacuole
Cm	Chloramphenicol
°C	Degree Celsius
Δ	Deletion mutant
DAPI	4',6-diamidino-2-phenylindole
DMEM	Dulbecco's Modified Eagle Medium
DMSO	Dimethyl Sulfoxide
DNA	Deoxyribose Nucleic Acid
Dot	Defect in Organelle Trafficking
EGFP	Enhanced Green Fluorescent Protein
ER	Endoplasmic Reticulum
FBS	Fetal Bovine Serum
GE	Genomic Equivalents
::Tn	Gene disruption by transposon insertion
HA	Hemagglutinin
HRP	Horse radish peroxidase
Icm	Intracellular Multiplication
IF	Immunofluorescence
Kan	Kanamycin
kb	Kilo-base pair

kDa	Kilodalton
LAMP-1	Lysosomal associated marker protein - 1
LB	Luria-Bertani medium
TFEB	Transcription factor EB
TFE3	Transcription factor E3
LB	Luria-Bertani
LPS	Lipopolysaccharide
g	Gram
µg	Microgram
µL	Microliter
µM	Micromolar
mg	Milligram
mL	Millilitre
mm	Millimetre
mM	Millimolar
M	Molar
MCS	Multiple cloning site
MOI	Multiplicity of infection
3×FLAG-	N-terminally 3×FLAG-tagged
ng	Nanogram
OD	Optical density
%	Percent
PBS	Phosphate-buffered saline
PCR	Polymerase Chain Reaction
PMSF	phenylmethylsulfonyl fluoride
®	Registered trademark
RPMI	Roswell Park Memorial Institute
RT	Room Temperature

(Amp/Cm/Kan) R	(Antibiotic) resistance
rpm	Revolutions per minute
SOB	Super Optimal Broth
SOC	Super Optimal Broth with catabolite repression
SDS	Sodium Dodecyl Sulfate
SDS-PAGE	SDS- Polyacrylamide Gel Electrophoresis
siRNA	Short Interfering RNA
™	Trademark
TBST	Tris-buffered saline with 0.1% Tween 20
T4SS	Type IVB Dot/Icm Secretion System
V	Volt
v/v	Volume/volume
w/v	Weight/volume
WT	Wild type